Development of a microwave pyrolysis process applied to flax shives and sargassum : product characterization and wave-matter interaction

Lilivet Aracelis Ubiera Ruiz

Normandie Université

THESE

Pour obtenir le diplôme de doctorat

Spécialité Energétique

Préparée au sein de l'Institut National des Sciences Appliquées Rouen Normandie

Development of a microwave pyrolysis process applied to Flax shives and Sargassum: Product characterization and wave-matter interaction

Présentée et soutenue par
Lilivet Aracelis UBIERA RUIZ

Thèse soutenue publiquement le 08 Décembre 2021 devant le jury composé de		
M. Ulises JAUREGUI HAZA	Professeur, INTEC, Saint Domingue, République Dominicaine	Rapporteur
M. Gabriel WILD	Directeur de Recherche CNRS, Université de Lorraine, Nancy, France	Rapporteur
M. Bechara TAOUK	Professeur, INSA Rouen Normandie, Saint Etienne du Rouvray, France	Examinateur
M^{me} Isabelle POLAERT	Maitre de conférences HDR, INSA Rouen Normandie, Saint Etienne du Rouvray, France	Directrice de thèse

Thèse dirigée par Isabelle POLAERT, **laboratoire LSPC - Laboratoire de sécurité des procédés chimiques**

INSA INSTITUT NATIONAL DES SCIENCES APPLIQUÉES ROUEN NORMANDIE

ED 591 PSIME

LSPC Laboratoire de sécurité des procédés chimiques

"No es amor el amor que cambia cuando un cambio encuentra
o que se adapta a la distancia al distanciarse.
¡Oh, no!, es un faro imperturbable
que contempla la tormenta sin llegar a estremecerse, es la estrella para un barco sin rumbo, de valor desconocido, aun contando su altura.
No es un capricho del tiempo, aunque los rosados labios y mejillas caigan bajo un golpe de guadaña. El amor no varía durante breves horas o semanas, sino que se confirma incluso ante la muerte."

Familia UBIERA RUIZ

¡Gracias!

ACKNOWLEDGMENTS

Throughout the writing of this dissertation, I have received great support. I would first like to thank my thesis director, Isabelle POLAERT, whose expertise was invaluable in formulating the research questions and methodology. Your insightful feedback pushed me to sharpen my thinking and brought my work to a higher level. Thanks for being there in my life's good and bad moments, boosting me, and encouraging me to be the best of myself. I will always be indebted to you.

Bechara Taouk, Lokmane Abdelouahed, Michel Delmotte and Dominique Seguin, thank you for wonderful collaboration. Without you, this journey could not be as successful today. I want to thank you for your patience, support, and the opportunities I was given to further my research. I am deeply grateful for your presence.

I wish to acknowledge and thank the MESCyT and INSA for having funded this research work and believing in the relevancy of this subject.

Thanks to my friends, Maxwell, Elizabeth, Oscar, Silvia, Cesar, and Wilson, this adventure was great. You have become my family in France. Also, I want to acknowledge all my INSA colleagues who have been part of this journey with me, the permanent staff from LSPC, and the students who worked on this project alongside me; Yu, Ghita, Lucille, Simplicio, Caroline, and Randal. My superheroes! Maria Pereira, Bruno Daronat, Sylvie Poubelle, Charles Lanel, and Christine Devouge Boyer helped me achieve this research without hesitating. This research could not be done without you.

My relatives (Ruiz and Ubiera's family), you know how much I miss you. I hope to give you back all the love and care you have given me one day.

My parents, Felix Ubiera and Lilian Ruiz, thank you for your wise counsel, a sympathetic ear, and unconditional love. Thank you for making me feel fully understood and loved. Thank you for being there to show me the right pathway to follow. I am here today because you did not give up on me.

Mis hermanitos, Felix Ricardo and Felix Joel. What would I do without you!? Thanks for your support, friendship, and implication and for being my inspiration. I love you.

TABLE OF CONTENT

TABLES OF FIGURES

LIST OF TABLES

LIST OF ABBREVIATIONS

$\vec{\nabla}$	Gradient
$\vec{E}$	Electric field in (V/m)
$\vec{B}$	Magnetic induction in ($Wb.m^{-2}$)
$\vec{D}$	Electric induction in (C/m^2)
$\vec{H}$	Magnetic field (A/m)
ε	Electric permittivity ($F.m^{-1}$)
ε_0	Electric permittivity in the void ($F.m^{-1}$)
μ_0	Magnetic permeability in the void ($H.m^{-1}$)
μ	Magnetic permeability ($H.m^{-1}$)
J	Electric current density ($A.m^{-2}$)
ρ	Electric charge density (C/m^3)
σ	Electric conductivity ($S.m^{-1}$)
σ_0	Electric conductivity in the void ($S.m^{-1}$)
λ_0	Wavelength in the free space
λ	Wavelength
c	Speed of electromagnetic wave
f	Frequency
$(\vec{E})$	Electric field component
$(\vec{H})$	Magnetic Field component
$\overrightarrow{(B)}$	Magnetic induction component
$(\vec{D})$	Electric induction component
(A)	Represent the fields ($\vec{E}$, $\vec{B}$, $\vec{D}$ and $\vec{H}$)
ω	Radian frequency

J	Electric current density
β	Wavenumber
v_p	Velocity of the wave
γ	Complex propagation constant
β_g	Wavenumber for a guided wave
$\beta_{c.}$	Cutoff wavenumber
Pi	Incident Power
Pr	Reflected power
Pabs	Absorbed Power
Ti	Irradiation time
PCA	Principal components analysis

ABSTRACT

Microwave pyrolysis is a relatively new and exciting option for biomass residues treatment in terms of energy efficiency and high-quality products. During this thesis, two types of biomass, Sargassum, and Flax shives, were studied under microwave pyrolysis conditions.

Preliminary studies were carried out to better understand the influence of temperature, moisture content, dielectric properties, biomass, and its pyrolysis products composition on the process. It was found that the thermochemical degradation of Sargassum occurs at a lower temperature in comparison to Flax shives; the increase in the moisture content increases the capability of biomass to convert microwaves into heat; and also, that Flax shives bio-oil and Sargassum bio-char were found to have interesting dielectric properties.

The incident power, irradiation time, flow rate, and biomass load were the main factors considered to evaluate the effect of operating conditions on the microwave pyrolysis products. The liquid bio-oil samples and the non-condensable gas samples were recovered from each experiment and analyzed through gas chromatography-mass spectrometry (GC–MS) and gas chromatograph by flame ionization detection (GC-FID) to identify and quantify the different molecules present. The three phases of pyrolysis, dehydration, primary devolatilization, and passive lignin/residue degradation were identified during microwave irradiation. Bio-oil production was found to depend on two main parameters: the energy absorbed and the internal heating rate of the system. High heating rates of at least 120 °C/min and up to 200 °C/min provided the best bio-oil yields, and such rates can only be achieved by microwave technology by internal heating.

The bio-oil and gas quality (in terms of chemicals families) was also discussed by using a principal component analysis (PCA) in order to visualize the global trend of the data and detect the main factors that enhance the formation or degradation of specific chemical families in the bio-oil or the non-condensable gases samples.

Also, a scheme to scale up a microwave pyrolysis process is proposed. Various factors such as the cavity design, dielectric properties of the treated material, electromagnetic compatibility of the system, and biomass circulation are discussed, sorting the desirable conditions for continuously operated microwave reactors.

Keywords: Intensification, microwaves, biomass pyrolysis, Flax shives, Sargassum

Highlights:

• Microwaves are the way to fast pyrolysis.

• Microwave pyrolysis leads to high bio-oil production.

• An optimum energy input exists for a maximum bio-oil production

RESUME

La pyrolyse par micro-ondes est une option relativement nouvelle et intéressante pour le traitement des résidus de biomasse en termes d'efficacité énergétique et de produits de haute qualité. Au cours de cette thèse, deux types de biomasse, les sargasses et les anas de lin ont été étudiés dans des conditions de pyrolyse micro-ondes.

Des études préliminaires ont été menées afin de mieux comprendre l'influence de la température, de l'humidité, des propriétés diélectriques et de la composition de la biomasse et de ses produits de pyrolyse sur le procédé en général. Il a été constaté que la dégradation thermochimique des sargasses se produit à une plage de température inférieure à celle des anas de lin. En outre, l'amélioration de l'absorption des micro-ondes par la teneur en humidité a été étudiée, où une augmentation de la teneur en humidité a augmenté la capacité de la biomasse à convertir les micro-ondes en chaleur. La bio-huile d'anas du lin et le biochar de Sargasses se sont avérés avoir des propriétés diélectriques intéressantes.

La puissance incidente, le temps d'irradiation, le débit et la charge de biomasse ont été les principaux paramètres considérés afin d'évaluer l'effet des conditions opératoires sur les produits de pyrolyse micro-ondes. Les échantillons de bio-huile liquide ainsi que les échantillons de gaz non condensables ont été récupérés de chaque expérience et analysés par chromatographie en phase gazeuse-spectrométrie de masse (GC-MS) et chromatographie en phase gazeuse par détection par ionisation de flamme (GC-FID) pour identifier et quantifier les différentes molécules présentes

Les trois phases de pyrolyse, déshydratation, dévolatilisation primaire et dégradation passive lignine/résidus, ont été identifiées lors de l'irradiation micro-ondes. La production de bio-huile s'est clairement avérée dépendre de deux paramètres principaux qui sont l'énergie absorbée et le taux de chauffage interne du système. Des vitesses de chauffe élevées d'au moins 120 °C/min et jusqu'à 200 °C/min ont fourni les meilleurs rendements en bio-huile et de telles vitesses ne peuvent être atteintes que par la technologie micro-ondes par chauffage interne.

La qualité du bio-huile et du gaz en termes de familles chimiques ont également été discutée en utilisant une analyse en composantes principales (ACP) afin de visualiser la tendance globale des données et de détecter les principaux facteurs qui favorisent la formation ou la dégradation de familles chimiques spécifiques dans les échantillons de bio-huile ou de gaz non condensables.

En outre, un schéma de mise à l'échelle d'un procédé de pyrolyse micro-ondes est proposé. Divers facteurs tels que la conception de la cavité, les propriétés diélectriques du matériau traité, la compatibilité électromagnétique du système et la circulation de la biomasse sont discutées en triant les conditions souhaitables pour les réacteurs micro-ondes fonctionnant en continu.

Mots clés : Intensification, micro-ondes, pyrolyse de biomasse, anas de lin, sargasses

Points forts :

• Les micro-ondes sont le moyen d'accélérer la pyrolyse.

• La pyrolyse par micro-ondes conduit à une production élevée de bio-huile.

• Un apport énergétique optimal existe pour une production maximale d'huile bio

General Introduction

GENERAL INTRODUCTION

There is no silver bullet to solve the global environmental, energy, and economic problems. Today, the increase in world population and energy demand plunges into insecurity the world economy and well-being due to consequences of a lifestyle based on non-sustainable processes.

The uncertainty of the availability of fossil fuels, the environmental contamination, and the actual energy market dynamic has boosted the research community to investigate new eco-friendly fuels productions over the last decade. This "eco-revolution" has submerged the energy sector in a profound and essential transformation where the expectation is the imminent shift from fossil fuels to biofuels.

Several routes can obtain biofuels, commonly divided into thermochemical or biochemical conversion. Also, depending on the type of feedstock (biomass) used to produce them, the type of biofuel can be classified into three types of generation: First generation biofuel if it comes from food crops, second-generation biofuels for the non-food crops and residues, and third-generation biofuels which are derived from algae biomass.

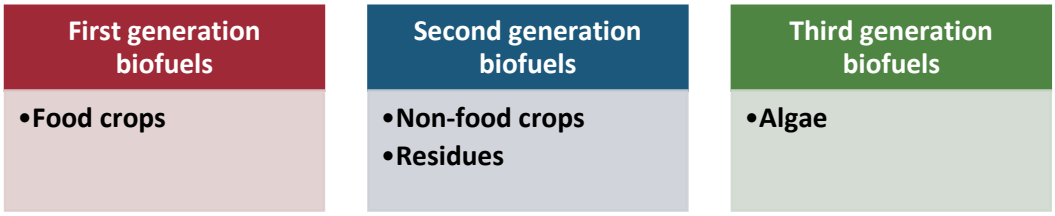

Figure 1.1-1. Biofuels generations description

The first insight into biofuels production was mainly based on crops as raw material. It is a controversial approach because it competes with food agriculture in terms of land use and by the environmental and climate change effect. The concerns of society turned the vision of first-generation biofuels to the use of non-edible raw materials (second generation) or algae (third generation) to produce sustainable biofuels.

Despite biomass being the oldest source of energy and currently accounts for 10% of total primary energy consumption in the form of fuel wood [1], the use of second and third-generation biomass in liquid biofuel production has shown rapid growth during the last decade. The use of liquid biofuels was expected due to the cost of transportation and storage. Still, the transition from the first generation to the third generation of biofuels is an ongoing debate. The first-generation biofuels are well established in terms of technology and economics, and second-generation biofuels are just in diapers in terms of the energy market.

The first step to gain the actual debate is to optimize the existing biomass sources and upgrade them to a biofuel that will be non-competitive to food production and waste recycling, helping solve both the economy and environmental issues. That said, lignocellulosic and algae biomass has no competition with food production and is considered waste. Both have the potential to be used as a raw material for liquid biofuel production.

The second step is finding a possible valorization of biomass into energy. There are two main routes to obtain bio-based fuels, the thermochemical and the biochemical ones. The biochemical one is commonly represented by anaerobic digestions and fermentation, and the thermochemical one by combustion, pyrolysis, and gasification [2].

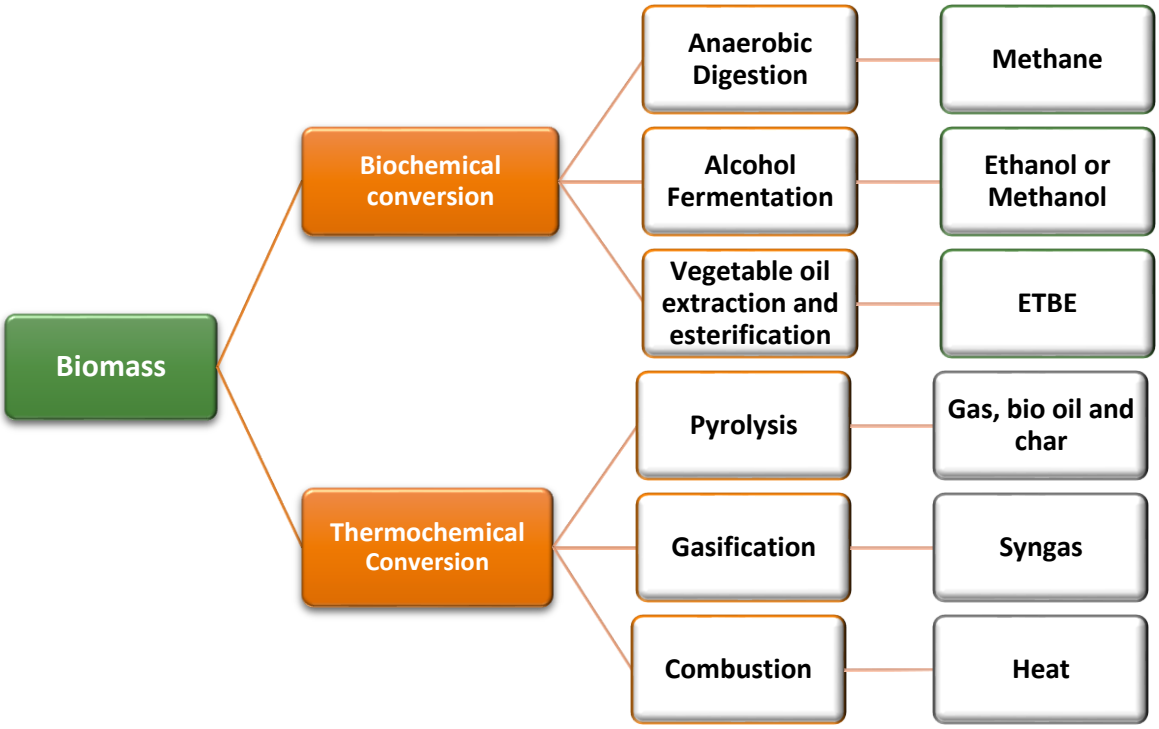

Figure 1.1-2. Biomass into fuels conversions processes

The biochemical conversion is mainly used to produce fuel like ethanol and methane by the hydrolysis of lignocellulose polysaccharides into simple sugars by fermentation organisms. However, one of the challenges that face this technology is the natural resistance of the plant cell walls to microbial or enzymatic biodegradation. This mechanism is also called “biomass recalcitrance”. This “resistance” is one of the main obstacles when discussing industrial transformation processes due to the degradation assistance steps that must be added to the process to have cost-effective fuel production.

In the other hand, thermochemical conversion processes to produce pyrolytic oil or bio-oil, syngas, and char, have an asset to the energy industry thanks to the adaptability of the present physical structure to these products, which can be easily transported, and with its moderate heating value can be burnt

directly in the conventional power stations. Also, the production time is shorter than the biochemical routes.

The most common thermochemical conversion processes are gasification, pyrolysis, torrefaction, and combustion. These processes are known as dry thermochemical processes and are defined by operational conditions such as temperature and presence of oxygen, for example, torrefaction 225-300 °C, without oxygen; pyrolysis 350-600 °C without oxygen; gasification 700-1400 °C, with or without oxygen; and combustion >1400 °C with oxygen.

Among these thermochemical pathways, pyrolysis, the thermal decomposition of organic in an inert atmosphere (absence of oxygen) to produce char, gas, and bio-oil, has a promising future and has received the attention of the research community due to the flexibility of use of bio-oil for power generation or chemical production. This technology has been extensively studied mainly focusing on increasing the bio-oil yield, where the conclusion is “high heat transfer rates, high bio-oil yields” [3]. However, providing the conditions to achieve this goal depends on giving the right residence time of solid and vapors and the challenge of providing the right energy to produce a high heating rate without degrading the product quality.

Microwave technology can provide a solution for energy and heat transfer rates. Microwave heating has been used for industrial processing applications over the competition from more conventional heating methods due to unique advantages, such as volumetric and selective heating, faster reactions time, space and energy savings, and security and quality improvement [4]. These characteristics make microwaves a promising technique to be implemented into the pyrolysis process.

Microwaves are part of the electromagnetic spectrum between the radio and infrared waves. Commonly used in the telecommunication industry, they were discovered during the Second World War and nowadays have taken an important place in the food and chemical industry as a heating method.

One of the drawbacks of using this technology for biofuels production is the difficulties of scaling up the processes due to the lack of knowledge of the microwave-biomass interaction and its influence on the reaction behavior. In this context, a proper knowledge of the wave propagation mode, wave penetration depth, the temperature-power density behavior, the electric field, and power density distribution are some of the different concepts to be evaluated before setting up a microwave process to have appropriate results.

In the case of the pyrolysis of biomass, evaluating the electromagnetic compatibility of all the system components is crucial to have a functional and highly performing process. The ability to deliver and absorb enough power to induce a high heating rate during pyrolysis is one of the first questions. Likewise, product separation and gas handling are other important points to discuss, as well as the reactor's temperature profile to avoid undesirable reactions.

The microwave pyrolysis of biomass has not been deeply studied in terms of the wave-matter interaction and its consequence on the pyrolysis reaction. The microwave pyrolysis applied to Flax shives and Sargassum has no background in the literature review, to the best of our knowledge. Understanding the

interaction between these biomasses and the microwave electromagnetic field and optimizing the operational parameters are the two main bases that would drive the industrialization of MW heating soon [2]. The latter implies that there is an interesting road ready to be discovered. Starting with the characterization of biomass unexplored in the field, the search for the right pyrolysis conditions to obtain the maximal product yield, performing the pyrolysis reaction under microwave irradiation, and finishing with the process development to scale-up towards a continuous flow operation. This thesis aims to achieve a concise scientific map, elaborated with theoretical and experimental evidence, to help along this path and set a precedent in the scientific community.

CONTEXT OF THE STUDY

The context of this research is based on the Caliope program, a collaboration of the Dominican Ministry of Higher Education for Science and Technology (MESCyT) and the French Embassy in the Dominican Republic to give birth an interuniversity association to bring into table scientifically tested solutions for waste valorization problem in both participating countries. According to this academic cooperation, the biomass of interest was selected according to the needs of both interested parties.

In the case of France, 200,000 tons of Flax shives are generated annually by the flax industry, being 80% of the world's production of scutched flax fibers originated in Europe, being France, the world leader [5]. The potential of this biomass to be integrated as a power source has not been completely explored. Some of the investigations done about the exploitation of Flax shives as raw material for the biofuel production by pyrolysis and combustion using the conventional heating method[6]–[8]; to the best of our knowledge, this is the first time that the Flax shives pyrolysis has been evaluated under microwave heating conditions.

In the other hand, the Caribbean region has suffered an inundation of pelagic seaweed Sargassum by the last years [9], [10]. Even if the presence of seaweeds lying on the beach are part of the ecosystem on many coastal regions, the dramatic increase in mass has become a trouble. For the Dominican Republic, a country that has a strong economy based on tourism, the tons of Sargassum smothering the coast deter tourists (see figure 2.1), also if not removed on time, the algae can turn into a malodourous morass which can produce toxic hydrogen sulfide from its anoxic interior, impacting negatively the environmental and economic productivity.

Figure 1.1-3. Algae inundation Punta Cana, Dominican Republic

AIM AND OBJECTIVES

The aim of this thesis is to investigate step by step the way to valorize two selected biomass, Flax shives and Sargassum, by microwave pyrolysis, following a rigorous methodology to develop a feasible continuous process. This objective can be divided into the next steps:

- Identify and characterize the type of biomass according to the context of the study.
- Study the dielectric properties of the biomass to be used and the product obtained during pyrolysis (gas and bio-oil).
- Study the volatilization kinetics of the selected biomass.
- Set up a semi-batch pyrolysis process under microwave heating to study the wave-biomass interaction, reaction performance, and behavior.
- Study the thermal gradient and microwave power behavior during the pyrolysis process
- Study the quality of gas and bio-oil obtained during the microwave pyrolysis batch process.
- Project the data to select a reactor and develop a microwave continuous flow pyrolysis process
- Evaluation of the compatibility of microwave irradiation and the continuous flow reactor selected according to the information gathered from the previous studies.

The latter is presented in five chapters. Chapter one is the state of the art of the technology that we aim to develop, focusing on the microwave technologies and microwave pyrolysis of biomass. Chapter two describes the methods and materials used to accomplish the research objectives. Chapter three gathers the preliminary studies, describing the biomass and pyrolysis product characterization in terms of dielectric properties and chemical compounds, as well as the behavior of the biomass in the absence of oxygen at different heating rates and the generalities of the volatilization kinetics. The semi-batch pyrolysis process under microwave heating is presented in chapter four. The evaluation of microwave pyrolysis conditions, product distribution, and product quality, as well as the relationship between process variables, are presented. In Chapter five, the development of a microwave pyrolysis continuous flow reactor is presented

CHAPTER 1
State of the art

1. STATE OF THE ART

1.1. MICROWAVES GENERALITIES

Born and developed during World War II, microwave technology has been spread from its use in telecommunications to other industrial applications like organic chemistry, food industry, bioenergy, etc. Nowadays, microwave heating is well established as a process intensification assistance technique.

Microwaves are electromagnetic radiations characterized by the presence of two oscillating modules, the electric and magnetic fields. These fields are perpendicular to each other and transversal to the propagation direction. As a part of the electromagnetic spectrum, its frequency range, between 300MHz and 300 GHz, is placed between the radio and infrared waves. For industrial applications, the frequency values most used are 2.45 GHz and near 900 MHz [11].

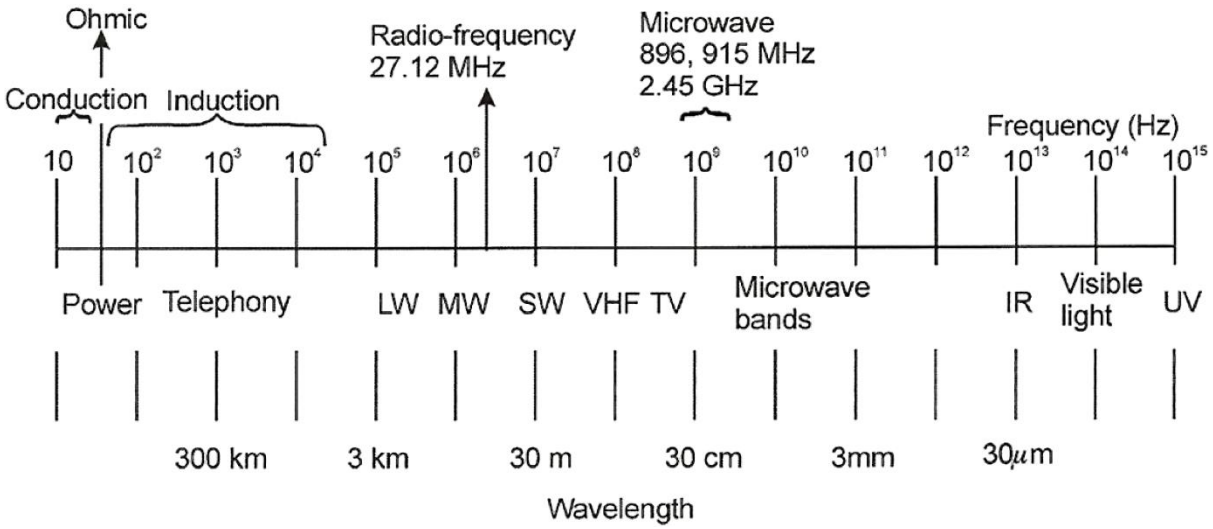

Figure 1.1-1 Industrial frequency bands[12]

Depending on the frequency or wavelength, the use of microwaves can be categorized into different applications, especially to avoid interference with the telecommunications signals. As said before, the most used microwave frequency for domestic, medical, and industrial use is 2.45 GHz. However, the regulations of use can change according to the region; for example, in the United Kingdom is 896 MHz. According to the Code of Federal Regulations from the united states [13], the frequency the microwaves can be classified into three categories:

- UHF - Ultra high frequencies from 300 MHz to 3 GHz
- SHF -Supra high frequencies from 3 GHz to 30 GHz

- EHF- Extra high frequencies from 30 GHz to 300 GHz

Also, for microwaves located between 1 and 100 GHz there is a special classification in sub ranges published in the IEEE Standard 521-2002 letter for frequency bands[14] .

Table 1.1-1 Sub-ranges of microwaves classification [11]

Sub range	Frequency (GHz)	λ_0
L	1 to 2	30 to 15 cm
S	2 to 4	15 to 7.5 cm
C	4 to 8	7.5 to 3.75 cm
X	8 to 12	3.75 to 2.5 cm
Ku	12 to 18	2.5 to 1.67 cm
K	18 to 27	1.67 to 1.11 cm
KA	27 to 40	1.11 to 0.75 cm
U	40 to 60	0.75 to 0.5 cm
V	60 to 80	0.5 to 0.375 cm
W	80 to 100	0.375 to 0.3 cm

To understand the table 1.1 and the relevance of the wavelength, in the inferior frequency limit of the microwave range inside the electromagnetic spectrum, 300 MHz, the wavelength in the air or vacuum is 1 meter, and in the superior limit of 300 GHz, the wavelength in the air or vacuum is 1 mm. The higher the frequency, the smaller the wavelength.

Each sub-range of the classification is aligned to a field of application. For example, de sub-range L appertain to radio astronomy services, army radars, and scientific research, and the range X for telecommunications and radio purposes [14]. In the case of the food and chemical industry, the microwave frequency range is the S, and more specifically, at a value of 2.45 GHz, as mentioned before.

1.1.1 Microwaves general equipment for chemical industry application

From the first microwave heating applications to the large-scale domestic microwave ovens and, more recently, to the development of industrial applications, the equipment used for microwave heating has largely evolved. However, there is a basic structure of the microwave heating system composed of three principal elements: the microwave power source, the microwave applicator, and the workload. These components have specifics objectives in the microwave heating path; the microwave energy is produced in the microwave power source, propagated by the microwave applicator, and applied to the workload to be heated. A description of the component is presented below.

1.1.1.1 *Microwave power source*

The core of the microwave heating system is the microwave generator. There are three types of microwave generators used for heating purposes solid-state generators, magnetrons, and klystrons. The solid-state generator is the newest technology, and it consists of a microwave small-signal generator, a high-power amplifier, and a power supply system [15]. The magnetron is a high vacuum electronic valve that generates the microwave power from a high-voltage source of DC power, and the klystron is an electron tube that amplifies the microwave signals using an electron beam [11]. The magnetron is the most used microwave generator for industrial applications due to its efficiency-cost advantages.

The magnetron, as mentioned before, is a high vacuum electronic valve composed of a cylindrical diode with an anode and cathode. The anode is incorporated into a resonant cavity structure that at the center has an electron-emitting cathode. The anode has a set of vanes projecting radially and forming slots that are mutually coupled via the fringing fields and forming a resonant circuit.

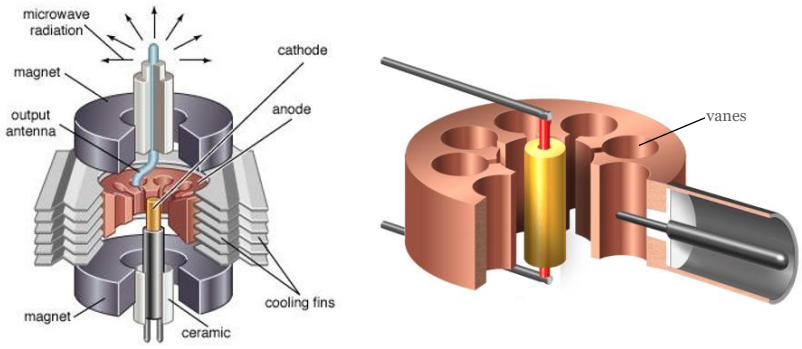

Figure 1.1-2 Microwave power generation

In operation mode, the power of several thousand volts passes through the cathode releasing electrons and charging the vanes of the anode; this creates a radial electric field. At the same time, a magnet placed on the limbs of the anode helps to create a stable magnetic field. The combination of both fields guides the trajectory of the electrons in a cycloidal form to the anode resonant cavity turning the electron's vibrations into electromagnetic oscillations radiated by an antenna enclosed in one of the envelopes of the vanes. In a fixed-tuned magnetron, the oscillations are designed to release the microwave energy at a certain frequency.

The power output of the magnetron is controlled by the time the magnetron is switched on divided by a time base, meaning internment on and off-cycle. The microwave energy output from the magnetron is measured in watts. This energy is going to travel inside the microwave applicator until being in contact with the sample/ load to be heated.

The power output of the magnetron can be affected by overheating resulting from the reflected microwave. The reflected power occurs when the traveling electromagnetic energy (microwaves) is not absorbed by the sample/load, and the flow of energy is partly in the reverse direction: towards the magnetron. This is the reason why there is mandatory to have a security protection system. Typically, the microwave generator has the following security interlocks: Water cooling, air cooling, anode temperature sensor, reflected power sensor, etc.

1.1.1.2 *Microwave applicator system*

The microwave applicator system aims to ensure wave-matter interaction in a safe environment. It is made from conductive materials like metals and conceived to handle microwave irradiation without leaks or secondary effects.

The microwave applicator system can be divided into three types, the traveling waves, the near-field, and the resonant cavities. The traveling wave applicators are hollow metal conductors connected to a microwave generator on one side and a terminating load on the other side. Near-field applicators are defined as the small distance according to the wavelength between the workload and the applicator. The resonant cavities, which are the most common ones are applicators, can be divided into the single-mode applicator and multi-mode applicators.

The resonant cavity applicator system starts with a hollow conductor that will allow the propagation of the electromagnetic energy produced by the magnetron until the workload is heated. The electromagnetic wave can have different propagations modes while traveling in a confined space. One or several propagation modes can coexist in the same space depending on the geometry of the conductive space and the frequency of the wave. When the applicator allows just one mode of propagation, it is called a single-mode applicator. If it allows several modes simultaneously, it is called a multi-mode applicator.

The multi-mode applicator system is the most used one. It is present in daily life as the microwave oven, but it is the most difficult to provide proper data in terms of precision. In principle, it is a closed metal box where microwaves entering the cavity are repeatedly reflected from wall to wall, allowing different directions and wave propagations mode.

On the other hand, the single-mode applicators consist of a metallic hollow structure into which the microwave energy generated by the magnetron will be reflected in the preferred direction giving rise to a standing wave pattern that, for some simple structures, will be very well defined in space.

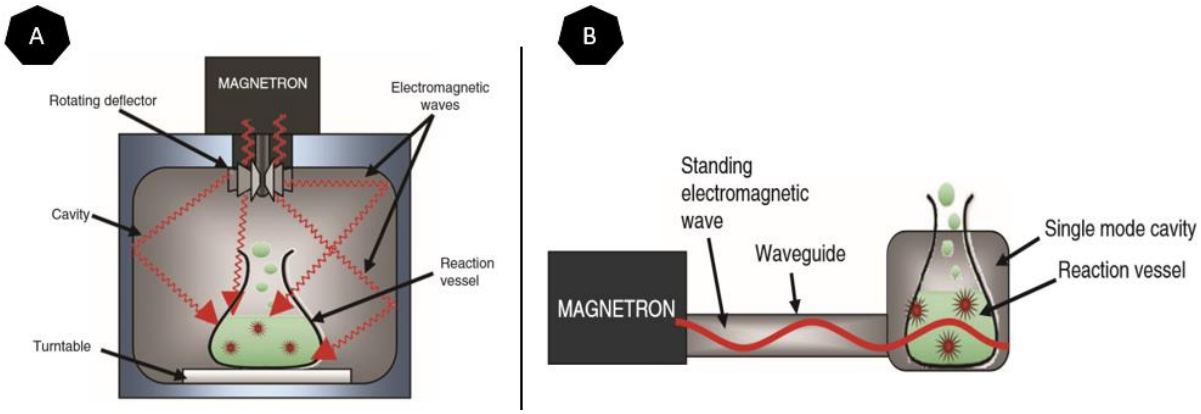

Figure 1.1-3. Types of microwave applicators [16]

Another essential element in the microwave applicator is the waveguides. The waveguide couples the microwave generator to the applicator while the applicator is designed to create a favorable EM field distribution around the workload to be heated. Waveguides are hollow metal pieces that can be rectangular or cylindrical used to transmit the microwave energy from the magnetron to the heating cavity.

In microwave engineering, the design of a waveguide with the low-loss transmission of microwave power is a must-do. Waveguides have the advantages of high-power handling capability, avoiding the mismatch of the irradiation and the workload. For the purposes of industrial scaling of microwave processes, a well-adapted waveguide to a single-mode cavity leads to higher electromagnetic field densities and thus higher heating rates. The following section will discuss the theoretical aspects of the traveling wave and the relevance of microwave assistance to the process intensification.

1.1.2 Understanding the wave propagation phenomena

1.1.2.1 *Electromagnetic phenomena: Maxwell equations*

To design microwave heating systems in which the microwave energy can be transferred to the workload without losses and predict the degradation of the energy into heat by the absorption of the wave during the wave-matter interaction, it is mandatory to know the electromagnetic behavior and the propagation modes of the wave.

First, both frequency and wavelength in the free- space, used to classify the range of application of every part of the microwave spectrum, are related, and their relationship is expressed by the following equation:

Equation 1 :

$$\lambda_0 = \frac{c}{f}$$

$\boldsymbol{c = 3 \times 10^8\ m/s} = Speed\ of\ electromagnetic\ wave\ in\ the\ air\ or\ vacuum$

$\boldsymbol{f} = frequency\ of\ the\ microwave\ \ in\ s^{-1}$

However, the electromagnetic energy propagates through free space at 3×10^8 m · s^{-1} independently of the frequency. It is composed of two inseparable components, the electric field (E) and the magnetic field (H), which have magnitude and direction in space and oscillate sinusoidally with time. To describe the behavior of the electromagnetic field in space at a macroscopic level, James Clerk Maxwell unified the work of Coulomb, Gauss, Ampere and Faraday, summarizing the electromagnetic science in fourth equations that are the heart of the wave phenomenon ([17]).

The general form of Maxwell's equations is represented considering the influence of the electric ($\vec{E}$) and magnetic ($\vec{H}$) field associated to the properties of the medium (ε , μ and σ) and their result as either magnetic ($\vec{B}$) and electric ($\vec{D}$) induction. These relations can be expressed by the equations presented below, which are linear but not independent of each other.

Equations 2 : Maxwell's equations :

Maxwell-Faraday	$\vec{\nabla} \times \vec{E} = -\frac{\partial \vec{B}}{\partial t}$	Maxwell-Gauss	$\nabla \vec{B} = 0$
Maxwell-Ampere	$\vec{\nabla} \times \vec{B} = \mu \vec{J} + \varepsilon\mu \frac{\partial \vec{E}}{\partial t}$	Maxwell- Flux	$\nabla \vec{E} = \frac{\rho}{\varepsilon}$

These equations can be solved by using the equations that link up the magnetic and electric field with the medium dielectric properties: electric permittivity (ε), magnetic permeability (μ) , and electrical conductivity (σ).

Equations 3: Connection equations to solve Maxwell's equations:

Electric induction	$\vec{D} = \varepsilon \vec{E}$	Electric current density	$\vec{J} = \sigma \vec{E}$
Magnetic Induction	$\vec{B} = \mu \vec{H}$		

The foregoing equation, for the medium dielectric properties are essentially applicable in free space and air:

- Electric permittivity in free space $\varepsilon_0 = \frac{1}{36\pi.10^9} \quad (\frac{F}{m})$
- Electric conductivity in free space $\sigma_0 = 0 \quad \left(\frac{S}{m}\right)$
- Magnetic permeability in free space $\mu_0 = \frac{1}{4\pi.10^{-7}} \quad (\frac{H}{m})$

When the electromagnetic wave travels in a free and homogenous medium, the dielectric properties are expressed by complex numbers that define the wave-matter interaction.

Equation 4: Complex number of electric permittivity:

$$\varepsilon = \varepsilon' - j\varepsilon''$$

Equation 5: Complex number of magnetic permeability:

$$\mu = \mu' - j\mu''$$

These complex numbers are composed of a real and an imaginary term, in which each term represents the specific behavior of the material undergoing microwave radiation. The real part (ε', μ') represents the phase lag of the electromagnetic wave in the material. Otherwise, the imaginary part (ε'', μ'') represents the loss or absorption of electromagnetic energy within the material. In other words, the higher the value of the real part, the higher the tendency to reflect the electromagnetic waves. Likewise, the higher the value of the imaginary part, the higher the ability of the material to convert the electromagnetic energy into heat. The dielectric properties can be normalized, taking as a reference their values in the void, as presented in equation 6.

Equation 6: Normalization of complex dielectric properties:

$$\varepsilon_r = \frac{\varepsilon}{\varepsilon_0} = \varepsilon_r{}' - j\varepsilon_r{}''$$

1.1.2.2 *First study case: Propagation in free space*

The wave propagation aspects and the relevancy to the investigation context are first explained by the solution of the Maxwell equations for a basic wave in the free space. The simplest way electromagnetic energy propagates consists of a sinusoidally varying electric field, vertically polarized, and horizontally polarized in phase with the magnetic field. This propagation form is also called a plane wave, in which the propagation direction is normal to the plane.

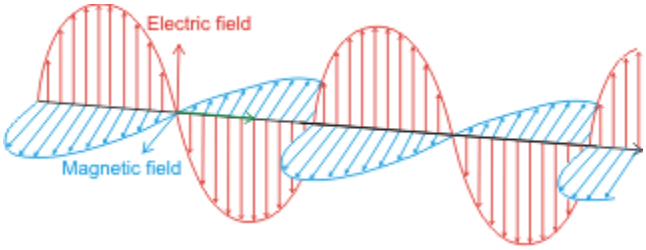

Figure 1.1-4. Basic plane wave example

The propagation behavior is deduced by resolving the previously presented, Maxwell equations. These are in general time-varying equations. For microwaves at 2.45 GHz, most of the work comprises fields with sinusoidal or harmonic time dependence. In this case the preceding equations can be written to include an implied time dependence in a sinusoidal function form (Phasor form).

Equation 7 General phasor form of wave fields quantities:

$$\vec{A}\,(x,y,z,t) = Re\left[\vec{A}'(x,y,z)\right] \cdot e^{j\omega t}$$

Where: (A) represent the fields ($\vec{E}$, $\vec{B}$, $\vec{D}$ and $\vec{H}$), ω represents the radian frequency and J the electric current density.

Assuming a sinusoidal time dependence ($e^{-j\omega t}$) , the time derivatives of Maxwell's equations in a source-free, linear, isotropic, and homogeneous region for the electric field and magnetic fields can be replaced by $(j\omega)$, resulting in:

Equation 8: Phasor form electric field:

$$\vec{\nabla} \times \vec{E} = -j\omega\mu\vec{H}$$

Equation 9: Phasor form magnetic field:

$$\vec{\nabla} \times \vec{H} = -j\omega\varepsilon\vec{E}$$

This equations system can be solved for either the electric or magnetic field, resulting in Helmholtz equations.

Equation 10: Helmholtz equation for electric field:

$$\overrightarrow{\nabla^2}\,\vec{E} - \varepsilon\mu\omega^2\vec{E} = 0$$

Equation 11: Helmholtz equation for magnetic field:

$$\overrightarrow{\nabla^2}\,\vec{H} - \varepsilon\mu\omega^2\vec{H} = 0$$

A constant called wavenumber, is the spatial equivalent of frequency and is obtained from solving the Helmholtz equations. For a plane wave in the free space, it is defined using the symbol (k), however, when talking about transmissions lines or waveguides, this "constant" is defined as the phase constant and is written as:

Equation 12: phase constant or wavenumber:

$$\beta = \omega\sqrt{\mu\varepsilon} = \frac{2\pi}{\lambda}$$

For a basic plane wave in free space, a solution can be found by solving the Helmholtz equations considering an electric field as a vector with only one component ($\hat{x}$) and uniform according to the (x) and (y) direction. This hypothesis allows reducing the Helmholtz equation for the electric field to:

Equation 13: Helmholtz equation for electric field for a plane wave in the free space:

$$\frac{\partial E_x}{\partial z^2} + \beta^2 E_x = 0$$

Others wave propagation' factors are the velocity of the wave and the wavelength. The speed of the wave defis ined as the velocity at which a fixed phase point travels, it is given by:

Equation 14: Velocity of the wave

$$v_p = \frac{\omega}{\beta}$$

The wavelength (the distance between two maxima or minima) is deduced from the wavenumber and expressed as a function of the velocity of the wave:

Equation 15 : Wavelength

$$\lambda = \frac{2\pi}{\beta}$$

In the case of lossy medium, the Maxwell's equations must be re written and the wavenumber must be adapted to the new medium where dielectric properties are complex numbers. The wavenumber as shown in equation 12 is replaced as shown in equation 16. More details on the subject will be detailed in the next section.

Equation 16: Wavenumber for lossy medium:

$$\beta = \omega\sqrt{\mu\varepsilon}\sqrt{1 - j\frac{\sigma}{\omega\varepsilon}}$$

1.1.2.3 *Second case of study: guided wave propagation*

Unlike the propagation of a plane wave in the free space, where the wave moves into the propagation direction, there is another type of situation where the wave is forced to move into a specific direction in order to harness its energy. The latter is the case of industrial microwave applications for heating purposes, and it is called guided propagation.

To guide the wave into the desired direction, a hollow, metallic or dielectric, structures are used. For example, transmission lines, which include many structures (two-wire, coaxial, optical fiber, etc…) and waveguides. Besides guiding the wave, another advantage of these structures is the low-loss transmission of microwave power.

Of the different structures mentioned before, one that attracts the attention of this work is the waveguide. Waveguides are a particularly important element in microwave heating systems because they are responsible for transferring the microwave power from the generator to the applicator with a minimal energy loss. Usually, the waveguides have a rectangular or cylindrical geometry, and the dimensions are set by boundaries conditions, which are calculated according to the wave's different properties.

Inside the waveguide, the electromagnetic wave propagation occurs by the multiple wave reflections generated by the conductive walls of the structure with a certain magnetic and electric field distribution. Whether the propagation frequency increases or the wavelength is reduced, the distribution pattern of the electric and magnetic field inside the structure is going to change, and when the wavelength value

becomes comparable to the cross-sectional geometry of the conductive structure, more distribution patterns appear.

The distribution pattern of the electromagnetic fields depends on the propagation mode inside the waveguide. The propagation modes are figured by solving the Helmholtz equation (Equations 10 and 11) in conjunction with a set of boundary conditions depending on the geometrical shape and materials of the waveguide. At any point in the space, one of the components or both, of the electromagnetic wave (electric and magnetic field) are transverse to the propagation direction and cannot align in the direction of propagation. The propagation patterns can be divided into two general categories: $TE_{m,n}$: Transversal electric mode, characterized by $E_Z = 0$ and $H_Z \neq 0$, and $TM_{m,n}$: Transversal magnetic mode, characterized by $H_Z = 0$ and $Z_Z \neq 0$.

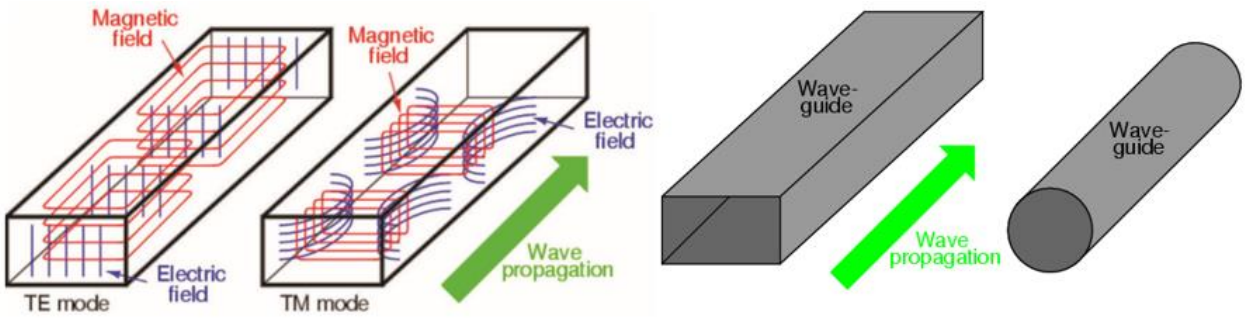

Figure 1.1-5 Wave propagation patterns [18]

In each case, the field (magnetic or electric) is perpendicular to the wave propagation's direction. The suffixes m & n represent the half of wavelength along the coordinate directions of the field which is perpendicular to the propagation direction.

In general, to describe the guided wave propagation, the Maxwell's equations in a phasor form described in the previous section (Eq 8 and Eq 9) are solved with respect to a system of orthogonal curvilinear coordinates designated by q_1, q_2, q_3. The most common used system to apply these equations are the rectangular and cylindrical coordinates which refer to the cylindrical and rectangular waveguides or transmission lines structures. For the rectangular coordinates system: $q_1 = x\,, q_2 = y,\ q_3 = z$. In order hand, for the cylindrical coordinates case: $q_1 = \rho\,, q_2 = \varphi,\ q_3 = z\,.$ The solution for a wave that propagates along a guide in the axe q_3 is:

Equation 17 :

$$\vec{e}\,(q_1, q_2, q_3, t) = \vec{E}\,(q_1, q_2) e^{-\gamma q_3} e^{j\omega t}$$

Equation 18 :

$$\vec{h}\,(q_1, q_2, q_3, t) = \vec{H}\,(q_1, q_2) e^{-\gamma q_3} e^{j\omega t}$$

$\vec{e}$ and $\vec{h}$ are the fields instant complex values and, $\vec{E}$ and $\vec{H}$ are the complex amplitude on the transversal plane γ is the complex propagation constant a characteristic parameter of the guided propagation. Its definition depends on the propagation context, for example:

Equation 19:

- Propagation without loss: $\gamma = j\beta$

Equation 20 :

- Propagation with loss: $\gamma = \sigma + j\beta$

1.1.2.3.1 Wave propagation in rectangular waveguide

Rectangular waveguides are one of the first studied transmission lines, used to transport microwave signals. The rectangular waveguide allows the propagation on TE and TM modes. In order to analyze the $TE_{m,n}$ propagation mode, it is assumed that the guide is filed with a material with permittivity (ε) and permeability (μ) with dimensions according to the standard convention: the longest side of the waveguide along the x-axis.

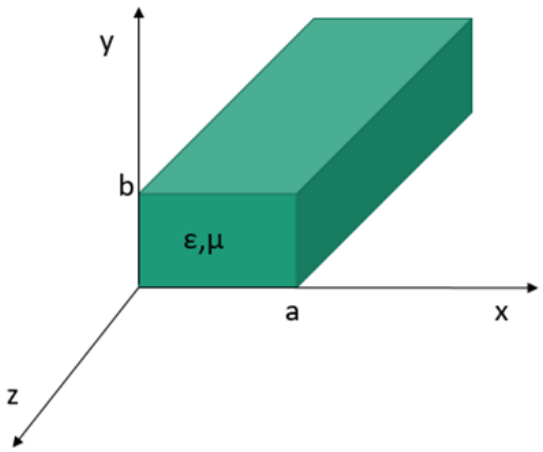

Figure 1.1-6 Rectangular waveguide

The propagation of TE modes is characterized by a transversal electric field in the propagation direction, while the magnetic field must satisfy a reduced two-dimensional wave equation from the Helmholtz equation for hz:

Equation 21: Two-dimensional equation for TE propagation mode:

$$\left(\frac{\partial^2}{\partial x^2}+\frac{\partial^2}{\partial y^2}+\beta_c^2\right)h_z(x,y)=0$$

With boundary conditions on the wall of the guide: $\frac{\partial^2 H_Z}{\partial n}=0.$ By solving this equation, a generator function is obtained:

Equation 22: Generator function:

$$H_z(x,y)=H_0\cos\frac{m\pi x}{a}\cos\frac{n\pi y}{b}$$

The cutoff wavenumber β_c comes from the following relation:

Equation 23: Cut off wavenumber βc:

$$\beta_g^2=\sqrt{\beta^2-\beta_c^2}$$

Where β_g is the wavenumber for a guided wave and β is the wavenumber in the free-space. The cutoff wave number determines the possibility of propagation inside the waveguide. Where the propagation will be possible if $\beta > \beta_c$. where β_c for a rectangular waveguide is defined by:

Equation 24: Cutoff wavenumber for rectangular waveguide:

$$\beta_c^2=(\frac{m\pi}{a})^2+(\frac{n\pi}{b})^2$$

1.1.2.3.2 Wave propagation in cylindrical waveguide

Cylindrical waveguides were just used as attenuators, phase shifters or turning joint for a long time. At the decade of 70's where with the rise of telecommunication industry, this geometrical structure takes the attention of engineers.

To adapt the Maxwell's equations for the electric and magnetic field in phasor form (Equations 8 and 9) to the cylindrical geometry, the solution is presented in cylindrical coordinates (ρ, φ, z). In this case, the time dependence of the variation of the fields is expressed by $e^{-jn\varphi}$, which is an angular function $F(\varphi)$. The solution of Maxwell's equations for cylindrical waveguides in the case of << $E_z = 0$ >>, use higher mathematics including Bessel's function and is presented below:

Equation 25: Maxwell's equation solution for cylindrical waveguide:

$$H_z = H_0 J_n(\beta_c \rho) e^{-jn\varphi}$$

Where J_n is a Bessel's function and with some boundary conditions.

Guide wall boundary condition: $\frac{\partial H_z}{\partial n} = \frac{\partial H_z}{\partial \rho} = 0$ when $\rho = a$

From the generator function, it is possible to obtain the expressions forms for both TE and TM:

Equations 26: Generator function expressions forms for both TE and TM:

$$E_\rho = -H_0 \frac{\omega \mu n}{\beta_c^2 \rho} J_n(\beta_c \rho) e^{-jn\varphi}$$

$$E_\varphi = jH_0 \frac{\omega \mu}{\beta_c} J'_n(\beta_c \rho) e^{-jn\varphi}$$

$$H_\rho = -H_0 \frac{\gamma}{\beta_c} J'_n(\beta_c \rho) e^{-jn\varphi}$$

$$H_\varphi = jH_0 \frac{\gamma n}{\beta_c^2 \rho} J_n(\beta_c \rho) e^{-jn\varphi}$$

The Bessel function Jn (u) is canceled for a series of values of "u" which are the roots of Jn and defined as u'_{mn}. Each of these roots corresponds to a mode of propagation. The mode corresponding to the root

"m" of a function of order "n" is called mode TEmn . The roots u'_{mn}, are used to calculate the cutoff conditions in the cylindrical waveguides and the discreet values of them are presented below.

Equation 27: Cutoff wavenumber for cylindrical waveguide and discreet values:

$$\beta_c = \frac{u'_{nm}}{a}$$

u'_{nm}	Discreet value
$\mathbf{u'_{0,1}}$	*3.832*
$\mathbf{u'_{1,1}}$	*1.841*
$\mathbf{u'_{2,1}}$	*3.054*
$\mathbf{u'_{3,1}}$	*4.201*
$\mathbf{u'_{0.2}}$	*7.016*
$\mathbf{u'_{1,2}}$	*5.332*
$\mathbf{u'_{2,2}}$	*6.706*
$\mathbf{u'_{3,2}}$	*8.013*

1.1.2.4 *Relevancy of understanding guided wave phenomena for microwave heating applications*

Microwave heating technology has been used for industrial processing applications over its competition, the conventional heating method, due to special advantages, such as faster reactions time, space and energy savings, and security and quality improvement. One of the drawbacks of this technology is the difficulties in scaling up the processes. In this context, proper knowledge of the wave propagation mode,

wave penetration depth, and the electric field distribution are some of the different concepts to be evaluated to have appropriate results.

For example, in the case of the pyrolysis of biomass, the evaluation of the electromagnetic compatibility of all the elements of the systems, including the biomass, is crucial to have a functional and highly performing process. Choosing the wave propagation mode, designing the waveguides according to the cutoff conditions, and screening the electric field distribution inside the microwave applicator to know where the ideal wave-matter interaction point is, are just the first steps. Subsequently, we must work on how to deliver enough microwave power to induce pyrolysis in safe conditions, without power loss and microwave leaks. The latter example makes clear the need to understand the basic physics of microwave propagation to design a proper microwave heated process.

1.1.3 Microwave-matter interaction: From microwave energy to heat

In a general, microwaves can be absorbed, reflected, or pass through the materials without changes. This behavior is used to classify the materials as transparent or insulators, absorbents or dielectric, and reflective or conductors. The insulators allow the wave to pass through them without losing energy, and they are used to make supports, vessels, and reactors to be used inside microwave ovens. The reflective materials are used to make waveguides and microwave cavities, and the absorbers are the ones that microwaves can heat.

The medium properties characterize the interactions between the microwaves and the matter as the electric permittivity and the magnetic permeability (ε and μ). Usually, in the chemical process field, the materials lack magnetic properties; therefore, most of the interactions of the microwaves with matter are caused by the electric field. The electric component can induce the current of free charges (ionic conduction) and equally the local reorganization of linked charges (electric polarization). Four mechanisms can describe the electric polarization phenomena:

- **Orientation Polarization:** This mechanism is present when the molecules with a permanent dipole moment exhibit a reorientation of the dipole because of the electric field.
- **Electronic Polarization:** The electronic cloud's displacement around the atom concerning the core because of the influence of the electric field.
- **Ionic Polarization:** It is the elastic displacement of the ions from their equilibrium positions. This type of polarization happens in molecules with ionic bonding. The dipoles present in the molecule are annulled by the molecular structure's symmetry caused by the electric field's application.
- **Interfacial Polarization:** It is also called the Maxwell-Wagner Effect. It occurs in heterogeneous materials with different phases, each with different dielectric properties. When the electric field is applied, a separation of the positive and negative charged particles is produced within the material or at the interface between different materials.

Both electronic and ionic polarization can be classified as induced polarization because the materials do not have a permanent dipole. Still, it appears after the distribution of charges produced by the effect of the electric field. These interactions are at the intramolecular level due to the elastic movements and molecular vibrations where the resistance to this movement is not sensible to the temperature. On the other hand, orientation polarization is a rotational process that implies non-elastic movements and intramolecular interactions, strongly dependent on the temperature.

1.1.3.1 *Microwave heating*

Microwave heating results from the degradation of the electromagnetic energy into heat that can be produced by two mechanisms: Ionic conduction and dielectric relaxation. The electromagnetic energy degradation by ionic conduction occurs when dissolved ions oscillate due to the influence of the oscillating electric field. This oscillation creates a current that faces an internal resistance because of the collision between the charged and non-charged ions. As a result, the kinetic energy of the system will degenerate into heat. This phenomenon is also called "Joule's effect".

The second mechanism occurs when the molecules have a permanent dipole moment, and an oscillating electric field is applied. This induces the rotations of the polar molecules, which try to follow the rate of the oscillating field. When these molecules cannot follow the rate of the field, a delay between the electromagnetic stimulation and the molecular response is produced; this delay is also called dielectric relaxation. The reorganization of the molecules due to the electric field force faces resistances due to thermal agitation and the inertia of the surrounding molecules, causing an increment of the entropy and, therefore, the degradation of the kinetic energy of the molecules into heat by the mechanical frictions. The ability of the material to convert electromagnetic energy into heat at a specific frequency and temperature can be expressed by the ratio between the imaginary and real term of the dielectric permittivity, defined as the loss tangent.

Equation 28: Loss tangent:

$$\tan\delta = \frac{\varepsilon_r''}{\varepsilon_r'}$$

1.1.3.2 *Improving microwave heating by microwave absorbers*

Microwave heating relies on the ability of the material to absorb microwave energy, taking advantage of the different microwave-matter interaction phenomena to produce heat. However, the materials used are not always good microwave absorbents, and, in some cases, they can even be transparent. This

makes the use of microwaves not feasible unless the addition of either reagents or catalysts is polar enough to absorb the microwaves and raise the overall dielectric properties of the medium.

To address this issue, a microwave absorber has been used as a susceptor or substrate to facilitate the heating of the substance that cannot be heated efficiently under microwave irradiation. This approach is also known as hybrid heating.

The most common microwave absorbers used are silicon carbide, carbon materials, biochar, and metal oxides. Also, the carbonaceous residue from biomass pyrolysis can be used as a microwave absorber [19]–[24].

Microwave absorbers can have indirect or in situ effects during irradiation. For example, the ceramic crucible used to hold the treated substance has a high microwave absorption that can turn the microwave energy into heat uniformly, heating the samples via the different heat transfer phenomena. However, microwave efficiency has its maximum effect if the absorber is directly added to the treated materials.

In this context, silicon carbide is one of the strongest materials in the world, a ceramic material with a strong microwave absorptivity and is chemically inert. These qualities make it attractive as a microwave absorber element for chemical processes. With a melting point of 2700 Celsius, it can be used at extremely high temperatures. It also has an exceptionally low thermal expansion coefficient and an excellent resistance to corrosive environments. Nowadays, SiC is used to produce microwave absorbent vessels, support the catalyst for microwave-assisted pyrolysis of biomass, reactors, and is also used in situ to help poor microwave absorbent solutions/substances to heat [25].

1.2. BIOMASS: A RENEWABLE SOURCE OF ENERGY

Biomass is by far the oldest source of fuel energy and currently accounts for roughly 10% of total primary energy consumption in the form of fuelwood. Is it defined by the standard ANSI/ASABE S593 as "Organic materials that are plant or animal-based, including but not limited to dedicated energy crops, agricultural crops and trees, food, feed, and fiber crop residues, aquatic plants, forestry, and wood residues, agricultural wastes, bio-based segments of industrial and municipal wastes, processing by-products and other non-fossil organic materials".

Depending on the feedstock available for energy production, the types of biomass can be classified into three groups: dedicated crops, which can be edible or not, waste materials, and algal biomass. Despite the traditional use of biomass as fuel in the form of wood (first generation biofuel), the competition of various primary biomass sources in the land use with the food crops is one of the questions today. Even if the surface available for biomass production was not a problem, the environmental impact of the frequent use of the land in terms of the soil's productivity quality is another fact to consider. Lignocellulosic biomass has been presented as a promising solution [1], [26], [27]. Producing biofuels from lignocellulosic biomass has the potential to overcome some limitations of the first-generation biofuels. Since the materials used to produce lignocellulosic biofuels are mainly residues from the harvesting and food processing or can be grown on marginal lands that are not suitable for food crops, it solves the problem of the land competition. Like lignocellulosic biofuels, the use of algae as raw material for third-generation biofuels production is an interesting solution because algae grow faster and do not require potable water or arable land and are easy to feed (CO_2 and sunlight) [28]. Algae production does not compete for land use. It helps with climate change by lowering CO_2 emissions and has a better and faster feedstock growth rate compared to terrestrial crops [29], [30].

The contemporary society is looking forward to sustainable energy feed. In that context, biomass, which is the only renewable source of fixed carbon that can contribute to reducing greenhouse emissions and help with the alarming climate change issues, has become a remarkable solution. The advantage of using biomass as a source of energy is due to the connection to the carbon cycle, where the dioxide carbon emitted to the environment by the energy production is consumed by the plants that are used to produce this energy reducing the air pollution on the earth. Nevertheless, inserting biomass into the energy sector and giving it a leading role can become a reality if the society's needs, resources, and technologies are well defined, exploited, and optimized.

1.2.1. Lignocellulosic biomass and algae

1.2.1.1. Lignocellulosic biomass

Lignocellulosic biomass is the most abundant one in nature. It comprises three major pseudo components or biopolymers (Cellulose, hemicellulose, and lignin) with small amounts of other components like acetyl groups, minerals, and phenolic substituents [31]. These pseudo-components are organized into non-uniform three-dimensional structures with varying relative compositions depending on the type of species, tissues, and maturity of the plant cell wall.

Each one provides a reinforcing effect defied by how they are bonded between them. For example, Hemicellulose and lignin are individually bonded to cellulose via hydrogen bonds and covalent bonds. Cellulose is a linear carbohydrate polymer made up of solely D glucose. In contrast, hemicellulose is a branched carbohydrate polymer composed of various monosaccharides, and lignin is a non-carbohydrate, highly complex, aromatic polymer assembled by irregularly arranged phenylpropane units for structural rigidity [32]. This combination of these polymers results from the evolution of lignocellulose to resist degradation, having an impeccable blend of the crystallinity of cellulose, hydrophobicity of lignin, and encapsulation of cellulose by the lignin–hemicellulose matrix [31]. In general, the lignocellulosic biomass comprises 10.5–40.4 wt.% hemicellulose, 25.0–44.2 wt.% cellulose, and 21.7–44.0 wt.% lignin, with the inconsiderable amount of ash and extractives [32].

- **Cellulose:**

It is the major component of the lignocellulosic biomass, representing a 35-50% by weight part of dry lignocellulosic biomass [31], [33]. It is known to be a polymer whose structure consists of extensive intramolecular and intermolecular hydrogen bonding networks, which tightly bind the glucose units. For example, A single cellulose molecule contains 5000-10000 units of glucose, with interesting properties such as hydrophilicity, biocompatibility, and stereoregularity [16], [18]– [20].

- **Hemicellulose:**

Hemicellulose is the second most abundant polymeric carbohydrate, representing 20-35% by weight of the dry biomass [16], [18]– [20]. In comparison to cellulose, the polymer chain consists of a branched structure, and it has a relatively low molecular weight with a random and amorphous structure, which is composed of several heteropolymers. The chemical and thermal stability of hemicellulose is generally lower than cellulose, probably due to its lack of crystallinity and lower polymerization degree [16], [18]–[20].

- **Lignin**

It is a three-dimensional polymer of phenylpropanoid units. It functions as the cellular glue which provides compressive strength to the plant tissue and the individual fibers. Depending on the materials, the percentage of lignin can be higher or lower. For example, hard biomass materials contain a lower percentage, whereas soft biomass materials contain a relatively high percentage of lignin. It is the third

important part which accounts for 10-25% by weight of dry biomass, depending upon the type of biomass. In terms of structure, lignin has amorphous so that it can exhibit more than one structure but with a highly branched three-dimension chain [16], [18]– [20].

- **Ash and inorganic minerals:**

Ash represents the residual mineral content present in biomass. These materials are found in different percentages depending on the type of biomass, and they can vary from 0.5% to 10 % as exposed by [34]. In typical biomass composition, minerals like potassium, sulfur, sodium, phosphorus, calcium, and magnesium are found. Also, these encountered minerals are thought to have an impact on the thermal biomass conversion pathways [35].

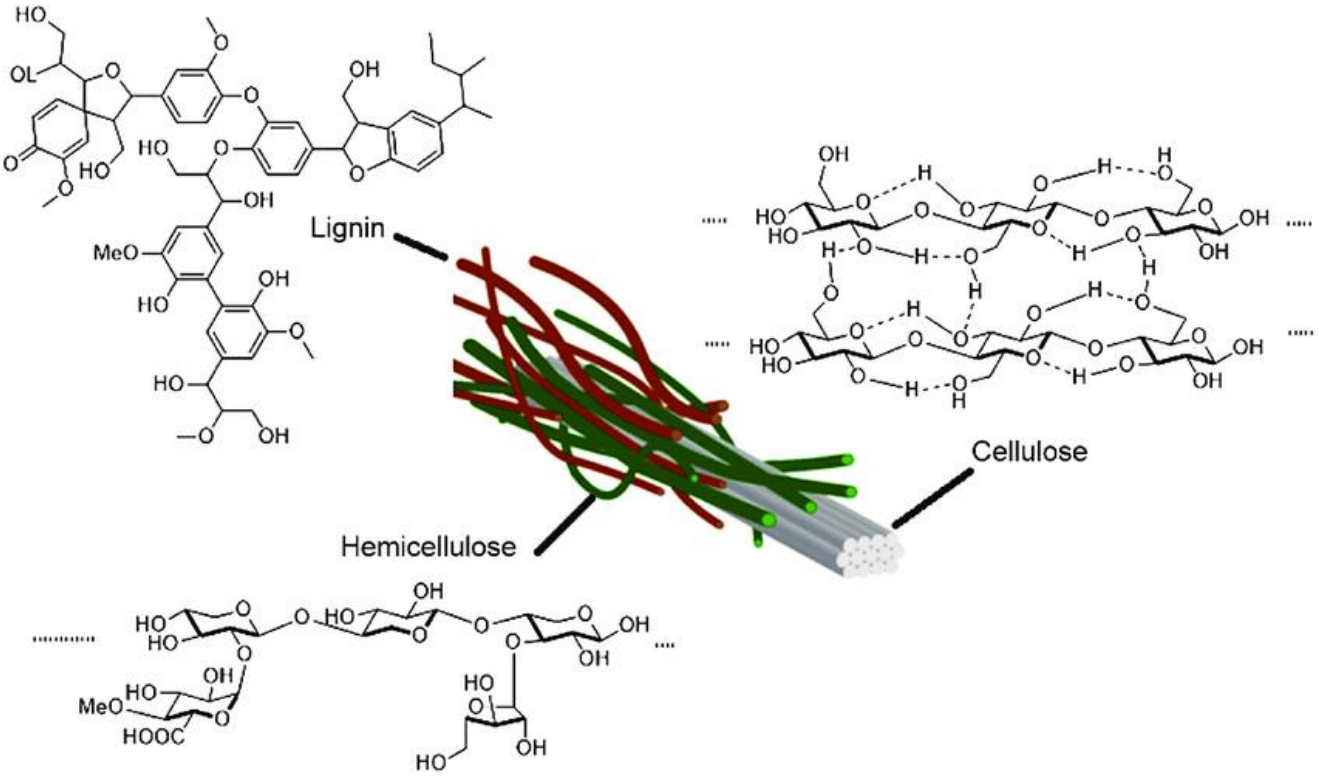

Figure 1.2-1 Pseudo-components of lignocellulosic biomass [36]

1.2.1.1.1. Flax shives

1.2.1.1.1.1. The flax plant:

Flax, also called linen (Linun Usitatissimum), is a dicotyledon of the Linacea Family. This plant it is between 80 and 120 cm high, with few branches and a small flower that can be easily recognized by its intense purple color (see figure 5). A general Cross-sectional schematic representation of flax stems is provided in figure 5.

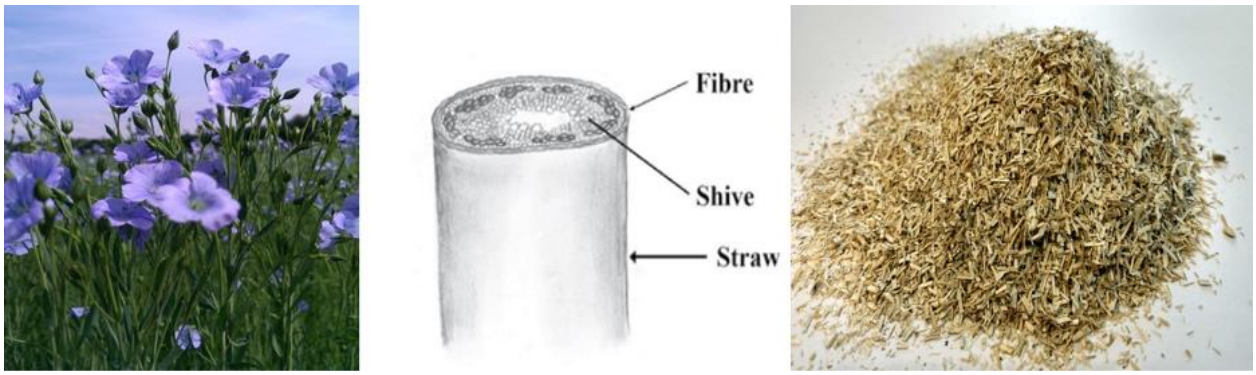

Figure 1.2-2. Flax and Flax shives

This plant is one of the oldest used on the textile industry, extensively used in Egypt from the 5th century for clothing and sails. Its cultivation use was developed throughout Europe, North Africa and Asia, and reaching a production of 400,000 tons of flax fiber through the word at the end of the 20th century[37]. The use of this plant is not limited to textile, but also for the paper, linseed oil, and composite products manufacture.

The principal component of flax fibers is cellulose, with smaller amounts of hemicellulose, lignin, pectin and oils and waxes. The location of constituents, as the chemical composition of the flax stem defines the flax fiber's properties. The lignocellulosic matrix is found in the cell walls determining the physical properties of the fibers[38].

1.2.1.1.1.2. Flax shives:

Flax shives are a secondary products while separating the fibers from the rest of the plant, by the scutching process[38]. Nowadays, there are limited applications of Flax shives and it is usually treated as a waste. Some applications found in the literature are animal bending, solid fuel for combustion processes, insulation material, cement additive, and for biochemical extraction [5], [8], [37], [39], [39]–[44]

As Flax shives have been treated with less importance in comparison to the flax as a whole, its specific composition has been less studied. [37] presented a general content distribution for the flax plants

giving a α-cellulose content of 40% to 50%, the hemicellulose content of 20% to 25% and lignin content of 20% to 25%. A more specific pseudo-components distribution for Flax shives presented in literature is presented in table 1.2-1.

Table 1.2-1 Pseudo-components distribution of Flax shives presented in literature

Component	[45]	[41]	[46]	[47]
Cellulose	53.1%	43%	33.3%	50.2%
Hemicellulose	13.2%	15%	21.9%	18.2%
Lignin	24%	34%	27.3%	22.7%
Ash	-	2%	1.5%	1.9%
Moisture	-	8%	16%	7%

1.2.2. Algae biomass:

Algae are defined as aquatic organisms which can be found in the marine area, freshwater, brackish estuaries, lagoon, and in sediments and soils [28]. The term algae, frequently used as a pejorative for weed growing where humans consider the wrong place, is now the focus of attention due to its potential use as a biomass source to replace conventional fossil fuels for producing biofuels and high value-added chemicals. More properly defined, the term algae include diverse categories of a photosynthetic, oxygen-evolving organism from various phylogenetic groups [48], [49]

The algae can be classified based on their color, size, and less clearness, by taxonomical groups. Based on their size, algae can be microscopic or macroscopic, also known as seaweeds. Microalgae are unicellular species found in fresh water and mire system, characterized by their ability to accumulate high levels of lipids and proteins. Macroalgae are multicellular organisms, mainly found in marine systems.

Based on their pigmentation, the algae can be divided into several major group: green, brown, and red algae [50].

- **Red algae**: Scientifically called as Rhodophyta, is the world's largest part of seaweed. The color of this algae is due to the presence of pigments called phycobilins. Some examples of red algae are laver and dulse.

- **Green algae:** There are two important races of green algae. The first one called Charophyta, is mainly found in fresh water in the form of sea grapes and sea lettuce. The green color is due to the presence of chlorophyll pigments *a* and *b*, and there is absence of phycobilin. The second type of green algae is the Streptophyta, also called freshwater algae.

- **Brown algae:** Also called Phaeophyta, are the dominant organism in many of coastal regions in the world. Responsible of forming undersea forest and host of high level of biodiversity [26]. The pigment Fucoxanthin is the cause of its brown color. These seaweeds are the main source of the industrial hydrocolloid alginate. Due to its very rapid growth rate is one of the interesting biomasses for biofuels production.

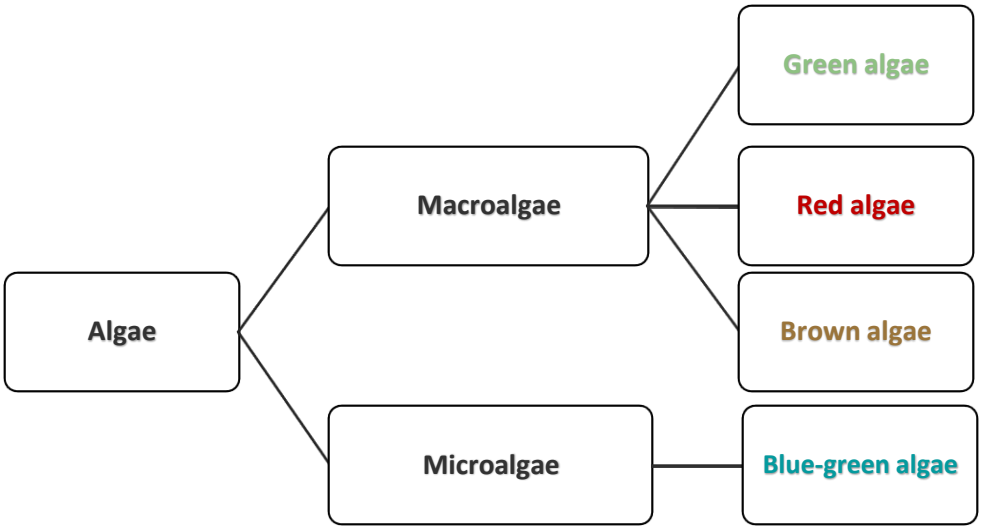

Figure 1.2-3. Algae classification

Unlike lignocellulosic biomass, algae inhabit the aquatic environment and do not need to develop a solid support structure composed of a matrix of cellulose, hemicellulose, and lignin. Thereby the main constituents of algae are active metabolic compounds such as protein, lipids, sugars, and nucleic acids.

- **Proteins:** Proteins are long chains of polymerized amino acids involved in cell structures. Proteins usually contain more than 80% of the total nitrogen in the algae [51]. The high percentage of protein in some algae makes them interesting as food and feed.

- **Carbohydrates:** Carbohydrates are the main product of photosynthesis, with different distributions depending on the algae species. Glucose is often the most present monomer for many species. Also, cellulose and hemicellulose are found in the cell membranes of green algae and the cell walls of the red algae [51]. In the case of brown algae, the main carbohydrates present are alginic acid, mannitol, lamarin, and fucoidan [52].

- **Lipids:** Lipids are long chains of hydrocarbon molecules with a carboxyl group at one end. They play both structural and energy storage roles as they are present as phospholipids,

glycolipids, fatty acids, and triglycerides. The percentage of lipids varies depending on the species of algae [51].

Inorganic and ash: The inorganics present in the algae are measured by the ash content. Includes metal oxides such as carbonates, nitrates, sulfates, phosphates, and chlorides. Also, a significant amount of sulfur can be present in the form of inorganic sulfate, sulfite, sulfide, and organic amino acids [51].

The chemical composition of the algae depends on the season, species, and culture conditions. For example, microalgae are generally composed of high levels of lipids 7–23%, carbohydrates 4–57%, and proteins 6–71% [53]. Contrasting, macroalgae only contain 10% -15% of dry matter with larger amounts of carbohydrates [53].

Algae represent an important group of organisms, and although they are widely found in aquatic habitats, they also inhabit terrestrial habitats, including extreme environments such as snow and glaciers in the Arctic and Antarctic. Some of the applications of microalgae are food supplements and animal feed, for example, Spirulina and Chlorella [54]. In the case of macroalgae, a large-scale production started several decades ago to be used as biomass [49], [49]. Unlike lignocellulosic biomass and the other terrestrial biomass sources, macroalgae cultivation for biofuels production offers specific advantages: It does not compete with food production, doesn't require fresh water, and has a high growth speed.

1.2.2.1.1. Sargassum:

Sargassum, named after the Sargasso Sea in the North Atlantic Ocean, is a genus of Phaeophyceae (brown algae). This type of algae was first described by C. Agardh (1820) [55], who was the first to start the new classification system for "algae". Sargassum belongs to the Fucale order, with more than 500 species described in the Guiry and Guiry 2020 algae database [55]. However, the taxonomy of the genus Sargassum is poorly understood; these species are very polymorphic, and even in scientific literature is difficult to have a very well-established description and classification of it.

Figure 1.2-4 Sargassum Natans

The genus Sargassum has, in general, a highly branched thallus to 10-200 cm or more in length with one to a few simple, terete to compressed stipes 1-20 cm long arising from a discoid-conical holdfast [56]. They have a brown or dark green color with a rough and muggy texture. If even most of them are glued to the land (Benthic), there are also species that are exclusively floating (Pelagic).

The distribution of the Sargassum species in the American continent is given in figure 1.11. It is found that in the Caribbean and Antilles, the main species are the S. fluitans, S. natans, and S. polyceratium. More specifically, in the Caribbean region, the most prominent species are S. natans and S. fluitans, being part of the problem of algae inundation of its coastlines [9], [30].

The problem of invasion of the Sargassum in the Caribbean has attracted numerous investigations to valorize this type of biomass. Just in 2015, the Caribbean recorded a peak daily influx of 10,000 tons of Sargassum [57], where the beach cast Sargassum was usually removed and disposed of as waste [10]. However, the genus Sargassum exhibit a wide application range that goes from food supplement, heavy metal absorber, fuel production, phytochemical source, and fertilizer [30], [49], [58]–[63].

In terms of the chemical composition of the pelagic species present in the Caribbean, there are not many studies presented in the literature. Oyesiku and Egunyomi [58] presented a proximate analysis of a mixture of these. The results are presented in table 1.2-2 with other studies performed on other types of Sargassum.

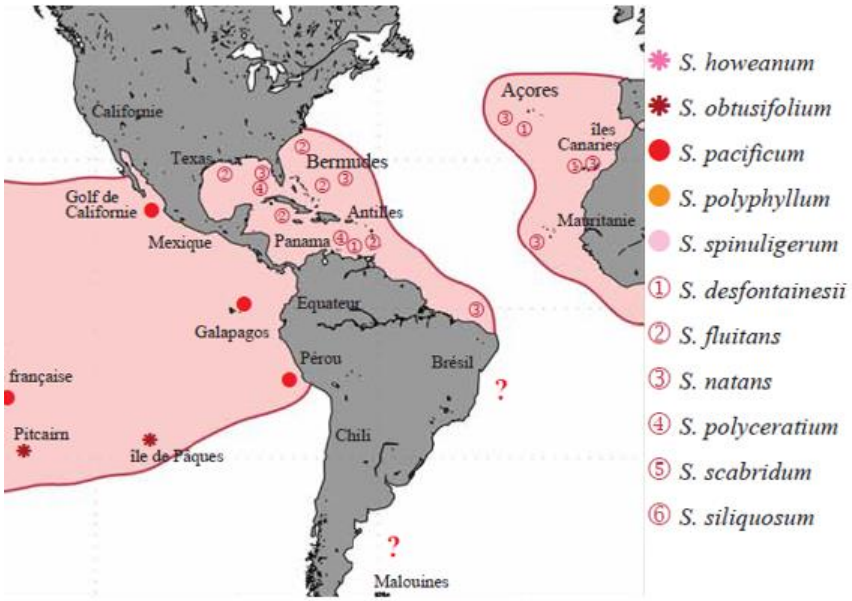

Figure 1.2-5. Distribution Sargassum Species[64]

As mentioned before, the chemical composition of algae depends on the species and this is valid even in the same genus (Sargassum). In general, the content of protein is higher than the content of lipids, as the quantity of hemicellulose which is almost twice the value of the other pseudo components.

Table 1.2-2 Composition of various species of Sargassum

Components/ Content Percentage	*S. natans and S. fluitans [58]*	*Sargassum spp [65]*	*Sargassum horneri [65]*	*Sargassum naozhouense [66]*	*Sargassum subrepandum [67]*
Carbohydrates	57.3%	-	-	-	-
Protein	15.4%	9.7%	18.5%	11.2%	3.2%
Lipids	-	-	0.8%	1.1%	3.6%
Ash	8.65%	-	-	-	-
Cellulose	-	20.5%	5.5%	4.8%	7.0%
Hemicellulose	-	43.2%	27.4%	29.7%	10.2%
Lignin	-	7.4%	14.6%	-	-

1.3. PYROLYSIS: TRANSFORMING BIOMASS INTO ENERGY

Thermochemical routes (gasification, pyrolysis, combustion, torrefaction, etc.) of valorizing biomass can generate useful products such as bio-oil, biochar, and syngas. Products that can be easily implemented in the actual energy market structure. These products have a wide range of applications: biochar as a solid fuel for electricity production or to produce activated carbon, bio-oil as liquid biofuel or as a raw matter to synthesize high value-added chemical products, and the syngas to produce synthetic natural gas or other chemicals as methanol.

The advantage of using pyrolysis as a valorization route is that the product distribution yield for char, bio-oil, and gas can be altered according to the process conditions, allowing to produce in the desired quantity the product of interest.

The concept of pyrolysis refers to the thermal decomposition of organic matter in the absence of oxygen at a temperature range from 450 to 600 Celsius. This reaction is also the first step in the combustion and gasification processes. The difference lies in the partial or total oxidation of the matter that occurs afterward [68]. It is an endothermic transformation which, by the temperature influence, produces different by-products such as:

- **Char (Carbonaceous residue):** Pyrolysis solid residue. A mixture of fixed carbon, ash, and minerals. Depending on how the reaction is carried out, the condition of the char can vary considerably in terms of microstructure, pH, surface area, etc.; Its quality defines the application of the char, which could be as soil quality enhancer, carbon sequestration, and activated carbon production.

- **Gas:** Gas collected from pyrolysis that could not be condensed is also called non-condensable gas. Mainly composed of CO, H_2, CO_2, and some low molecular weight hydrocarbons. It can be used as a direct combustion fuel for heat or electricity production.

- **Pyrolytic oil or bio-oil:** Liquid collected from the pyrolysis process by condensing the condensable gas phase. Generally, it is a dark brown organic and acid liquid consisting of a mixture of oxygenated molecules and water in very high percentages (15-50%) [69]. The main organic families present in the oil chemical matrix are carboxylic acids, ketones, aldehydes, alkenes, phenols, furans, guaiacols, esters, and sugars [68]–[71]. Usually, bio-oil is the target product in the implemented pyrolysis process due to its suitability to be used in applications like those of conventional fuel.

1.3.1 Types of pyrolysis

The products mentioned before are always produced, but the proportions can be very different depending on the adjustment of the process conditions. For example, pyrolysis typically occurs at operating temperatures above 400°C and depending on the thermal environment and the final temperature. Pyrolysis will yield mainly biochar at low temperatures and mainly gases at high temperatures, greater than 800°C; At an intermediate temperature (500°C) and under relatively high heating rates, the main product is bio-oil. Parameters such as temperature, solid residence time, heating rate, biomass particle size, vapors residence time, etc., have a strong influence on the process outcomes and are also used to determine the pyrolysis operational mode, as shown in table 1.3-1.

Table 1.3-1 Different pyrolysis conditions [61]

Pyrolysis reaction mode	***Temperature (°C)***	***Vapors residence time (s)***	***Heating Rate (°C/s)***	***Product distribution***		
				Liquid (%)	**Char (%)**	**Gas (%)**
Fast	±500	± 2	>1000	75	12	13
Intermediate	500-600	10 – 20	10 – 200	50	20	30
Slow	±400	300- 1,800	0.1- 1	30	35	35
Gasification	±800	>20		5	10	85

As seen above, there are three primary pyrolysis operational modes:

- **Slow pyrolysis:** Takes place at a low heating rate (0.1 to 1 °C/s) and high vapors and solid residence time. The low heat transfer produced during the reaction period allows for an increase in char production by up to 35%. However, long residence time requires extra energy input.

- **Intermediate pyrolysis:** Intermediate pyrolysis mode works with a high heating rate, short vapors residence time, and accurate control of temperature between 500- 600 °C. The product yield on a weight basis is 40-60% for oil, 15-25% for char, and 25-35% for gas, depending on the biomass type.

- **Fast pyrolysis:** The most promising pyrolysis mode to produce bio-oil, achieving up to 75% of bio-oil yield. This method can be described as the fast biomass volatilization due to the extremely high heating rates and temperature (up to 1000 °C) and short vapors residence time (±2 seconds). Despite the high oil yield, the thermal stability and corrosiveness of the oil produced are some drawbacks of implementing this scenario.

Contrary to slow pyrolysis, fast pyrolysis is preferred according to the bio-oil and gas yield target. The yield of either liquid or gas depends on the residence time and heating rate. With a low heating rate and long gas residence time, a high temperature will result in a higher gas yield [72]). Low temperature, high heating rate, and short residence time will maximize the bio-oil yield for fast pyrolysis.[68], have stated that the maximum bio-oil yield (75%) is obtained at around 500°C coupled with high heating rates and very short residence time.

The effect of the residence time on the bio-oil and gas yield is explained by the time of heat exposure of the organic matter present in the biomass [73]. When increasing the residence time to 10-20s, secondary cracking reactions of the products appear, increasing the gas yield. In addition, to the rapid heating, the rapid quenching of the condensable gases will avoid the breakdown reactions of the higher molecular weight species into lighter gaseous products [74]. Also, there are significant differences in liquids produced from different pyrolysis modes in terms of water miscibility tolerance. Bio-oil resulting from fast pyrolysis can tolerate up to 30-35 wt.% water before phase separation occurs, while liquid from slow pyrolysis has water miscibility tolerance of only about 20 wt.% [68].

1.3.2 Pyrolysis reaction: Mechanism

Knowing that the pyrolysis product's distribution is highly dependent on reaction conditions, understanding the biomass pyrolysis mechanism and kinetics is considered a necessary subject to optimize the process. In terms of basic pyrolysis chemistry, pyrolysis starts with the partial depolymerization of carbohydrate polymers into a short chain of sugars. It occurs at low temperatures (<200°C) within long reaction times, usually hours. Below 300°C, slow dehydration takes place along with a reduction of the sample weight, thus leading to subsequent reactions forming unsaturated polymers and, finally, char. When a high temperature (~300°C) is applied, fragmentation dominates where it involves depolymerization into anhydrous-glucose compounds and light volatiles. Upon heating at even higher temperatures, volatile species will escape, thus giving rise to the formation of tars when efficiently removed from the reaction zone and condensed. Also, the production of C_{2-4} oxygenates from the extensive breaking of the C-C bond takes place at this stage. When the heating goes beyond 700°C, a valuable mixed gas product is generated, which consists of CO, CO_2, H_2, and CH_4.

To convert biomass into energy, it is vital to understand the thermal behavior of the major chemical constituents of biomass.

1. The first component to decompose is the hemicellulose. This component is highly susceptible to pyrolysis at low temperatures (200–300 °C) due to its low degree of polymerization, amorphous structure, and shorter carbohydrate chains [75]. It usually decomposes below 250 °C and depolymerizes to rearrange the glycosidic ring structure caused by the dehydration and dissociation of the acetyl group to form acetic acids [76]. The mixture of various polymerized monosaccharides of hemicellulose then

decomposes at around 300 °C to produce dominantly volatile products such as CO_2, CO, H_2O, and condensable vapors [32].

2. Between 250–300 °C, the hemicellulose depolymerization and the fragmentation of monosaccharide units coincide [77]. Thermal degradation of cellulose starts at temperatures close to 320 °C, and it is completely degraded at 500 °C. During decomposition, cellulose undergoes several phenomena such as water elimination, condensation, and fragmentation reactions forming gases, liquid, and char residues [3], [78].

3. The final stage is characterized by lignin degradation. Lignin steadily decomposes in the temperature range of 250–500 °C due to the complicated aromatic structure [77]. Lignin has the most influential effect on pyrolysis product distribution due to the high carbon and low oxygen contents [32], [79]. The high content of lignin is correlated to the high yields in biochar up to 50 wt.% [77].

In a simple overview, biomass could be treated as a solid consisting of volatile matters, fixed carbon, ash, and fixed water content. Still, the complexity of biomass matrix is one of the challenges when studying the pyrolysis behavior, and even more when considering that each feedstock of biomass has a different quality giving different products yield results.

Many studies have been performed to understand the degradation behavior of biomass [8], [80]–[82], [82]–[90], in general, with the assistance of thermogravimetry analysis. The studies indicate a decomposition of biomass in three stages: the first stage refers to the release of water, carbon monoxide, and carbon dioxide at temperatures no higher than 200 °C, then the main decomposition occurs at the second stage in temperatures between 475 and 655 °C. Finally, the decomposition reaction slows down in the third stage at a temperature above 600 °C. This decomposition behavior is intimately related to the decomposition behavior of biomass pseudo-components. As mentioned in the previous section, the thermal degradation of each pseudo-component is summarized as 220-315 °C for cellulose, 315-400 °C for hemicellulose, and 150-900 °C for lignin.

Contrary to lignocellulosic biomass, the pyrolysis of algae biomass is often decomposed in the degradation of lipids, proteins, and carbohydrates. Initially, bond breaking, and water content are removed. In the second stage, lipids, proteins, and carbohydrates are decomposed during the active pyrolysis phase, and at the final stage, carbon-rich residues are formed.

In earlier studies [91], Spirulina platensis (SP) and Chlorella protothecoides (CP) were analyzed in terms of devolatilization behavior and pyrolytic characteristics. Both biomasses are mainly devolatilized between 150 and 560 °C with a total volatile yield of 71 %. Interestingly, higher lipid content was correlated with the maximum yield of liquid (52–55% w/w), gas (33–36% w/w), and biochar (15% w/w). As the heating rate increased, a shift to higher temperatures was observed in their thermograms, and

the instantaneous maximum and average reaction rates in the devolatilization stage were increased while the activation energy was decreased.

The kinetics of algal biomass pyrolysis is commonly represented by an independent and simultaneous reaction of lipids, carbohydrates, and proteins into biochar and volatiles [28]. The degradation process is explained in the scheme below:

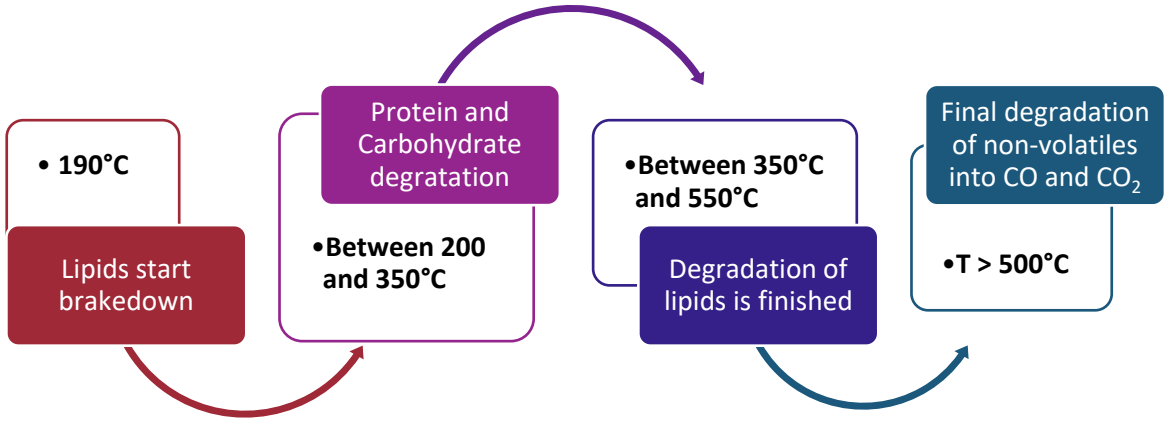

Figure 1.3-1 Algae biomass pyrolysis behavior

Lipids begin to break down at 190 °C [92]. Between 200 and 350 °C starts, the degradation of proteins and carbohydrates [93]. When reaching the temperature range between 350 and 500 °C, there are almost no lipids to be degraded, and the remaining proteins and carbohydrates are converted into volatiles through depolymerization, decarboxylation, and cracking. The non-volatile materials will only degrade and vaporize into CO_2 and CO when the temperature is > 550 °C [94]. Generally, the favorability of bio-oil production from algal pyrolysis follows the trend: lipid > protein > carbohydrate [95].

Chemical compositions (carbohydrate, lipid, and protein) can be converted into different species. Usually, lipid undergoes decarboxylation, decarboxylation, and fragmentation of glycerides [96]. This complex process primarily forms aldehydes, ketones, alcohols, and acids with long carbon chains from its triglycerides and fatty acids [97]. In addition, fatty olefins, paraffin, and aromatic compounds are formed from lipid constitutes. Carbohydrate pyrolysis produces light organics, carbonyls, acids, and alcohols [96]. Furans, pyrazines, and pyrroles are formed from the carbohydrate thermal decomposition at temperatures above 300 °C [97].

Nitrogenous compounds such as amines, amides, pyridines, pyrroles, pyrazoles, pyrazines, Poly heteroaromatics, nitriles, imidazole, and indoles are produced from the pyrolysis of high protein algae biomass [97].

In terms of reaction mechanisms, several schemes are proposed in the literature to describe the pyrolysis process, but two general approaches are generally presented. One-step global reaction and multicomponent reactions model. When referring to biomass as a homogeneous component, the general reaction mechanism is described as a first-order single-step reaction, where biomass is converted into char and volatiles. The volatiles are composed of condensable gases or bio-oil and non-condensable gases. This model is one of the most frequently used [98] [84].

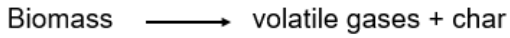

Also, another commonly used method is the multicomponent model. Ranzi et al. (2008) [99] use this model for cellulose pyrolysis. The model consisted of a multistep lumped mechanism of cellulose pyrolysis from cellulose to active cellulose at 280 °C and then by competitive reactions to bio-oil, gas, and char. This model also considers different steps of solid fuel volatilization and secondary gas-phase reactions, the decomposition of cellulose in acids and levoglucosan at high heating rates, and the production of gas and char at the low heating rates.

Concerning the kinetics model, simulating the the biomass pyrolysis mechanism of the reaction and finding the kinetics parameters are important steps. Models such as Kissenger Model, Isoconversional method, NLSM (Nonlinear least-square minimization), and Genetic algorithm have been used to describe pyrolysis reaction mechanism [78]. The Kissenger method is used in the case of biomass, taking into consideration the hypothesis of a homogenous monomolecular solid with a single reaction mechanism. The isoconversional method considers pyrolysis as an infinite number of independent and parallels reactions. The NLSM and the genetic algorithm are fitting models based where it is needed to have previous knowledge of the reaction mechanism to determine the kinetic parameters by a convergence criterion between the experimental and the modeling results. A first-order kinetic model could be used as a first approximation and for a general view of the process.

1.3.3 Reactors used for biomass pyrolysis

A pyrolysis process consists of four main steps, starting with the feed station, including biomass pretreatment as drying. Biomass is redirected to the reactor where pyrolysis takes place. The third step in situ or ex-situ of the reactor is the solid separation of volatiles. The fourth and last stage of the process is the separation of condensable and non-condensable gases by a system of condensers.

Selecting the type of reactor is essential and has a strong influence on the final product distribution and quality. Many processes have been proposed in the literature. Some of them are at large scale units. Still, in general, the leading technologies offered include bubbling fluidized bed, free, circulating fluidized bed, rotating cone, ablative pyrolysis, free fall, and the auger (screw) system.

Bubbling Fluidized Bed:

Bubbling fluidized bed (also known as a fluidized bed) reactors have been used for decades and nowadays are one of the most common reactors used for commercial-scale pyrolysis [100]–[103]. Its popularity is due to the ability to provide a high heat transfer rate of the large contact area between the fluid and the solid particles. This system uses fluidizing gas, fed at the bottom of the column, which controls the vapor and solid residence time. Also, the fluidizing gas carries out the products by the top of the reactor and passes through cyclones to separate the char and then to a condensation system when the bio-oil is condensed. Advantages such as bio-oil yield up to 75%, reuse of non-condensable gases as fluidizing gas, simple reactor configuration, and high heat transfer are presented. However, it has limitations in terms of the size of the particle (<3mm) and difficulty in recovering the oil due to the decrease of the vapor pressure. Also, the flow of the gas and particle sizes need to be carefully controlled so as not to blow the biomass out of the reactor or let it fall to the bottom of the reactor. The operating temperature is between 500 and 800 °C, and the heating is provided either by hot fluidizing gas, indirectly through the reactor walls and/or immersed heating tubes, hot sand, or microwaves.

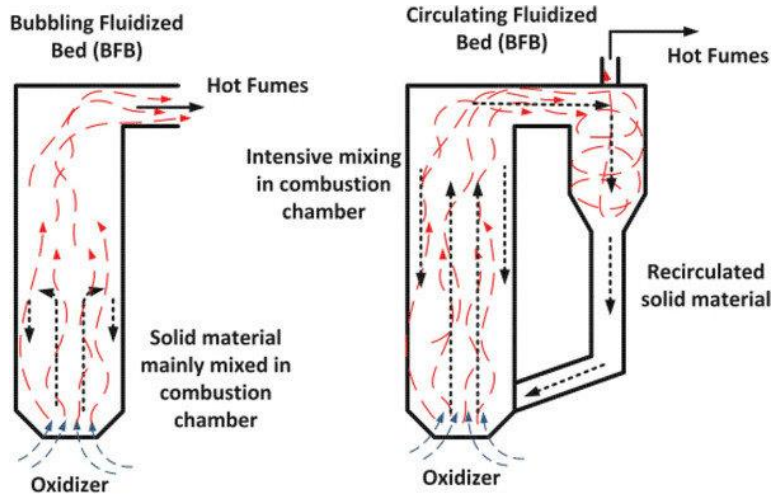

Figure 1.3-2 Bubbling and circulating fluidized bed reactor

Circulating Fluidized Bed (CFB)

Circulating fluidized bed and bubbling fluidized bed are similar. The main difference is that CFB technology uses higher gas velocity, which results in shorter solid and vapors residence times. The heating method commonly used is a mix of hot fluidizing gas and hot sand, which also assists in lifting the biomass particles in the reactor. High oil yields of over 70% can be achieved. Additionally, the particle size can be more diverse. However, these reactors are more challenging to design, and like bubbling fluidized beds, it has the drawback of removing particulate matter from the gas and oil due to high gas flow rates. This type of system leads to high char content in products. Recently, companies like Metso, UPM, and Fortum developed a circulating fluidized bed continuous flow reactor with a capacity of 400 kg/h[104]–[107].

Rotating Cone:

This technology was developed at the University of Twente for flash pyrolysis of biomass. It consists in mixing the biomass with hot sand in a rotating cone inside a container. Unlike a fluidized bed reactor, it does not require using an inert gas, allowing to reduce the size of the reactor and the condenser [68], [108], [109]. This provides excellent heat transfer without the issues associated with high gas flow rates. Under the optimum reactor working conditions, the bio-oil yield is between 60% and 70 wt%. The main disadvantage of the rotating cone process is its complexity of ensuring the sealing and movement of the cone simultaneously. Also, it can only be performed at a small scale with small particle sizes [110], [111].

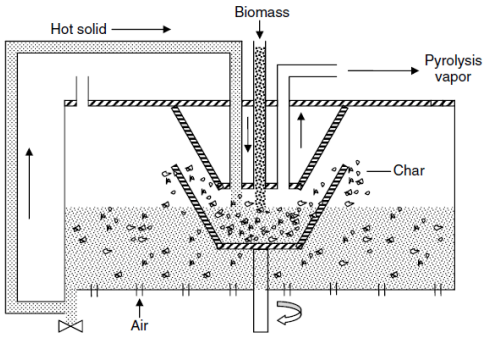

Figure 1.3-3 Rotating cone reactor

Ablative Pyrolysis:

Unlike the other technologies, in this type of reactor, the biomass particles are pressed against a moving hot metal surface for rapid heating [112], [113]. The ablative force is applied to the particle through either high gas velocity flowing tangentially to the reactor walls (gas ablation) or mechanically using a rotary disc/blade [68]. The force allows removing the char layer formed on the particle's surface during the reaction. Although extremely high pyrolysis oil yields of over 80% have been reported, the poor heat transfer, and the complexity of setting the right particle - reactor wall pressure - reactor wall temperature combination, have slowed down the implementation of this technology.

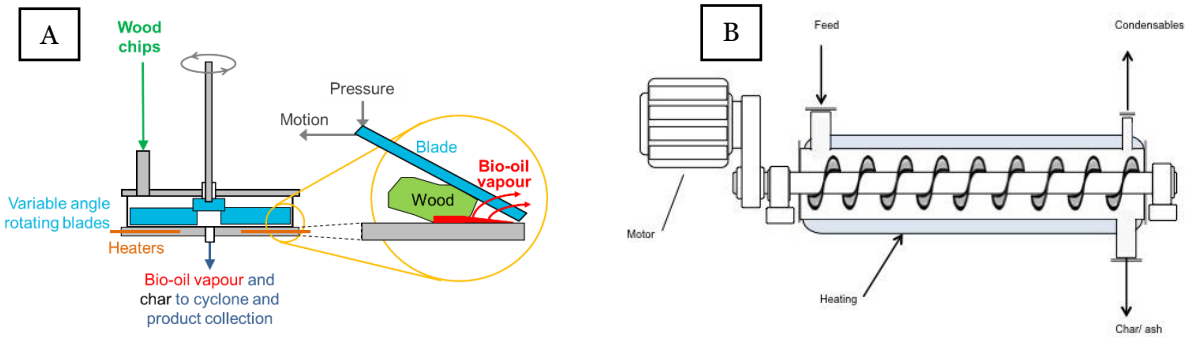

Figure 1.3-4 (a) Ablative pyrolysis reactor and (b) auger reactor

Auger Reactor

Auger reactor and fluidized bed are the two most used reactors for pyrolysis. The auger reactor pushes biomass through a reactor with heated walls. A carrier gas pulls out the vapors released from pyrolysis. The main advantages of the auger reactor are its simplicity and flexibility in terms of feed particle size and shape (Bridgwater, 2012). However, the solid and vapors residence time inside the reactor for this technology is long compared to the fluid-transported technologies leading to high biochar and low liquid yields (Bridgwater, 2012). ABRI-Tech Canada, Lurgi–Ruhrgas process in Germany, and Renewable Oil Intel in the USA are some of the producers of large-scale auger reactors. [114]–[116]

Rotatory Kiln Reactor

Rotary kiln reactors feature a spinning tube angled so that biomass tumbles down the reactor. It can for continuous or semi continuous flow processes. [102]–[104]. The feed is usually introduced at one end of the kiln, and the rotating motion enables the processed material to be transported along the length of the kiln to the exit Heat is provided by firing the outer wall of the reactor.

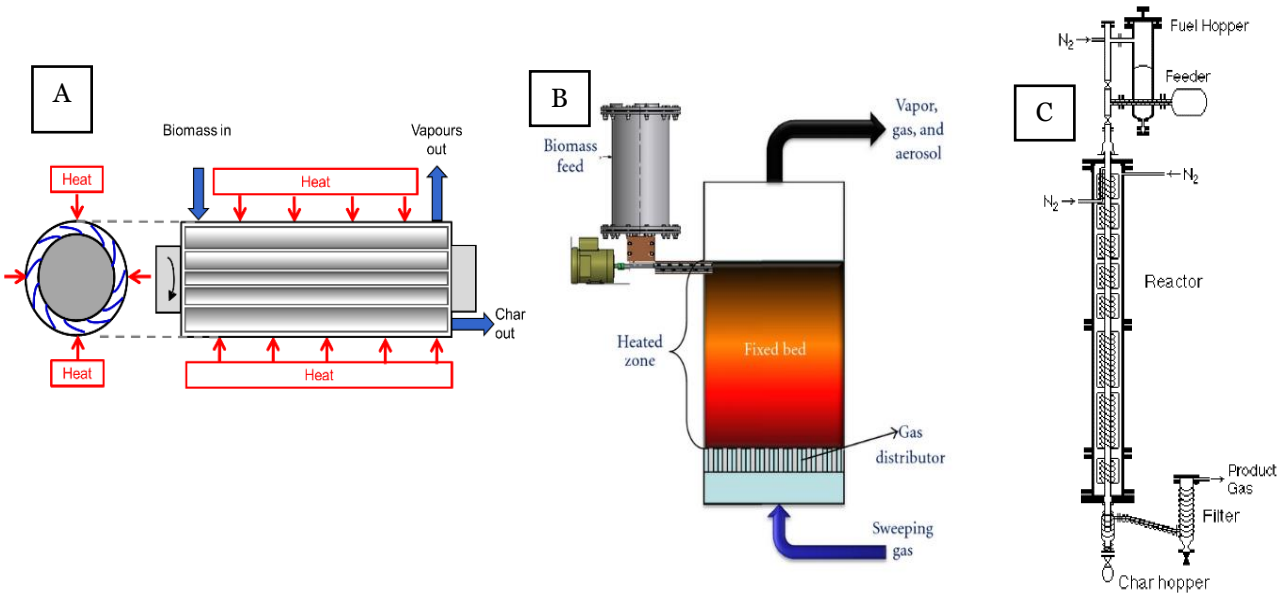

Figure 1.3-5 (a) Rotatory kiln, (b) fixed bed and (c) free fall reactor

There are not many references in literature about using this type of reactor which can be due to some issue with heat transfer and long residence times[117]–[119], have been extensively used within the solid processing industries, and have also been used for biomass processing[117]–[119].

Fixed bed:

Fixed beds are the simplest reactors for pyrolysis. However, they are usually used for slow pyrolysis and at a laboratory scale because they are not flexible with respect to process changes. As its name says, it has a fixed bed of biomass, and a carrier gas enters and passes through the bed to carry both the condensable and non-condensable gases to the condenser [120]–[123]. This type of reactor has been used to perform the conventional pyrolysis of coconut shell [77], rice straw[65], wheat straw, beech wood[6], Flax shives[124], and switchgrass, corn stover, Napier grass, etc. The operating conditions are about 10 -30°C/min of heating rate , 300-700° C, and 30 – 120 min of reaction time. The best results for bio-oil yield were found in the pyrolysis of coconut shells at a heating rate of 20°C/min, a temperature equal to 575°C for 50 % bio-oil, 27% biochar, and 23% gas[77].

Free fall:

Free-fall or drop-tube reactors are in principle a simple technology. The particles fall through the length of the reactor while heated by the reactor's wall. Biomass is fed from the top of the reactor and char is captured in a collector at the bottom of the reactor. The volatile gas passes through a cyclone to remove solid particles before entering a condenser[125], [126]. Campanella et al. (2012)[126] studied the non-catalytic and catalytic pyrolysis of microalgae were carried out in a free fall reactor. The impacts of several process variables on the fast pyrolysis were studied, the higher bio-oil yield (48%) was obtained using CO_2 as sweeping gas and 500 °C. The authors concluded that the liquids yields were higher than those during pyrolysis in a fixed bed with the same feedstock.

1.4 MICROWAVE PYROLYSIS OF BIOMASS

1.4.1 Microwave pyrolysis vs conventional pyrolysis

Similar to conventional pyrolysis, microwave pyrolysis is divided in three stages: moisture evaporation, primary decomposition or active phase of pyrolysis, and secondary reactions or passive phase of pyrolysis. Unlike the conventional method based on radiation, convection, and conduction as a heat transfer phenomenon, microwave pyrolysis is based on the interaction of biomass and the electric field component to produce heat. The heat transfer produced by conventional pyrolysis results, in most cases, in a longer heating period and high energy loss because the heat is transferred from the surface to the center of the material, being mandatory a physical contact between the sample and the heating source. For microwave heating, the sample is directly heated in the core without physical contact with an inverse heating pattern from the inside to the outside [11]. Many studies have been conducted on microwave pyrolysis of biomass materials, and in most cases, they have outlined the effect on energy efficiency, product yield, and quality [21], [77], [127]. Also, the use of microwave irradiation for pyrolysis as an in-situ energy conversion into heat has been validated by several authors as a preferred option in comparison to the conventional heating method [4], [23], [128]–[131].

Microwave technology can provide a solution in terms of energy transfer rate. Microwave heating has been used for industrial processing applications over the competition from more conventional heating methods due to special advantages, such as volumetric and selective heating, faster reactions time, space and energy savings, and security and quality improvement. Due to the low thermal conductivity of organic solid plant residues (0.15 to 0.2 W/m.K for wood and approximately 0.05 W/m.K for sawdust), conductive heating through a wall or by infra-red heating is hardly possible, which makes vegetable fibers extensively used as thermal insulation. The use of microwave irradiation for pyrolysis processes, as an in situ energy conversion into heat, has been long recognized to provide better quality bio-products in shorter reaction time due to the direct sample heating and the particular heating profile resulting from the interaction of biomass with the electric field component of an electromagnetic wave [132]–[134]. Budarin et al. [12] reported that microwave pyrolysis can reduce the pyrolysis temperature up to 150°C compared to conventional pyrolysis. They have shown that microwave pyrolysis can be performed at temperatures between 100 and 200°C. This leads to a favorable energetic balance for microwave pyrolysis. The microwave power density absorbed by a material (W/m3) is usually in the order of 108 W/m3, as reported in the literature [135]–[137].[138]

Shra'ah and Helleur 139] reported higher yields of levoglucosan amorphous cellulose at 260 °C in microwave pyrolysis, while conventional pyrolysis required a much higher temperature (400° C). Zhao, Zhang [140] reported a greater syngas volume and biochar yield (30–50 wt.%) than conventional pyrolysis. Similarly, Dominguez et al.[141] investigated the pyrolysis of sewage sludge using microwave and electric ovens as the sources of heat. It was found that the desired gas production (H_2 + CO) was in a higher proportion by microwave pyrolysis than by conventional pyrolysis, with a maximum value of

38% for H2 and 66% for H2 + CO. Muley et al (2016) concluded that the microwave heating yielded higher aromatic compounds than the conventional heating methods [142]. Additionally, Afolabi et al. found that microwave pyrolysis could enhance the caloric value and mechanical properties of biochar via densification [143].

In terms of energy transfer rate, microwaves are preferable to be used for solid organic residues, the low thermal conductivity of which does not favor conductive heating or infrared heating. Huang et al., 2016 reported that the heating rate of microwave pyrolysis could be up to 42% higher than that of conventional pyrolysis. Concluding that less time and input energy are required to reach the desired temperature, leading to decreased processing time, capital costs and even enhancing material properties as the microstructure of char [144]. Also, Miura et al. (2004) studied the temperature gradient and the mass transfer for both conventional and microwave heating, concluding the advantages of using microwave heating due to the absence of secondary reactions activated by the pass of volatiles from low-temperature zones inside the biomass to high-temperature zones at the surface of biomass [145].

Also, microwave heating is very tolerant of water. Usually, conventional pyrolysis needs a biomass humidity percentage of 10%, so a pre-drying step is required [68]. This is not the case with microwave pyrolysis, where the amount of water inside the biomass helps to increase the heating rate of biomass. Yin [128] confirmed that a certain amount of moisture in biomass can increase heating rates during microwave-assisted pyrolysis, improving the overall microwave energy utilization efficiency. Also, Robinson et al. [129], [146] demonstrated that the water content of wood biomass alone meets the required microwave absorbing properties for efficient heat generation during microwave pyrolysis.

The rapid core heating results in a rapid reaction development, increasing the surface area and favoring the quick release of volatiles, which will be rapidly condensed due to the lower temperatures at the surface, reducing a second cracking reaction [147]. These features reduced the preliminary steps needed in the conventional heating process (drying, grounding, and extra condensation steps), which are where responsible for important contributions to acidification, eutrophication, and photochemical oxidant formations, and, therefore, to the global warming potential [148].

In terms of security, microwave pyrolysis can be said to be much safer as compliance with a safe working environment due to the easy on and off power ‘system developed for microwave irradiation. The latter will avoid explosions or other hazards that could be higher risks when compared to conventional pyrolysis plants where the heat production and heat inertia cannot be controlled. Moreover, pyrolysis is an endothermic reaction type, and therefore runway effect of reaction temperatures can also be prevented [138]. Time-saving is another advantage due of volumetric heating. In fact, the use of a microwave oven will achieve heating rates higher than the conventional reactors due to the interaction of molecules within the material. This, in turn, benefits from greater control of the heating process. Thus, obtaining high heating efficiency from microwave pyrolysis is possible.

1.4.2 Microwave pyrolysis mechanism

The scale of energy conversion efficiency of microwave heating depends on the material's molecular dielectric properties. The ability of the material to align itself with the frequency of the electromagnetic field applied determines the amount of generated heat. The ability to be polarized by the electric field is also called the dielectric constant, and as said before, this property reflects how much energy can be stored in the material. The efficiency of the material in converting this stored energy into heat is the dielectric loss factor.

In the case of microwave pyrolysis, the feedstock dielectric properties and its evolution during the reaction are incredibly important to achieve the desired results. The analysis of the dielectric properties of biomass will reflect the ability to be heated. If the feedstock is a transparent material, a microwave absorber will be needed. However, the moisture content can also induce heat production due to the water's dielectric properties.

Secondly, as well as in conventional pyrolysis, microwave pyrolysis is composed of three stages. Water evaporation, active pyrolysis phases, and passive pyrolysis phase [149]. As water is a good susceptor to microwaves, a sharp decrease in dielectric properties is observed because the dried biomass feedstock has difficulties absorbing microwave energy. However, Robinson et al. [146] demonstrated that the water content of wood is sufficient to induce the pyrolysis because even if the water is evaporated, the char produced takes the role of microwave absorber, enhancing the feedstock microwave absorption. Once the active pyrolysis phase starts, the dielectric properties of the medium change and the biochar and bio-oil dielectric properties influence the ability to produce heat.

Finally, the biochar dielectric properties direct the microwave energy absorption in the third stage. It must be said that dielectric properties change during the pyrolysis reaction. Robinson et al. (2009) proved during their investigations a non-linearly change in the dielectric properties of biomass while increasing the temperature during the microwave pyrolysis of wood pellets [146]. Also, the loss of tangent for water and most organic compounds decreases with increasing temperature [22].

Motasemi et al. (2015) [150], the latter was also studied. The authors studied the microwave dielectric properties of agricultural biomass at high temperatures in an inert environment. The results showed that the dielectric properties of oat and barley straw were almost independent of the microwave frequency in the drying and pyrolysis temperature range. During the drying stage, the dielectric properties decreased from room temperature to 75°C for barley and then remained roughly constant until ~200°C. In the pyrolysis stage, the dielectric properties dropped between 200°C and 350°C (reflecting the breaking of bonds and the release of volatile matter), after which the constant values up to 450°C indicate a reaction. Also, they noticed that the penetration depth remained almost constant during the drying stage. At the same time, it increased significantly during the pyrolysis stage and decreased dramatically as the temperature increased from 450°C to 700°C in the char stage. Similar behavior was also reported by Li et al. (2019), in the study of the dielectric properties of five biomass-pyrolusite mixtures at high temperatures [151]. Contrary, in the dielectric characterization of

switchgrass reported by Motasemi et al. (2014), the microwave dielectric properties of switchgrass at 915 and 2450 MHz under nitrogen (N_2) decreased during the drying and pyrolysis stage. Still, it increased dramatically in the char region, indicating the strong microwave absorption capability of the char[152].

Another point is the effect of microwave irradiation on the lignocellulosic biomass. Microwave irradiation has been used to fractionate the lignocellulosic materials. The depolymerization and breakdown of the crystalline structure of the cellulose have been reported, as well as a decrease in the hemicellulose content after a microwave pre-treatment irradiation [153]. Ahmad Al Shra'ah and Robert Helleur studied the microwave pyrolysis of cellulose, and they found that the pyrolysis reaction was successfully performed at low temperatures (200 to 280 °C) in comparison to the conventional method, with a maximum bio-oil yield (45%) obtained from amorphous cellulose at 260 °C [139]. Also, they found that microwave-derived bio-oil product composition was influenced by cellulose crystallinity, where high yields of levoglucosan were obtained from amorphous cellulose at 260 °C.

Hongqiang and Xu (2014) studied the microwave pyrolysis of lignin. The authors found that in terms of bio-oil quality, phenols, methoxy phenols, and alkylphenols were the most important chemical compound from the microwave pyrolysis of lignin [154]. Also, the thermal degradation of lignin occurs over a broad temperature range and the production where several varieties of reactive volatile components are produced during the degradation process. However, there is no dominant component in the products. In contrast, levoglucosan is dominant in the cellulose pyrolysis process [154].

Similarly, Krieger-Boquet [155] studied the microwave pyrolysis of wood. The author claimed that residue (char) increased from 10 to 33% as carbon content increased. Tar yields were quite variable, with 15-31% being typical and the chemical species present reflected the chemical structure of the biomass (levoglucosan for cellulose; phenols, guaiacols for lignin).

1.4.3 Reactors used in microwave pyrolysis

Microwave pyrolysis has been generally studied in batch and semi-batch reactor conditions, being the fixed bed reactors the most used ones. The literature presents other types of reactors with promising advantages for both batch and continuous operating modes. The type of operating mode influences the type of reactor to be used. For example, when using batch operation mode, the mixing of biomass is required, and the uniformity of the process is achievable but less scalable [156], [157].

A rotatory kiln reactor has been proved to be a good choice for microwave pyrolysis because it provides a homogeneous heating profile inside the reactor, which is desired for fast microwave pyrolysis to avoid hot spots. However, some drawbacks include low power density distribution and residence time [77]. The advantages of the rotary kiln reactor are due to the rotating motion, which tumbles the biomass without compressing it. This type of reactor has been used for the microwaves heated calcining of uranium concentrate [158]. Another reactor used in microwave pyrolysis is the conveyor belt. The continuous microwave pyrolysis of oil-contaminated drill cuttings was studied by Robinson et al.,

remarking advantages such as high-power densities and uniformity in power distribution along the conveyor belt [159]. Biomass processed through the conveyor belt concept is in contact with power densities much higher and uniform compared to the rotary kiln reactor, with a shorter residence time [21]. Fluidized beds have been successfully used for the fast pyrolysis of chlorodifluoromethane into tetrafluoroethylene. The authors concluded that the fluidized bed allows a high-heat flux for a small reactor volume without overheating the reactor wall, resulting in an advantage in performing fast microwave pyrolysis [160]. Another interesting reactor is the auger screw conveyor, which can provide an efficient power density distribution while stimulating the heat transfer between the biomass load and pyrolysis products and harvesting the bio-oil, biochar, and gas [21], [77]. Li et al. used a dual-stage system based on an auger pyrolysis reactor operating in a continuous mode to process 20 kg/h of a solid residue from the bio-ethanol production process [161].

1.4.4 Influence of operating parameters in microwave pyrolysis

The operating parameter of a microwave heated process can significantly alter the final product quality and yield. The critical parameters to consider are type, size and water content of biomass, reaction temperature and time, heating rate, microwave incident power and reactor's configuration.

1.4.4.1 Effect of temperature and irradiation time:

The liberation of the main product of pyrolysis depends on the temperature, residence time, and type of feedstock. Each parameter influences the yield of bio-oil, biochar, and gas. It is imperative to understand the processing conditions to obtain the desired quality and yield of the pyrolysis products. The effect of the temperature in the microwave pyrolysis process has been outlined by many researchers [129], [140], [141]. Zhao et al. (2012) studied the microwave pyrolysis of wheat straw on a modified domestic oven of 3000 watts and 2.45 GHz. The results showed an increase of 200°C increased the gas yield from 17.69 wt.% to 22.7 wt.%. Also, an enhancement of the structure of the char was produced. Domínguez et al. (2006) [141] studied the gasification temperature under pyrolysis conditions. At 1040°C, the volatiles produced undergo a secondary cracking reaction increasing the gas yield and improving the syngas production. Increasing the reaction temperature leads to a reduction in char yield and an increase in the gas yield, while intermediates temperature with high heating rates and short residence favors the bio-oil production [22], [162], [163]

1.4.4.2 Effect of moisture content

The moisture content has been remarked as one of the contrast points between conventional and microwave pyrolysis. While the moisture content is an undesired characteristic in the feed for the conventional pyrolysis, the amount of water significantly influences the material's dielectric properties when the biomass undergoes the microwave heating process. Robinson et al. (2009) [146] studied the effect of water content on dielectric properties of a wood sample, and they observed that with an increasing water content of up to 22%, both the liquid and gas yields were decreased to 3.5% and 4.5%

respectively. Also, they identified that at room temperature, the dried wood sample was transparent to microwave energy, whereas the water-containing wood sample was a good microwave absorbent material. Also, Yin [164] concluded that the amount of moisture in biomass increase heating rates improving microwave absorption.

1.4.4.3 Effect of biomass size input

The effect of biomass size comes from the microwave heating pattern (inside to outside). To have high heating rates with low energy consumption, a reduction of the biomass size is generally required [128]. However, too small particles may lead to an extremely large surface area and too large to an incomplete, according to Suriapparao et al. (2017) [165] and [131]. Robinson et al. (2015) [129] claims that the appropriate type and size of the biomass could reduce the energy and time of the microwave pyrolysis process. Microwave pyrolysis is more efficient than conventional's one [140], [145]. For example, it took 120 min for microwave heating whereas 300 min for the electric heating to pyrolyze a corn stalk bale with a size of 100 cm × 60 cm × 60 cm [166]

The microwave pyrolysis of wood using different biomass sizes was studied by Miura et al. (2004) [145]. The pieces of larch had diameters ranging from 60 to 300 mm. The experiments were carried out using two types of microwave ovens (1.5 kW and 3 kW). The results showed a higher temperature at the core of the wood being higher than the surface and easier heating of the larger woodblock can be than a smaller wood block when using the right microwave process configuration.

Bartoli et al. (2016) [167] concluded that the particle size influenced bio-oil production using microwave pyrolysis at 2.45 GHz and 3 kW. Using materials with smaller particle sizes (powder) increased bio-oil yield.

1.4.4.4 Effect of microwave incident power

The microwave incident power contributes to the heating rate and final temperature. Low incident power is traduced on the lower heating rate and high incident power in higher heating rates, despite the type of biomass. The latter was studied by Huang et al. 2016 [168], where seven types of biomasses were analyzed. The results showed that both final temperature and heating rate have a linear relationship with the microwave power level. Also, they found that reaction rates at higher power levels are higher than those at lower power levels.

Hu et al. (2012) [169] studied the effect of microwave incident power in the microwave pyrolysis of Chlorella vulgaris. The experiment was performed using a 3750 watt and 2.45 GHz microwave oven. It was discovered that when the microwave power level increased from 750 to 2250 watt, the temperature level increased from 200 ºC to almost 800 ºC, thus improving the yield of gas production but decreasing the solid fraction yield. The maximum bio-oil output (35.83 wt.%) was obtained at a 1500 watt of

incident microwave power level, whereas the maximum gas yield was obtained at an incident power of 2250 W.

Miller et al. (2021) [170] studied the microwave-induced selective decomposition of cellulose through a computational and experimental mechanistic study. The experiment was carried out in a fixed bed reactor. They concluded that all microwave incident power and fixed temperature led to the formation of CO, CO_2, and H_2, along with some CH4 and benzene. Reaction under 500, 750, and 1000 watt of incident power at constant temperature (305 °C) revealed that higher power decomposes cellulose to mainly CO, H_2, and CO_2.

1.4.4.5 Effect of microwave absorber

The biomass materials are found to be poor microwave absorbers [171], [172], and several studies have suggested the use of microwave absorbers to improve the microwave absorption [8], [9], [113], [116], [126], [128], [135]–[137]. According to Salema and Ani [175], the microwave absorber ratio to biomass has optimum to achieve the highest bio-oil production. This conclusion was obtained by an experiment carried out with four different ratios of biomass to carbon. They found that when no microwave absorber was added, no pyrolysis occurred at power settings of 180 W and 450 W and that with a 10% addition of carbon to the biomass, the bio-oil yield was found at its minimum, while char yield was at its maximum value, and for biomass to carbon ratio of 1:0.5 the maximum bio-oil yield and phenol content in the bio-oil were obtained. In the same way, Beneroso et al. (2016) [176] claimed that the addition of increasing amounts of microwave absorbent (up to 40%) impairs microwave penetration, resulting in heterogeneous heating of the bulk. Hence, there is, therefore, an optimum proportion that balances heat conversion and penetration depth. Mushtaq et al. [177] concluded that the effect of the heating aid (activated carbon from coconut) has

a linear increase in bio-oil yield at high microwave power, whereas bio-oil profit decreased with increasing heating aid at low microwave power.

The effect of microwave absorbers is seen in the product distribution and the quality of the product. Abdelsayed et al. (2019) [178] studied the impact of mixing pine wood biomass with coal in microwave pyrolysis at 550 ° C. They found that the high O/C ratio and low fixed carbon content in a biomass structure relative to coal affect the product distribution during microwave pyrolysis. Also, a higher aromatic-to-aliphatic fraction was observed under the microwave for the coal/biomass mixture. Also, Huag et al. (2017) [179] studied the microwave pyrolysis of Chlorella and Spirulina using activated carbon or magnetite as a microwave absorber. They concluded that microwave absorbers had no significant impact on the bio-oil yield. However, magnetite catalyzed the formation of aliphatic instead of aromatics while activated carbon enhanced dehydration reaction, which formed nitrogen-containing aromatics.

1.4.4.6 Effect of operation mode and cavity type

Despite the numerous investigations on microwave pyrolysis, the continuous operation mode is not as developed as for conventional pyrolysis [21], [77]. The relevancy on the microwave continuous flow reactor was outlined by Moseley and Kappe [180]which concluded that that the microwave heating at laboratory-scale single-mode microwave reactors is energy inefficient, and that scaling up to pilot scale resulted in higher energy efficiency. In terms of type of cavity, high power densities are provided by single mode applicators; however, the processing volume is extremely limited when using batch reactors due to the heterogeneous heating and penetration depth issues. Also, both multimode and single mode cavities have been tested for the microwave pyrolysis of several lignocellulosic biomass, and for each cases the single mode cavity resulted in a higher yield of bio-oil for a same type of biomass [77], [181], [182]

1.4.4.7 Effect of the type of biomass

Lignocellulosic biomass has been extensively studied as a carbon-neutral resource to produce renewable biofuels by pyrolysis reaction. Several studies also have been performed on microwave pyrolysis of biomass, including feedstock such as wood [146], rice husk [182], corn stover [183], straw bale [140], paper cups [83], pinewood [178], palm fiber [130], sugarcane bagasse, sugarcane peel, waste coffee grounds, and bamboo leaves,[184]. In general, the solid, liquid, and gas yields were 18–22, 40–50, and 30–40 wt.%, respectively. The feedstock type greatly influences bio-oil production because of the different proportions in pseudo-components characteristic to each type. Lo et al. [184] carried out the pyrolysis of lignocellulosic biomass, including rice straw, rice husk, corn stover, sugarcane bagasse, sugarcane peel, waste coffee grounds, and bamboo leaves, using a single-mode microwave oven operating at 2.45 GHz frequency. The authors concluded that for a microwave power level of 500 W, the solid yields of the seven types of biomasses were almost the same, but the liquid and gas yields were different. The higher gas yield was found in the Corn stover (40 wt%) but the lowest liquid yield (40 wt%). On the contrary, rice husk had the lowest gas yield (30 wt%) but the highest liquid yield (48 wt%). It can be noticed the competition between the gas and bio-oil yield is related to the feedstock type.

Microwave pyrolysis of algae is known for producing pyrolysis products with higher heating values than the conventional process [185]. Also, The bio-oil from algal biomass was characterized by a higher heating value (about 21 MJ/kg) and nitrogen content (2.68%) when compared with lignocellulosic biomass [186]. Regarding pyrolysis products yields, the microwave pyrolysis of Chlorella sp. at 750 watt and 480 °C reports a 28% bio-oil yield. Increasing the temperature records a higher gas yield of 35% at 540 ◦C and 1250 watts. Concerning bio-char, the yield was 28% at 362 ◦C and 500 watts (28%) [187]. Also, Hong et al. [188] carried out the pyrolysis of Spirulina, Chlorella, and Porphyra with catalyst SiC at various temperatures of 400, 500, and 700 °C, concluding that the bio-oil yield and the nitrogen content increased with temperature, as well as nitrogenated compounds in bio-oil were derived from protein in algae. At the same time, carbohydrates led to the formation of PAHs.

The pyrolysis of macroalgae tends to encourage gas and char production [28], [188]. For the Gelidium variety, the microwave pyrolysis using an incident power of 200 – 300 W promoted the generation of syngas faction (37.15 wt%) with lighter compounds [189]. Similarly, in another study, the algae Porphyra produced the highest syngas yield (87 wt%) [188]. The feedstock, Scenedesmus almeriensis was also suitable for generating gas products [190]. At 800 °C, the maximum syngas yield was reported to be 94 vol% with the highest H_2/CO ratio by reducing CO_2 and light hydrocarbons. Zhang et al. [191] investigated the microwave-induced pyrolysis of naturally blooming algae. By increasing the microwave power from 400 to 800 W, the yield of the liquid product was improved from about 35 to 47 wt%. Gas product was also improved accordingly while biochar product was diminished drastically from 47 to 25 wt%.

Table 1.4-1 Compilation of results for the microwave pyrolysis of lignocellulosic biomass

Lignocellulosic Biomass	*Type of cavity*	*Type of reactor*	*Incident Power*	*Reaction time*	*Reaction temperature*	*Microwave absorber*	*%Solid*	*%Liquid*	*%Gas*	*Reference*
Wheat straw		Batch reactor	1-2 kW	1-5 minutes			17.8%	27.9%	46.1%	[155]
Sewage sludge	Sigle mode	Batch reactor	1 kW	6 minutes	1000 °C	Char	10.7%	4%	16.5%	[141]
Sewage sludge	Multimode	Batch reactor	1 kW	6 minutes	1000 °C	Char	10.1%	3.0%	24.2%	[141]
Coffee hulls		Batch reactor	-	20 minutes	500°C	Char	30.20%	7.9%	61.9%	[192]
Pine wood sawdust				12 minutes	470°C	SiC	36.7%	22.7%	60%	[193]
Rice straw	Single mode	Batch reactor	300 W		407°C		28.07%	22.56%	49.37%	[194]
Corn stover		Batch reactor	700W	8 minutes	650°C		23.9%	33.72%	42.36%	[195]
Agricultural residues			2 kW		400°C		33.4%	20%	46.6%	[196]
Larch			1.5kW	18 minutes			21%	18%	60%	[145]
Aspen			875W	20minutes	450°C		25.2%	35.9%	38.9%	[197]
Rice husk			700W	20minutes	600°C		43%	22%	35%	[182]
Sugar cane bagasse	Single mode	Batch reactor	500W				18%	43%	40%	[184]

Waste coffee grounds	Single mode	Batch reactor	500W				21%	44%	35%	[184]
Bamboo leaves	Single mode	Batch reactor	500W				22%	44%	34%	[184]

Table 1.4-2 Compilation of results for the microwave pyrolysis of algal biomass

Algal Biomass	*Type of cavity*	*Type of reactor*	*Incident Power*	*Reaction time*	*Reaction temperature*	*Microwave absorber*	*%Solid*	*%Liquid*	*%Gas*	*Reference*
Chlorella sp.		Batch reactor	500 W	20 minutes	462°C	char	28%	26%	24%	[187]
Microalgae			250W		400°C		32.4%	23.1%	44.4%	[190]
Macroalgae waste					750°C		27.8%	35%	37.2%	[189]

1.5. PRELIMINARY CONCLUSIONS

The chapter on state of the art has provided the knowledge to understand the purpose and context of this thesis. It presented the generalities of microwave technologies, biomass, pyrolysis, and microwave pyrolysis, which led to understanding the experimental section presented in this research. The absence of the literature on microwave pyrolysis of Flax shives and Sargassum exposes the first axis of investigation.

Biochar, bio-oil, and the non-condensable gases from thermochemical processing of both lignocellulosic and algal biomasses acquired much significance recently due to their application and the percentages of chemical families present in their structure. When focusing on bio-oil production, the mechanism for decomposition of biomass components into simpler products must be understood to optimize the critical parameters that yield higher bio-oil and higher quality.

Also, the type of biomass affects the product yield and quality, the heating rate, and temperature according to the dielectric properties. The study of the physical and chemical properties of biomass and the behavior under microwave irradiation vs. devolatilization mechanism is recommended. The moisture of the biomass helps the heating rate but increases the water content in bio-oil.

The reactor design should allow a uniform distribution and contact of the microwave energy. The design of the microwave pyrolysis process is different from the design of conventional pyrolysis due to the different heating modes and other parameters that are not usually considered, such as the electric field distribution, the position of the guide waves, the power supplied, the dielectric properties of the material, the material of the reactor and the operation mode.

Chapter 2
Materials and Methods

2 MATERIALS AND METHODS

This chapter describes the methodologies used during the investigation to characterize the biomass and pyrolysis products and describe the microwave pyrolysis process used to obtain these products. The first part of the chapter describes the methodologies used to understand biomass behavior under microwave pyrolysis; methodologies such as thermogravimetric analysis and dielectric properties measurement. Then, the experimental pyrolysis setup and procedure are presented and the mass balance and product characterization. At the end of the chapter, the mathematical equations used to quantify the pyrolysis products, the chemical families presented in bio-oil, and the data analysis are explained. This chapter supports the next chapters, where the results will be presented and discussed.

2.1 CHARACTERIZATION OF BIOMASS SAMPLES

The samples for this study were Flax shives and Sargassum spp. The Flax shives and lignocellulosic biomass are provided by “La cooperative Terre de Lin” located in the Normandy region in France. The samples of Sargassum spp. were collected at the Punta Cana Beach in the Dominican Republic, then dried under the sun. After receiving them from the suppliers, the biomass materials were left open for air drying. Both biomass samples were ground and sieved at our laboratory “LSPC”, located in Rouen, France. The average particle size was between 300 and 400 μm.

2.1.1.1 Thermogravimetric Analysis

2.1.1.2 Description of apparatus and principle

The thermogravimetric analysis is a technique where the mass of the sample is monitored over time in a specified atmosphere (inert or oxidizing) in relation to changes in temperature. This measure can give information about the weight loss curve, changes in sample composition, and thermal stability, and can help obtain the thermal decomposition reaction's kinetic parameters. The thermogravimetric analysis experiments done during this investigation were performed in an SDT Q600-TA Instrument analyzer. The objective of the analysis was to evaluate the volatilization behavior of the two biomasses studied.

Figure 2 shows the equipment used. It is composed of a bifilar wound furnace, with two holders connected to a horizontal balance type dual beam, a Platinum/Rhodium thermocouple located in each holder to measure the temperature in situ, and a mass flow controller with automatic gas switching. The

balance sensitivity is 0.1 µg, and the temperature sensitivity is 0.001 °C. The temperature ranges from ambient to 1500 °C with a calorimetric precision of ±2%.

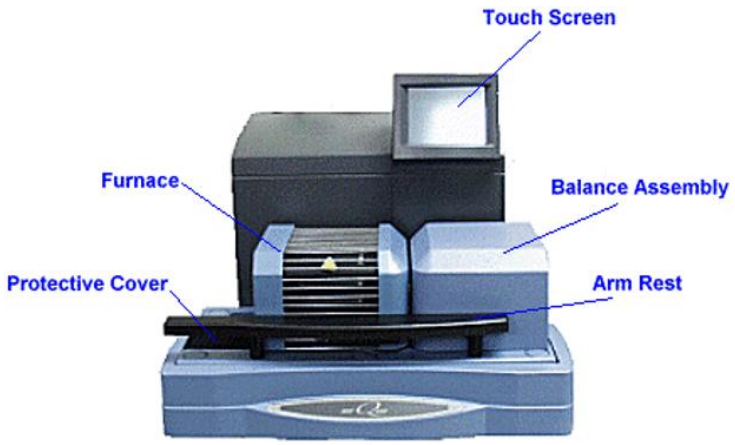

Figure 2.1-1. Thermogravimetric analysis equipment. SDT Q600-TA

The measurement is based on a sensitivity-calibrated balance. The mass difference of each holder, the standard, and the one with the sample to be studied is evaluated according to the changes in time, temperature, and gas flow. As the thermocouples are placed in each holder, it is possible to enable simultaneous signal output of temperature and weight simultaneously. The signals obtained are translated and solved to obtain information about the behavior of the sample in a programmed environment.

2.1.1.3 Protocol analysis for a thermal decomposition study

During this investigation, two biomasses were evaluated in terms of thermal decomposition behavior in an inert environment. The biomass samples were, Flax shives and Sargassum. The sample size was kept around 8 and 15 mg. Nitrogen was used as inert carrier gas under a flow rate of 50 ml min^{-1}. The heating rate varied from 2 up to 200 ˚C min^{-1} in a temperature range from room temperature up to 1000 ˚C.

The samples were introduced at room temperature and atmospheric pressure. The heating rate program included a temperature ramp at a desired heating rate followed by five minutes of isothermal conditions at 1000 ˚C and then proceeded to cool down the furnace. All the experiments were repeated three times to have an average value and to test the repeatability of the experimental conditions. The figure 3 shows the data obtained from the TGA experiment. The graphic presents the evolution of the percentage of weight according to the evolution of temperature and the weight derivative, but also it is possible to have the evolution in time.

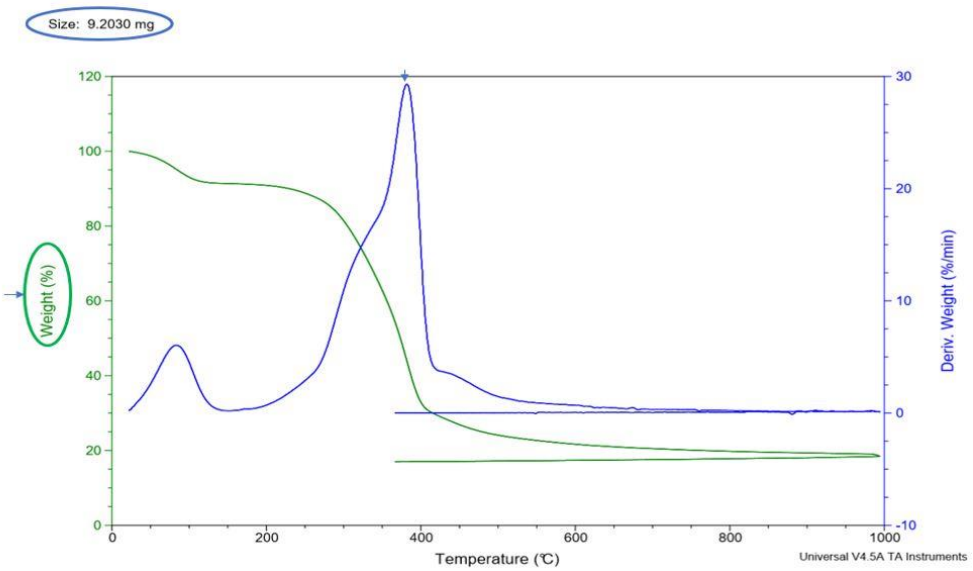

Figure 2.1-2. Example of TGA graphic results

2.1.1.4 Proximate analysis

The proximate analysis covers the determination of moisture, volatile matter, fixed carbon, and ash of biomass. During this study, the proximate analysis was performed by thermogravimetric methodology, which measures weight changes in a material with temperature. This analysis estimates the biomass efficiency for the thermal conversion system as pyrolysis. It is important to remind that a parameter such as heating rate and carrier gas is critical to have proper data when using a TGA method. The procedures used are described in the American Society for Testing and Materials (ASTM) standard. The proximate analysis was performed in an SDT Q600-TA Instrument analyzer with thermogravimetric programming, which considered two different analysis steps and a default sample mass of 10±1 mg. The first step was conducted under an inert atmosphere to obtain the moisture and volatiles content values, and the second one under an oxidizing atmosphere to determine the fixed carbon content and the ash. The protocol performed is validated by the ASTM standards method: D1102-84[198], E872-82[199], and E871-82 [200].

As presented in figure 2.1, the first step of the analysis was conducted under nitrogen with a gas flow rate of 50 ml min-1. During this step, the moisture and volatiles content was determined. For moisture content determination, the heating step was up to 110 C with a hold time of 15 minutes. Then, the temperature was increased up to 600 °C for volatiles determination with a hold time of 30 minutes. When the mass stabilization was completed, the carrier gas was switched from nitrogen to air, which started the second step. In this step, fixed carbon and ash were determined.

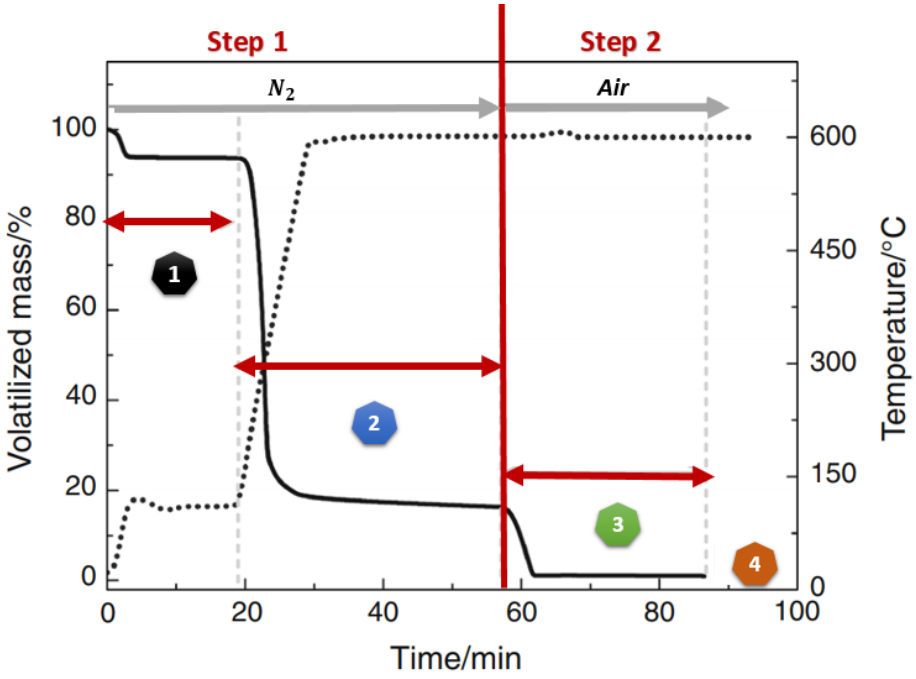

Figure 2.1-3. General scheme of proximate analysis method based on thermogravimetric analysis

In figure 2.1-3, it is shown the changes in volatilized mass by time and temperature. The first mass loss is due to the vaporization of the water, which allows determining the moisture content. The second mass loss is due to degradation of the organic matter with temperature (volatiles content). The combustion of fixed carbon causes the third variation in weight. The final step (number four in figure 2.1) is the final residue representing the biomass sample's ash content.

2.1.2 Dielectric properties measurement

2.1.2.1 Description of apparatus and principle

The measurement of the interaction between the matter and the electromagnetic field at microwave and radio frequencies is defined as dielectric measurement. The phenomena occurring during the interaction between electromagnetic waves and materials are briefly presented in chapter 1. In general, each material has different and inherent dielectric properties, which depend on temperature, frequency, pressure, etc. [11].

For microwave heating purposes, the measurement of interest is the interaction of the matter with the electric field, also called permittivity. This value is expressed as a complex number. The real part describes the potentiality of energy storage of the sample measured, and the imaginary part describes the energy losses or the ability to convert the energy into heat [11].

The study of these properties is a compulsory step toward understanding the dielectric behavior of the biomass during microwave heating [201].

To measure the dielectric permittivity, there are different commercial methods available. A coaxial line measurement technique was employed to obtain the dielectric permittivity data from the biomass and pyrolysis products (bio-oil and char). The equipment employed consists of an Agilent network analyzer N5230A PNA-L with an 85070E Dielectric Probe Kit. This system allows measurements within a frequency range from 0.01 to 50 GHz. This system is well-known for its simplicity and usefulness when measuring dielectric properties for solids and liquids samples of medium and large losses (tanδ>0.05, where tanδ= $\varepsilon''/\varepsilon'$).

The permittivity is measured by immersing the probe into a liquid sample or touching the flat face of a solid material. When the probe is in the right position, the measurement starts when the network analyzer sends an incident wave signal to each frequency point within the frequency range. The reflective wave, which is the reflected part of the incident wave that interacted with the sample, is analyzed by the network analyzer giving a measure response (permittivity) at the frequency range tested.

Before the measurement, a three-term calibration is required using a shortcut, air, and distilled water at 25°C as standards. The calibration corrects the measurement errors, but it is mandatory to avoid cable instability, air gaps, or inadequate sample thickness/volume.

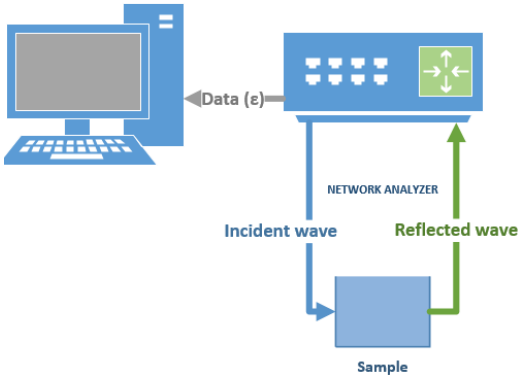

Figure 2.1-4. Dielectric properties measurement general scheme

2.1.2.2 Protocol

The protocol includes three main steps. Sample preparation, calibration, and measurement. The three of them are important to have a reliable measurement data. The preparation step is different between solid and liquids. In the case of liquids where the slim probe is used, a five millimeter of immersion inside the sample is required as a minimum and around the tip of the probe. In case of solid samples, a minimal thickness of $\frac{20}{\sqrt{\varepsilon^*}}$ millimeters where $\varepsilon^* = \sqrt{\varepsilon'^2 + \varepsilon''^2}$ with a particule size smaller than 0.3 millimeters, is required.

The sample is placed in contact with the probe and the calibration step is done for both type of probes, the high temperature and slim probe. The calibration is done using air, distillated water and shortcut. After the calibration is completed, a measure of air and distillated water is performed to compare the results of permittivity with the literature standards values and assure the accuracy of the measure. After confirming the accuracy, the measure is performed and repeated three times to have a repeatability.

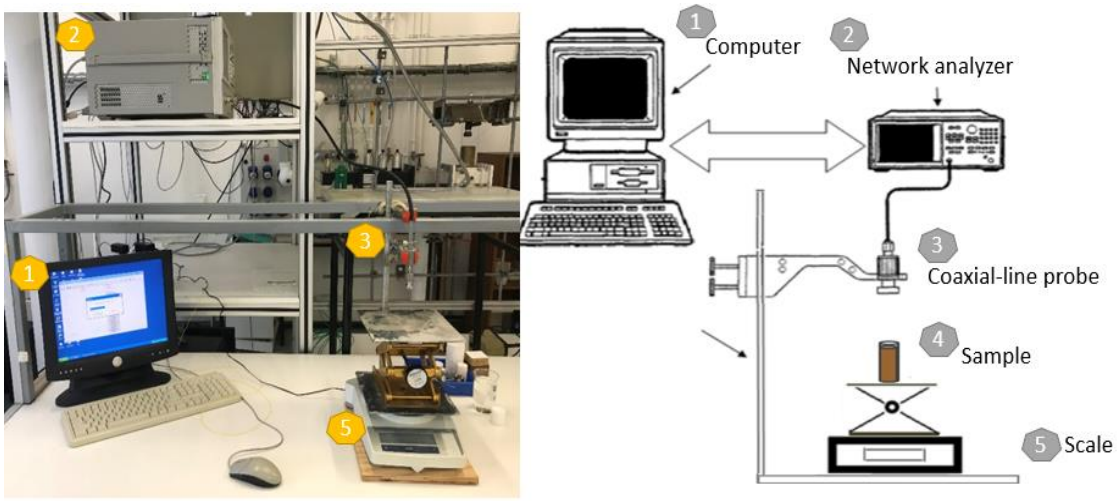

Figure 2.1-5.Dielectric measurement instrument

2.2 MICROWAVE PYROLYSIS EXPERIMENTS IN A ROTATORY REACTOR

2.2.1 Description of apparatus and principle

The figure 2.6 shows the experimental setup used to perform the microwave pyrolysis in batch conditions. The experiment was performed using a single-mode cavity microwave to guide the microwave energy generated by a SAIREM magnetron at a frequency of 2.45 GHz and a power between 0 and 2000 watts and through a standard WR430 waveguide. To measure the energy absorbed by the system, the incident and reflected waves were recorded using a system composed by two bolometers connected to a wattmeter box. In addition, a system of three manual sliding short-circuit was connected to the waveguide to assure the impedance matching, in other words, to maximize the interaction between the reactor and the microwave energy.

The pyrolysis reaction took place in a rotatory kiln quartz reactor placed horizontally inside the cavity and set to rotate at 65 rpm at atmospheric pressure. The quartz reactor is a cylinder of 17 cm of length and 3 cm of internal diameter. The temperature inside the reactor vessel was measured using a thermocouple type K sensor and the temperature at the surface was recorded using an optical fiber. To maintain an anoxic atmosphere, a flowrate of nitrogen was maintained during the experiment.

A set of three condensers in series at a constant temperature of -14 °C was connected to the rotatory reactor to condensate the volatiles compound produced during the pyrolysis reaction, and the non-condensable gases were recovered in a sampling bag to be later analyzed. The data recollected during the experiment, such as temperature, incident and reflected power were recorded in time by using a LabVIEW program.

2.2.2 Protocol

For each pyrolysis experiment, a weighed quantity of biomass and 20 percent in mass weight of silicon carbide are mixed and added to the quartz reactor and then fixed in the position with the help of quartz wool. When the reactor was filled, the reactor was placed horizontally inside the microwave cavity and connected to a motor which ensured the rotation of the reactor. Then the gas inlet, output, and condenser were connected. When the experimental set-up was completed, the reactor was purged with a maximum nitrogen flowrate allowing the reduction of the oxygen content inside the reactor, and then the nitrogen flow rate was adjusted to the desired value.

To measure the temperature at the surface, an optical fiber was placed in contact with the outer surface of the reactor. A thermocouple was used to measure the initial temperature inside the biomass bed and took off before turning on the microwave power.

The microwave power was turned on after setting the required incident power. When starting the microwave heating, the adjustment of the sliding short-circuit was made to minimize the reflected power. The heating time was measured, and after reaching the required time for pyrolysis, the microwave power was turned off. When turning off the microwave power, a thermocouple was immediately introduced inside the reactor to measure the final biomass/char bed temperature.

The solid left in the reactor was collected, as well as the bio-oil condensed in the set of condensers by flushing all the glassware with acetone and collecting the final solution. The gas was collected in a sampling bag. The bio-oil recovered at the end of the experiment was analyzed by GC-FID and the gas by a GC-FID/TCD method.

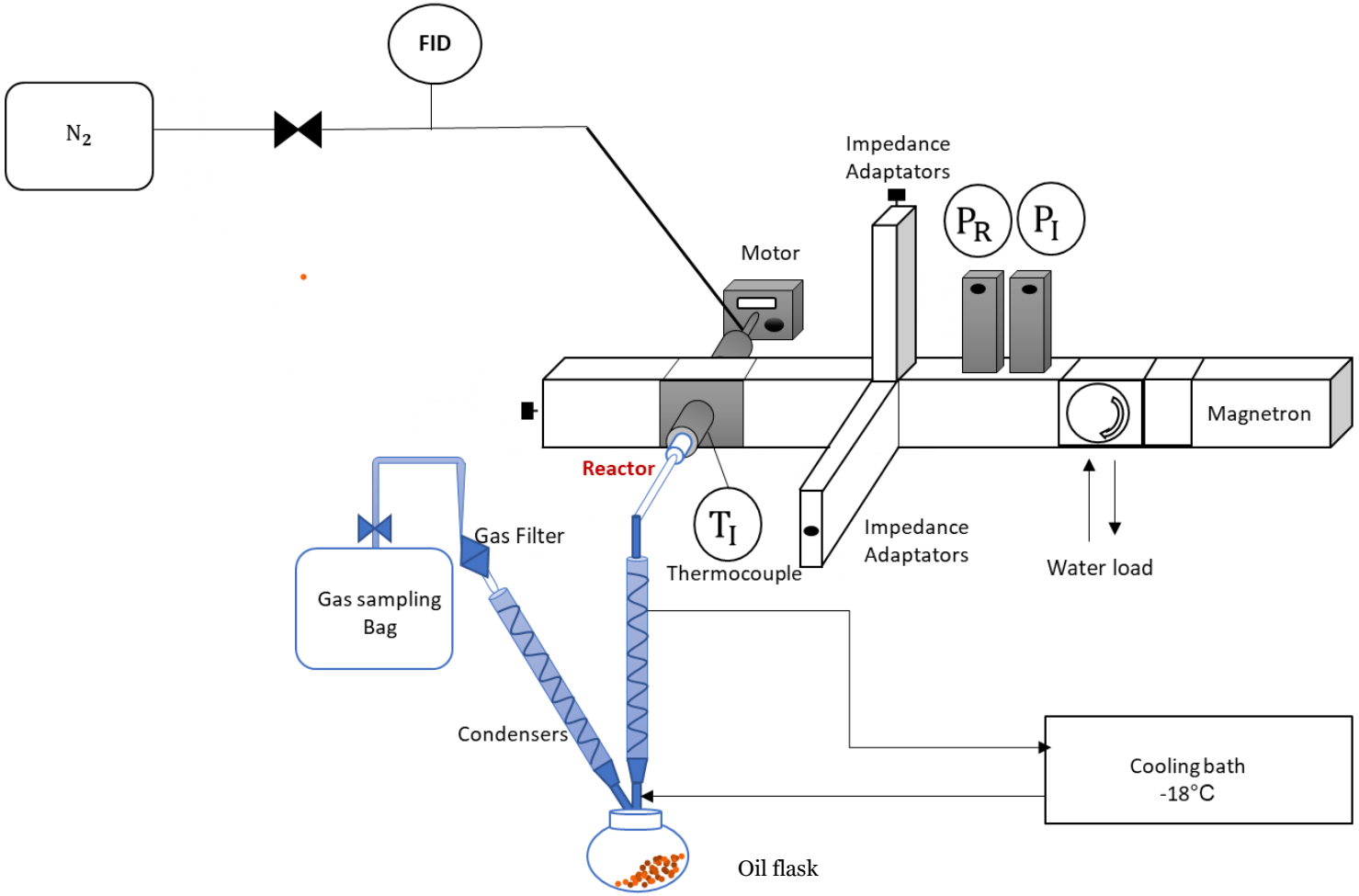

Figure 2.2-1 Microwave pyrolysis set-up scheme

Figure 2.2-2 Photo of the microwave pyrolysis set-

2.3 CHARACTERIZATION OF PYROLYSIS PRODUCTS

The products of pyrolysis are influenced by the properties of the biomass used to be produced, not only by that but also by the operating condition such as heating rate, the residence time of the vapors, final temperature, and microwave power used.

Part of developing a microwave pyrolysis process is to identify the characteristic of the products obtained to select the optimal conditions that yield the highest quantity of the product desired with the best quality possible. In this context, chromatography is an analytical technique employed to examine the liquid and gas product obtained to correlate the operating condition used with the final characteristic found in the products. In this section, the chromatography methods used are going to be described, as well as the protocols employed.

2.3.1 GC-MS

The analysis and identification of the recovered pyrolysis products (gas and bio-oil) was performed using a gas chromatograph-mass spectrometer instrument. For the liquids, the samples were injected via an autosampler onto a capillary column which is inside the GC-MS (Varian 3900-Saturn 2100T). The sample molecules were separated either by electron or chemical ionization and the analyzed according to their mass/charge ratio. The column used was a VF-1701ms commercialized by Agilent with a film thickness equal to 60 m × 0.25 mm × 0.25 μm.

The temperature program used started with a temperature in the oven at 45 °C for 4 minutes and then heated by performing a heating rate of 4 °C min^{-1} until reaching a temperature of 280 °C. The final temperature was held for 20 minutes. Helium, an inert gas, was used as a carrier gas with a constant flowrate of 1 mL/min. 1 μL of the bio-oil/acetone solution was injected into a split injector with split ratio 30:1 and heated at 250 °C.

The electron ionization energy to perform the mass spectrometer was 70 eV. The chromatogram was obtained by performing a full scan mode and the library used to identify the analyzed components was the Varian Worsk Station and NIST 2002 software. The peaks were identified by comparing the mass spectrum obtained to mass spectra from the NIST library and selecting the one which fit the best.

The sample of gases were also analyzed, and the product identified by GC-MS. The equipment was a PERKIN Clarus 580+SQ S8S. The column used was a Restek RTQ Bond t with a film thickness equal to 30 m × 0.25 mm × 8 μm. The temperature program used started with a temperature in the oven at 35 °C and then heated at a heating rate of 10 °C min^{-1} until reaching a temperature of 280 °C. The final temperature was held for 20 minutes. Helium, an inert gas, was used as a carrier gas with a constant flowrate of 0.8 mL/min. 500 μl of the gas sample was injected into a split injector with split ratio 10:1 and heated at 280 °C. The chromatogram was obtained by performing a full scan mode and the library used to identify the analyzed components was the Varian Work Station

2.3.2 GC-FID

After identifying all the components presents in the bio-oil by using GC-MS, the characterization of the bio-oil samples diluted in acetone of each pyrolysis experiment was analyzed by using a chromatograph instrument with a flame ionization detector, GC-FID, type Scion 456-GC Bruker. The column used was the same as in the GC-MS, a VF-1701ms commercialized by Agilent and the temperature program was also the same as the one employed at the GC-MS analysis. Depending on the sample, a number between 200-300 species were identified by this method and then classified in chemical families according to the principal functional group of the compound. The characterization method of the bio-oil is explained further in section 2.4.3.

2.3.3 GC-FID/TCD

The non-condensable gases were analyzed by using a gas chromatograph instrument commercialized by Perkin Elmer, type Clarus 580. Equipped with a Shincarbon st 100 120 column, a hydrogen generator and a methaniser. Also, the instrument has two different detectors, one of flame ionization (FID) and other of thermal conductivity (TCD). The compounds detected are H_2, N_2, CO, CO_2, and the carbonated components.

The gas sample was connected to the instrument. The analysis last 15 minutes and then the chromatogram was exploited by integrating the peaks obtained. Those peaks were already identified, and the peak area were correlated to a calibration curve done for each component detected. The result from the treatment was a component volumetric yield.

2.4 CALCULATIONS

2.4.1 Volatilization kinetics of biomass

To exploit the volatilization kinetics, a single reaction model was assumed. The kinetic parameters are based on the determination of the pre-exponential factor, activation energy and reaction order. The Kissinger method was used to calculate the kinetic parameters. This method is extensively used in literature when the case is a monomolecular solid and the reaction mechanism is assumed to be a one step or single reaction mechanism.

The hypothesis for the system studied during this thesis was a singles reaction mechanism:

Equation 29 : Single reaction mechanism

$$C_xH_yO_zN_xS_y \longrightarrow \text{Volatiles} + \text{Char} + \text{Ash}$$

The mass loss of the sample is used to calculate the conversion rates and is defined as

Equation 30 : Conversion rate

$$\alpha = \frac{m_T - m_f}{m_0 - m_f}$$

Where m_T is the mass at a specific temperature in kilograms, m_o is the initial mass and m_f is the final mass. The reaction rate can then be expressed by the following relation:

Equation 31 : Reaction rate

$$\frac{d\alpha}{dt} = k(T)f(\alpha)$$

Where k (T) is the rate constant and f (α) is the most commonly used kinetic model for the solids volatilization. The latter terms are defined as follows and are also used to obtain the kinetic parameters: exponential factor and activation energy.

Equation 32: Rate constant and kinetic model

$$\begin{cases} k(T) = A \times \exp\left(\frac{-E_a}{RT}\right) \\ f(\alpha) = (1-\alpha)^n \end{cases}$$

Where A is the pre-exponential factor (in s-1), Ea is the activation energy (in kJ.mol-1), R is the ideal gas constant (8.314 JK-1.mol-1) and n is the order of the reaction.

The final form of the biomass decomposition kinetics for the two models described below is written as follows:

Equation 33 : Biomass decomposition kinetics

$$\frac{d\alpha}{dt} = A \times \exp\left(\frac{-E_a}{RT}\right)(1-\alpha)^n$$

To determine the kinetic parameters, a right kinetic model adapted to the experimental conditions must be chosen. In the case of fast pyrolysis, the free kinetic models such as Kissinger and the iso-conversational method are generally considered. The kinetic parameters are calculated based on variations in heating rates, and in the case of the free models, specific knowledge of the reaction mechanism is not required.

2.4.1.1 Kissinger method:

The Kissinger method is the most widely used method for mono-molecular solids. The decomposition of biomass can be modeled as a single reaction as expressed before and mathematical relationship for this case is written as follows:

Equation 34 : Kissinger method

$$\ln\left(\frac{\beta}{T_{max}^2}\right) = \frac{-E_a}{RT_{max}} + \ln\left(\frac{AR}{E_a}\right)$$

Where β is the reaction rate and Tmax is the temperature of the maximum peak of the DTG dα / dt curve of the ATG analysis.

This method is based on determining the temperature Tmax corresponding to the maximum reaction rate. However, this relation gives global kinetic parameters. The detailed decomposition kinetics of biomass, according to three parallel and independent reactions of cellulose, hemicellulose, and lignin, are carried out using the Tmax of each pseudo-component (cellulose, hemicellulose and lignin).

2.4.2 Microwave pyrolysis mass balance

The section 2.4.2 explained the protocol used to perform the microwave pyrolysis of biomass. After each experiment, the products were collected in different points of the experimental set-up. The gas was collected in a sampling bag at the exit of the condensers set-up, the bio-oil was gathered by washing all the condensers with acetone and the char, was the remaining solid in the reactor.

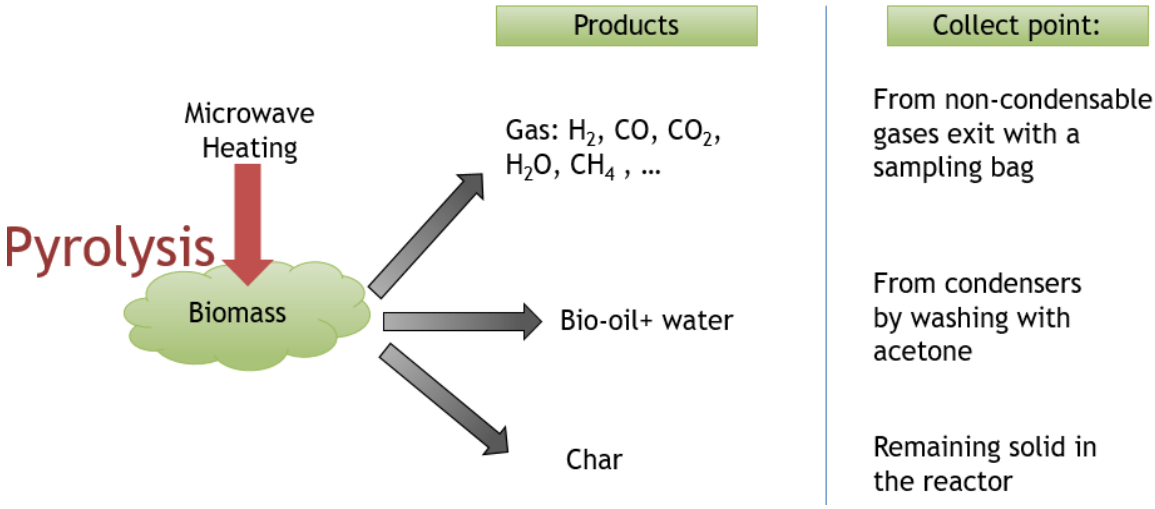

Figure 2.4-1. Microwave pyrolysis products collect point

The mass balance was done by weighing the solid and liquid (bio-oil without acetone) products. The mass of the gases was determined by using the GC-FID/TCD analysis. After having the volumetric yield obtained in the GC-FID/TCD results for nitrogen and all the gases detected (H_2, N_2, CO, CO_2, C_2H_2, C_2H_4, C_2H_6, C_3H_2, C_3H_4 and C_3H_6), the mass of each gas was obtained as a derivate calculation from the total nitrogen volume used and the density of each gas.

Equation 35: Global pyrolysis mass balance

$$Mass\ balance = mass\ char + mass\ \ bio - oil + mass\ \ gas$$

$$Weight\ gas = \sum volume_{xi}\ (ml) * \rho_{xi}\ (\frac{gr}{ml})$$

Where x_i = H_2, N_2, CO, CO_2, C_2H_2, C_2H_4, C_2H_6, C_3H_2, C_3H_4 and C_3H_6.

2.4.3 Characterization of bio-oils

The first step on the bio-oil characterization is the identification of components by GC-MS as explained in section 2.5.1. This step is followed by the quantification of components. To quantify the components, the bio-oil samples are analyzed by GC-FID with the protocol presented in section 2.5.2. The characterization of bio-oils follows a cascade of event described in the following scheme:

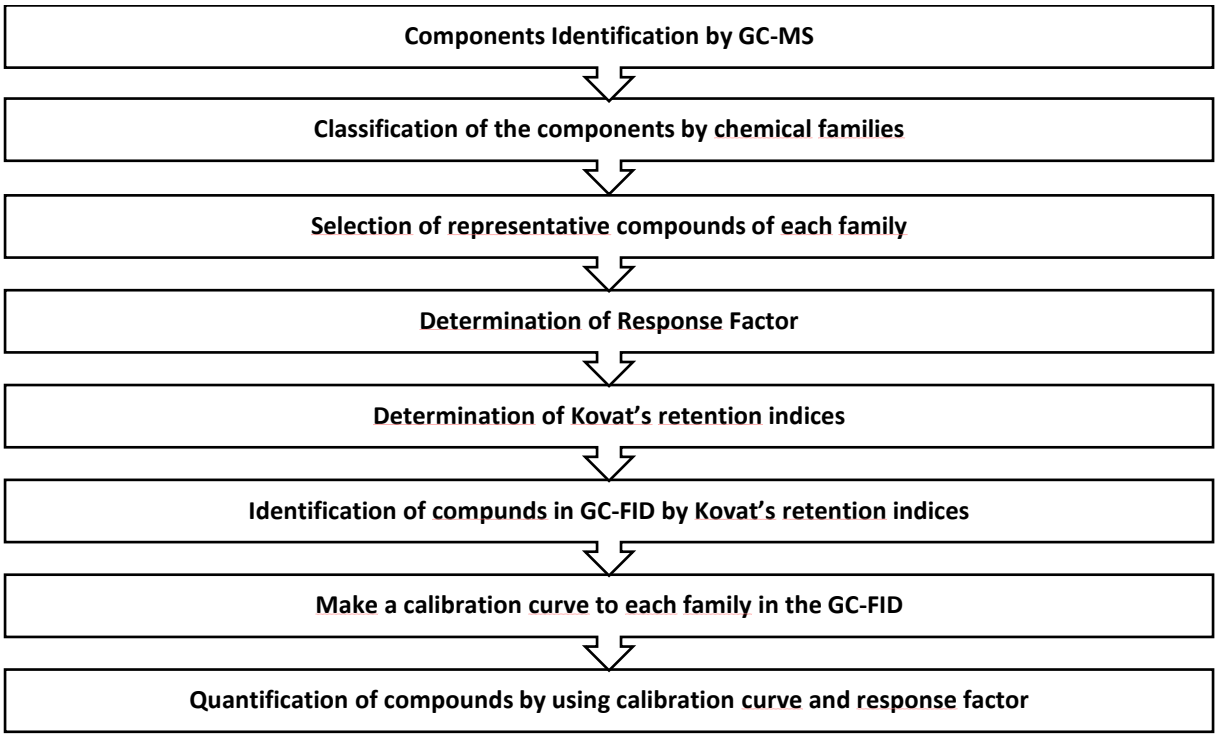

Figure 2.4-2. Process scheme of bio-oils characterization

The first step in the bio-oil characterization process is to detect the compounds in the GC-MS and group them into chemical families as shown in table 2.4-1. From each family, a representative component was chosen. The purpose of the representative component was to calculate a response factor for each component detected in the same family and then to be able to quantify the component later.

The response factor is calculating by correlating the molecular weight and the effective carbon number by the following equation:

Equation 36 : Response factor

$$\frac{Molecular\ weight\ xi * ECN\ standard}{Molecular\ weight\ standar * ECN\ xi}$$

Table 2.4-1 Chemical families and representative compounds in bio-oil

Chemical Family	Representative compound
Carboxylic acids	Acetic acid
Esters	Allyl butyrate
Amides	Benzamide
Aromatics	Dodecene
Furans	Furan
Aldehydes	Furfural
Sugars	Levoglucosan
Phenols	p-cresol
Alcohols	Phenol
Alkanes	Dodecane
Ketones	2-cyclopenten-1-one
Guaiacols	methyl-4-methylcatechol

Where the standard is the representative component of the family, xi is the component detected and the ECN is the effective carbon number. This method is explained in the literature by Scalon and willis, 1985[202].

The next step was to calculate the Kovats's retention indices of the identified components. This number helps to relate the component identified at GC-MS with their retention time in the GC-FID. The retention indices are calculated by linking the retention times of a reference compound, in this case alkanes, with the retention time with the identified components in both instruments GC-MS and GC-FID.

In order to obtain the standards retention times in the GC-MS and the GC-FID, alkanes from C_7 up to C_{20} are injected in both instruments. Once obtained the standard retention time, the Kovats's retention

indices can be calculated for each component identified in the GC-MS and the GC-FID. For an identified component, even if the retention time is different in both instruments, the value of Kovats's retention indices is the same independently of the instrument used. This method allows to find a component detected in the GC-MS, in the GC-FID spectrum.

The Kovat's retention indices are calculates as following:

Equation 37 : Kovat's retention indices

$$100 * N.C\ Standard\ \ 1 + \frac{Retention\ time\ xi - Retention\ time\ of\ std\ 1}{Retention\ time\ of\ std\ 2 - Retention\ time\ of\ std\ 1}$$

Where N.C. Standard 1 is the number of carbon atoms of the smaller alkane used as standard (std1), the standard 2 is the largest alkane used as standard (std 2) and xi is the component identified. The retention time of the component identified is in between the retention time of the two alkanes.

After identifying the components in the GC-FID spectrum, the following step is the quantification of the components and families. First, a calibration curve of six points using the representative component of each family is done. The calibration curve was obtained by injecting different diluted samples of the representative components to the GC-FID. The peak area obtained from each component was related its concentration in the sample injected. The samples were prepared by diluting a mother solution into six daughter solutions at six different concentrations. The mother solution was prepared by mixing 1000µl of liquid sample into 3000µl of ethanol. This solution was then transferred to a GC vial and sealed with a PTFE/Silicone septum. Dodecane was used as internal standard and the five daughter solutions had a gap of ten milliliter between them.

For the analysis of each sample, 3µl of sample was injected with a split ration of 1:20 to the GC and a column flow of 1ml/min. The temperature program started with an initial temperature of 40 °C held by four minutes and then heated to 200 °C with a heating rate of 1.3 °C/min. Then the heating rate was increased to 2.7 °C/min up to 300 °C followed by a holding period of 1 hour.

After having the calibration curve with a determination coefficient superior to 0.98, a calibration equation was obtained. The calibration equation is type Ax+ B, where A and B are constant obtained from the calibration curve and x is the peak area of the component acquired from the GC-FID analysis. The concentration in mol/ml of each identified compound was found by multiplying the response factor of the component with the calibration equation results.

Once the components are identified and quantified, the results are presented in percentage of each family. The chemical family distribution depends on the amount in mass of compound produced during the pyrolysis reaction which are also influenced by the operating conditions. The characterization of the

bio-oil samples is done to each experiment performed in order to study the changes on the bio-oil composition according to the changes in the operating conditions.

2.4.4 Microwave total effective energy

When using microwave processes, one of the key points is the power absorbed evaluation. Both the incident power and the reflected power during the pyrolysis experiment are recorded during time. The absorbed power is calculated by the difference between the incident and reflected power.

As the performance of the incident and reflected power changes with the changes in the biomass bed during the pyrolysis reaction, the total effective energy which does not depend on the changes on the incident and reflected power over the time, it is calculated for every experiment. The total effective energy is expressed as by:

Equation 38: Total effective energy

$$E = \int_{t0}^{tf} Pabsorbed\ dt$$

2.4.5 Principal Components analysis

The principal components analysis (PCA) is a variables' reduction method for large data sets which allows to have a smaller dimensional graphic that contains most of the information of the original variables data set. The purpose of this analysis is to understand the correlations between variables and at the same time the amount of variance of each variable. This analysis allows to see tendencies in data sets that have many different variables with or without evident relation between them. This analysis is used to study the tendencies between the product's compositions and operating conditions for both of biomasses, Flax shives and Sargassum. To better understand the PCA analysis, an example will be presented during this section. The PCA analysis starts with the standardization of the range of initial variables so that each one of them contributes equally to the analysis. (See table 2.4-2).

Table 2.4-2 PCA Standardization step

Variable	Observations	Minimum	Maximum	Average	Standard deviation
H_2	4	0,032	0,035	0,033	0,002
CO	4	0,587	0,607	0,593	0,009
CH_4	4	0,069	0,081	0,074	0,005
CO_2	4	0,289	0,309	0,301	0,009
C_2	4	0,013	0,038	0,029	0,011
C_3	4	0,007	0,013	0,011	0,002
Final Temperature	4	570,000	820,000	698,383	114,568

Once the standardization is done, a covariance matrix is calculated. The objective of the covariance matrix is to understand the correlations between the input variables. The relevant information on the covariance matrix is the sign of the covariance; positive sign means that the two variables increase or decrease together (positively correlate), the negative sigh means that the variables are inversely correlated.

Table 2.4-3 PCA- Pearson covariance matrix

Variables	H_2	CO	CH_4	CO_2	C_2	C_3	Final Temperature
H_2	**1**	**0,984**	-0,591	-0,859	0,615	**-0,987**	0,726
CO	**0,984**	**1**	-0,588	-0,874	0,538	**-0,975**	0,786
CH_4	-0,591	-0,588	**1**	0,122	-0,909	0,711	-0,895
CO_2	-0,859	-0,874	0,122	**1**	-0,130	0,775	-0,416
C_2	0,615	0,538	-0,909	-0,130	**1**	-0,709	0,686
C_3	**-0,987**	**-0,975**	0,711	0,775	-0,709	**1**	-0,814
Final Temperature	0,726	0,786	-0,895	-0,416	0,686	-0,814	**1**

The matrix allows to obtain the eigenvectors and eigenvalues to identify the principal components. The characteristic vectors represent the direction of the axes including the higher amount of information. They are also called Principal components. The eigenvalues are the coefficients attached to eigenvectors, which give the amount of variance carried in each eigenvalue. In the example there are three characteristic vectors (eigenvectors), and the F1 and F2 includes the maximum amount of useful information to understand the input variables correlations.

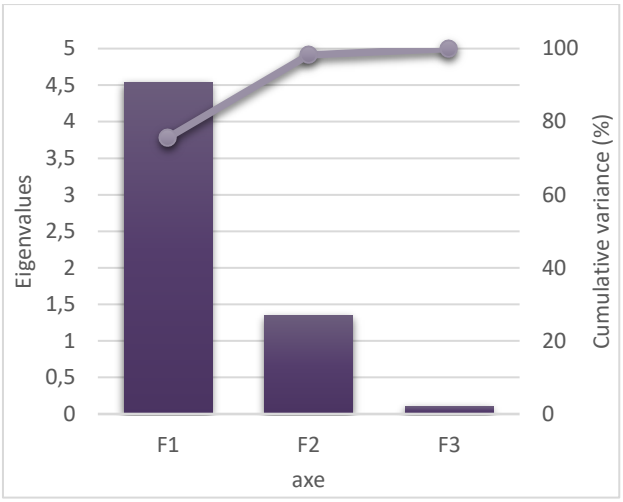

Figure 2.4-3 PCA Eigenvectors and eigenvalues

The eigenvalues or principal components are new variables constructed by the linear combinations of standardized input variables. The PCA tries to put the maximum amount of information into the first vector and the remaining information in the others until covers all the information available. Normally, the first two vectors are chosen to produce a two dimensions graphics, providing a best angle to see and evaluate the initial data. In figure 2.4-4 , the PCA plot is presented. To understand the graphics, the following keys should be considered:

- The larger the variance carried by a line, the larger the dispersion of the data points along it,
- The larger the dispersion along a line, the more the information it has.
- Acute angles represent positive correlations,
- Obtuse angle, negative correlations
- Right angle, not relevant correlation

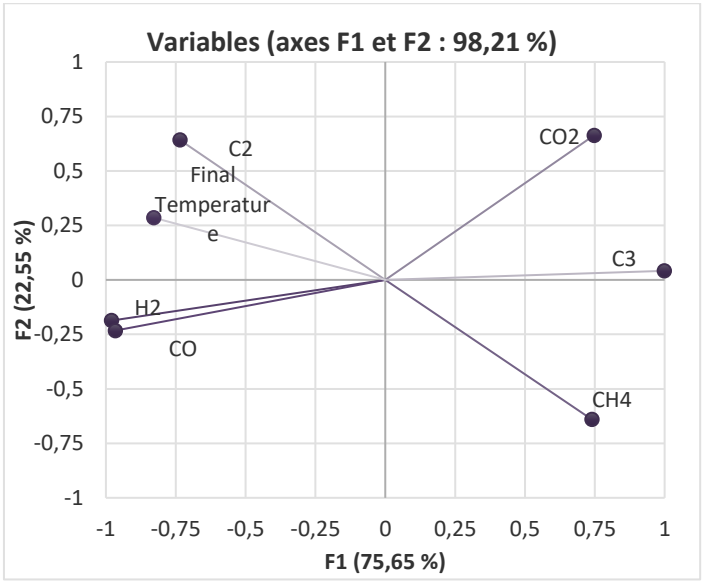

Figure 2.4-4 PCA graphic

2.5 MICROWAVE THERMOGRAPHY

2.5.1 Description of the apparatus and principle

Once chosen the wave propagation mode, the screening of the electric field distribution must be done. For that, a simple and inexpensive technique is available. Thermography consists in mapping the microwave electric field intensity by using a thermal paper. The latter technique can be a preamble to have some preliminary results that can help on the process scale-up development.

The waveguide couples the generator to the applicator. The applicator is designed to create a favorable EM field distribution around the material to be irradiated. The wave propagation mode is an electrical transverse mode TE11. The TE11 propagation mode is characterized by a uniform and circular polarization according to the diameter, and this particularity leads to improvement in the uniformity of the electric field across the section of the dielectric, as well as heating larger workloads.

The basic reactor structure to be studied is composed by a cylindrical cavity of 600 mm of length with an internal diameter of 100 mm. The transition element that connects the rectangular waveguide with the cylindrical cavity has 375 mm of length. Beside this element, a shaftless spiral is placed inside of the cylindrical cavity to ensure the passage of the biomass through the reactor. The combination of the cylindrical cavity and the shaftless spiral it is like a screw conveyor. (Fig 2.5.1)

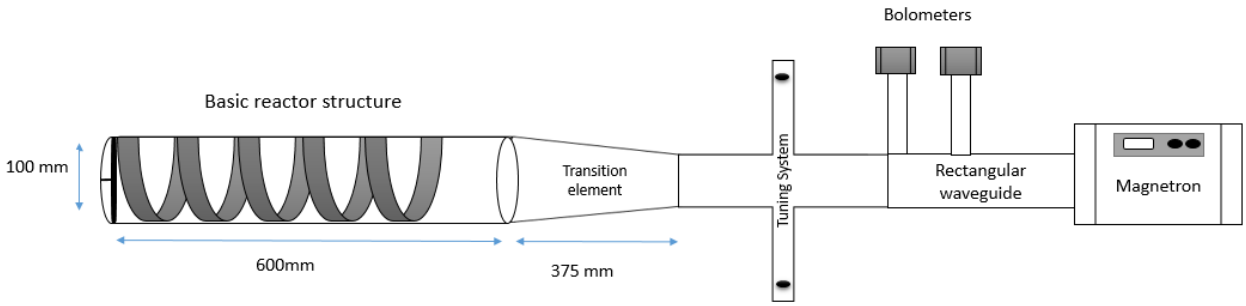

Figure 2.5-1 Basic reactor structure

To record the mode pattern inside the cavity, a piece of thermal sensitive paper is placed between two pieces of cardboard and fixed inside the cavity along its length. The cardboard will heat up when encountering the electric field, and the thermal paper changes its color from white to black due to the temperature rise. The time of contact and the incident power must be tuned to avoid spots too dark or not visible. After an adequate time of contact with established incident power, the power generation is turned off, and the paper is removed to be analyzed. The figure below presents examples of thermography using the method later described.

The black spots are generated where the intensity of the electric field is the highest, but because of thermal transfer, the spot can be spread in the thermal sensitive paper. For this reason, it is vital to have the right time of irradiation.

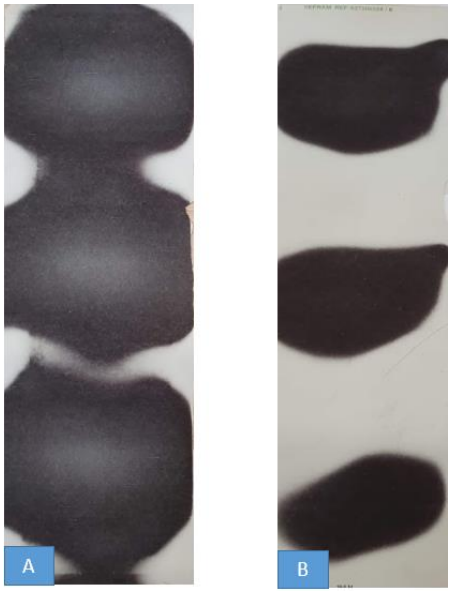

Figure 2.5-2 Example of thermography result A.Thermography using and incident power of 900 watt and a time of contact of 20 seconds. B.Thermography using and incident power of 900 watt and a time of contact of 10 seconds.

Two different types of shaftless spirals was tested and at the end, the cavity/reactor, filled with various workloads of biomass. (See figure 2.5-3)

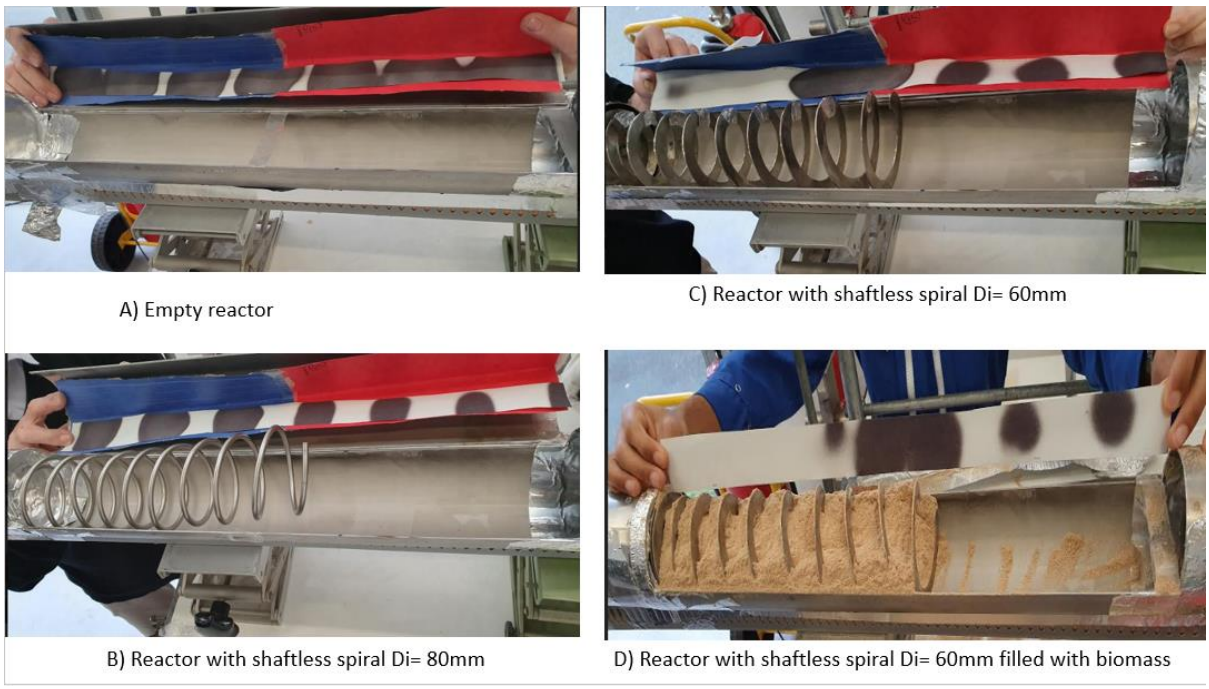

Figure 2.5-3. Different configurations tested on the thermography analysis.

Figure 2.5-4. Placement of thermal paper inside the cavity

2.6 PRELIMINARY CONCLUSIONS

The different methods used during the thesis are explained in this chapter. Starting with the characterization of biomass samples in terms of elemental compounds, volatilization kinetics, and dielectric properties, which served to better understand the base of the microwave- biomass interaction related to pyrolysis reaction.

This technique is particularly useful because the volatiles produced are the same as the volatiles obtained during pyrolysis by applying the right temperature/carrier gas program. In this way, the characterization of the bio-oil obtained is reliable. After obtaining the chromatogram, a mass spectral library is used to identify each peak.

The second step of the experimental methodology was the description of the pyrolysis reaction protocol in a semi-batch reactor and the characterization of the products. The results from these sections will be presented in chapter 4 and the influence of the relationships between the variables studied.

Finally, thermography, the physical mapping of the electric field, was described to study both the electric field mapping and the biomass-microwave interaction. These methods are fundamental for the discussion of chapter 5.

CHAPTER 3
Biomass and pyrolysis' products characterization

3 MICROWAVE PYROLYSIS: PRELIMINARY STUDIES

The chemical structure, the major organic compounds, the thermo-chemical decomposition behavior, and the dielectric properties of biomass have a strong influence on the development of a microwave pyrolysis process. Similarly, the choice of the right operating conditions. Before studying the wave matter interaction during the pyrolysis reaction, there are preliminary studies to be done.

First, in this chapter, biomass, as well as the products obtained by pyrolysis, are characterized. Then, the devolatilization behavior in an anoxic atmosphere is studied to understand the influence of temperature in the decomposition reaction. After evaluating the latter, the evolution of the microwave receptivity in a changing biomass load is considered by analyzing the dielectric properties of biomass with different humidity percentages, the bio-oil, and finally, the biochar. This gives us a general idea of how the feedstock will behave concerning the wave-matter interaction during microwave-assisted pyrolysis.

The products obtained by pyrolysis are also studied in terms of chemical families. The percentage of chemical families in the bio-oils and non-condensable gases gives a notion of the utility of the products for the chemical or energy industry. Also, the results are compared with literature.

3.1 BIOMASS ELEMENTAL AND PROXIMATE ANALYSIS

The total C, H, and N contents were measured on sub-samples using an elemental analyzer Flash 2000 (Thermofisher Scientific) in an external laboratory. The results are presented below:

Table 3.1-1 Elemental Analysis[1]

Elemental analysis (% w: w)				
Flax shives	Carbon	Hydrogen	Nitrogen	Oxygen
	45.70	5.77	0.41	48.12
Sargassum	26.62	2.97	1.65	NM*

*NM = Not measured

In the case of Flax shives, there are not reference values for C,H,N and O contents, however it was found similarities to other lignocellulosic biomass (beech wood) presented in literature [124] [8]. Concerning Sargassum, there are many different families, and as expressed in chapter one, the Sargassum used during this thesis is the Sargassum Natans from the Caribbean coast at Dominican Republic.

Table 3.1-2 Proximate analysis

Proximate analysis (% w: w)				
Flax shives [6]	Humidity	Volatile Matter	Fixed Carbon	Ash
	8.28	69.22	19.97	2.53
Sargassum	14.6	57.2	22.8	6.36

The proximate analysis of Flax shives was previously performed in our laboratory, and the results are presented in Table 3.1. In general, the value of volatile matter is lower than those presented in numerous literature reviews [58], [81], [81], [96], [188], [190]; however, the content of C, H, N, and O is similar to most of the agricultural residues studied.

The proximate analysis for Sargassum was performed following the protocol described in section 2.1. Results are presented in table 3.1-2. On the other hand, the volatile matter of Sargassum natans is similar to the results presented by Yesiku and Egunyomi in 2014 for a mixture of Sargassum natans and fluitans (57%)[58].

The ratios of volatile matter, fixed carbon, ash content, and moisture are indicators of pyrolysis product yields. In general, biomass with high volatile matter produces high quantities of bio-oil and syngas, whereas fixed carbon increases biochar production. Moisture content in biomass influences the heat transfer process with significant effects on product distribution [69] [203]. It has been observed that an increase in moisture content increases liquid product yield while solid and gas yields decrease [204]. This is because moisture produces large quantities of condensate water in the liquid phase. Friedl et al. [205] found that feedstocks with low mineral and nitrogen contents favor bio-oil and syngas production.

In addition, the organic fraction was evaluated by calcination, and hemicellulose, cellulose, and lignin fractions were determined by biochemical fractioning following the AFNORFD U44-162 method (results reported in Table 3.3). Analysis confirms that Flax shives are lignocellulosic biomass, contrary to Sargassum, where the main constituents are active metabolic compounds such as protein, lipids, sugars, and nucleic acids.

Table 3.1-3 Organic Matter by calcination

Organic matter by calcination (% w: w)			
Flax shives	Hemicellulose (% Organic Matter)	Cellulose (% Organic Matter)	Lignin (% Organic Matter)
	19.4	41.5	20.9
Sargassum	4.6	13.6	11

3.2 THERMO-CHEMICAL DECOMPOSITION BEHAVIOR

Thermogravimetric analysis (TGA) is used to evaluate the thermo-chemical decomposition behavior of Flax shives and Sargassum and to determine the decomposition temperature range. The curves of mass fraction and first derivative of mass loss are presented in this section. The data is used to determine the kinetic parameters using the Kissinger method.

3.2.1 Flax shives

The study of the thermal decomposition of Flax shives was previously carried out by Abdelouahed et al. [82] at low heating rates. For this thesis, the interest was to evaluate decomposition at high heating rates, comparable to those used during microwave heating. Figure 1 shows an example of the thermal decomposition of Flax shives for various heating rates ranging from 1 to 200 °C / min.

Figure 3.2-1 shows the mass loss as a function of temperature. In general, a first loss of mass can be expected that starts at room temperature up to around 100-150 °C relative to the evaporation of water. For low heating rates (1 and 2 °C / min), it is observed how the decomposition of the biomass begins just after the evaporation of water, for medium or high heating rates a stability zone is observed between 150 C to around from 250°C to then trigger an abrupt loss of mass up to around 500 °C. A last zone of stability can be observed that indicates the completion of decomposition, leaving the coal and ash as a residue.

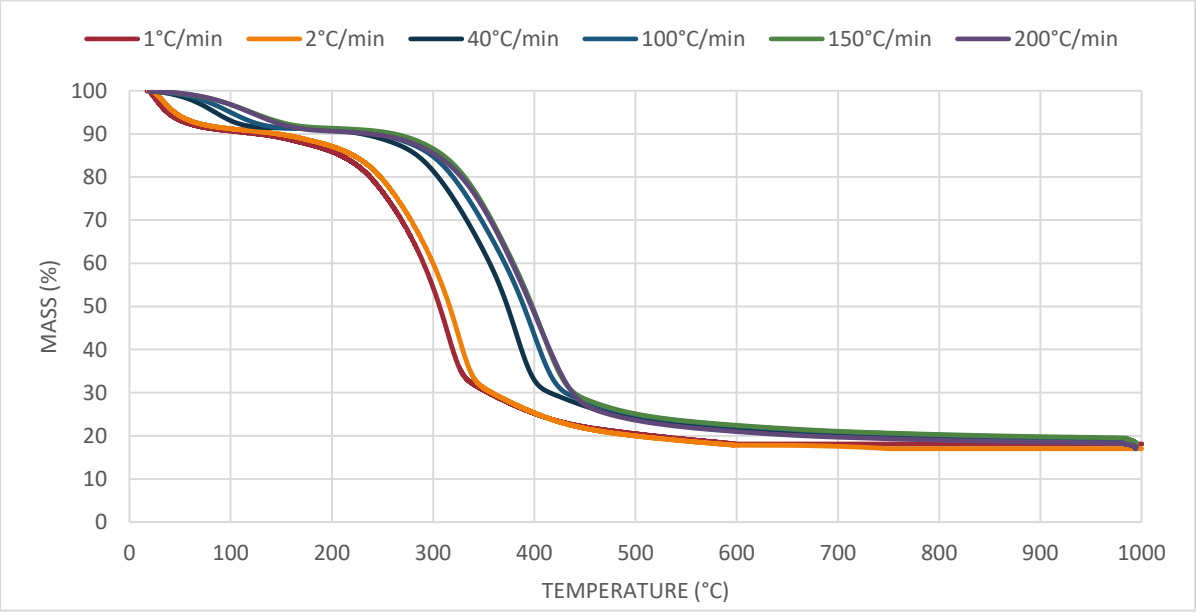

Figure 3.2-1. Flax shives - Mass loss as a function of temperature

Figure 3.2-2 shows the derived mass curves with respect to temperature, and indicates the points of maximum decomposition rate, which is a required data for the thermophysical characterization of materials. The largest peak of the curves is attributed to cellulose decomposition, this peak is

accompanied by a small shoulder at lower temperatures and indicates the beginning of hemicellulose decomposition. The decomposition of the third pseudo component of biomass, lignin, is evidenced in the small tail of the peak at higher temperatures. It could be summarized that the order in which the components begin to degrade is: Hemicellulose-> Cellulose-> lignin.

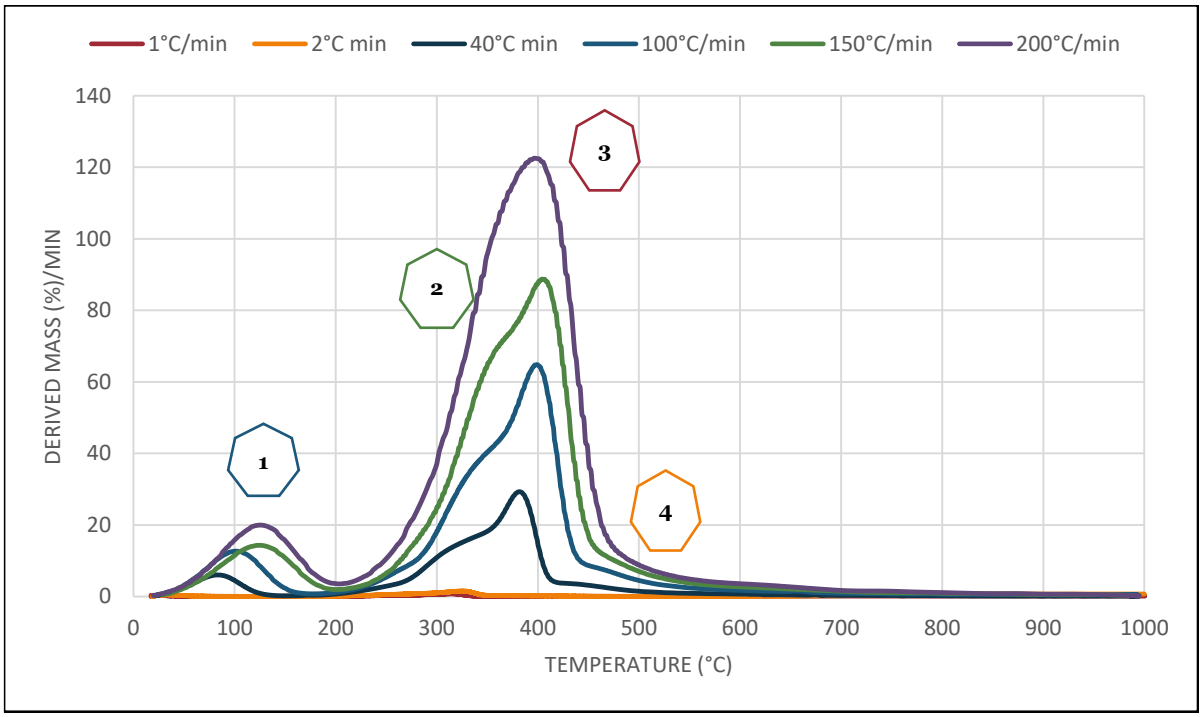

Figure 3.2-2 Derivative of mass as function of temperature

The forms of the peaks follow the trend of scientific publications to date where a first peak can be seen between room temperature and 200°C indicating the evaporation of water, as well as the presence of the largest peak that goes from 250-280°C according to the heating rate up to 330-450°C, indicating the decomposition of hemicellulose and cellulose, a pseudo-make up majority in Flax shives according to [8] [124] [82] and Table 3.1-3. The small tail (fourth peak) at the end of the peak that starts after 400 °C indicates the slow and long decomposition of lignin.

The effect of the heating rate on the decomposition rates is clearly evidenced, whereas the heating rates increase, the decomposition rates also increase. A thermal lag in the biomass behavior is observed due to the endothermic character of the pyrolysis reaction, as well as the possible limitations by mass and heat transfer for the high rates of heating.

When increasing the heating rates, an increase was also found between the temperature range of the water evaporation zone, which is closer to the pyrolysis zone. This phenomenon could be due to a relationship between the water content that resides inside the particles and that would have a limiting impact on the physicochemical behavior of the pyrolysis reaction and the residence of volatiles.

The curves in Figure 3.2.2. allow determining the maximum decomposition temperature for each heating rate, which is necessary to obtain the kinetic parameters by the Kissinger method described in

Chapter 2. Figure 3.2.3. shows the linear regression of the experimental data for Flax shives from which the activation energy and the pre-exponential factor are determined from the equation of the typical line y = ax + b, where a = (-Ea / R) and b = (ln (AR / Ea)), where R is the ideal gas constant.

Figure 3.2-3. Kinetics parameters calculation using the Kissinger method

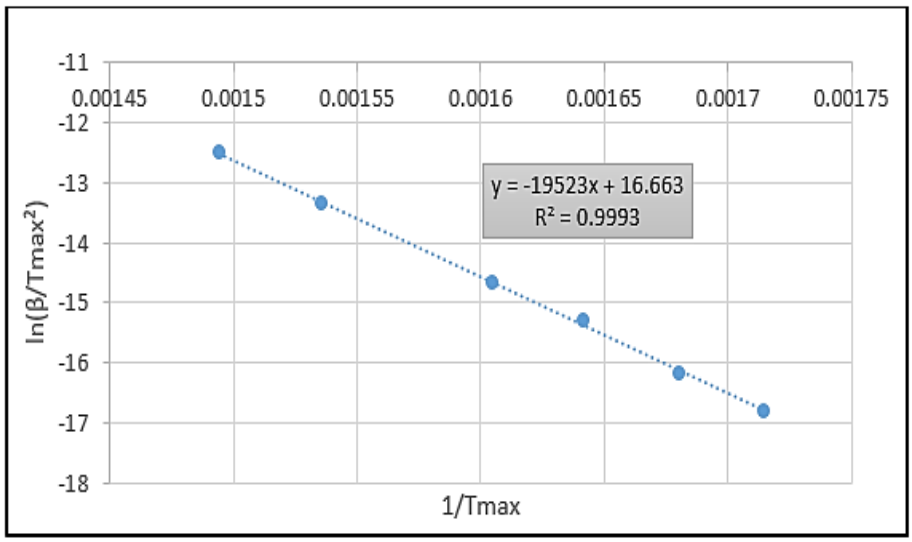

Ea (J/mol)	162314
A	3.3666E+11
log A	11.52

The global results obtained for the activation energy and the pre-exponential factor are indicated in figure 3. These results are different from the results obtained by [71] for Flax shives using the Kissinger method at low heating rates (from 2 to 40 c / min). A comparison between both results is presented below:

Table 3.2-1 Activation energy and Log A comparison with literature

Results	**Ea (J/mol)**	**log A**
Abdelouahed et al. [71]	187950	13.72
This thesis	162314	11.2

The activation energy of Flax shives was lower than the value found by Abdelouahed et al. and close to cellulose, the major pseudo-component present in Flax shives [71]. These results can lead to some hypotheses:

1. At higher heating rates, the decomposition reaction requires lower activation energy, meaning that the decomposition is easier.
2. The cellulose has a major influence on the reaction conversion

3.2.2 Sargassum

Sargassum's study has been previously evaluated in the literature and described as a highly complex thermal degradation process [81]. As expressed in Chapter 1, the Sargassum family of algae is broad, and each family comes with different pseudo-component distributions. In the case of Sargassum Natans, no previous studies concerning their decomposition behavior were found. However, the outcome of this study can be compared to some macroalgae results already published.

Figure 3.2.4 shows the loss of mass with respect to temperature for five different heating rates. A regular mass loss can be observed as the temperature increases and whose slope decreases until stability from 800 °C. The remaining mass after decomposition of the biomass was around 28%. This result is considerably low in comparison to other results found in the literature such as 46% for Sargassum spp. [81], 45% for Sargassum pallidum and 35% for Sargassum thunbergii . This remaining mass refers to the content of char + ash, given in table 1-3. Unlike Flax shives, the decomposition stages are not so visible in the curves of mass loss with respect to temperature, however the three main zones can be distinguished, at 150 °C the water evaporation stage ends, then at 200 °C begins the general decomposition of the biomass and at 850 °C a new zone of stability can be verified.

In stage 1, where the loss of cellular and external water take place, the moisture content of Sargassum Natans was higher than those found in the bibliography, with a value of 14.6%. The literature values were 9.34% -9.8% for Sargassum spp. [81], 10.3% for Sargassum pallidum (3) and 9.7% for Sargassum thunbergii (1). It should be noted that the Sargassum Natans samples used for this study were only dried 5 days under the sun and stored in room conditions. In figure 3.2-4, it can be observed that the maximum rate of decomposition tends to increase with the heating rate.

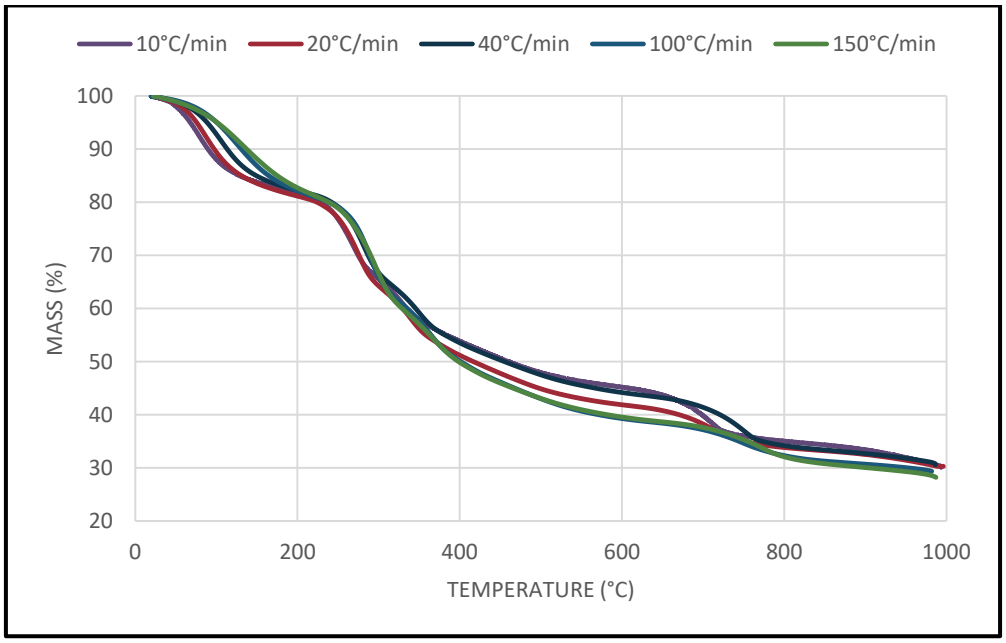

Figure 3.2-4. Sargassum Mass loss as a function of temperature

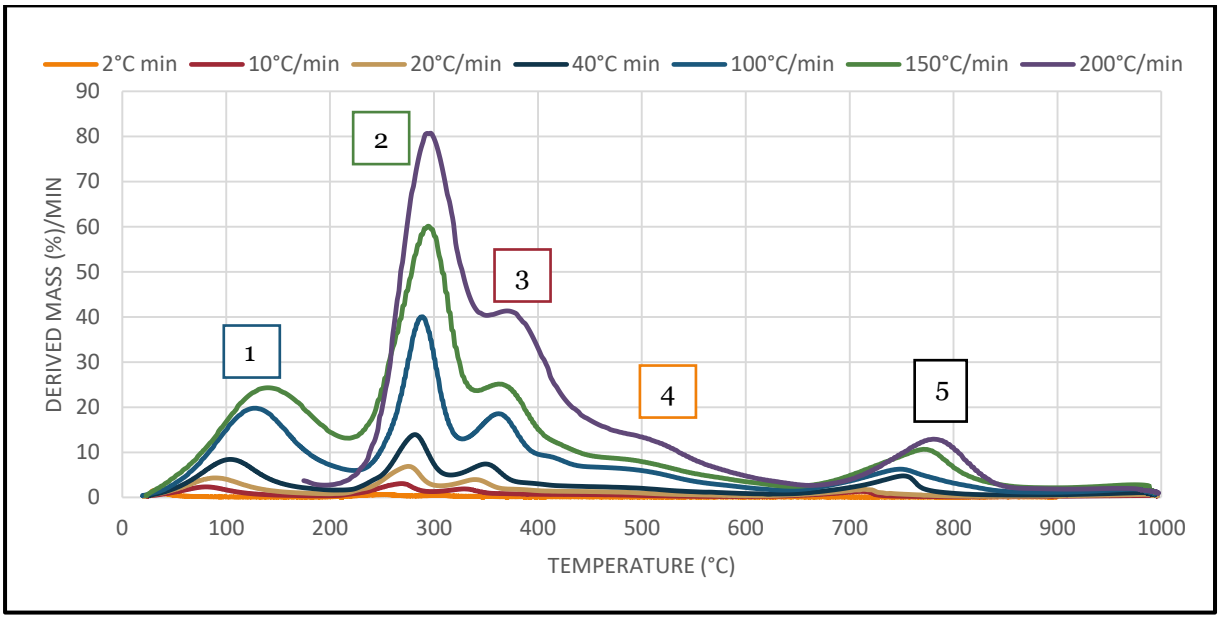

Figure 3.2-5. Sargassum Derivative of mass as a function of temperature

The active phase of the decomposition of biomass or 2nd stage can be better explained by observing the curves of the derivative of mass as a function of temperature. Each curve for each heating rate shows a first peak corresponding to the evaporation of the water, then three well-marked peaks (number 2,3 and 5) and a shoulder (number 4) between 400 and 650 °C can be observed.

Contrary to lignocellulosic biomass, the pyrolysis of algae biomass is often decomposed in the degradation of lipids, proteins, and carbohydrates. Initially, water content is removed. In the second stage, lipids, proteins, and carbohydrates are decomposed during the active pyrolysis phase, and at the final stage, carbon-rich residues are formed [91], [95]. According to Ali and Bahadar [81], the first peak of the active phase of biomass decomposition (peak number 2) corresponds to the decomposition of different fractions of biopolymers present in the biomass, the second peak (number 3) is attributed to the decomposition of carbohydrates and the third peak (number 4) to the decomposition of proteins [206], [207]. The overlapping of the peaks shows the complexity of the degradation of the molecular structure of Sargassum N.

In our experiment, the decomposition of Sargassum starts at 200°C. Between 200 and 500 ° C, there is an important weight loss, but after 500 °C, the decomposition rates decay. Considering the decomposition temperatures and comparing with the literature, the first peak, as mentioned above, refers to the evaporation of water. Peak 2, 3, and 4 refer to the decomposition of hemicellulose and biopolymers, cellulose and carbohydrates, and lignin and proteins, respectively [81]. The particularity of peak 4 or shoulder is that it shows the slow degradation of the lignin/protein present in the Sargassum samples. Peak 5 is the degradation of the char.

In earlier studies [91], Spirulina platensis (SP) and Chlorella protothecoides (CP) were analyzed in terms of devolatilization behavior and pyrolytic characteristics. Both biomasses are mainly devolatilized between 150 and 560 °C with a total volatile yield of 71 %. Interestingly, higher lipid content was correlated with the maximum yield of liquid (52–55% w/w), gas (33–36% w/w), and biochar (15% w/w). As the heating rate increased, a lateral shift to higher temperatures was observed in their thermograms, and the instantaneous maximum and average reaction rates in the devolatilization stage were increased while the activation energy was decreased. The degradation of the char is broader than the other components [88].

Table 3.2-2 Degradation temperature range of principal peaks- Sargassum f. DTG curves

Peak	**2** **Hemicellulose/biopolymers**	**3** **Cellulose/carbohydrates**	**4-** **Protein/Lignin**	**5** **Char**
Temperature Range (C)	200-350	300-440	400-650	650-850

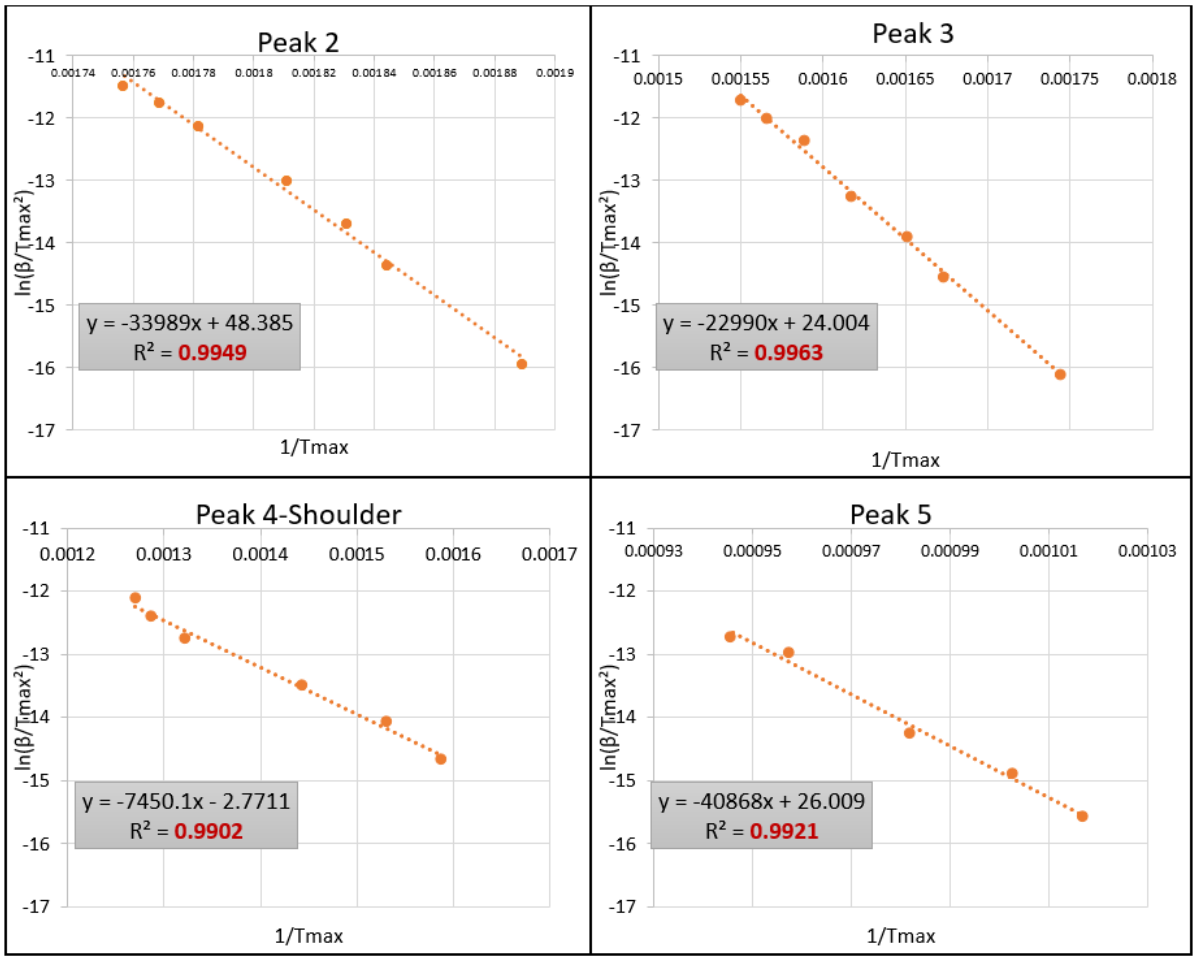

Figure 3.2-6. Sargassum linear regression graphics

Figure 3.2.6. shows the linear regression plots for each Sargassum N. peak with regression factors R2> 0.99. The values of the activation energy and the pre-exponential factor are presented in table 3.2-2

In table 3.2-3, a value that draws attention is that of lignin / protein, which although it is true is the lowest, it also refers to a more extensive peak temperature range, thus becoming a limiting stage in the pyrolysis process due to the relationship of lignin with the entire structure of the cell wall, preventing accessibility during the decomposition process[81].

Table 3.2-3 Kinetics parameters for Sargassum N. for each peak

Peak	**2 Hemicellulose/biopolymers**	**3 Cellulose/ carbohydrates**	**4 Lignin/ Proteins**	**5 Char**
Ea (J/mol)	282584	191138	61939	339776
Log A	25.54	14.78	5.07	15.04

By comparing the results of the third peak (cellulose decomposition) for Flax shives and Sargassum, it can be noticed that the global activation energy for Sargassum N. (191 kJ/mol) is higher than Flax shives (162 kJ/mol). This means that Sargassum will require higher activation energy to decompose its cellulose fraction. However, most of this fraction decomposes between 280°C -and 300°C, which is a lower temperature range when compared to Flax shives. These experiments point out the major differences between lignocellulosic and algae pyrolysis. Flax shives pyrolysis is dominated by cellulose decomposition, while Sargassum pyrolysis is dictated by low carbohydrate pyrolysis requiring higher activation energy but occurring at a lower temperature range. Also, Sargassum seems to produce a char that will decompose at higher temperature conditions which is not the case for Flax shives.

3.3 DIELECTRIC CHARACTERIZATION OF BIOMASS AND PYROLYSIS PRODUCTS

The acquisition of data on the dielectric properties of materials is a fundamental stage in the implementation of a microwave process. In chapter 1, the phenomenon of wave-matter interaction is described. However, it is important to remember that the heat phenomena appear through the interaction of the dielectric material with the electromagnetic field in the microwave frequency used.

There are numerous studies on the dielectric properties of biomass, but nonspecific were found for Flax shives and Sargassum Natans. The experimental data concerning the Flax shives and Sargassum are presented and their pyrolytic product (solid and liquid). The effect of water content and SiC content is also studied.

3.3.1 Dielectric characterization of Flax shives and its pyrolysis products

The relative permittivity (dielectric constant and loss factor) for Flax shives was evaluated at 20 °C. The method used was that of a coaxial probe for a frequency range between 500 MHz and 20 GHz. The protocol used, as well as well as the equipment, are described in chapter 2.

The biomass samples were dried in the oven at 105 °C for 24 hr. Then, the moisture content was determined, which was equal to ±5 %. Different moisture contents from 5 to 34% were achieved by adding water to the dry biomass. Table 3.3-1, figure 3.3.1. and 3.3.2. show the results of the measured dielectric properties for dried biomass and with different moisture contents, at 20 ° C.

Table 3.3-1 Dielectric Properties of Flax shives for different moisture content

At 2,45 GHz and 20°C	ε'	ε''	Loss tangent (tanδ=ε''/ε')
Flax shives + 5% Moisture Content Room conditions	2.3	0.2	0.07
Flax shives + 14% Moisture Content	2.9	0.4	0.14
Flax shives + 27% Moisture Content	5.5	1.2	0.3
Flax shives +35% Moisture Content	8.9	1.9	0.2

As expected, the relationship between dielectric properties and moisture content presented how the real part ε ' and the imaginary part ε" at room temperature become more pronounced with increasing water content. This behavior was also published by [208], who affirms that the dielectric constant of different hardwoods increase with the water load because the water loss factor has higher values than wood, and by increasing the water within the matrix of the wood, the relative permittivity of the sample increases. This result is particularly visible in table 3-7, where the loss tangent increase from 0.07 to 0.3 when increasing the moisture content from 5 to 27%. This response was also observed by Ellison et al (2018)

in their study of the potential for using bentonite as a microwave absorber for microwave pyrolysis. The dielectric properties of bentonite at different moisture contents were measured using a coaxial line dielectric probe and vector network analyzer in the microwave frequency range from 0.2 to 4.5 GHz at room temperature, and both dielectric constant and dielectric loss factor increased linearly with increasing moisture content[209].

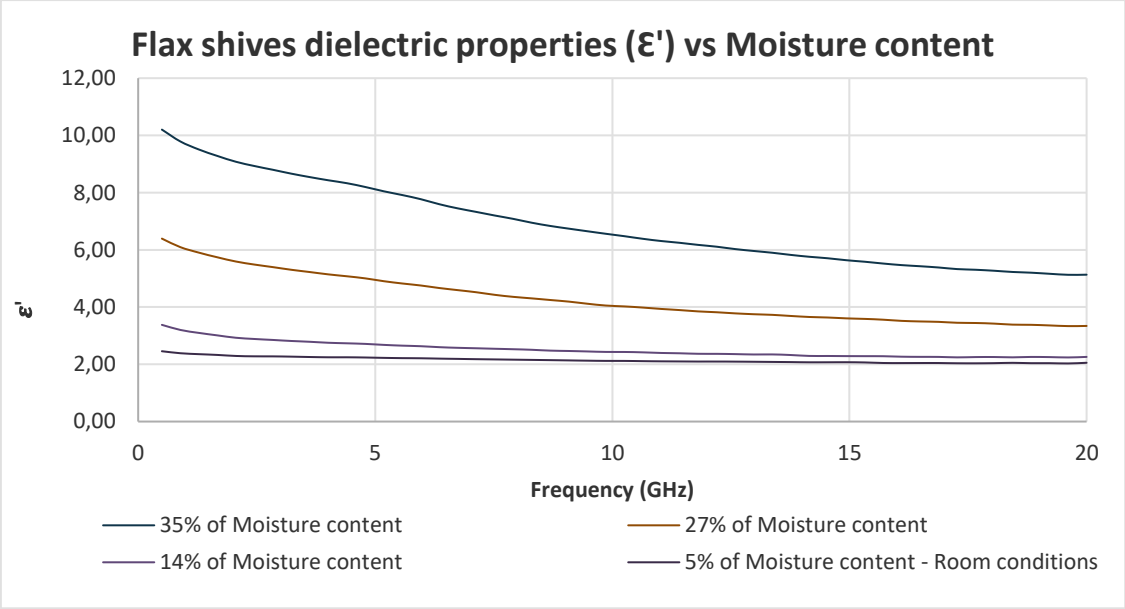

Figure 3.3-1 Flax shives dielectric constant loss at 20 °C with frequency

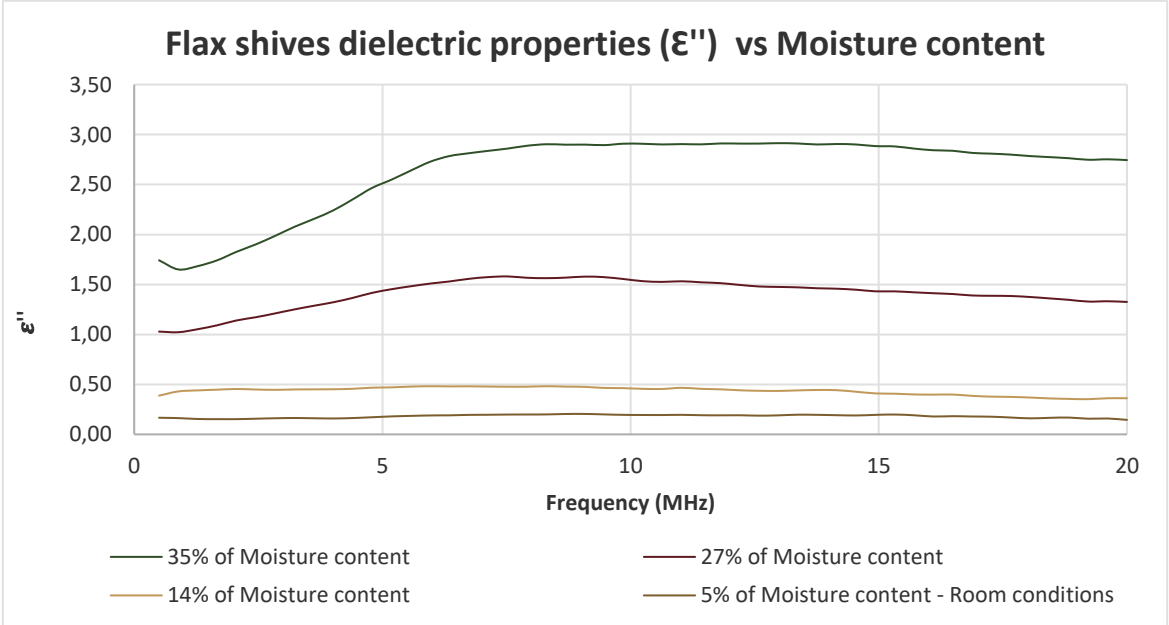

Figure 3.3-2 Flax shives dielectric loss at 20°C with frequency

Water content is not the only parameter related to the increase of the dielectric properties of the matrix of biomass. Furthermore, the polar components inside the Flax shives matrix reach higher liberty of rotation at higher moisture content [208]. The latter contributes to better dielectric behavior. The presence of water is then an asset in terms of microwave heating, as already established in literature [208].

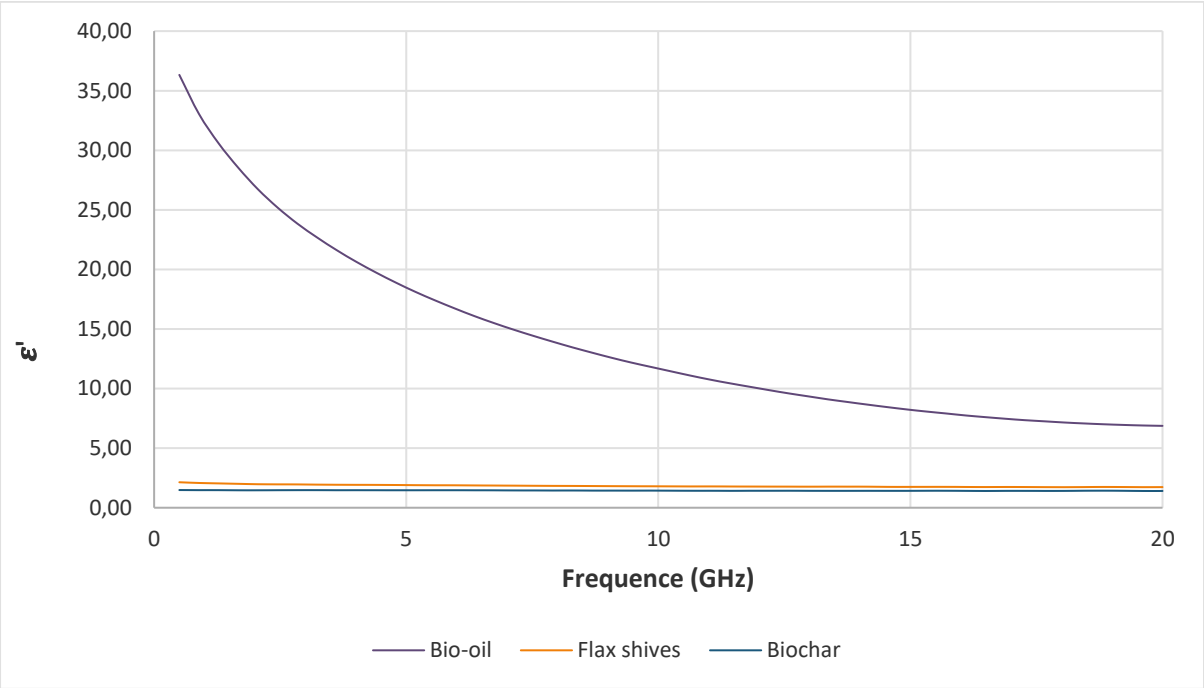

Figure 3.3-3. Flax shives and pyrolysis product's dielectric constant at 20°C with frequency

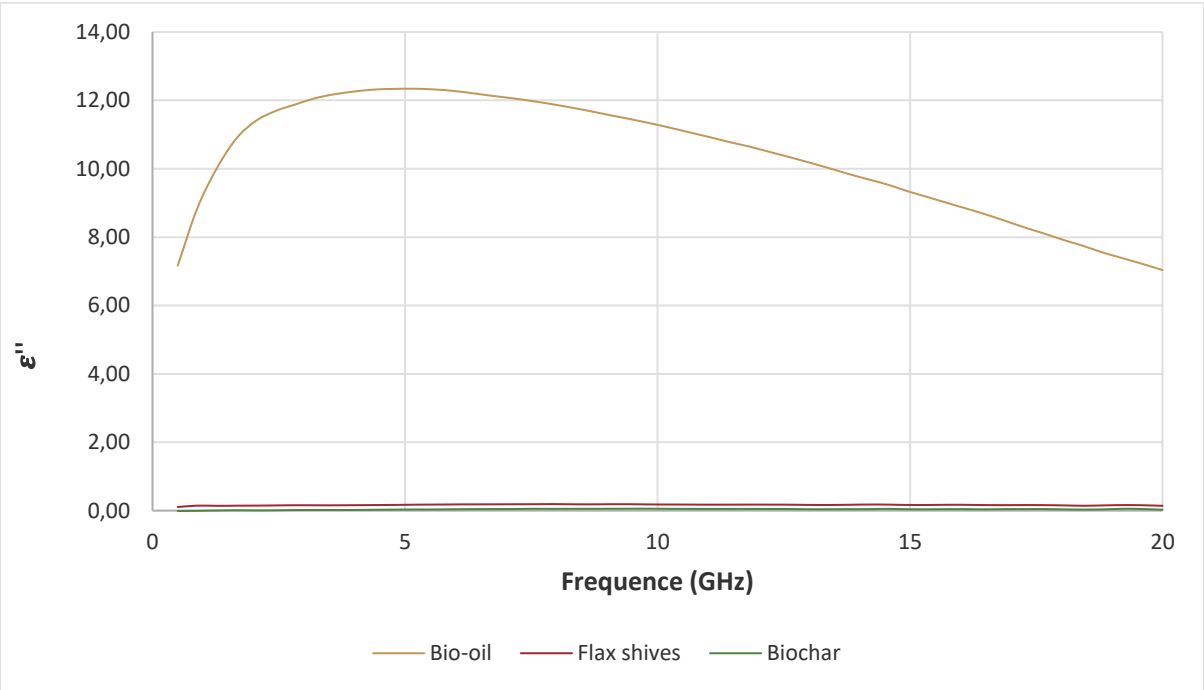

Figure 3.3-4. Flax shives and pyrolysis product's loss factor at 20°C with frequency

It is also important to study the dielectric properties of the Flax shives pyrolysis products obtained at a pyrolysis temperature of 650°C. Figure 3.3-3 and 3.3-4 show the dielectric properties of the products. From the results, it can be observed that the biochar has similar values compared to the biomass. Also, it was found that the product with the most interesting dielectric properties is bio oil, having values at 2.45 GHz and 20 C of: ε '= 30.67 and ε' '= 11.08, meaning to have a crucial role in the electromagnetic field propagation in the reactor.

3.3.2 Dielectric characterization of Sargassum and its pyrolysis products

The study of dielectric properties for algae biomass is not very extensive. Itolikara and Kurtadikar [210] studied the dielectric properties of dry and moist green algae at 5 GHz at room temperature. The conclusions were like those for Flax shives. As the moisture content increases, the dielectric properties increase. Figures 3.3-5 and 3.3-6 present the results of the dielectric constant and the loss factor, respectively, for Sargassum N. and the char and bio-oil obtained from the pyrolysis of this biomass.

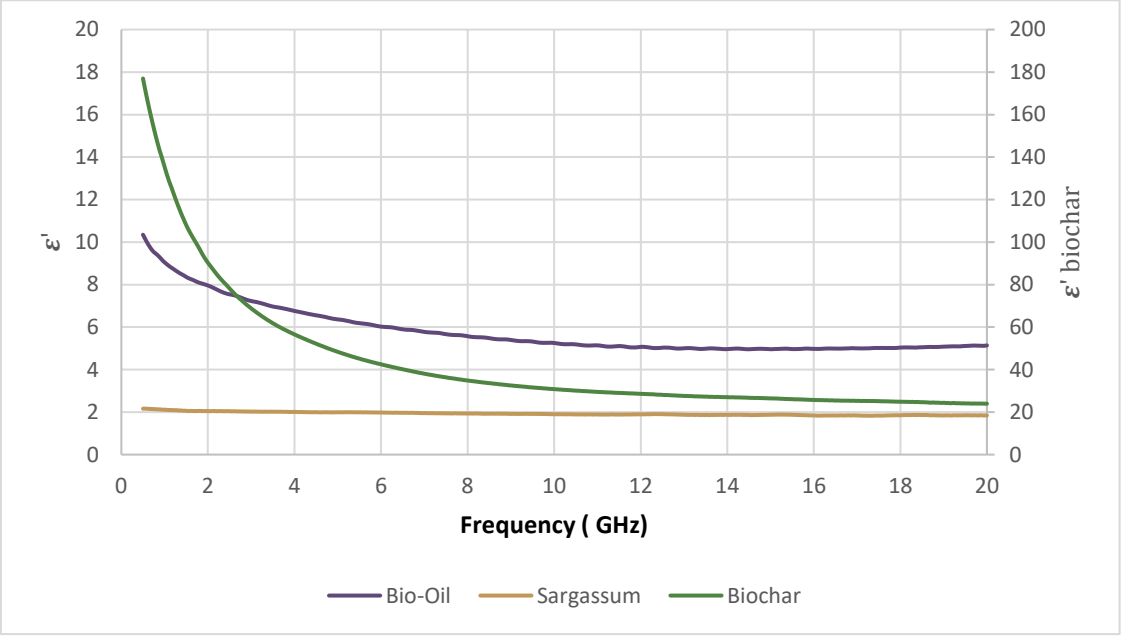

Figure 3.3-5. Dielectric constant for Sargassum (ε') with frequency

It was found that for Sargassum, at low frequencies, the dielectric constant of bio-oil was higher than that of biochar, while at higher frequencies, biochar had higher values. This was also reported by Tripathy et al.(2015) while studying the effect of microwave frequency on dielectric properties of oil palm shell and char synthesized by microwave pyrolysis[211].

Contrary to Flax shives and hardwoods [208], the char obtained from the pyrolysis of Sargassum has remarkable potential as a microwave susceptor with high dielectric constant and loss factor values.

Ellison et al. [212] also studied the dielectric properties of biochar from 0.5 to 20 GHz at room temperature, concluding that the dielectric properties increase quadratically with increasing biochar content in a biochar/biomass mixture. Similar role to water which is undoubtedly a good microwave absorber, the carbonaceous characteristic of the biochar also plays a crucial role in developing high polarization in the material. The char structure can be a medium to absorb microwaves due to the Maxwell-Wagner effect; polarization that occurs due to the difference in conductivities and dielectric constants of the substances at the interfaces thus leading to field distortions and dielectric loss, and eventually causes the heating effect (Lam and Chase, 2012)[12]. From these results, it can be concluded that the biochar behaves as a conductive matter. Able to be used as a microwave susceptor in microwave assisted pyrolysis

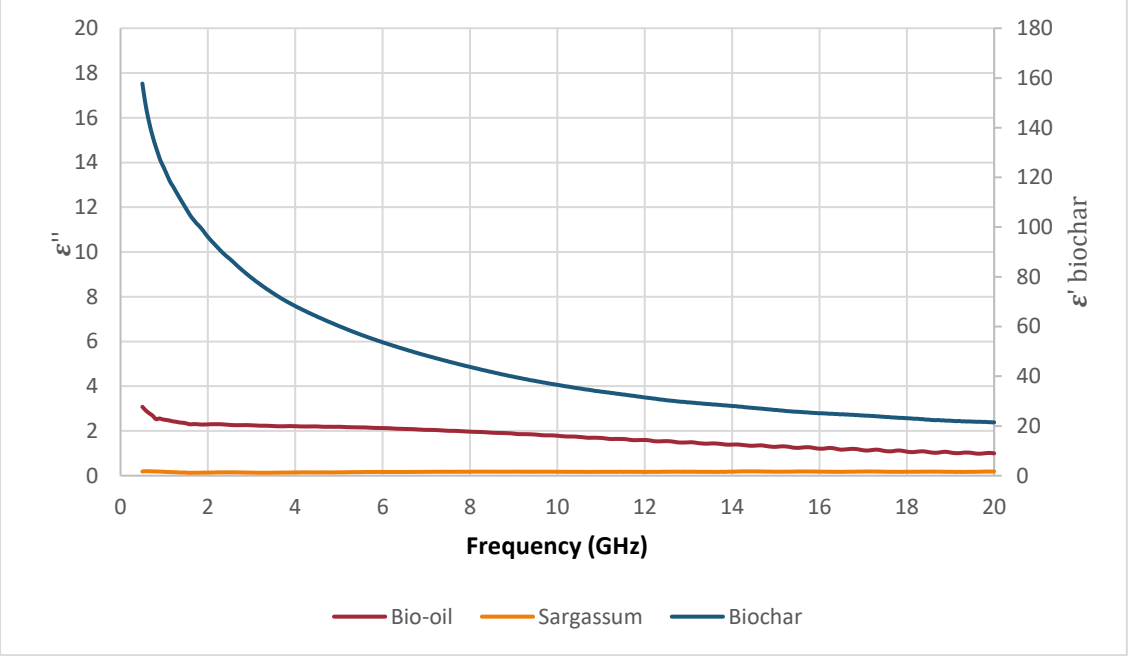

Figure 3.3-6. Loss Factor for Sargassum (ε") with frequency

3.3.3 Dielectric characterization of SiC and its interaction with biomass

As both Flax shives and Sargassum N. are feedstock with low dielectric properties, a microwave absorber is needed to achieve the temperature of pyrolysis. Silicon Carbide is generally used as a microwave absorber, so we decided to test it in both biomasses.

The dielectric properties of Silicon Carbide were studied by Benamara during her thesis research [25]. To understand the effect, SiC in the feedstock load, dielectric properties measurements, were done. The results for a mixture of Flax shives and 20% w:w of SiC are presented in figure 3.13. The results did not show an improvement in the dielectric properties of the biomass + SiC mixture. On the contrary, the dielectric properties were almost identical to those of biomass alone.

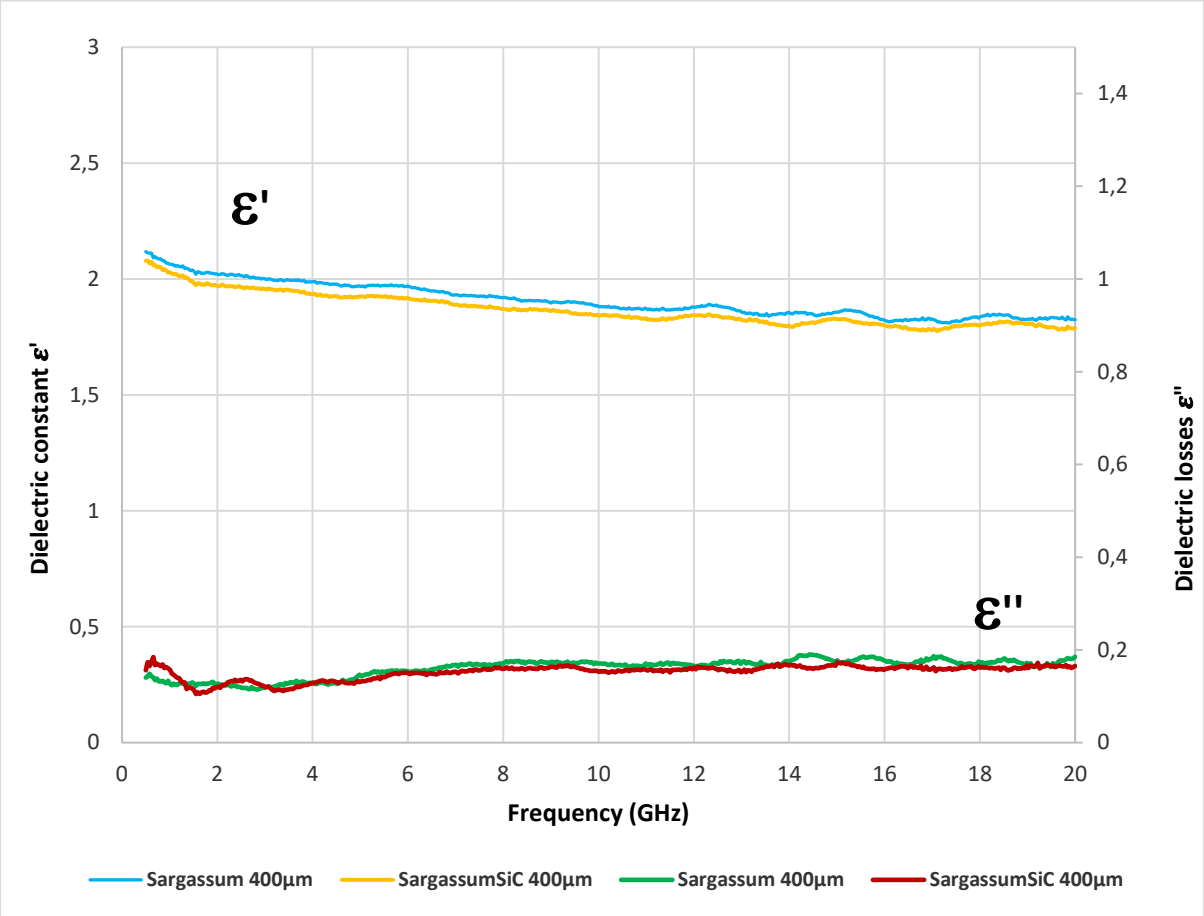

Figure 3.3-7. ε' and ε'' for biomass (Sargassum) and Sargassum + SiC

This unexpected result can be explained by the difference in the particle size of the tested biomass (400µm) and the silicon carbide (1600 µm), allowing the presence of air inside the sample and producing a heterogeneous medium which cannot ensure a valuable coaxial probe method's measurement.

3.4 PYROLYSIS PRODUCT'S COMPOSITION

GC-MS was used to analyze the pyrolysis products (oil and gas) composition as a preliminary step to further understand the influence of the operational conditions of the microwave's pyrolysis process on the quality and composition of the products obtained in bio-oil and non-condensable gases. The quantitative and qualitative study of bio Flax shives oil has been previously carried out under conventional pyrolysis conditions in an intermediate pyrolysis regime by Mohabeer et al. [124] and the analysis of non-condensable gases by Sulman et al. [7]. Regarding Sargassum Natans, no studies were found in the literature on the characterization of bio-oil and non-condensable gases specific to this type of biomass. However, we will refer to studies on the characterization of bio-oils for microalgae [188], common algae species [189], and brown algae [213].

The bio-oil obtained from pyrolysis of Sargassum Natans et de Flax shives was analyzed by GC-MS as detailed in chapter 2. After identifying all the components, they were divided into 12 major chemical families. Once the peaks were identified, a GC-FID was used to quantify the components with the percentages divided into the families concerned. The quantification of these compounds and the influence of the operational parameters on them will be discussed in Chapter 4.

There are many types of organic compounds in the bio-oil produced by pyrolysis. The classification of the detected compound is explained in section 2.3.1. There are three types of groups of compounds present in the bio-oil, as discussed by Vreugdenhil et al. (2009). They are called primary tars, secondary tars, and tertiary tars. The first product belongs to levoglucosan, furfurals, and methoxy phenols, which are cellulose, hemicellulose, and lignin-derived compounds. Secondary tars are characterized by olefins and phenols, whereas tertiary tars are characterized by aromatic compounds such as benzene, toluene, and PAH species. Oxygenates compounds such as acids, alcohols esters, ethers, aldehydes, and ketones, are mostly produced in a temperature range of 350-650°C. Aromatic compounds are mainly generated at higher temperatures >700°C.

This section aims to provide a general characterization of the products obtained by the pyrolysis of biomass in microwaves that will then serve as a basis for the quantitative analysis and the influence correlations of the operating conditions with the quality of the products obtained.

3.4.1 Bio-oil

After analyzing the Flax shives bio-oil, 196 different compounds were found, of which the compounds listed in Table 3.8 stand out, with their respective retention times and chemical family. From Table 3.4-1, the species found in notable area percentages in the GC-MS chromatogram are mostly acetic acid, phenol, phenol isomers, and smaller PAH species such as fluorene, styrene, and naphthalene. The analyzed bio-oil species are composed of many chemical families (Carboxylic acids, alkenes, ketones, esters, alcohols, furans, aldehydes, sugars, alcohols, and guaiacols).

It is worth noting that the bio-oils from lignocellulosic biomass usually contain a higher proportion of oxygen than fossil oils (due to carboxylic acids). Therefore, they are quite not as stable as fossil fuels,

where their characteristics can change rapidly during condensation and under storage conditions (Onay, 2007). The presence of phenol compounds in the bio-oils was more important in microwave-pyrolyzed oils than in the bio-oil obtained by Mohabeer et al. [124] for Flax shives. Similar composition on the GC-MS spectrum is found in the oil palm fiber bio-oil [177].

Table 3.4-1 Principal peaks detected on Flax shives bio-oil

Fax Shives GC- MS Principal peaks detected		
Retention Time	**Component**	**Chemical Family**
7.155	Benzene	Alkenes
8.905	Acetic Acid	Carboxylic Acids
10.078	2-Propanone, 1-Hydroxy-	Ketones
12.12	2-Nitroethyl Propionate	Esters
14.12	1-Propanol, 2-Methyl-	Alcohols
14.787	Furan, 2,5-Dimethyl-	Furans
14.81	Furfural	Aldehydes
15.353	Styrene	Alkenes
15.575	L-Glucose	Sugars
17.71	2-Furanmethanol	Alcohols
22.61	2(5H)-Furanone	Ketones
25.372	Phenol	Phenols
26.155	Phenol, 2-Methoxy-	Guaiacol
28.541	Cresol	Guaiacol
34.66	2-Methoxy-4-Vinylphenol	Guaiacol
34.942	Biphenyl	Alkenes
37.066	2-Ethenylnaphthalene	Alkenes
38.806	Trans eugenol	Guaiacol
42.003	Fluorene	Alkenes
46.403	Levoglucosan	Sugars
60.501	Benzo[C]Fluorene	Alkenes

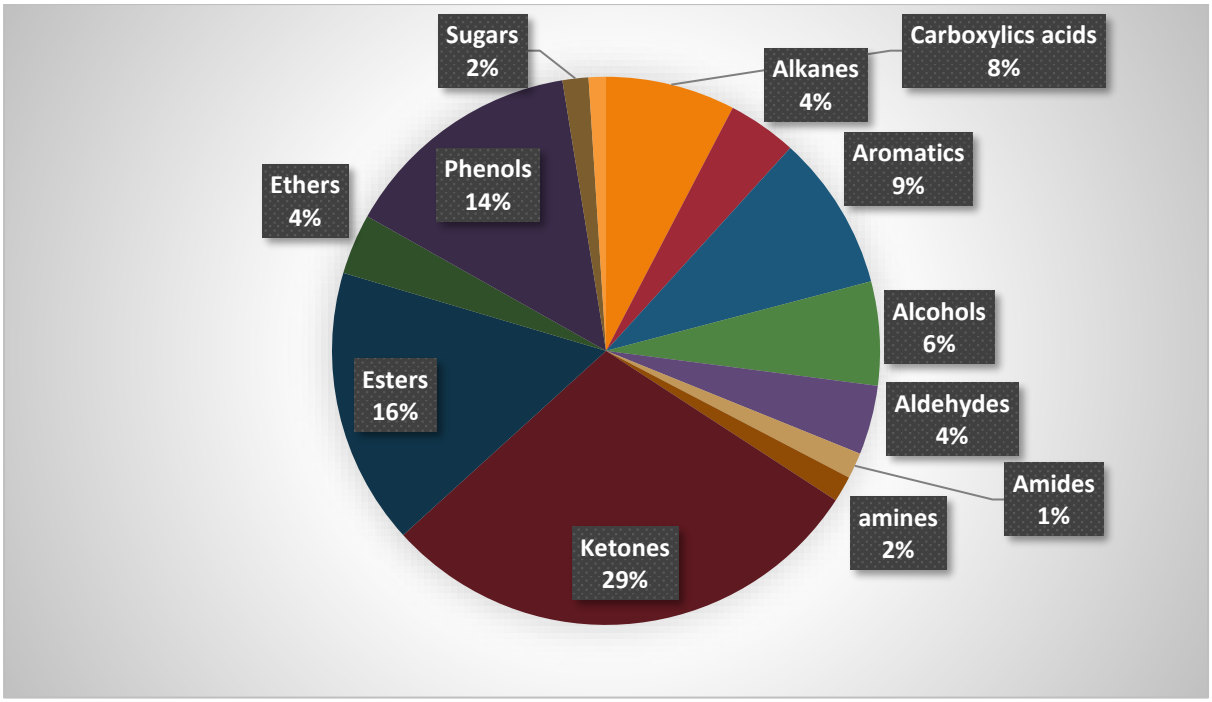

Figure 3.4-1 Percentage of number of detected compounds by each chemical family in Flax shives bio-oil

In the case of Sargassum, 208 compounds were detected and classified into 13 chemical families. Unlike Flax shives, this algae biomass has a non-negligible nitrile content. The chemical families of the detected compounds as well as the list of the most important detected peaks are listed in table 3.4-2. Compounds as Proline, Glycylsarine and D-Fucose, are amino acids, normally found in the bio-oil from the algae pyrolysis, Dianhydromannitol war similarly found in the pyrolysis of brown algae [51].

Compounds as toluene, styrene, furans, 2-methyl phenol, acetid acid, drianhydromannitol, benzenacetonitrile and 3-penten-2-one, are some of the common compounds found in macro algae feedstock. For example: from pyrolysis of Chlorella vulgaris, compounds such as 1H-indole; 1H-indole-3methyl, benzenepropanenitrile (C9H9N); benzyl nitrile (C8H7N); propanenitrile (C3H5N); 4-methyl-pentanenitrile (C6H11N), toluene, styrene, ethylbenzene, methylphenol, phenols were detected in the pyrolytic products as derived from protein fraction [153,162]. From the pyrolysis of algal biomass, a variety of organic and inorganic compounds are formed and distributed into three main pyrolytic products.

Table 3.4-2 Sargassum Natans GC-MS principal peaks detected

Sargassum GC-MS principal peaks detected		
Retention time	Component	Chemical family
8.596	Acetic Acid	Carboxylic Acids
10.44	Pyridine	Aromatics
11.455	2,4,4-Trimethyl-2-Oxazoline	Amines
13.649	P-Xylene	Aromatics
14.647	Furfural	Aldehydes
16.421	2-Pentanone, 4-Hydroxy-4-Methyl	Ketones
17.933	2-Cyclopenten-1-One, 2-Methyl-	Ketones
17.507	2-Furanmethanol	Alcohols
18.726	Furan, 2-Ethyl-5-Methyl	Furans
18.977	Proline	Carboxylic Acids
21.276	2-Furancarboxaldehyde, 5-Methyl	Aldehydes
22.391	Bicyclo[3.2.0]Heptan-2-One	Ketones
25.238	Phenol	Phenols
27.03	Phenol, 2-Methyl	Phenols
28.261	Naphthalene	Aromatics
28.337	P-Cresol	Phenols
30.245	Glycylsarcosine	Carboxylic Acids
31.698	1,4:3,6-Dianhydro-.Alpha.-D-Glucopyranose	Sugars
32.503	Dianhydromannitol	Furans
34.056	D-Fucose	Sugars
34.873	Naphthalene, 2-Ethenyl	Aromatics
36.361	3-Methoxy-Alpha,Alpha-Dimethylbenzyl Alcohol	Alcohols
38.736	Acetoisovanillone, Trimethylacetate	Esters
40.667	Orcinol	Alcohols
41.998	L-Threonine, O-Tert.-Butyl-N,N-Diethyl-, Methyl Ester	Esters
45.149	7,11,15-Trimethyl-3-Methylidenehexadec-1-Ene	Aromatics
46.036	Levoglucosan	Sugars
50.383	Hexadecanenitrile	Nitriles
52.122	Hexadecanoic Acid	Carboxylic Acids
54.088	Octadecanamide	Amides
60.437	Hexadecanamide	Amides

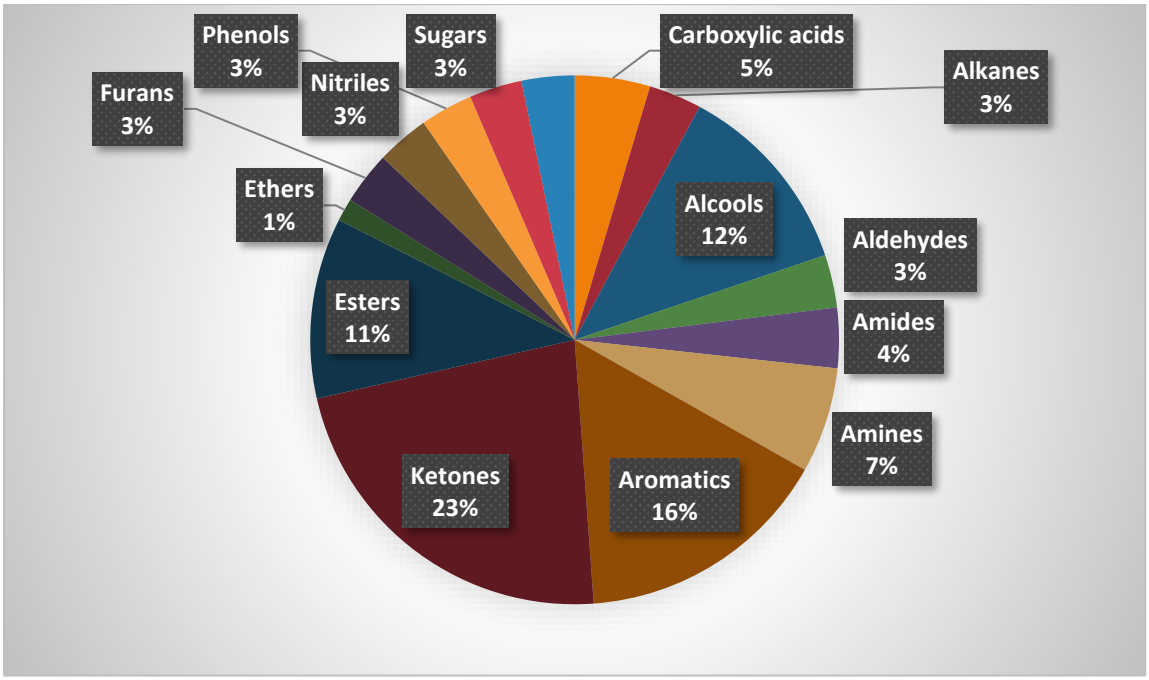

Figure 3.4-2 Percentage of number of detected compounds by each chemical family in Sargassum bio-oil

3.4.2 Non-condensable gases

The composition of non-condensable gases depends on the feedstock organic matrix. The main compounds are CO_2 , CO, CH_4 and H_2 for both of biomass. To detect heavier compounds, a GC-MS analysis was implemented. In the case of Flax shives C_3 and C_4 compounds as Ethylene, Ethane, propene et propane were found in the GC-MS analysis. The presence of this compounds in the non- condensable gases composition for Flax shives were already presented by Mohabeer et al. [116] and Sulman et al. [5] On the other hand, compounds heavier than C_3 were not detected in the Sarsassum N. gas sample.

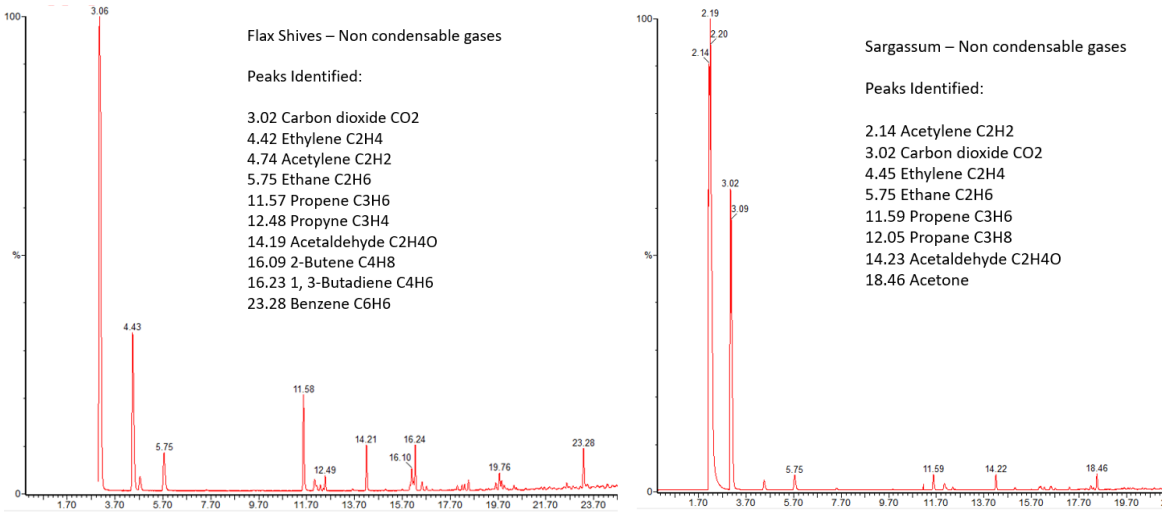

Figure 3.4-3 Flax shives and Sargassum GC-MS results of non-condensable gases

3.5 PRELIMINARY CONCLUSIONS

The elemental and proximate analysis results were presented at the beginning of the chapter. It was found differences between the percentage of C, H, and N for both biomasses and humidity, volatile matter, fixed carbon, and ash content.

The thermochemical decomposition behavior was also studied. Flax shives presented abrupt weight loss when increasing temperature while Sargassum N. behavior was more stable. The temperature at which the decomposition starts is ±225°C for Flax shives and Sargassum, but Flax shives have a maximum decomposition rate of around 400°C while 300°C for Sargassum. However, despite the difficulty in comparing the results in the values of the global kinetic parameters, the pattern in the decomposition of the biomass is consistent with the literature review.

The dielectric properties of biomass and pyrolysis products were measured at room temperature for a frequency range between 500 MHz and 20 GHz. This study indicates the dependence of permittivity on frequency, biomass type, and moisture ratio. Dielectric properties increased with increasing the humidity content for all biomasses. Dry biomass materials require a considerable amount of microwave energy to reach high processing temperatures by microwave irradiation due to low dielectric properties. Biochar, a byproduct of Sargassum pyrolysis, was a good microwave absorber and can be used as an additive to biomass feedstocks to increase microwave absorption in the bulk material and accelerate heating rates.

The number of chemical compounds analyzed in bio-oil obtained from Sargassum is higher than in Flax shives. However, the non-condensable compounds from Flax shives were heavier than those from Sargassum.

CHAPTER 4:
Microwave pyrolysis of biomass

4 MICROWAVE PYROLYSIS

The effect of microwave heating using a rotatory quartz reactor for Flax shives and Sargassum is presented in this chapter. First, the relationship between microwave irradiation and temperature profile is presented, followed by the influence of microwave irradiation on general pyrolysis behavior. Sections 4.2 and 4.3 discuss in detail the results of microwave pyrolysis of Flax shives and Sargassum separately, and section 4.4 is a comparison of the effect of the type of biomass on the microwave pyrolysis process. The conclusions are presented at the end of the chapter.

4.1 MICROWAVE IRRADIATED PYROLYSIS

In a process where the thermal energy and heat transfers are the main variables to consider, temperature becomes a crucial parameter. High heating rates, reaction temperature between 400° C up to 550°C, short vapors residence time and high cooling rate are expected to increase the bio-oil production. These features are achievable in a microwave heated environment and this section will explain the relationship between the microwave irradiation and the thermal profile.

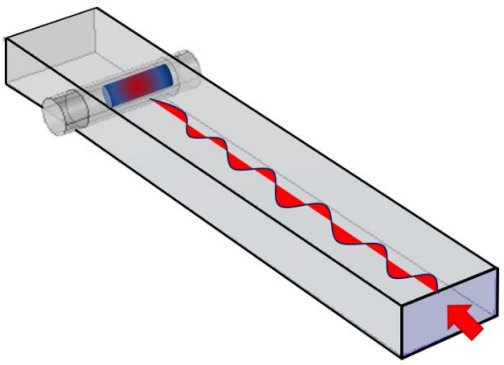

Figure 4.1-1 Microwave irradiated reactor

First, figure 4.1.1. represents the quartz reactor in contact with the electromagnetic wave. As presented in the figure, there is a gradient of temperature between the center of the reactor and the surface. The temperature produced inside the reactor is proportional to the absorbed microwave power from the sample. The absorbed power is the difference between the incident power and the reflected power measured by the bolometers.

Equation 37: $$Absorbed\ power = Incident\ power - Reflected\ power$$

When the microwave irradiation starts, the microwaves travel inside the waveguide until they encounter the biomass load inside the reactor, creating instability in the reflected power measured by the bolometers. This instability is due to the interference of the reactor load to the microwave irradiation path. Figure 4.1.2 shows the behavior explained before in terms of equation 37 for the microwave heated rotary reactor in time.

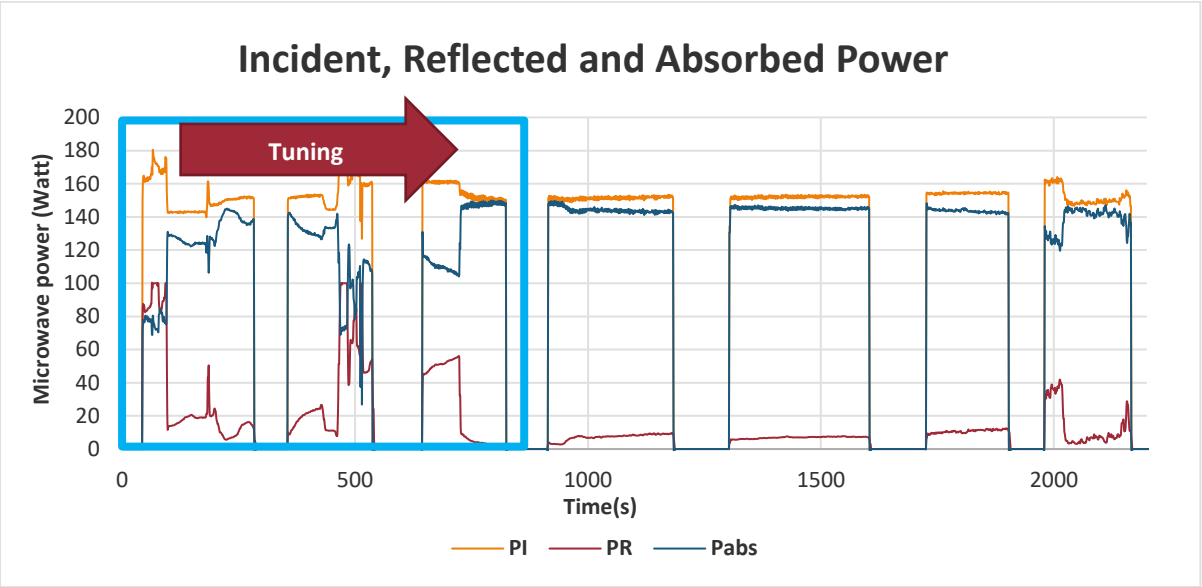

Figure 4.1-2 Incident, Reflected and absorbed power: Tunning phase

The orange line represents the incident microwave power, the blue one absorbs microwave power, and the red one reflects microwave power. Inside the blue square, the unstable microwave power behavior can be noticed. To solve this problem, a microwave "tuning" is done using impedance adaptors (See figure 2.2-1). The "tuning phase" is present in each microwave pyrolysis experiment, and it is considered when evaluating the exploitable experiences. This phase is extremely important. Thanks to it, the percentage of absorbed power increases up to 97%, with an average value of 92%, as presented in table 4.1-1. The time of the tuning phase must be considered. It can take up to 20% of the irradiation time.

Also, during microwave irradiation, there are dramatic changes in the physicochemical properties, dielectric properties, and load volume/weight causing a general instability and heterogeneity inside the reactor. The latter results in a change of the electric field pattern inside the cavity as well as its intensity location inside the cavity. When performing microwave pyrolysis, the irregular intensity of the electric field is going to interfere with the biomass load-wave interaction "point," and a second tuning phase to readapt the absorbed power is expected.

Once the "tuning phase" is mastered to obtain a higher ratio of absorbed power, the relation between microwave power and temperature is studied. Some remarkable findings were observed regarding the temperature profiles during microwave irradiation over the biomass load and during microwave irradiated pyrolysis.

Table 4.1-1 Microwave's tuning phase and microwave absorbed power

Incident Power	Irradiation Time (min)	Absorbed power after Tunning (%)	Tunning required Time (s)
150	6	92%	57
200	6	86%	8
250	6	95%	35
300	6	96%	44
300	6	93%	86
300	6	97%	38
300	6	94%	23
300	6	95%	47
350	6	91%	53
350	6	96%	57
400	6	88%	58
400	6	90%	20
600	5	87%	32
900	3	87%	36

The surface and internal temperatures were measured during a microwave heating experiment to study the magnitude of the temperature gradient between the center of the reactor and its external surface. The quartz rotatory reactor was placed inside the cavity, loaded with a mixture of 4.5 gr of Flax shives and 0.9 gr of SiC. An optical fiber was used to measure the reactor surface temperature during the experiment. When the optical fiber achieved a temperature equal to 150 °C, the microwave generation was turned off. Then a thermocouple was inserted until the bottom of the reactor to measure the internal temperature. This procedure was repeated four times. The results are presented in figure 4.1.3. The blue square represents the “tuning phase”.

As seen in figure 4.3, the temperature data recorded between the optical fiber and the thermocouple differs one from the other. This hot spot and cold spot effect are quite common in microwave-heated systems. For example, Salema and Afzal (2015) presented the intense heating at different spots when simulating a microwave heated reactor, as well as Robinson et al. (2015) [138], [159], [196].

Also, the variation of the intensity of the electric field at different locations in the cavity leads to changes in the temperature distribution of the sample. This difference between two points, the center, and surface of the reactor, was also evidenced by Salema and Afzal (2015), which observed an irregular electric field intensity from the top to bottom of the cavity where the minimum electric field intensities occurred at the center and maximum on the periphery of the material.

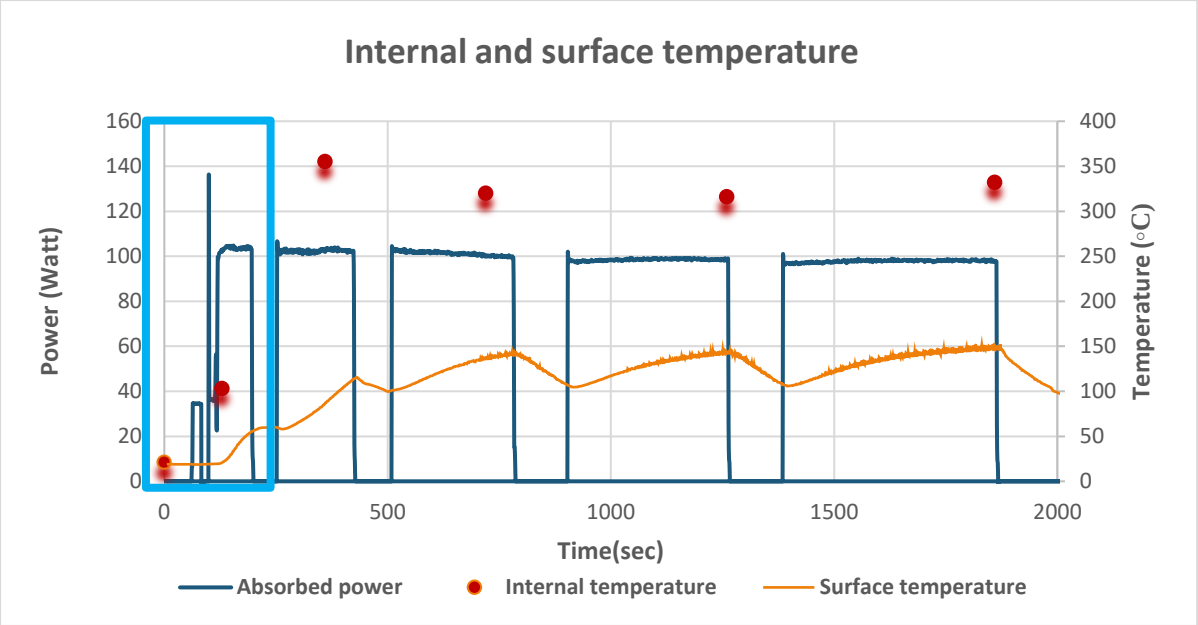

Figure 4.1-3 Microwave absorbed power vs reactor's internal and surface temperature

In our case, the maximum took place at the center of the reactor and the minimum at the surface. This was also supported by Guo and Lua (2000), which observed the same patterns in the treated sample: the internal temperature of a sample being subjected to microwave heating can be up to a hundred degrees higher than the surface temperature.

Another difference between measurements may be due to the " material in contact". The optical fiber is in contact with the quartz wall of the reactor and the thermocouple with the mixture biomass+SiC. The quartz is a transparent material to microwaves, so it is heated by a heat conduction mechanism from the heated biomass. On the contrary, SiC is a microwave absorber, which helps the biomass be heated quickly and intensely.

The next step was the study of the internal temperature of the reactor and the microwave power. The temperature measurement during the high-temperature process is very controversial due to the uncertainty of measurement. To validate the temperature measurement, relatively low and high-temperature measurements were carried out.

Figure 4.1-4 presents the evolution in time of the internal reactor's temperature related to the microwave incident power. The temperature was measured with an optical fiber placed in the center of the reactor, for a temperature range between 20 and 200°C.

The tendency was clear, the higher the incident power, the higher the temperature. A linear tendency was also found for the final temperature at the center of the reactor versus the absorbed power, in a range of 300 to 800 °C. The absorbed energy increased linearly with the incident power as the final temperature with the absorbed energy (see figure 4.1-5). For these experiments, the heating rate was between 0.3 - 4 °C/s depending on the incident power. This result is considerably higher than that

achieved using electrical heating (0.16–0.33°C/s) or for other biomasses under microwave heating, according to the literature [214].

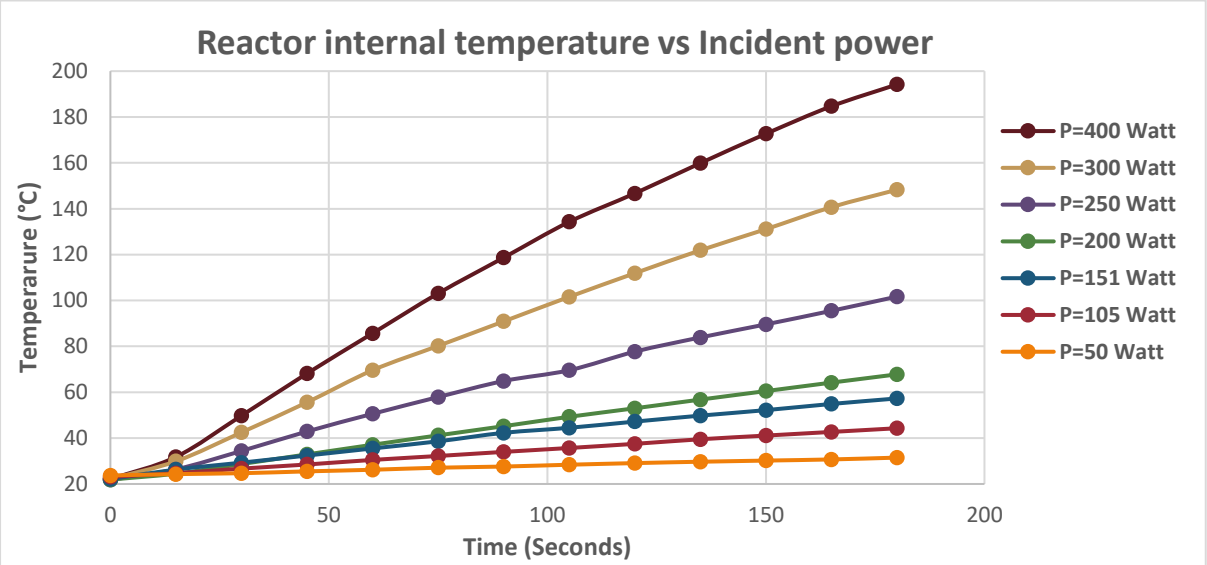

Figure 4.1-4 Reactor Internal Temperature vs Incident Power

However, even if the temperature, heating rate, and absorbed energy have a linear correlation with incident power, the different steps of the pyrolysis reaction interfere with the stability of the microwave power. As explained in chapter 3, section 3.2, the pyrolysis of biomass is often divided into three phases, a drying phase followed by an active reaction phase and finishing with a passive reaction phase.

The performance of the incident and reflected power mirrored the different biomass decomposition phases. For example, figure 4.1-5. presents the profiles of the incident, reflected, and absorbed powers during a pyrolysis experiment. The first zone inside the blue square corresponds to the tuning and water evaporation phase. The second zone in which both incident and reflected power are unstable corresponds to the active pyrolysis zone in which an abrupt mass loss and evolution of the medium permittivity occurs. At the end of the experiment, a new stable phase begins that can also be called the passive phase, which corresponds to the slow break-in of lignin.

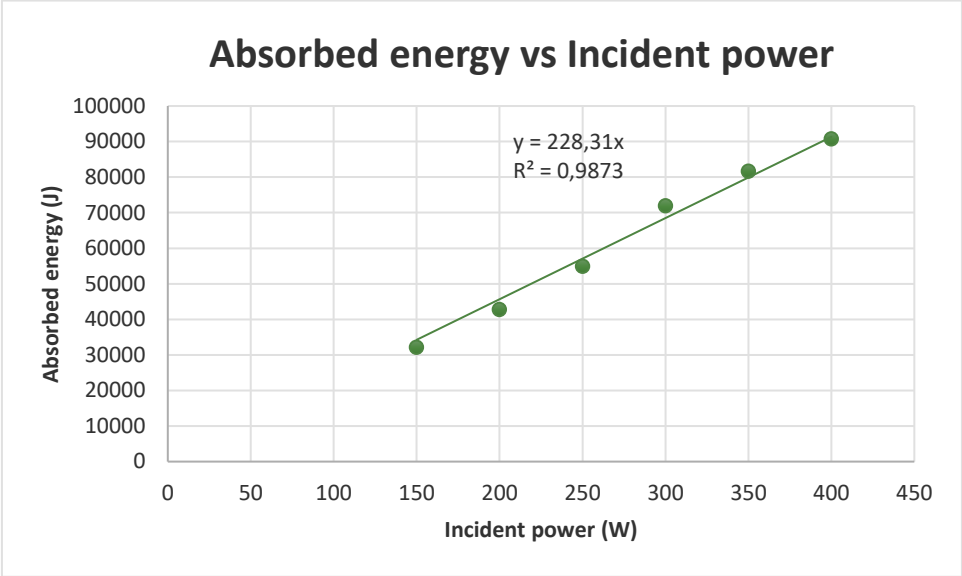

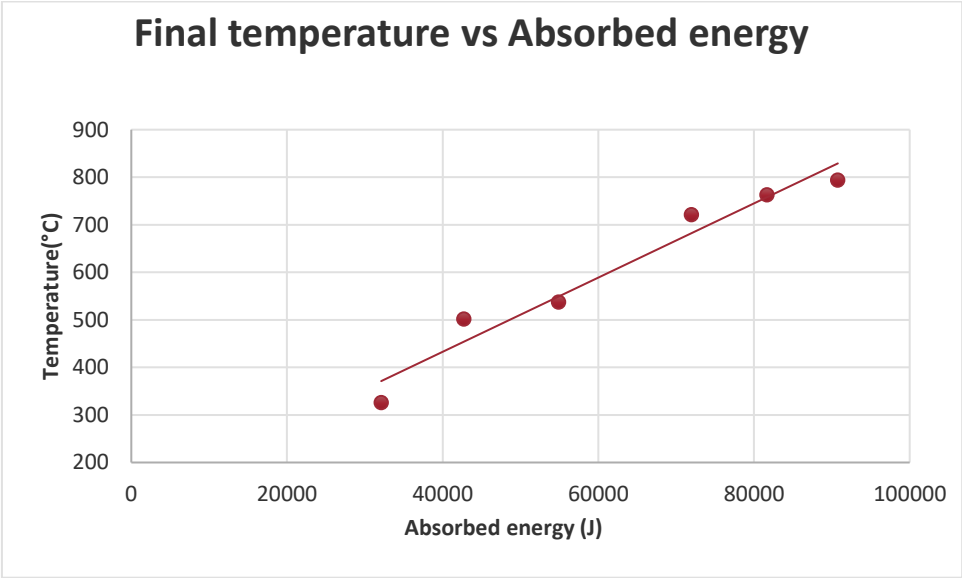

Figure 4.1-5 Incident power, Absorbed power and Final Temperature relationship

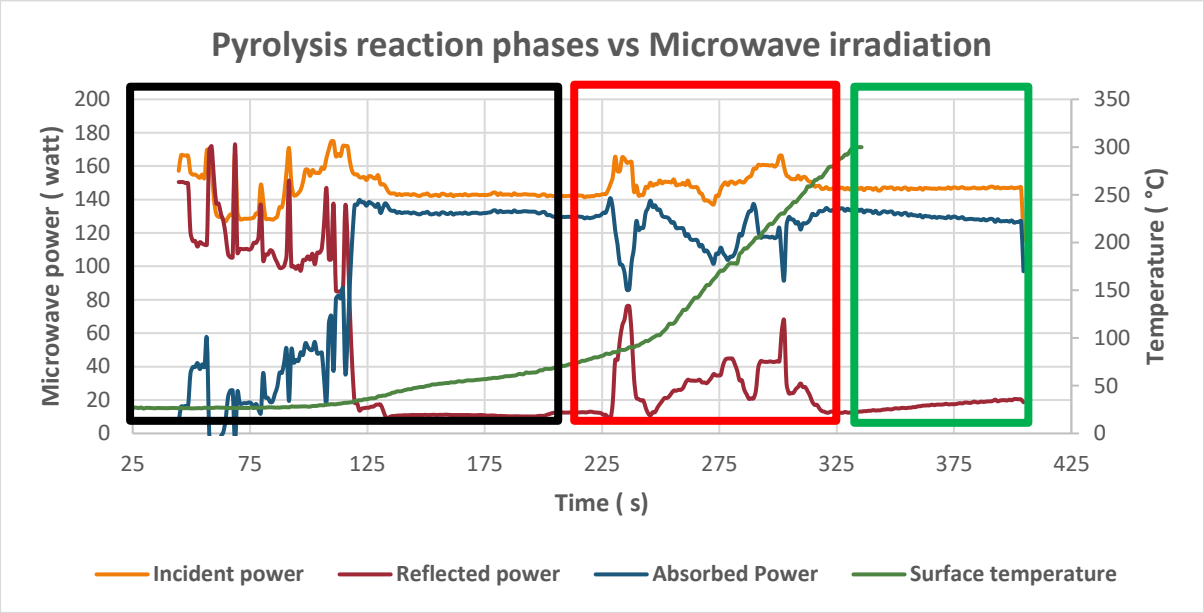

Figure 4.1-6 Pyrolysis reaction's phases during microwave irradiation

The temperature profile observed in figure 4.1-6 reflected the behavior for pyrolysis of Flax shives at 150 watts, 6 minutes of microwave irradiation, and a sweeping gas flow rate (QN2) of 600 ml/min. The alternate instability/ stability behavior of the incident and reflected microwave power is regularly observed in the experiments done during this thesis. The microwave pyrolysis behavior is characterized by the slow increase of temperature up to 120°C during the drying phase, followed by a sharp temperature increase during the active pyrolysis phase.

During the active phase, an abrupt weight loss and a change of dielectric properties of the feedstock load occur. The temperature increases, indicating the considerable heat given to the sample. The sharp increase can be related to the dielectric properties of the SiC and the bio-oil formed from the reaction. Beneroso et al. (2015) also found that the dielectric properties of municipal solid waste being heated from room temperature to 800°C increased significantly from 400°C to 600°C [196].

The last phase is more stable than the first two phases. There is not much organic matter to pyrolyze, and the thermal degradation of the lignin is quite slow. The dielectric properties of the medium are not changing since the main component on the reactor bed are SiC and char.

The active and passive pyrolysis phases can be put in evidence when observing the volatiles production during the experiment. Inside the active pyrolysis zone, devolatilization of cellulose and hemicellulose and a significant mass loss occurs, leading to massive volatile's production (See figure 4.1-7 A). The following passive phase is characterized by the slow degradation of lignin and a minimal weight loss, traduced in a non-perceptible volatile's production (See figure 4.1-7 B).

A. Pyrolysis active phase B. Pyrolysis passive phase

Figure 4.1-7 Active and passive pyrolysis phases: Volatile's production

For each microwave pyrolysis experiment, the absorbed power was deduced from the difference between the incident and reflected measured powers. The energy absorbed during each experiment was calculated as the integral over irradiation time of the absorbed power as shown below:

Equation 38: Absorbed energy

$$E = \int_{t=0}^{t_{final}} P_{abs}(t)\, dt$$

By comparing the power profiles measured during the experiments, we find that these three phases can occur over different times depending on the operating conditions applied. Figure 4.1.8. compares the pyrolysis of 4.5 g of biomass for different applied incident powers (280 W or 762 W) over different times (6 or 4 min).

Table 4.2 reports the energy absorbed by the system during each of the three phases and the total energy absorbed. The water evaporation phase is visible in both cases (delimited by the black square) and characterized by a reflected power of 40 to 45% of the incident power. Then comes the pyrolysis phase (red square). The reflected power fluctuates intensely, and the manual adjustment of the impedance by the shortcuts is difficult, especially at high incident power. This behavior was also noticed by Motasemi et al. (2015), who investigated the microwave dielectric properties of two types of agricultural biomass in the temperature range of 30°C to 700°C at 915 and 2450 MHz in a nitrogen (N_2) environment. Their results showed a penetration depth dramatically decreased as the temperature increased from 450°C to 700°C[215]. Combined with the important biomass weight loss, the latter could be responsible for the drastic drop in stability during the active pyrolysis phase.

Also, we find that this phase has a variable duration depending on the power applied (about 260 s in figure 4.1.8.a and 140 s in figure 4.1.8.b). With the high-power irradiation (figure 4.1.8.b and line 2 of Table 4.2), less energy was absorbed during the pyrolysis phase than when using low power. The third phase is the decomposition of the lignin. It is easy to control because the medium evolves slowly and allows to adjust the reflected power to its minimum.

As the production of the volatiles in this phase is not that important, the irradiation time expended in this stage can last, depending on the desired gas yield. In our example, the energy absorbed was much higher during the high-power irradiation. It should be noted that the final temperature reached was also higher (T= 820°C against 720°C for the conditions of fig 4.1-8a).

Table 4.1-2 Absorbed energy repartition during the three pyrolysis phases and final temperature

Conditions	**Phase 1: Evaporation (J)**	**Phase 2: Pyrolysis (J)**	**Phase 3: Lignin decomposition (J)**	**Total Energy (J)**	**Final temperature (°C)**
Figure 4.8 a	2525	51954	19814	74293	720
Figure 4.8 b	4353	26638	61727	92717	820

In general, the overall absorbed energy varies linearly with the incident power for the different experiments conducted over 6 minutes of microwave irradiation. Similarly, the final temperature reached has a linear correlation with the total energy absorbed as seen in the figure 4.1.5. This indicates that despite the thermal losses and inertia of the system, the energy is properly transmitted to the biomass and that the medium is relatively homogeneous in temperature, regardless of power applied.

Also, the inertia of the system was evaluated. Both continuous and alternate microwave irradiation were tested for the same operating conditions. The experiment consisted in 7 minutes of microwave irradiation: the first one, 7 minutes “on” under continuous irradiation, and the second one, 7 minutes divided in 4 minutes of irradiation, 1 minute off followed by 3 minutes of irradiation. The results are presented in figure 4.1-9 for the absorbed energy, final temperature, and cooling behavior.

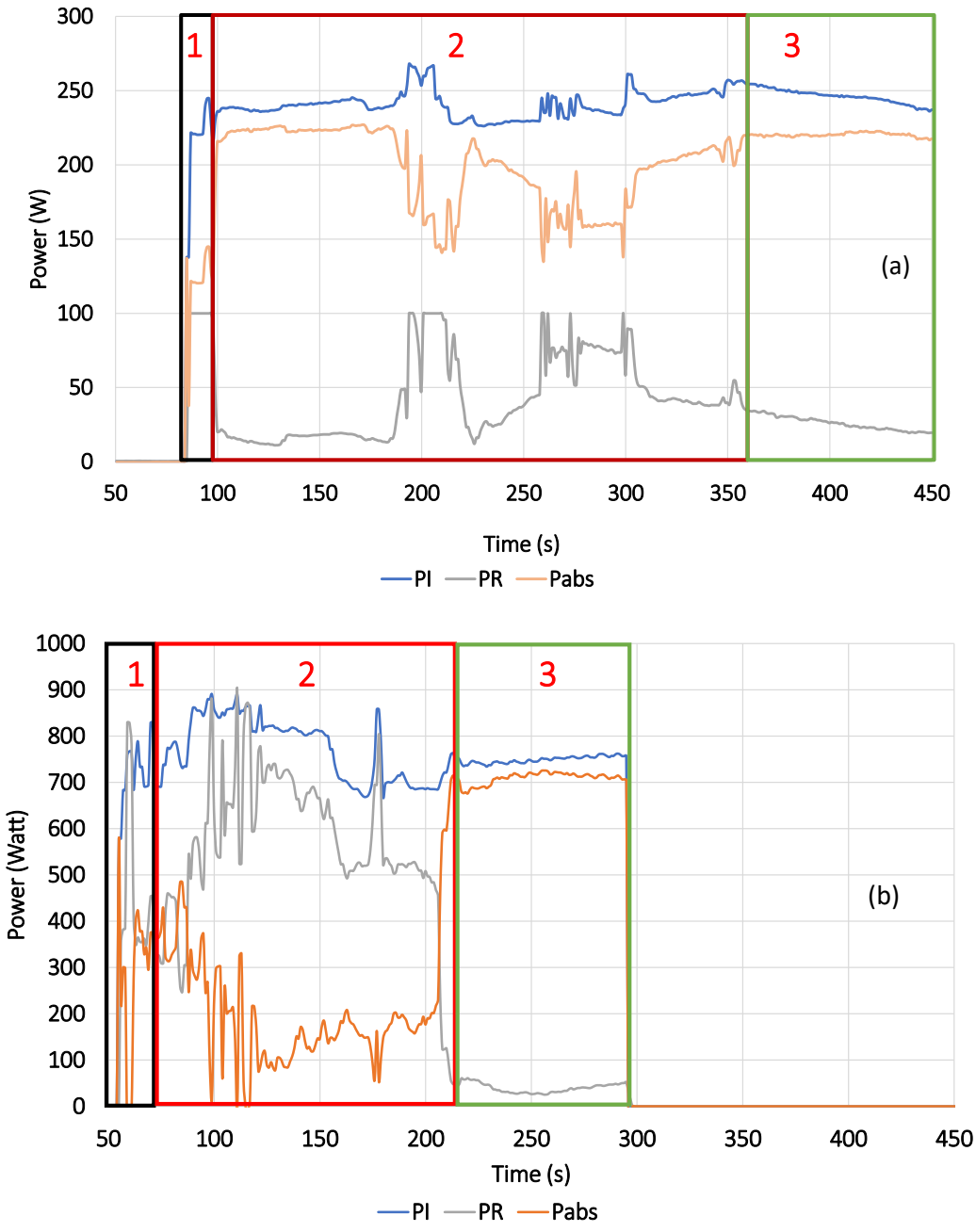

Figure 4.1-8 Incident, reflected and absorbed powers profiles (PI, PR and Pabs respectively):

a) $PI_{average}$ = 280 W; $t_{irradiation}$ = 6 min; m = 4.5 g; Q_{N2} = 300 ml/min.

b) $PI_{average}$ = 790 W; $t_{irradiation}$ = 4 min; m = 4.5 g ; Q_{N2} = 600 ml/min.

Table 4.1-3 Maximum temperature and energy for continuous and alternate irradiation mode

Type of irradiation	Tmax measured (°C)	Energy (j)
Continuous	529°C	85563
Alternate	580°C	66680

It was found that the alternate irradiation mode consumed less energy, and the final temperature was a little bit higher than for the continuous irradiation mode. The effect of the alternate irradiation mode on the final temperature can be explained by the reduced time under the third phase of pyrolysis and the extension of the second phase of pyrolysis.

By dividing the experiment into two periods, the first irradiation period is consumed by the evaporation of the water and the ignition of the active pyrolysis zone. The minute the microwaves were off, the system's inertia allowed to continue the pyrolysis but at a lower degree. As the pyrolysis was not completed, the active pyrolysis zone was extended when re-starting the irradiation. When measuring the final temperature, it was higher due to the dielectric properties of the mixture of bio-oil, char, and SiC remaining on the reactor bed. Figure 4.1-9 presents the power and temperature behavior for the alternate irradiation mode to better understand the latter. (Incident power in green, reflected in brown, and absorbed in blue. The surface temperature is purple, and the final internal temperature is red). The alternate microwave heating was also studied by Wang et al. (2012), concluding that it was a practical energy-saving method while manipulating the heating operation exothermic reactions and allowing to selectively collect primary pyrolysis products at specific heating times [164].

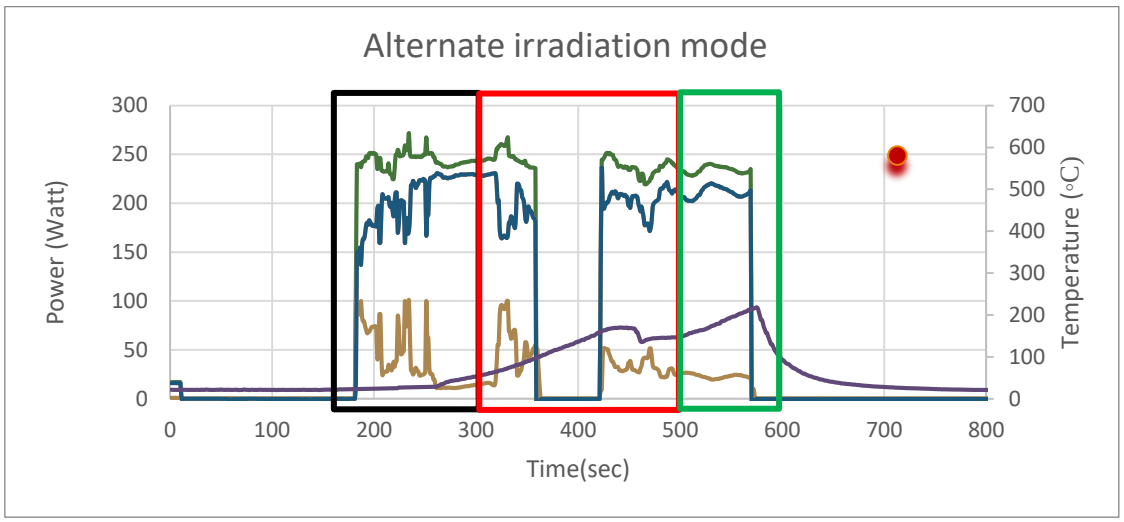

Figure 4.1-9 Alternate irradiation mode with temperatue

4.2 MICROWAVE PYROLYSIS OF FLAX SHIVES

Microwave heating leads to high temperatures and heating rates, and the rotary reactor configuration favors the homogeneity of the process. The incident power, proportional to the absorbed power, heating rate, and temperature, is the main parameter affecting the amount of energy for biomass fragmentation. Variations in the biomass products (liquid, gas, and char) are observed when changing the operating conditions and the kind of biomass feedstock selected. His section aims to understand the relationship between operating conditions and the Flax shives microwave pyrolysis products. The microwave pyrolysis setup and protocol used in this chapter are described in chapter 2.

4.2.1 Influence of operating conditions on bio-oil, gas, and char distribution

The fractional yield of bio-oil, gas and char for the results of pyrolysis of 4.5 g of Flax shives mixed with 0.9 g of SiC, under a nitrogen flow rate of 600 ml/min during 6 minutes of microwave irradiation are presented in table 4.2-1. The number of repeated experiments for each operating condition was shown in the first column and the values displayed for product distribution, total energy absorbed, the surface and internal heating rate and final temperature reached values are averages of the values obtained. Thus, five experiments with identical operating conditions were conducted under a 300 W magnetron instruction, and this set of results allowed to evaluate at 4.6% standard deviation on energy absorbed, and respectively at +/-1.72%, 0.54%, and 3.62% absolute error on the percentages of char, bio-oil, and gas.

Table 4.2-1 Absorbed energy, heating rates, final temperature and products distribution vs incident power; mbiomass= 4.5 g; mSiC = 0.9 g; QN2 = 600 ml/min; Irradiation time = 6 min.

Number of repeated experiments	PI Magnetron (W)	Absorbed energy (J)	Surface heating rate (°C/min)	Internal heating rate (°C/min)	Final temperature (°C)	% Bio-oil	% Char	% Gas
1	150	32105	19	51	326	41.1	33.6	25.3
2	200	42741	57	80	502	47.5	23.0	29.5
1	250	54916	69	86	537	49.9	18.0	32.1
5	300	71977	81	117	721	56.6	17.7	25.6

From table 4.2-1, the yield of bio-oil obtained increases with the increase of the incident power and consequently with the absorbed energy. The heating rate and temperature also tend to increase. Contrary, the char content tends to decrease, and the gas is less stable in yield. There is a maximum between 80 and 86 °C/min regarding the heating rate and gas yield. Higher heating rates are more

favorable for bio-oil production than gas. Also, from a certain point, the decrease in char yield at higher temperatures is believed to occur due to solid char cracking that favors gas formation.

Normally, an increase in gas and a decrease in bio-oil are expected at higher temperatures when referring to conventional pyrolysis due to the secondary cracking of pyrolysis vapors. However, in our case, the higher temperature did not decrease the bio-oil percentage to favor gas production. This is expected since the heating rate of the microwave pyrolysis was quite high due to the instantaneous volumetric heating of the sample.

The latter was also observed by Isahak et al. [18] and Mohan et al. [19], who proposed that the high yield of bio-oil is due to cracking reactions promoted at a higher heating rate.

To have competitive results compared to conventional pyrolysis, the microwave pyrolysis bio-oil yield must be 50-60%. In this study, the liquid yield was found to be between 40 and 60%, with an average between all the experiments and operating conditions of 51%.

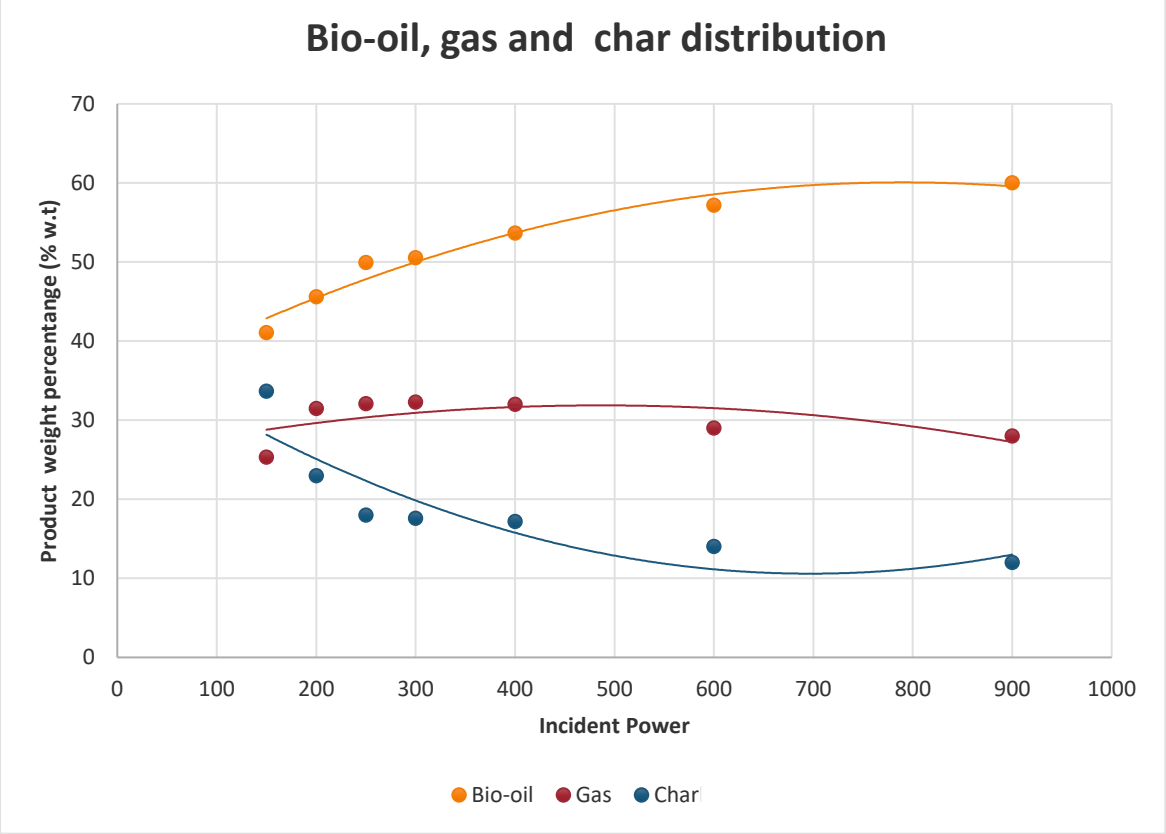

Figure 4.2-1 Bio-oil, gas, and char distributions vs incident power

Figure 4.2.2 shows a maximum bio-oil production at around 72000 J in terms of absorbed energy. A minimum amount of energy must be brought to the system to break down chemical bonds and decompose the biomass, essentially hemicellulose and cellulose. We can also see this in char production, which decreases sharply between 30000 and 60000 J: the first points do not correspond to the char

production but rather to a mass of partially pyrolyzed biomass remaining at the end of the experiment. The amount of char tends to reach around 17-18%, which corresponds perfectly to the value obtained at high temperature by TGA. At higher energy delivered, bio-oil production tends to stagnate. The bio-oil is mainly produced during the rise in temperature up to 350°C - 400°C by the decomposition of hemicellulose and cellulose. Still, beyond that, the decomposition of the remaining lignin does not allow for more oil production. Zhao et al. (2017) observed this pattern in the study of the distribution of volatiles products and the influence of temperature. It was found that, for each sample pyrolysis, pyrolysis temperature and their chemical structures played an important role in the yields, composition of bio-oil, and bio-gas. The optimal temperatures for bio-oil production from cellulose, hemicellulose, and lignin focused at 500 °C, 450 °C, and 600 °C, respectively, and cellulose made a greater contribution to bio-oil formation [216].

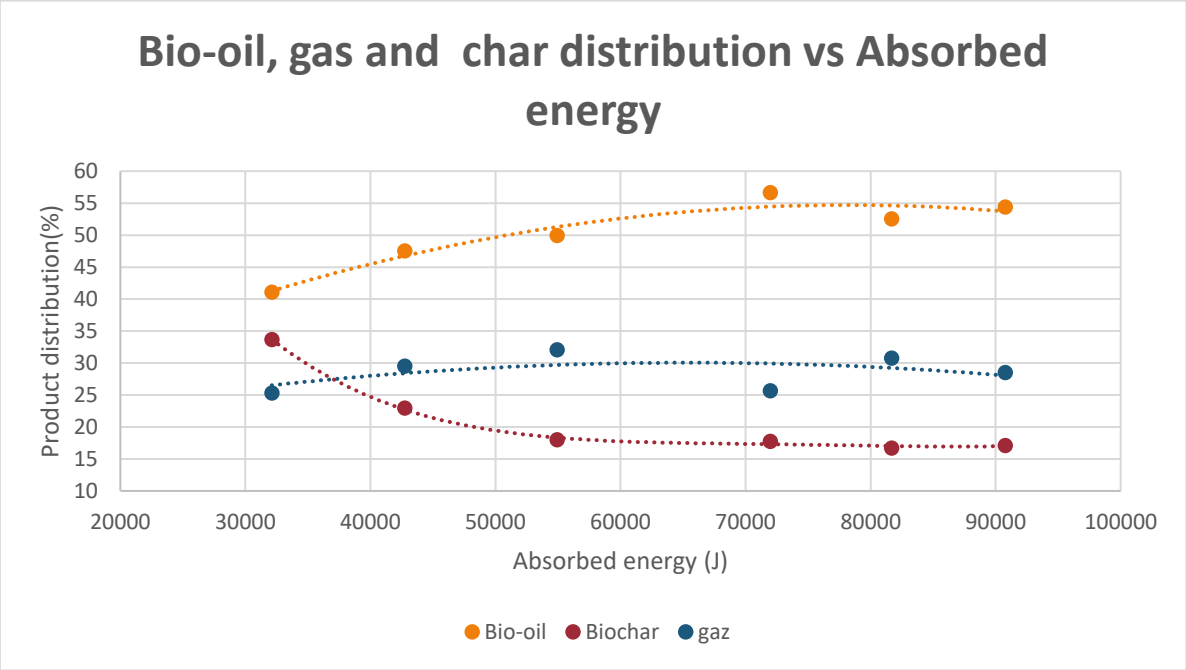

Figure 4.2-2 Products distribution with absorbed energy

Given the previous results, the next step was to study the effect of the irradiation time correlated with the incident power. Table 4.2-2 presents the results of pyrolysis of 4.5 g of Flax shives mixed with 0.9 g of SiC, under a nitrogen flow rate of 600 ml/min for different irradiation times and incident power. It is observed that the higher yield on bio-oil was obtained at 900 watt and 4 minutes of irradiation. The higher yield of gas was obtained at 500 watt and 5 minutes of irradiation, as well as the lower yield of char. Also, for the same incident power, the increase of the irradiation time was more favorable to produce gas than the production of bio-oil. It can be concluded that high incident power with short irradiation time favors bio-oil, and intermediate incident power with high irradiation time benefits the production of gas.

Table 4.2-2 Irradiation time and incident power effect on bio-oil, gas, and char fractions

Incident Power (watt)	Irradiation Time (min)	Bio-oil %	Char %	Gas %
300	2	53%	42%	6%
300	4	59%	17%	23%
300	7	**60%**	**15%**	**25%**
500	5	**47%**	**17%**	**36%**
600	4	57%	15%	28%
900	4	64%	16%	20%

The energy absorbed per unit mass is an alternative to reconcile the data of absorbed energy and the biomass load inside the reactor. Across the range of experiments conducted, the absorbed energy did show and influence with respect to the bio-oil liquid yield. In the other hand when increasing the biomass load, the absorbed energy is also increased because of the volume to be heated. The maximum point of bio-oil yield is achieved at 30325 J/ g for a 70% with a tendency to increase with the quantity of energy applied to biomass.

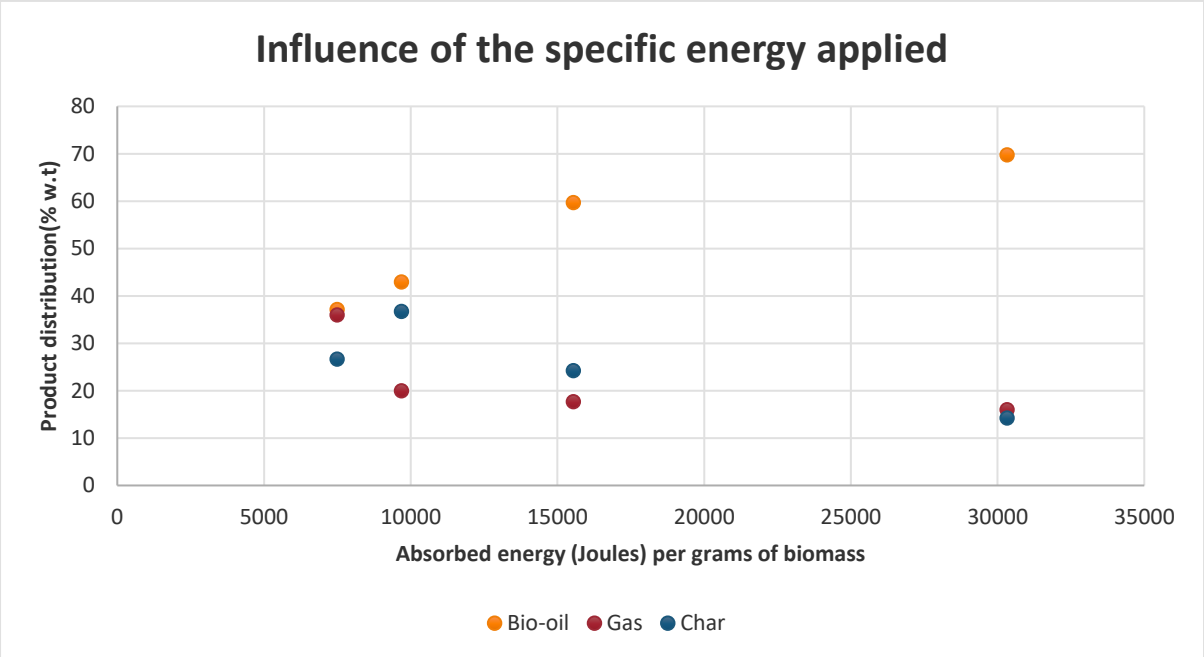

Figure 4.2-3 Influence of the absorbed energy per grams of biomass

The maximum point of gas production is achieved at 9388 J/g for a 37%. The maximum point for the bio-oil yield was achieved by applying an incident power of 300 watt to a biomass load of 2.25 g and the maximum of gas was produced by applying the same incident power to a biomass load of 6.75 gr. This effect can be closely related to the biomass load that is known to influence the pyrolysis yield. Thus, larger feedstock loads have greater temperature gradients in the center and a slower heating rate between the surface and the center. Also, the mass transfer barrier becomes more pronounced where volatiles produced from primary reactions are facing higher resistance offering opportunities for the vapors to undergo extensive secondary cracking reactions leading to a higher gas yield.

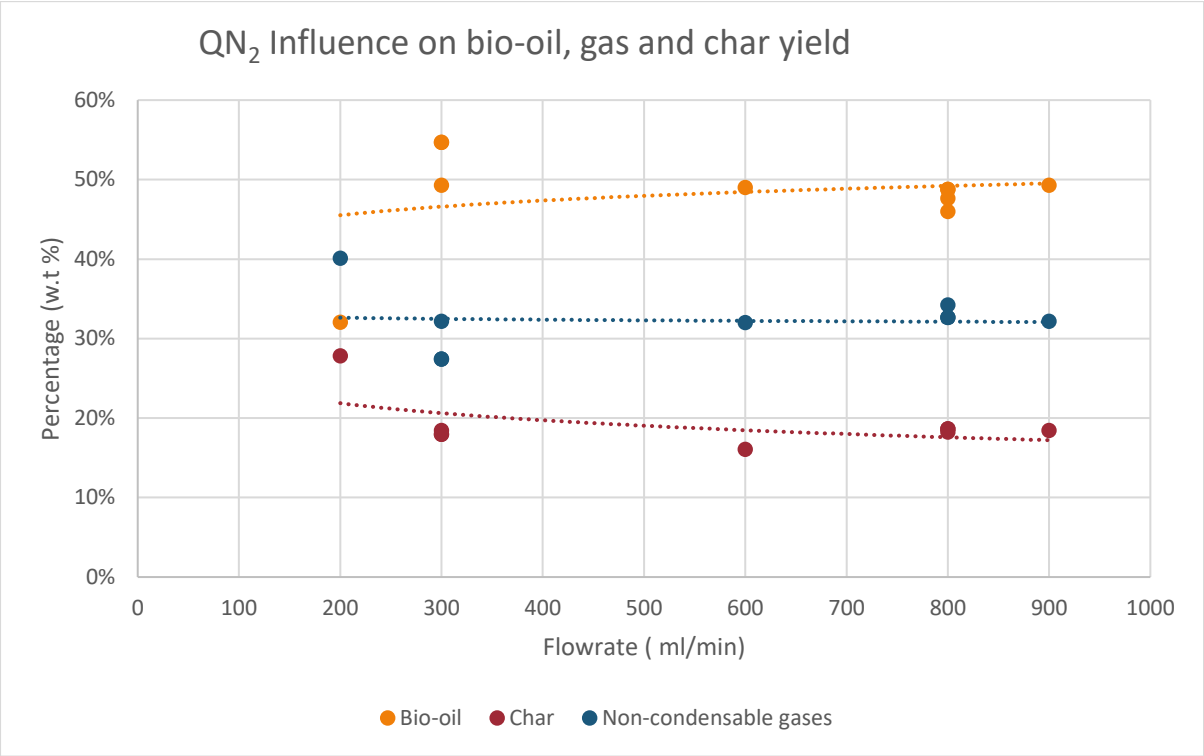

Figure 4.2-4 Influence of the sweeping gas flowrate on bio-oil, gas and char yield

The influence of the sweeping gas flow rate over the bio-oil, char and gas yield was also evaluated for the pyrolysis of 4.5 g of Flax shives mixed with 0.9 g of SiC at 300 watts of incident power and 6 minutes of microwave irradiation. In general, increasing the sweeping gas flow rate decrease the residence time. Short residence time also leads to an increase in bio-oil yield due to the rapid exclusion of organic gasses from the reactor, which minimizes the secondary reaction, according to Bridgewater [3], [68]. In general, bio-oil production exceeds gas production for the different possibility of flow rates.

Mushtaq et al. [177] studied the effect of the nitrogen gas flow rate in the pyrolysis of oil palm shells. The results showed that the nitrogen flow rate strongly influenced the bio-oil yield. Increasing the flow rate did increase the bio-oil yield. However, a further flowrate increase, up to 5L/min, decreased the bio-oil yield, showing an optimal operating condition.

Low flow rates favor the char yield. According to Koufopanos et al. (1991), the secondary reactions at high residence times enrich the carbon content of the final residue when it interacts with the

carbonaceous solid, leading to primary products reforming into char and secondary volatile products [217], [218]. The gas yield has similar behavior to the char yield. At a nitrogen flow rate of 200ml/min, the longer residence time tested at 300 watts, the yield of gas was higher than the yield of bio-oil also the yield of char and bio-oil were very close. As mentioned before, long residence time favors the production of gas and char.

4.2.2 Influence of operating conditions on bio-oil chemical families

The GC-MS analysis performed in the bio-oil samples for different conditions, put in evidence the existence of more than 150 compounds which were grouped into 13 families listed in section 2.3.1. The composition of the bio-oil is variable. We observed that carboxylic acids, phenols, and ketones which come from the hemicellulose break down are the major compounds. The percentage of sugars, guaiacols and alkanes was less than 0.5%. As these percentages were less than the error margin of the apparatus used to quantify the oils, they have not been retained.

The composition of the bio-oil seems to depend more on the sample's nature than on the operating conditions of pyrolysis studied here. Even at high heating rates, the composition is close to the average composition obtained on all our experiments, however, the trends of the mass percentages of the main compounds are studied below.

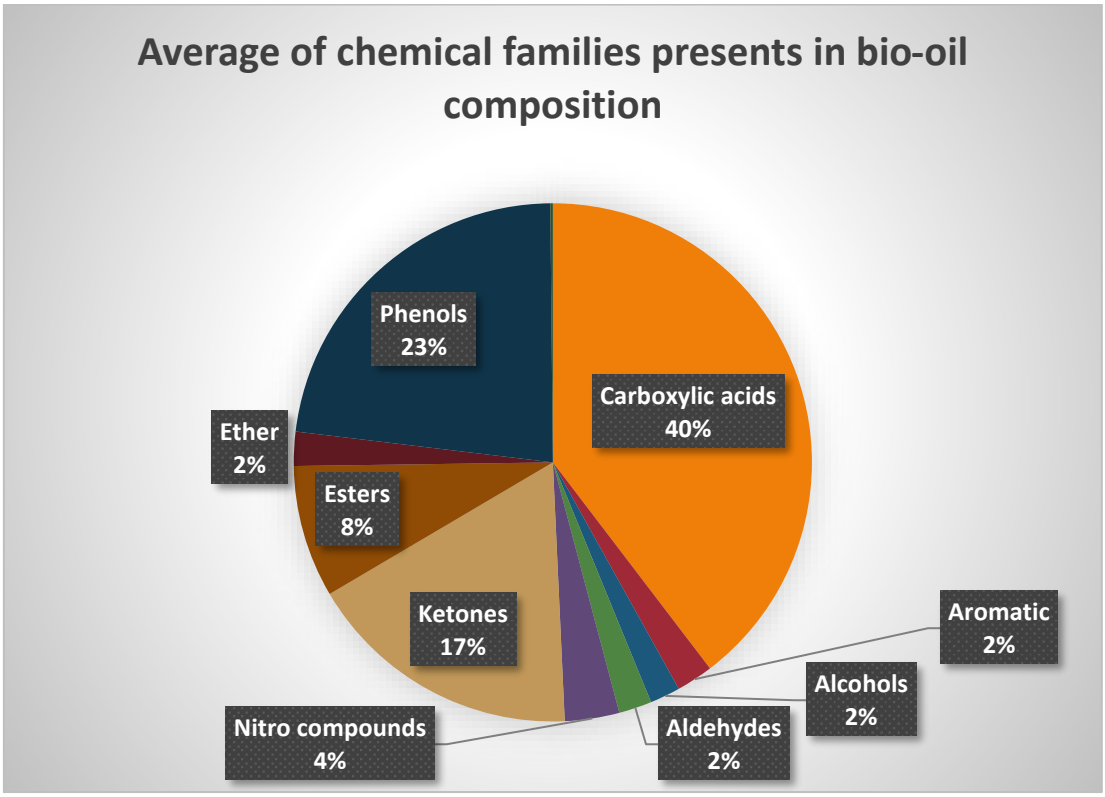

Figure 4.2-5 Average of chemical families presents in bio-oil composition for all experiments

The carboxylic acids production first increases and then decreases while increasing temperature, with a maximum value at 530° C (figure 4.2.6). The latter behavior was also reported for the carboxylic acids obtained for beech wood [219] . This trend can be explained by the formation of complex molecules at low temperature, that break down when temperature increases, and escape in gaseous form. The low-temperature dehydration phase does not promote the acids production because the time is too short, giving the way to depolymerization. However, Flax shives are rich in cellulose (more than hemicellulose), which favors the production of syngas at high temperature [220], the high temperature is quickly reached and the decomposition of cellulose results in a high proportion of gas of the same composition as the other experiments, in detriment of the carboxylic acids molecules.

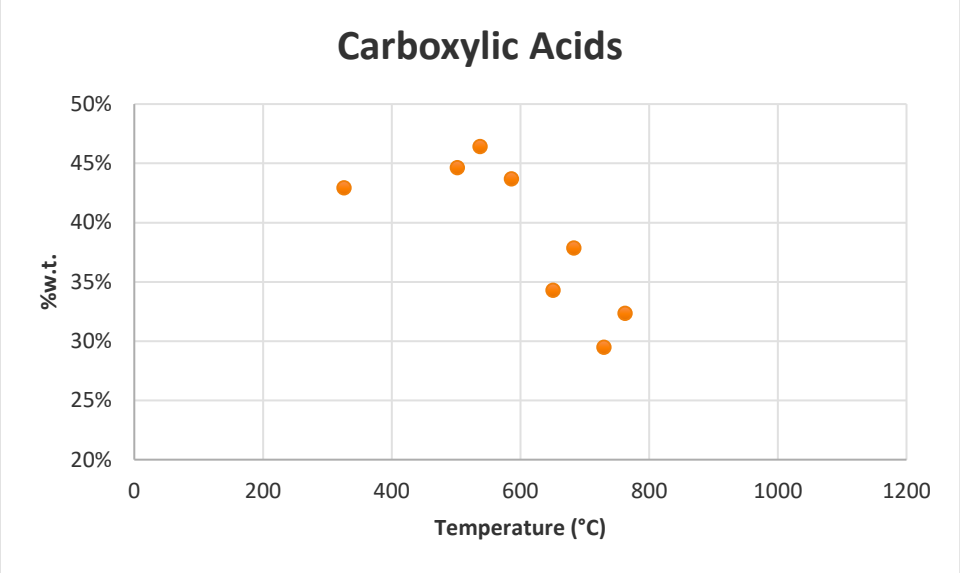

Figure 4.2-6 % w.t of Carboxylic acids at different temperatures

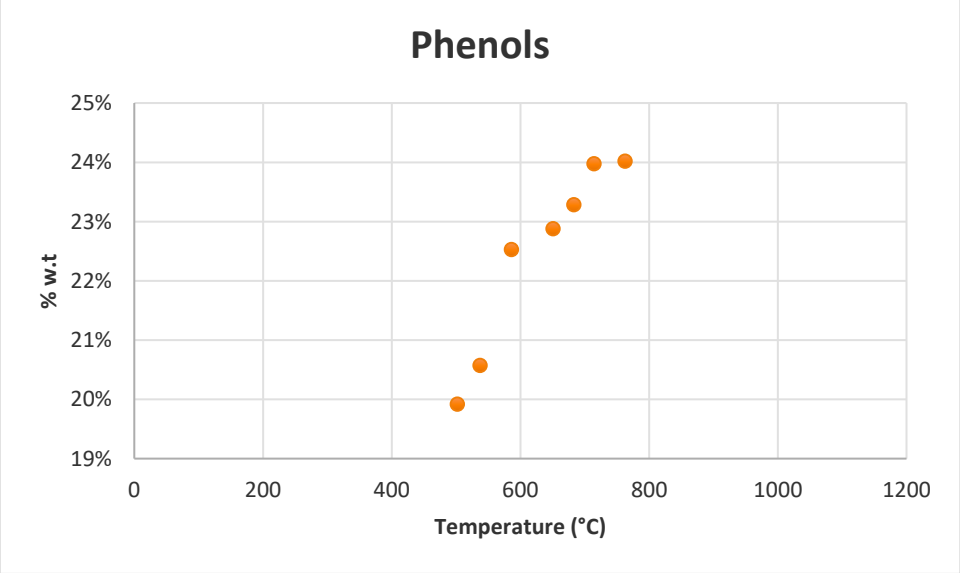

Figure 4.2-7 % w.t of phenols at different temperatures

Phenol compounds in the bio-oils were observed, in greater quantities in microwave-pyrolysis oils. Phenolic compounds are the second major compound of the Flax shives pyrolysis bio-oil. The

percentage of phenols fluctuates with temperature from 20 to 24%, increasing with temperature. Mohabeer [219], explained in her thesis work that the percentage of phenolic compounds came from the lignin fraction of the biomass. However, the global trend found here was not similar to the trend found by Mohabeer [219] in a fixed bed reactor and conventional heating, where the percentage of phenols decreased after 600 °C. The aromatic compounds were found in concentrations between 1.6 and 2.8 w.t %. An increase with temperature was found, but only until 700°C (figure 4.2-8). This means, that to increase the aromatics compounds, the temperature limits must be 650°C while evaluating other parameters as flow rate and the use of catalyst.

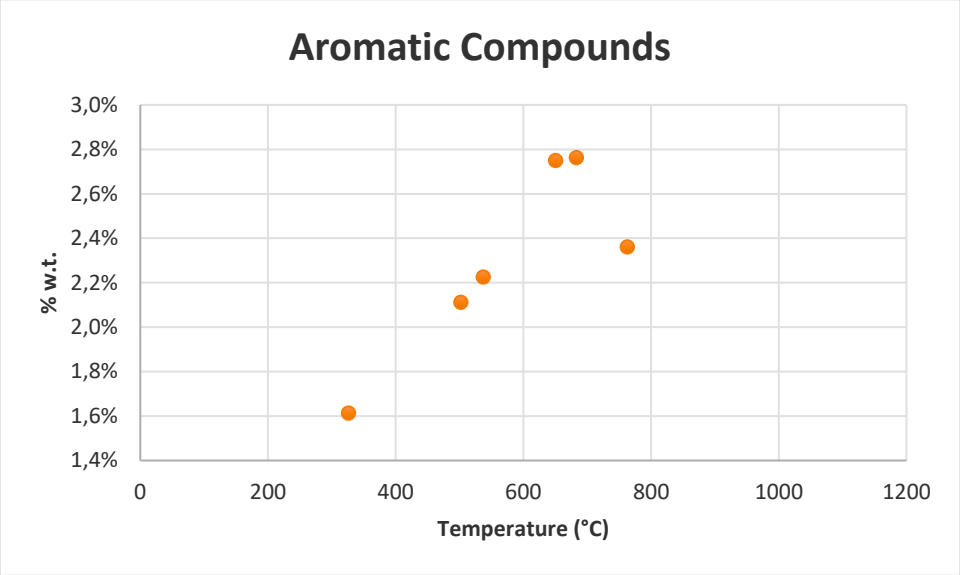

Figure 4.2-8 % w.t of aromatic compounds at different temperatures

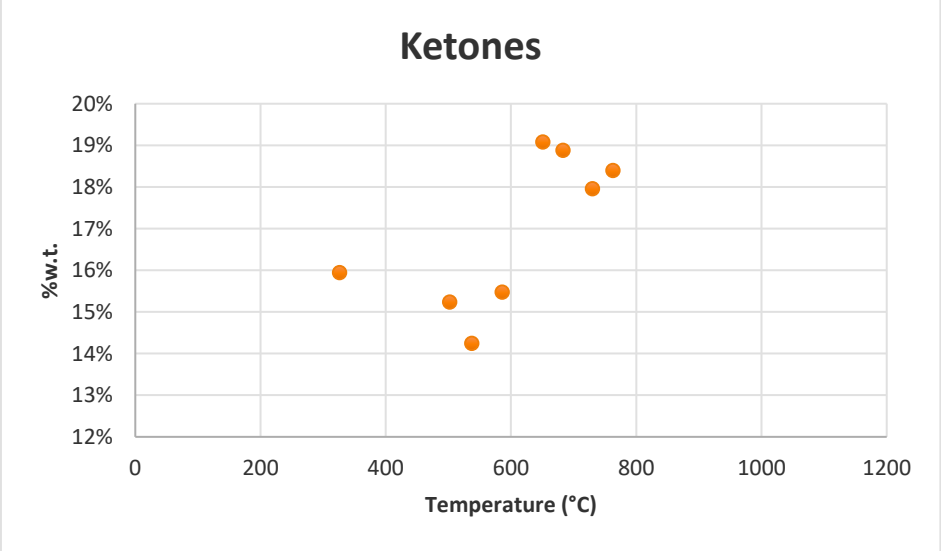

Figure 4.2-9 % w.t of ketones at different temperatures

Contrary to carboxylic acids, after 650°C, the percentage of ketones increased. However, the percentages are dispersed, and other factors should be studied deeply to better understand the ketones behavior. An explanation could be the time and kinetics of hemicellulose' degradation path, given that the bio-oil of hemicellulose is higher in acids and ketones, and the higher temperatures could lead to secondary cracking reactions of the hemicellulose bio-oil [216].

4.2.3 Influence of operating conditions on gas composition

The gas or non-condensable is the third product of pyrolysis and is mainly composed of H_2, CO_2, CH_4, and CO with traces of C_2 and C_3 species. This set of species is a consequence of secondary reactions such as volatile cracking and interactions between volatiles with gas or volatiles with the char during pyrolysis. Nitrogen, which is used as sweeping gas, is also found in the sample of gases, but as it is an inert gas used to produce the anoxic atmosphere during pyrolysis, it is not considered for the gas quality study. First, the results obtained for 300-watt pyrolysis of 4.5 gr of Flax shives mixed with 0.9 gr of SiC and 600 ml/min of N_2 flow rate are shown in figure 4.2.10. It is observed that at 3 minutes of microwave irradiation, the main specie produced is CO_2. At a temperature between 300 and 400°C, CO_2 and CO are the main species produced. This is corroborated by Zhao et al. (2017), which indicate that up to 280°C, the degradation of cellulose go together with CO_2 and CO production. At that time, the temperature is between 300-and 400°C [216]. Three minutes later, the CO_2 production decreased abruptly with the increase of temperature up to 700°C. The latter behavior of CO_2 is due to the secondary reactions intensified by the increase in temperature.

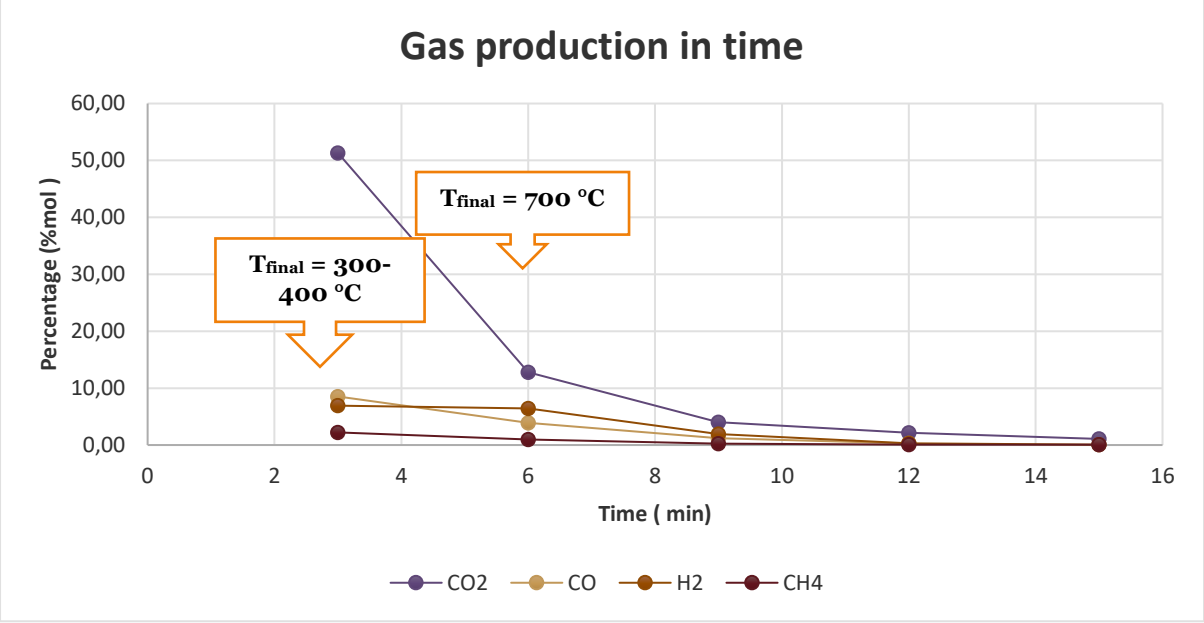

Figure 4.2-10 Gas species production in time for a 300 watt pyrolysis of 4.5 gr of Flax shives mixed with 0.9 gr of SiC and 600 ml/min of N2 flowrate.

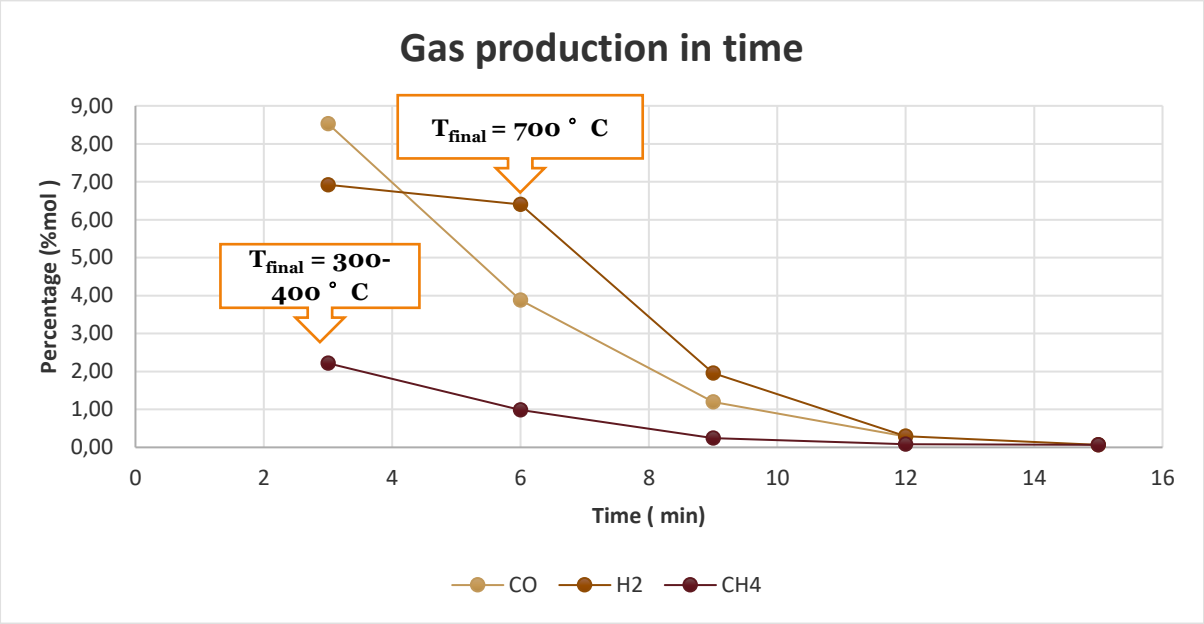

Figure 4.2-11 CO, H2 and CH4 production in time for a 300-watt pyrolysis of 4.5 gr of Flax shives mixed with 0.9 gr of SiC and 600 ml/min of N2 flowrate.

Considering the other species, the production of H_2 exceeds the production of CO and CH_4 when increasing the temperature. The increase of H_2 is due to the first part of char formed inside the core of the material that becomes the microwave absorber. It has a higher capacity to absorb microwave energy resulting in a higher temperature in the char matrix and an ignition of the char gasification reaction.

The effect of the incident power on the global gas species production was studied. As observed in Table 4., H_2 and CO production increase slightly, whereas CO2 and CH_4 decrease as the incident power increases. The increase in CO with simultaneous reduction of CO_2 concentration at higher incident power which results in higher temperatures indicates that the Boudouard reaction is taking place [221]. Also, the fact that CO_2 is released first and H_2 later in the pyrolysis process while the peak of CO formation follows CO_2 formation indicating secondary reactions of tar cracking, steam reforming, and char gasification, was reported by Zhang et al. (2017) [206]. This char gasification is a result of the unique heating path inside the biomass produced by the microwave heating and increasing CO and H_2

Table 4.2-3 Gas species production for different incident powers at 6 minutes of microwave irradiation for pyrolysis of 4.5 gr of Flax shives mixed with 0.9 gr of SiC and 600 ml/min of N2 flowrate

Incident power (W)	H_2 %w/w	CO %w/w	CH_4 %w/w	CO_2 %w/w	C_2 %w/w	C_3 %w/w
200	3,2%	58,8%	8%	30%	1,3%	1,3%
400	3,2%	59,1%	7%	31%	2,7%	1,2%
900	3,3%	59,2%	6%	27%	3,1%	1,1%

.

Miller et al. (2021) concluded from their research about the microwave-induced selective decomposition of cellulose that gas products revealed that applying 250 W of MW power led to the production of CO, H_2, along with some CO_2 and CH_4. Reaction under 500, 750, and 1000 W of power revealed that higher power led to the complete decomposition of cellulose to mainly CO and H_2 [223]. This could explain the increase of CO and H_2 at higher incident power at the expense of the pyrolysis of cellulose. Mohabeer et al. [198] also studied the effect of temperature on the non-condensable gas species for Flax shives. She concluded that the CO_2 production decreased with increased temperature while the other species increased [219]. In our case, the tendencies for CO_2 were similar, but only CO, H_2, and the C_2 increased with the incident power and consequently with temperature. The C_3 and CH_4 decreased. Regarding the residence time of the non-condensable gases related to the total gas flow rate, the CO_2 production was favored at lower flow rates while C_3 at the higher flow rate. The other species found a maximum mass percentage at 600 ml/min.

Table 4.2-4 Gas species production for different N2 flowrate at 300 watt at 6 minutes of microwave irradiation for pyrolysis of 4.5 gr of Flax shives mixed with 0.9 gr of SiC.

Flowrate (ml/min)	H_2 **%w/w**	CO **%w/w**	CH_4 **%w/w**	CO_2 **%w/w**	C_2 **%w/w**	C_3 **%w/w**
200	1,9%	43%	2,0%	53%	1,0%	0,8%
600	3,2%	58,7%	7%	31%	3,5%	1,2%
800	3,0%	55%	6,8%	30%	3,3%	1,9%

4.3 MICROWAVE PYROLYSIS OF SARGASSUM

4.3.1 Experimental approach

The pyrolysis of Flax shives allows us to understand the influence of the microwave pyrolysis parameters on the bio-oil, char, and gas yield. A factorial experimental approach was implemented to compare the global trend of those results to the ones of Sargassum's microwaves pyrolysis. The experimental approach and combination of operating parameters is presented in the figure below:

Figure 4.3-1 Factorial experimental system for Sargassum.

Flow rate (ml/min)	200	200	800	800
Incident power (Watt)	**100**	**600**	**100**	**350**
Irradiation time (Minutes)	0.5	2	2	6
Incident power (Watt)	100	350	100	600
Irradiation time (Minutes)	10	6	10	6

4.3.2 Influence of operating conditions on bio-oil, gas, and char distribution

The weight-loss behavior of the Sargassum is presented in figure 4.3-1. Like Flax shives, the increased energy absorbed leads to higher temperatures and higher weight losses, which is also traduced to the amount of biochar remaining in the reactor after the pyrolysis reaction. When comparing both Flax shives and Sargassum weight loss with time (section 3.2.2 and section 4.2.1), for Sargassum, the weight loss was less critical for the same amount of absorbed energy with a 10% the difference. Also, the behavior of temperature vs. the absorbed energy was studied for the minimal and maximal flow rates used. Figure 4.3-3 shows how the N2 flow rate decreases the maximal temperature achieved for a similar amount of absorbed energy. As the sweeping gas flowrate comes inside the reactor at room temperature, it cools down the biomass bed.

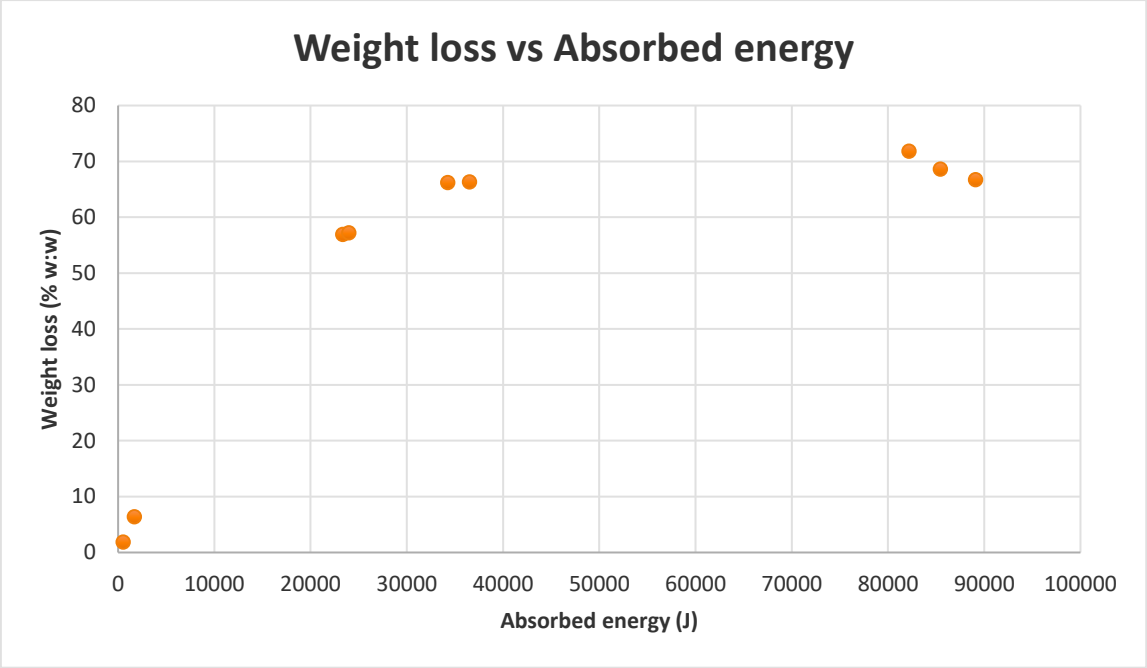

Figure 4.3-2 Sargassum feedstock weight loss vs absorbed power

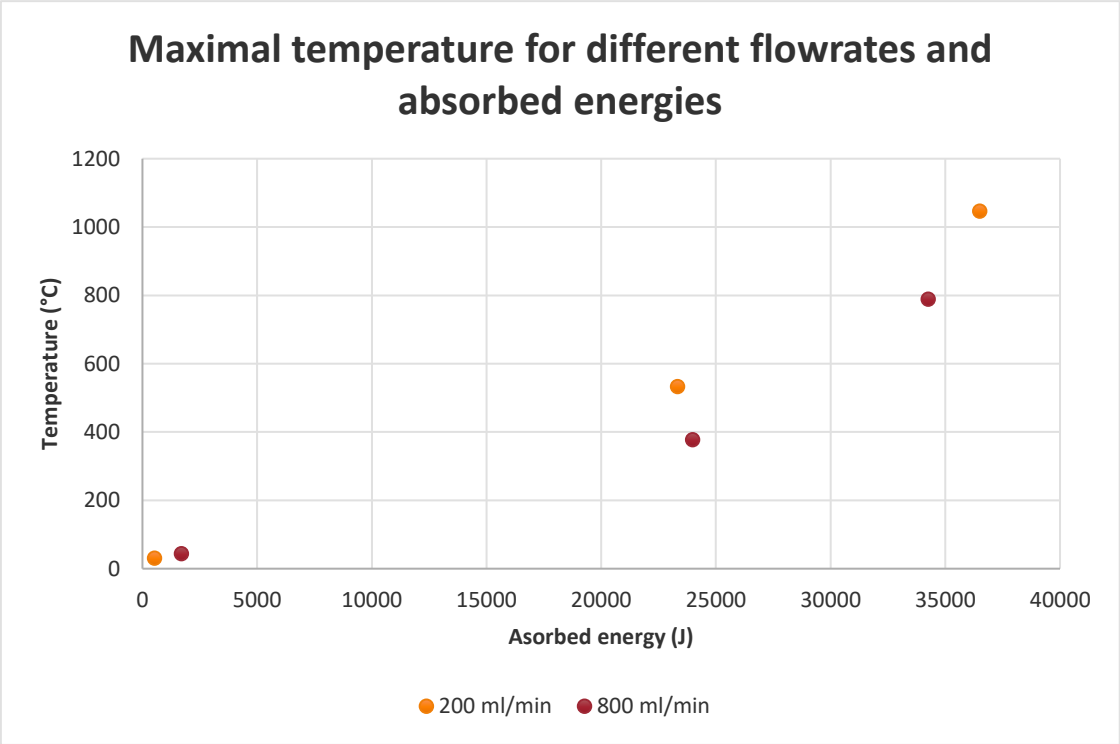

Figure 4.3-3 Sargassum maximal temperature under different flowrates vs absorbed energy

The pyrolysis temperature of biomass has an important effect on product yields, and it was found to be the best parameter to understand the results. With increasing temperature, there was also an increase

in the amount of bio-oil produced, up to 43.8 % at 1047 °C. The maximum change in bio-oil yield (an increase of 40%) occurred between 400 to 500 °C (Figure 4.3.4). Similarly, another researcher has studied the effect of temperature on liquid yields.

The liquid yields were determined from rapeseed cake based on increasing temperatures of 350, 400, 450, and 550°C via a home-built lab-scale semi-continuous pyrolysis reactor. They found that increasing temperature leads to higher liquid yields of 28.3, 34.3, 53.4, and 58.2 wt%, respectively [107]. In general, it is stated that temperature is an important parameter that plays a key role in getting pyrolytic yields.

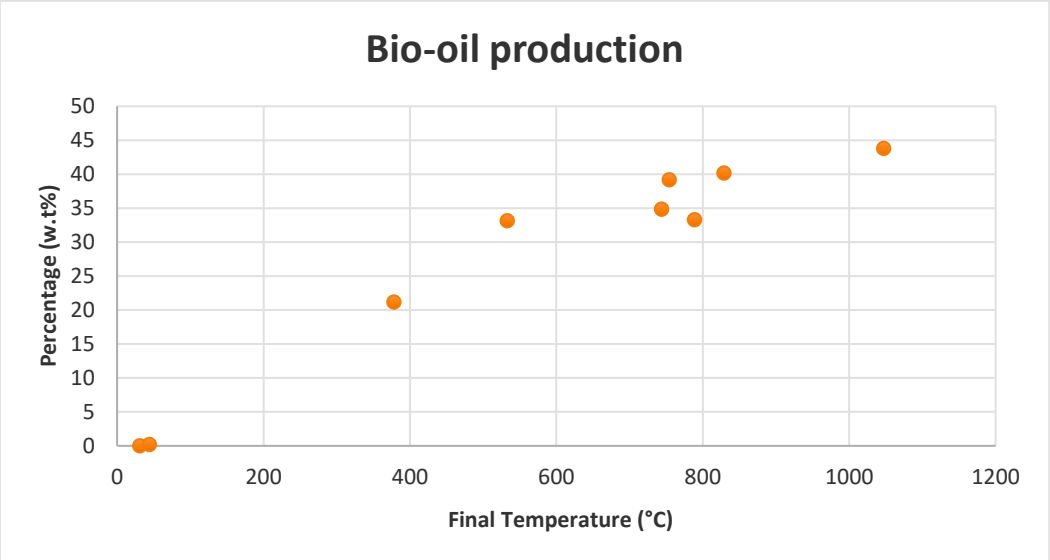

Figure 4.3-4 Sargassum's bio-oil production vs temperature

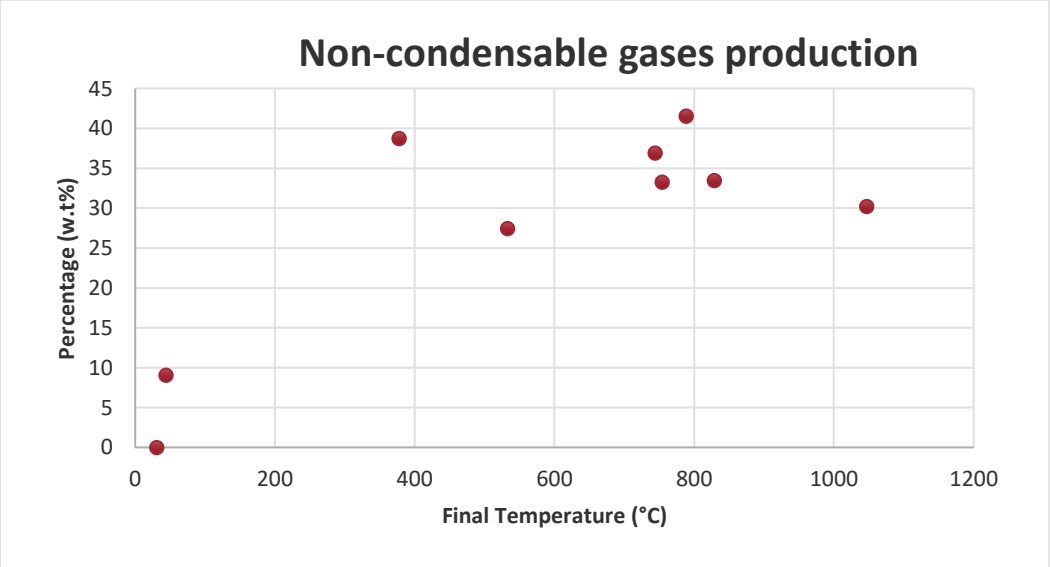

Figure 4.3-5 Sargassum's gas production vs temperature

Grierson et al.[222] investigated the slow pyrolysis using six microalgae species [222]. The study was conducted on aquatic microalgae Tetraselmis chui, Chlorella like, Chlorella vulgaris, Chaetoceros

muelleri, Dunaliella tertiolecta and Synechococcus. The observed oil and biochar yields were 24–43% w/w and 34 to 63% w/w. The yield had been improved by increasing the temperature from 300 ◦C to 500 ◦C. For instance, raising the 200 ◦C increases the gaseous products from 9.5% to 40.6% w/w.

In our work, the production of gas for Sargassum, presents the same tendency as for Flax shives. The gas production increases with temperature until a maximum point and then decreases. As the microwave pyrolysis was done for two different biomasses, a behavior closer to the literature (increase of gas with the increase of temperature and reduction of bio-oil yield) was expected. We believe that the heating rate inside the matrix is higher than expected favoring the bio-oil production over the gas yield, despite the final temperature.

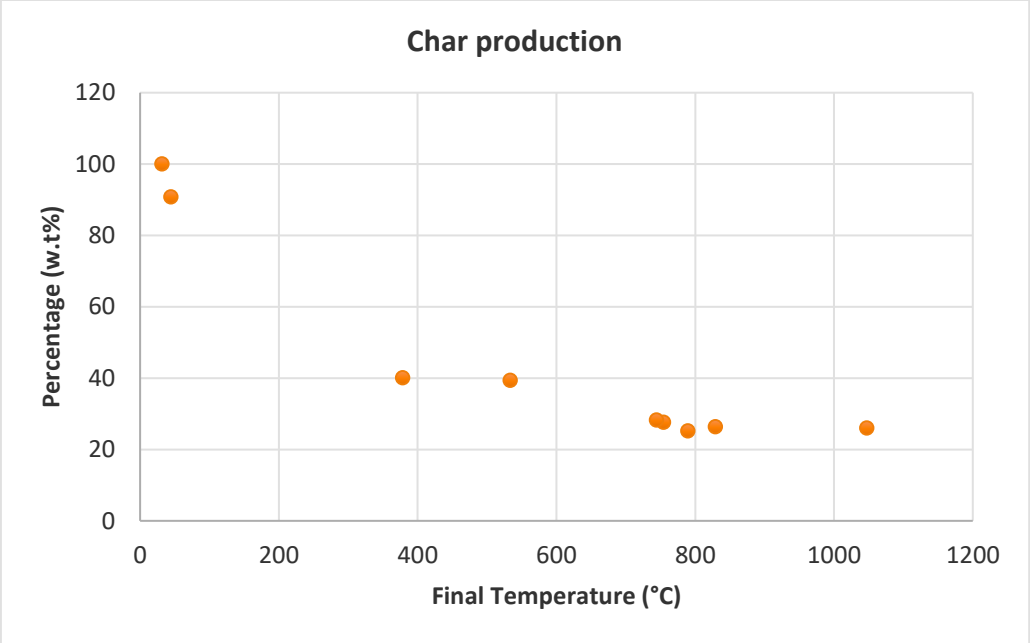

Figure 4.3-6 Sargassum: Char production vs final temperature

The biochar production decreases with the increase of temperature finding a minimum point at 1047°C equal to 26% mass percentage. This value is lower than the value obtained during the TGA experiments (section 3.2.2) at conventional pyrolysis conditions.

4.3.3 Influence of operating conditions on bio-oil chemical families and non-condensable gases species

Nitrogenated compounds, including amides and nitriles, were found in high yields in the bio-oils from Sargassum pyrolysis. Literature indicates that nitrogenated compounds were formed during the pyrolysis of Sargassum proteins. Also, no lignin derivatives, such as guaiacols, were detected in the bio-oil from Sargassum pyrolysis. Compared to the pyrolysis of Flax shives, the carboxylic acids and phenols content was lower. Furans, which were not present in the bio-oil obtained in the case of Flax shives, have an average mass percentage of 5.92%. Aromatic compounds were also found in higher yields. At the same flow rate and irradiation time, the carboxylic acids and furans increased with incident power, and the nitro compounds and ketones decreased. The incident power did not highly influence the other families.

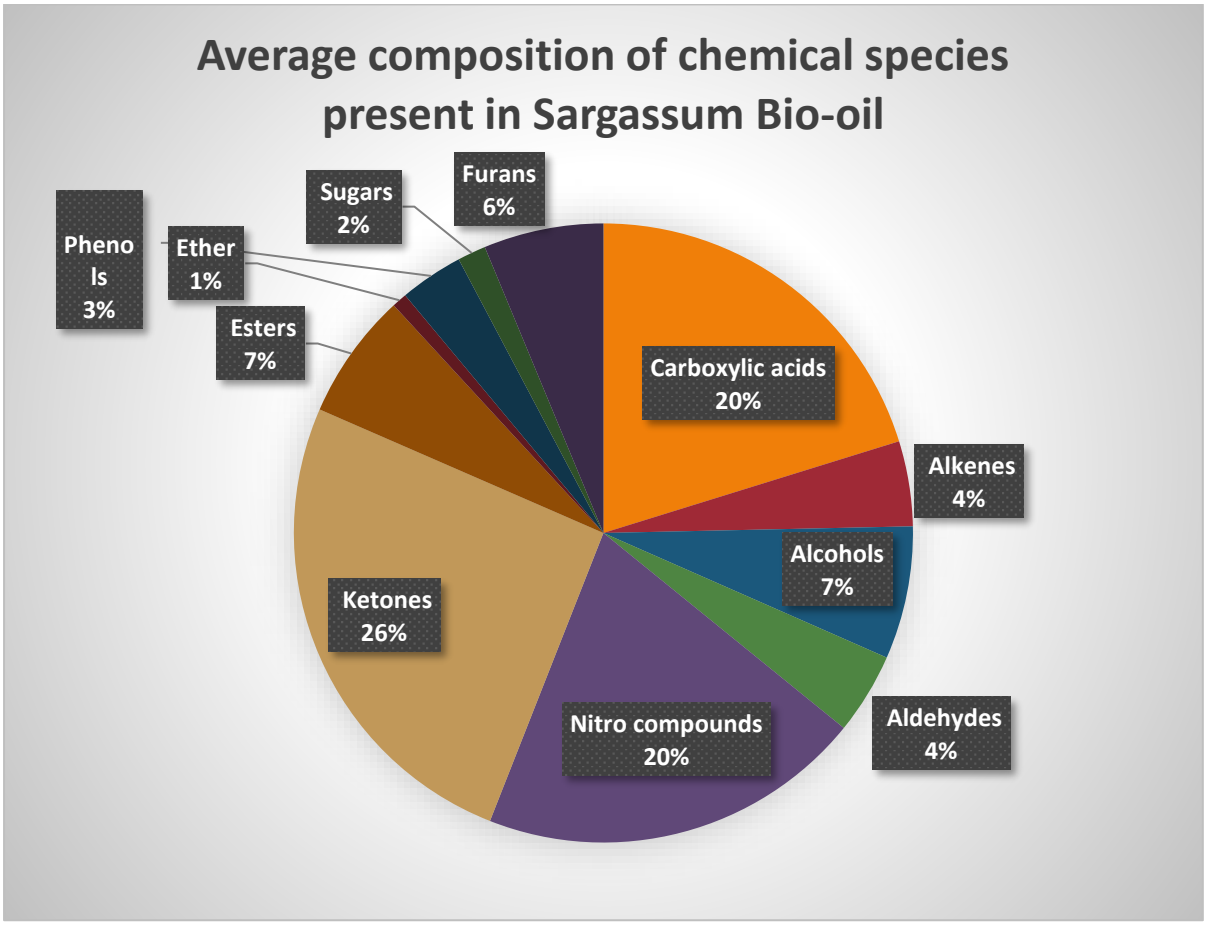

Figure 4.3-7 Average composition of chemical species present in Sargassum Bio-oil

Table 4.3-1 Bio-oil composition results for Sargassum microwaves pyrolysis (%w:w)

Inciden Power (Watts)	Irradiation time (min)	Flowrate (ml/min)	Carboxylic acids %w/w	Alkenes %w/w	Alcohols %w/w	Aldehydes %w/w	Nitro compounds %w/w	Ketones %w/w	Esters %w/w	Ether %w/w	Phenols %w/w	Sugars %w/w	Furans %w/w
100	2	200	20%	4%	5%	7%	15%	25%	7%	0%	11%	2%	5%
600	2	200	18%	5%	9%	4%	21%	25%	6%	1%	3%	1%	6%
600	2	800	20%	4%	8%	3%	19%	26%	7%	0%	5%	1%	6%
600	4	600	22%	4%	5%	6%	20%	26%	7%	1%	2%	2%	6%
300	4	600	17%	3%	5%	5%	23%	28%	9%	1%	2%	1%	5%
350	6	500	19%	5%	7%	9%	19%	17%	6%	2%	6%	2%	5%

The main compounds detected for the non-condensable gases were CO, CO_2, CH_4 and H_2. The mass percentages of CH_4 and C_3 were lower than Flax shives. When regarding the species distribution obtained at the different operating conditions, it is observed as how long vapors residence time with high incident power increase the production of H_2 and CO (Syngas). Also, short residence time, favors the CH_4 production. CO_2 yield is at its maximum point a short irradiation times and low incident powers.

Table 4.3-2 Non- condensable gases composition results for Sargassum microwaves pyrolysis (weight percentages % wt)

Incident Power (watt)	Irradiation time (min)	Flowrate (ml/min)	H_2 %w/w	CO %w/w	CH_4 %w/w	CO_2 %w/w	C_2 %w/w	C_3 %w/w
100	2	200	1,3%	51%	2,3%	44%	1,1%	0,0%
100	2	800	0,0%	15%	0,0%	84%	1,0%	0,0%
300	4	600	1,1%	61%	1,5%	36%	4,6%	0,8%
300	4	200	1,8%	42%	2,0%	51%	1,4%	1,0%
300	4	200	0,5%	19%	1,7%	76%	1,1%	1,2%
600	2	200	3,3%	71%	2,9%	20%	1,4%	1,1%
600	2	800	2,3%	50%	1,6%	44%	0,8%	0,7%
600	4	600	3,0%	60%	7,3%	30%	4,0%	1,2%
600	4	600	2,3%	57%	1,4%	40%	0,8%	0,9%

4.4 FLAX SHIVES VS SARGASSUM MICROWAVE PYROLYSIS BY PRINCIPAL COMPONENT'S ANALYSIS (PCA)

4.4.1 Flax shives

The operational parameters associated with heat: the incident power, the specific energy applied, and the final temperature are positively correlated. This was shown before in section 4.1. For Flax shives, the bio-oil is positively correlated with the incident power and negatively correlated with gas in terms of product distribution. Also, the gas is negatively correlated with both char and bio-oil. The energy and final temperature also have a positive impact on the bio-oil yield in the case of a constant irradiation time of six minutes. The gas production depends mostly on solid reduction (higher negative relation than bio-oil). This must be a cause of the disintegration of char or the pyrolysis of lignin in the passive phase of pyrolysis. Higher incident power and applied energy did not increase the production of gas. A phenomenon of temperature heating rate, the irradiation time, and pyrolysis active/passive phases must be studied deeply.

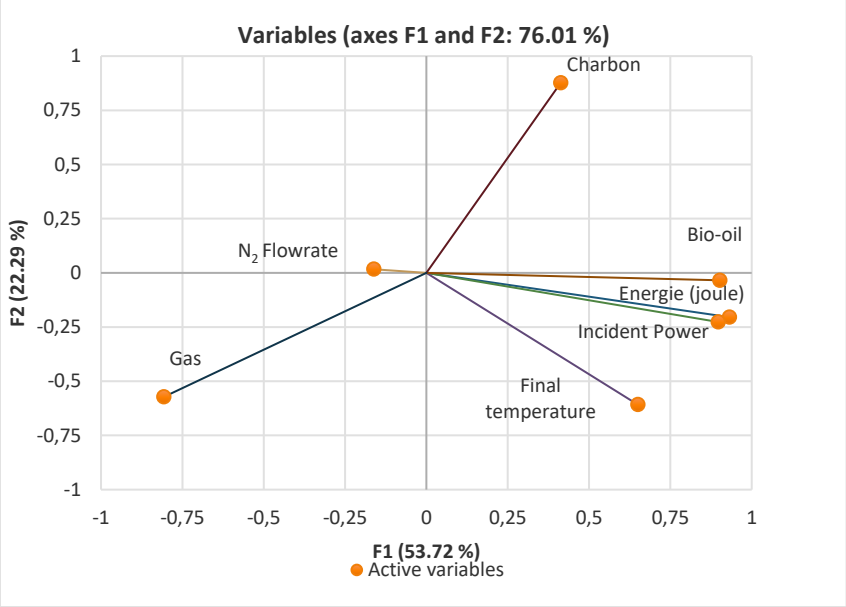

Figure 4.4-1 PCA for Flax shives operating conditions

The pyrolysis bio-oil is a complex mixture of several compounds that normally are divided into chemical families. In terms of bio-oil quality, the incident power positively influenced the phenols, ketones, esters, and aldehydes. On the other hand, the augmentation of incident power reduces the production of alcohols, carboxylic acids, and sugars. Also, there are interesting correlations between the bio-oil chemical families. Carboxylic acid is negatively correlated with ketones, aldehydes, aromatics, and phenols production and positively correlated with alcohols and esters. Aldehydes and ketones seem to be produced together, sugars, aromatics, and nitro compounds.

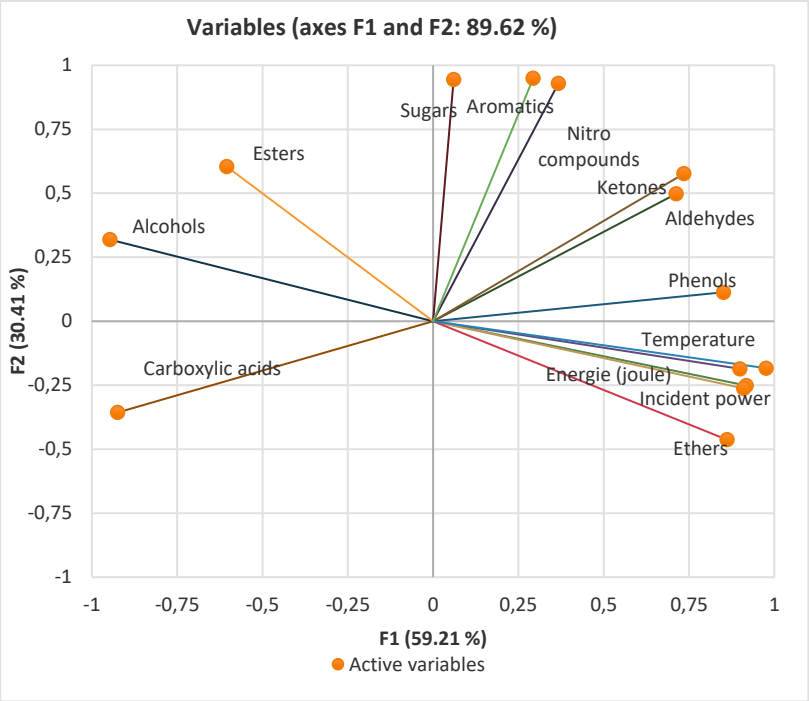

Figure 4.4-2 PCA of the chemical families present in Flax shives bio-oil

In the case of non-condensable gases, composition, temperature, energy, and incident power were negligible. Still, the flow rate positively influenced the CH_4, C_2, and C_3 production and had a negative influence on the CO_2 and CO. The irradiation time was favorable for hydrogen production but negative for producing the heavier species. The hydrogen production was negatively correlated with CO and CO_2 but positively correlated with CH_4 and the higher species C_2 and C_3.

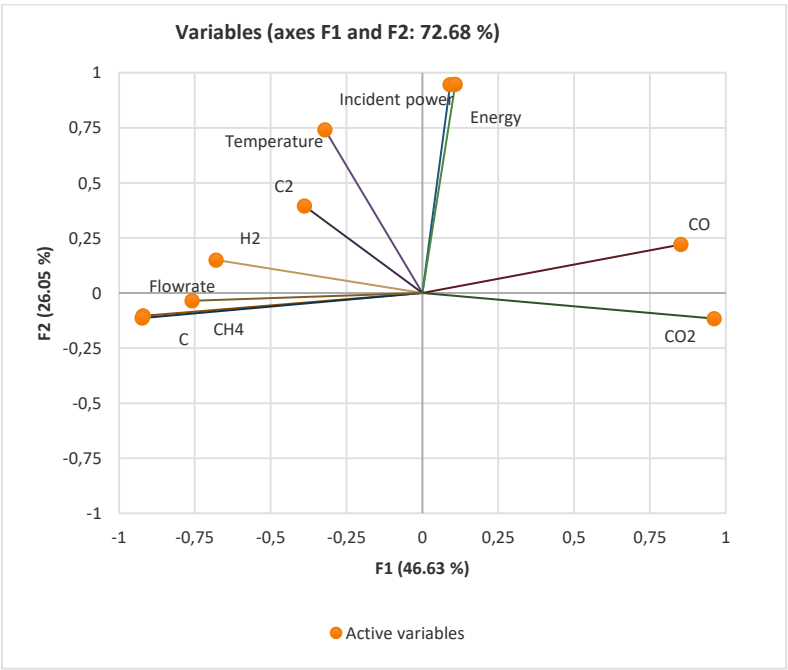

Figure 4.4-3 PCA Flax shives non-condensable gases

4.4.2 Sargassum

As for Flax shives, the operational parameters associated with heat: the incident power, and the specific energy applied are positively correlated. The bio-oil is positively correlated with the absorbed energy and the incident power and negatively correlated with char. The bio-oil and the gas are not negatively correlated. They are produced together, which could result in a competitive relationship.

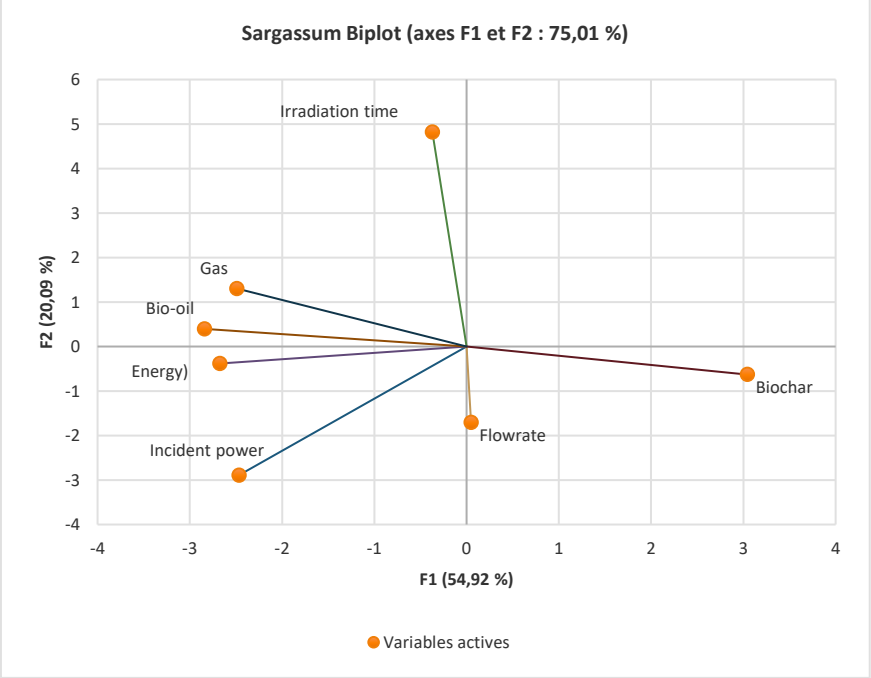

Figure 4.4-4 PCA Sargassum N. General operating conditions

In terms of the chemical families present in bio-oil, the production of carboxylic acids has a negative correlation with the production of most species and is favored at low incident powers. Phenols are promoted at high incident powers and temperatures. These results are like those found in Flax shives analysis. In terms of the correlation between chemical family's aldehydes, ketones, aromatics, and nitro compounds were positively correlated. Carboxylic acid is negatively correlated with ketones, aldehydes, aromatics, esters, and amines. The correlations between chemicals families for the Sargassum N. bio-oil were not very pronounced in comparison to Flax shives. In the case of non-condensable gases composition, the effect of temperature was not negligible for the syngas production and had a negative relation to the production of CH_4 and C_3. H_2 and CO are positively correlated, increasing with similar patterns.

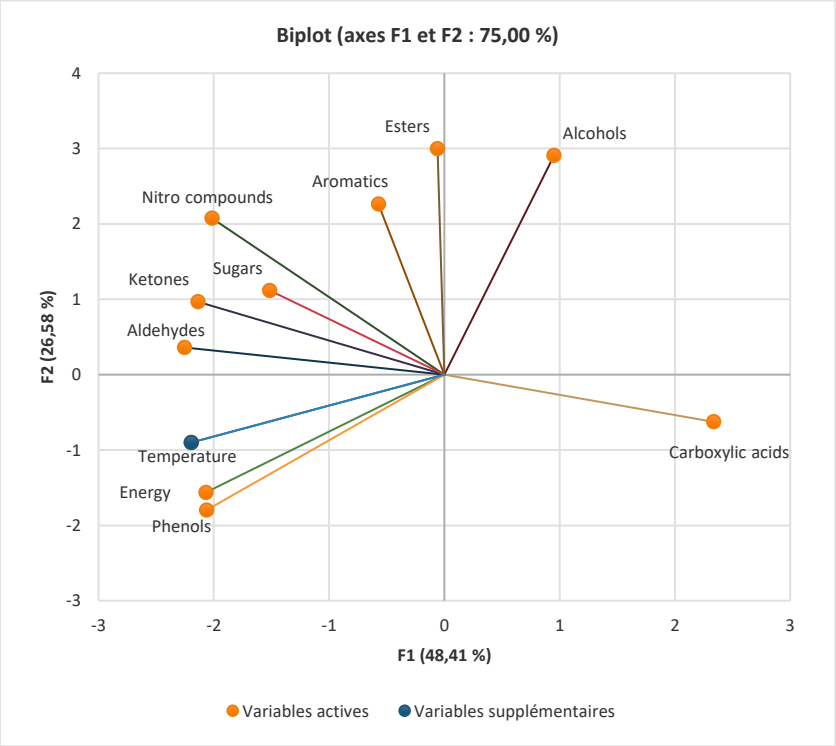

Figure 4.4-5 PCA Sargassum Bio-oil chemical families

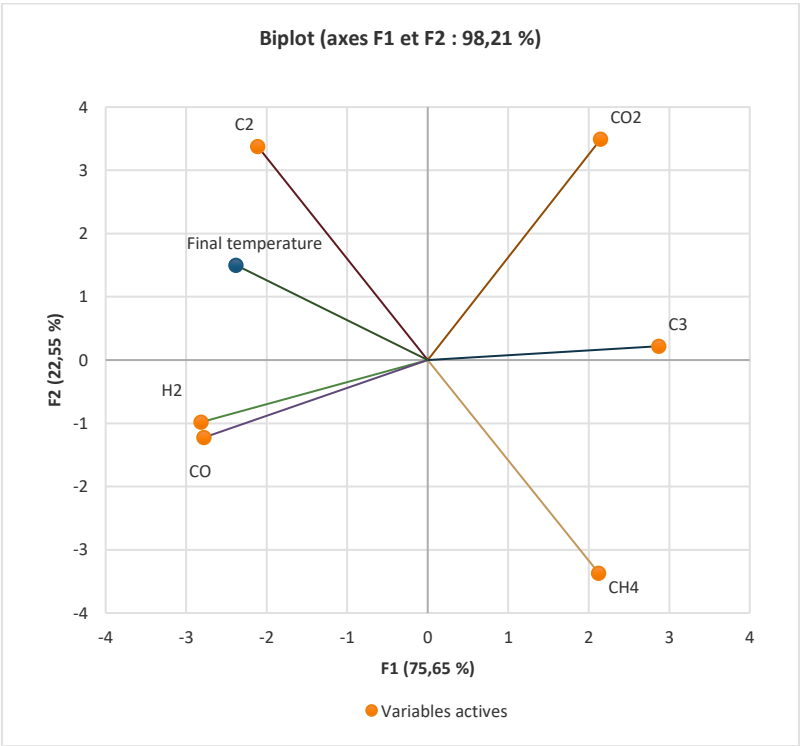

Figure 4.4-6 PCA Sargassum non -condesables chemical families

4.5 ENERGY OPTIMIZATION

The issue of energy optimization is essential for the industrial development of biomass waste pyrolysis. This energy optimization needs to be examined at several levels:

1-Are the products in my process energy or chemically interesting, and what products should I optimize?

2-What type of heating is desired for optimal production, i.e., lower energy cost production?

3-What technical improvements do I need to bring to minimize the energy consumption?

The answers to these three questions applied to this study start with the flax shive's properties and pyrolysis products. First, during pyrolysis, the amount of char produced quickly reaches a limit value close to 16-17% of the initial mass. This behavior is observed if the energy supplied is enough and regardless of how this energy is supplied. The char has thought-provoking properties, for example, the high heating value as a result of the increase of the degree of aromaticity while increasing temperature and the decreased elemental oxygen content [224], also as microwave adsorbents for being used as susceptor or as pollutant adsorbent for gas or liquid wastewater treatment. It would be interesting to characterize it more finely. Therefore, it is rather a by-product of pyrolysis, which will itself be best valued as fuel or as adsorbent.

Table 4.5-1 High Heating Values (HHV) of Flax shives/ hemicellulose/cellulose/lignin/Flax shives biooil and char

High Heating Values (kcal/kg)					
Flax shives	Cellulose	Hemicellulose (Xylan)	Lignin	Flax shives bio-oil	Flax shives char
4795	3812	3765	4622	3588 – 3827	6660

Second, the gas produced is low in CO_2 and can be reused as fuel or syngas. Lastly, the oils produced are also sufficiently energy-efficient (Table 4.5-1) to serve as fuel or fuel additives. However, they may need to be upgraded to reduce their acidity. Furthermore, an examination of their composition shows the presence of certain products of interest in chemistry, such as phenols and ketones, in interesting proportions. These compounds are widely used in the industry as antioxidants, paint components or oil additives for phenolated compounds, or as solvents for ketones. Therefore, the oils could be distilled to separate the compounds for use as basic chemicals. In this study, the production of oil from Flax shives was considered the most important and which we sought to optimize.

The microwave heating method was the chosen technology for this process concerning the second question. Obtaining a significant proportion of oil requires a significant energy supply within the system and very rapid temperature rises (from 140 to 200°C/min), which only microwaves can provide. To process a given mass, we have established an energy optimum, i.e., an energy value absorbed beyond which bio-oil production has no higher impact (approximately 72000 J for 4.5 g of processed biomass

(Figure 4.5.1 and 4.5.2). To confirm the existence of this optimum, we tested other masses and examined the production of oil/char/gas for a given absorbed energy. Table 4.5-2 shows that bio-oil production increases with the increasing energy absorbed per g of biomass treated at the expense of coal and gas. Up to 70% of the oil was obtained by irradiating the lowest amount of biomass (2.25 g). However, it is important to note that the electromagnetic wave/matter interaction becomes increasingly difficult to ensure when the mass decreases and the energy absorption condition may no longer be verified, especially if the microwave settings are not well controlled.

Table 4.5-2 Mass influence on absorbed energy, heating rates, final temperature and products distribution; QN2 = 600 ml/min

PI Magnetron (W)	Irradiation time (min)	Absorbed energy (J)	Mass (g)	Energy/mass (J/g of biomass)	Energy/mass (J/g of bio oil)	Internal heating rate (°C/min)	Final temperature (°C)	% Bio oil	% Char	% Gas
300	6	68232	2.25	30326	43240	138	740	70.1	16.1	14.6
300	6	60449	4.5	13433	25527	121	725	52.6	18.9	29.0
300	6	63375	6.75	9389	21786	137	823	43.1	20.1	36.9
300	6	67463	9	7496	20084	104	571	37.3	36.2	26.9

Finally, we calculated the energy absorbed per gram of oil produced for all the experiments presented in this work. This parameter is a way to estimate the cost of the process and compare it to other processes. Energy optimization, therefore, consists of minimizing the energy intake per gram of bio-oil produced while ensuring sufficiently advanced pyrolysis to make the proportion of char formed minimal.

Figures 4.5-1 show product yields obtained for Flax shives with this parameter. Logically, the higher the energy expenses, the more oil is produced. However, we can also see for Flax shives that a moderate expenditure (around 25000 J/g of oil produced) can volatilize 82% of the biomass in oil (51%) and gas (31%), and that to obtain a 3% more in volatiles, the quantity of energy has to be doubled. Thus, it can be concluded from Figure 4.5.1 that an energy density of around 25000 Joules per gram of oil produced, or about 13000 Joules per gram of processed biomass, is the best energy compromise. In addition, the power provided must allow a significant temperature ramp, at least 120°C/min, over the experiment.

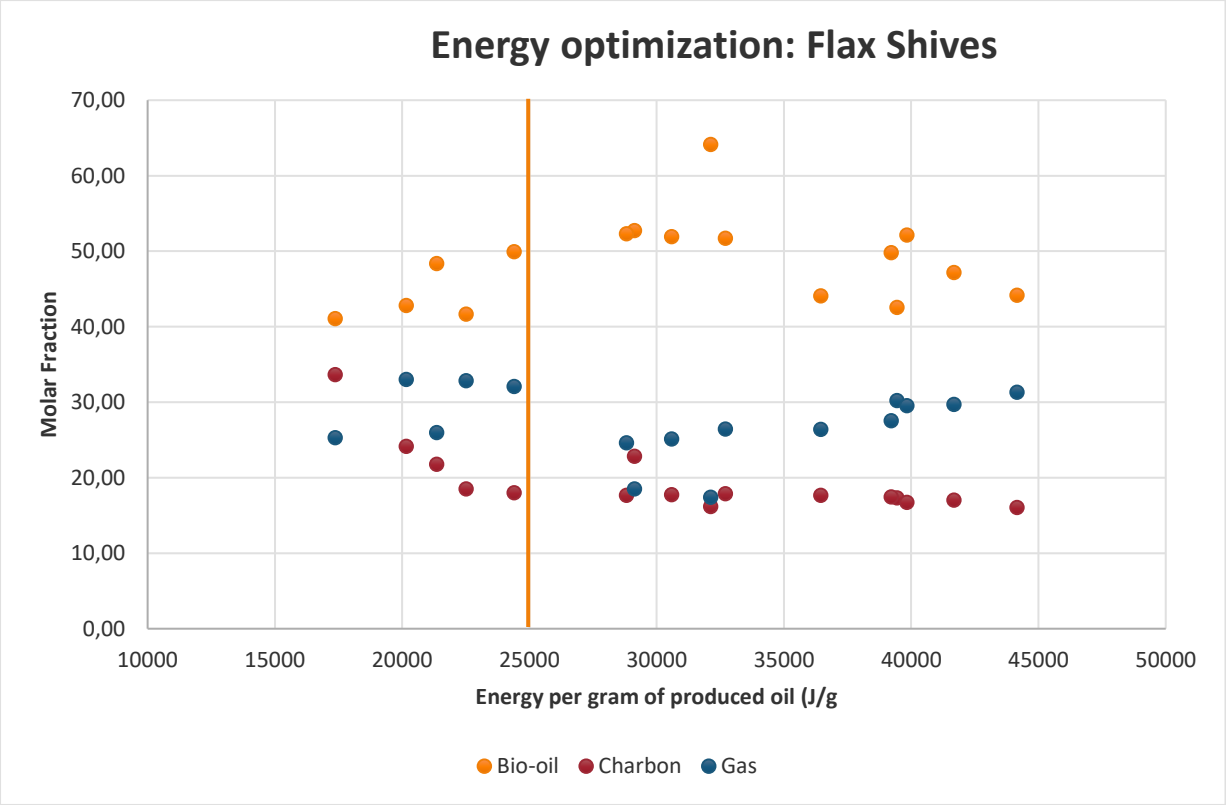

Figure 4.5-1 Flax shives: Products distribution as a function of the absorbed energy per gram of produced bio oil.

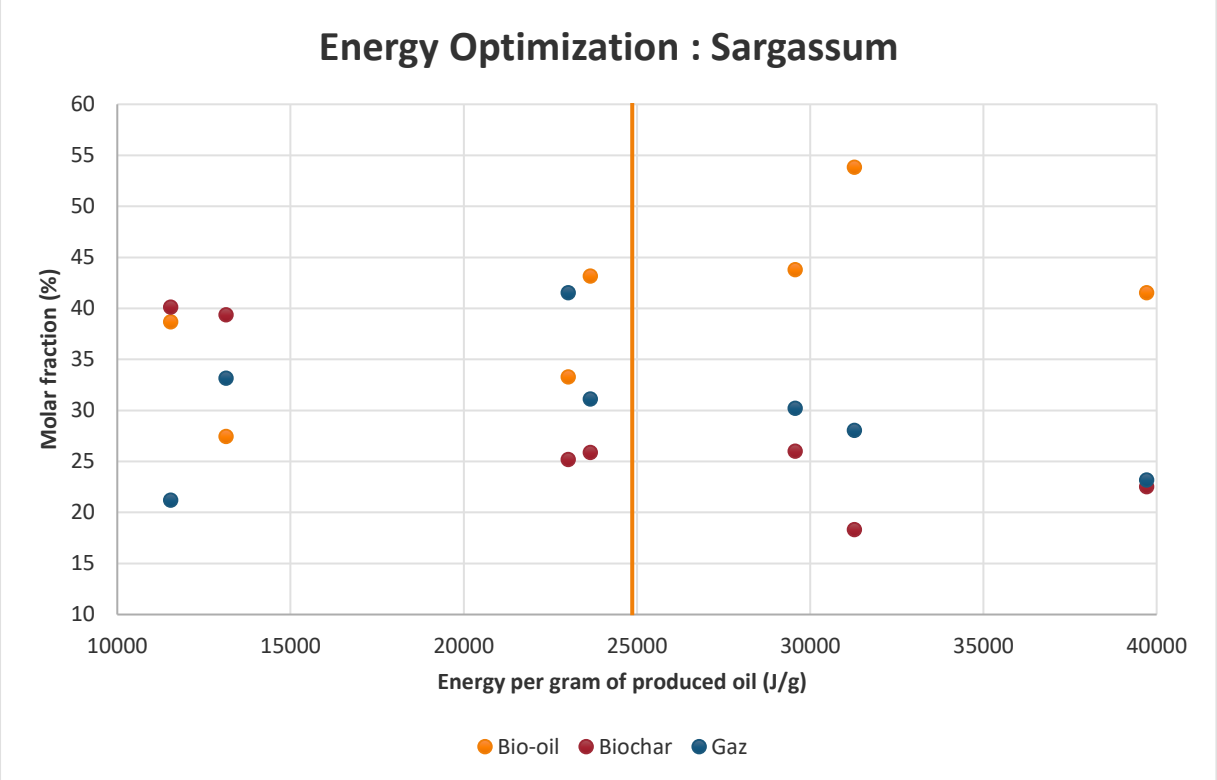

Figure 4.5-2 Sargassum: Products distribution as a function of the absorbed energy per gram of produced bio oil.

For Sargassum, results are less clear because of the high dispersion of the values. A moderate expenditure (around 30000 J/g of oil produced) can produce between 45 and 55% of oil and 28 to 30% of gas. The remaining char reaches the plateau of 24%, around 23000J/g of oil produced. Increasing the energy applied further does not affect much gas and oil production.

In response to the third question, maximizing the energy absorbed by the system is a crucial factor. An efficient cavity tuning system provided here by the three impedance adaptors is essential. It allowed us to obtain absorbed powers of about 85% of the incident power. The ideal would be to have automatic regulation based on minimizing the reflected power throughout the experiment. Controlling the temperature rise over time would allow the heating speed to be controlled by adjusting the incident power. Of course, effective isolation of the set-up will also reduce the energy cost. This will be discussed in chapter 5.

4.6 PRELIMINARY CONCLUSIONS

The feasibility of the microwave pyrolysis of Flax shives and Sargassum has been demonstrated. High heating rates are reachable, leading to an important temperature gradient between the center and the outer wall of the reactor. The rotation of the reactor homogenizes the load during the experiment, and oil and gas are produced in higher quantities than by classical heating.

The initial composition of the biomass seems to have a singular effect on bio-oil production. The difference in gaseous and oil products for the Sargassum N. and Flax shives could be attributable to the different elemental and organic compositions. Concerning the biochar, further studies should be performed in order to characterize the biochar obtained.

In terms of energy optimization, there are optimal conditions to increase bio-oil production under microwave irradiation. A minimum value of 72000 J for 4.5 g of biomass, to reach about 800 °C with a high heating rate (200 °C/min), yields up to 64% w/w of bio-oil, which is a very promising result compared to other published works. According to the review of Ge et al. [220], in which Table 2 reports the yields obtained for many biomasses, under microwave irradiation or not, the maximum value of bio-oil produced is 47% w/w, except for poplar pyrolysis. Flax shives are not listed there [208]. Also, none of the results are higher than the one obtained in this work for Flax shives. For Sargassum, results must be confirmed by additional experiments. The bio-oil shows a high-water content leading to low high heating values. Gas composition is interesting but shows higher contents of CO_2 and less CH_4 and H_2 than gas produced from Flax shives.

CHAPTER 5
Development of a scalable microwave pyrolysis process

5 MICROWAVE PYROLYSIS: TOWARDS CONTINUOUS FLOW

From the first application of microwave heating in chemistry until today, the enthusiasm of the scientific community has been promoted by the energy and time efficiency achieved when using this method. While one of the drawbacks of this technology is the difficulty of scaling up the processes, the market demand cannot be diminished. It is required to dig into a new, safe, and feasible way to upgrade this type of technology towards continuous flow operation.

The type of reactor, the wave propagation mode and its penetration depth, the relation temperature vs. microwave power density, the dielectric properties of the feedstock, and the power density distribution are the basic concepts that every microwave process should consider to operate in an industrial scale. In the case of the pyrolysis of biomass, the evaluation of the electromagnetic compatibility of all the elements of the systems, along with the ability to deliver enough power density to induce pyrolysis, is one of the first questions to be answered if the aim is to have a functional and highly performing process.

Chapters three and four, highlighted the predominant physical phenomena involved in biomass microwave pyrolysis. Consequently, optimum conditions for a microwave pyrolysis process were defined according to the desired characteristic of the products obtained (gas, bio-oils, char). These elements constitute a preliminary and necessary step for an industrial transposition.

Based on state of the art, the upgrading of a semi-batch process to a continuous flow under microwave irradiation should start by resolving the following points:

- Choosing the right geometry to ensure the microwave propagation
- Preparing the system to deliver enough power density to ensure the process's desirable temperature
- Ease of feedstock circulation and products separation.
- When studying the microwave pyrolysis of biomass for a continuous flow process development, other points are added to the list:
- The abrupt weight loss during the pyrolysis phase and the dielectric properties evolution of the medium.
- The gas handling and the bio-oil condensation in the reactor's colder zones
- Biochar recovery
- The use or not of a microwave absorber.

This section aims to provide the first theoretical elements to answer the previous points for continuous flow pyrolysis process development. First, the cavity choice and wave propagation mode are defined. The basic reactor structure is described, followed by mapping the electric field distribution using thermal paper (thermography) and COMSOL simulations. The objective is to have a first sight of the compatibility of the system and the difficulties that could arise while inserting new elements into the basic reactor structure.

5.1 REACTOR DESIGN

5.1.1 Choosing the type of reactor

As discussed before on state of the art, there are advantages or disadvantages to consider when transferring a new process from research and development to manufacturing. At this stage, many disciplines must converge to successfully and simultaneously produce pyrolysis products under microwave irradiation. Determining the scale-up parameters is possible by studying numerous situations (one of the objectives presented in chapter 4), which are going to be assembly with both "know-how" and "know why," serving as a basis for the equipment design and standard operating procedure.

Some of the reactors proposed in the literature have already been proved for microwave pyrolysis in continuous flow. For example, the conveyor belt system has been widely used throughout the drying and food processing industries. Biomass processed through the conveyor belt concept can be subjected to power densities much higher and uniform as compared to the rotary kiln concept. Moreover, the residence times can be very short, which is extremely important in promoting fast pyrolysis. The evolved volatiles from the pyrolysis process can be easily extracted employing a fan through specially designed materials perforations at the top of the cavity. A further advantage of this microwave processing concept is that the thermal inertia is very low; hence, start-up and shut-down of the process can be achieved within seconds.

Nevertheless, important challenges can be detected in this system. On the one hand, the design of electromagnetic chokes structures to limit the microwave leakage through the open feed boundaries allows the feed material and products to pass continuously through the cavity while containing the electromagnetic field is highly challenging. On the other hand, the compatibility of the belt material with microwave processing must be addressed; the belt material should be microwave transparent, mechanically robust, and thermally stable as high temperatures are promoted.

Fluidized beds have also been successfully used in pyrolysis of biomass at a large scale and proving to provide the large amounts of heat required. A homogeneous temperature can be reached because solid particles are perfectly mixed, enabling an efficient convective heat transfer and thus heating homogeneity. However, indirect heating must be used to obtain high-quality bio-oils instead of in-situ heating (e.g., hot carrier gases may promote bio-oil degradation) unless circulating fluid beds are used. Also, the fluidization behaviour is highly dependent on the type of biomass and particle size. For instance, hardwoods have a fibrous shape which makes the particles stick to each other during the gas flow, channelling and slugging behaviour being induced even at low gas velocities. Henceforth, previous biomass palletization treatment could be required.

Extrusion-based systems, such as the auger reactor, have attracted interest for pyrolysis applications as they can be operated continuously with almost no carrier gas. Pyrolysis processes can be processed through the rotation motion of one or multiple screw conveyors inside the reactor. This mixing motion enhances the heat transfer between solids, liquids, gases, the reactor wall, and the transportation of the particles towards the reactor outlet. Further biomass particles can be fed and pyrolyzed while char particles leave the reactor, thus allowing a continuous operation. The auger reactor can be especially appealing for its potential to reduce operating costs associated with bio-oil production. The main advantages of the auger reactor are its simplicity and flexibility in terms of feed particle size and shape [3]. Microwave-assisted pyrolysis of rice straw using an auger reactor was recently studied by Luo et al. (2021). They developed an 80 kg h−1 pilot-scale microwave-assisted pyrolysis Auger reactor continuously operated at 200–300 °C with five microwave waveguides with a total power of 15 kW, adjusted with the programmed temperature. The energy and economic analysis indicated this type of reactor is suitable for the mobile decentralized biomass conversion system [225].

To consider the type of reactor to choose, there are some parameters evaluated:

1. **Geometry compatibility with the single mode microwave cavity available:** The reactor should be compatible with the TE10 propagation mode available in our laboratory. A transition element could be connected from the rectangular cavity shape to the reactor's shape.

2. **Control of temperature, residence time and penetration depth:** To have results comparable to the semi-batch experiments, the temperature, residence time, and penetration depth should be controlled. Cold sweep gas is required for immediate quenching of the pyrolysis products, and at the same time, the temperature must be maintained below 700 °C. Otherwise, the operating condition will favour the gasification rather than pyrolysis. In the case of microwave pyrolysis, the heat for the reaction will be produced by the microwave interaction with the biomass inside the reactor and the pyrolysis products produced during the microwave irradiation time. In this term, a well-defined transition is needed to better match the microwave irradiation with the microwave absorption and the temperature generated. The penetration depth varies with the dielectric properties of materials and their microstructure and temperature. For example, the penetration depth of the water increases from 1.4 cm up to 5.7 cm when increasing the temperature from 20°C to 90°C at 2.45 GHz.
   Also, the penetration depth is a factor that cannot be neglected. It is often stated that microwaves can only penetrate between 1 and 2 cm of the materials, which is a limiting factor to the continuous flow scaling.

3. **Reactor's geometry:** Reactor geometries as small as 50mm are not viable due to the heterogeneous nature of the heating due to both the distribution of the electric field and conventional heat transfer. Using large reactors will result in significant charring/gasification within some areas of the process material and almost zero treatment within others. Biomass must therefore be transported and processed within a narrow geometry to promote

homogeneous treatment, only then can the liquid yields be comparable with conventional pyrolysis processes.

In order to fulfil the latter requirements, the auger reactor was chosen. The main feature of this technology is that the biomass material is fed to the reactor and moved inside it mechanically through a shaftless screw. Also, using this type of reactor allows for to creation of highly localized power densities and, at the same time controlling the biomass and char residence time.

In terms of electromagnetic combability, the auger reactor has a cylindrical shape, so the transition element is possible from a rectangular waveguide. Also, depending on the biomass flow direction, the biomass thermochemical degradation transition can be tuned according to the revolution per minute of the internal spiral. The general scheme of the system can be observed in figure 5.1-1.

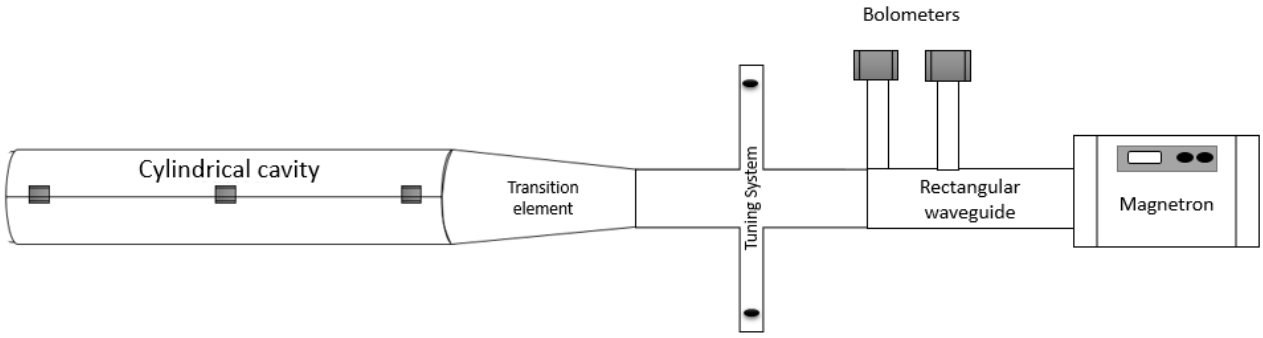

Figure 5.1-1 Reactor proposed scheme for microwaves continuous pyrolysis

5.1.2 Microwave propagation and attenuation

The reactors can be designed to maximize the microwave contact with the circulating biomass to accomplish two different roles, reactor and microwave applicator. The reactor's cylindrical shape can be considered a cylindrical waveguide, and the transition element can favor the wave propagation model in an electrical transverse mode TE11. A uniform and circular polarization characterize the TE11 propagation mode according to the diameter. This particularity improves the uniformity of the electric field across the section of the dielectric and heating larger workloads. However, some factors must be respected to ensure wave propagation along the reactor.

First, the cut-off diameter should be calculated to validate the minimal internal diameter d, of the reactor.

For $f = 2.45\ GHz$:

Equation 39 :

$$\lambda_0 = \frac{C}{f} = \frac{3.10^8}{2.45.10^9} = 0.1224\ m = 12.24\ cm$$

For a cylindrical cavity, the wave will propagate if:

Equation 40 :

$$\beta > \beta_c,$$

Where:

Equation 41 :

$$\beta = \frac{2\pi}{\boldsymbol{\lambda}}$$

For example, in the air:

$$\beta_0 = \frac{2\pi}{\boldsymbol{\lambda}} = 51.33\ m^{-1}$$

A wave will propagate in the air if:

$$\beta_0 > \beta_c$$

Where:

Equation 42 :

$$\beta_c = \frac{u'_{nm}}{\boldsymbol{a}}$$

Where a, is the internal radius of the guide and u'_{nm} = 1,841 according to Combes [226] for the TE1,1 mode.

$$\beta_0 > \beta_c = 51.33 > \frac{u'_{nm}}{\boldsymbol{a}}$$

The minimal radius required for a wave propagation in the air is:

$$a = \frac{u'_{nm}}{\mathbf{51.33}} = 0.0358\ m = 3.58\ cm$$

If the reactor is filled with biomass, the dielectric properties of the biomass must be included into the equation. The relative permittivity of the biomass can be related to the cut-off wavelength by:

Equation 43 :

$$\frac{\varepsilon'_r}{\lambda_0^2} = \frac{1}{\lambda_c^2} + \frac{1}{\lambda_g^2}$$

Where:

$$\frac{\varepsilon''_r}{\varepsilon'_r} \ll 1 \quad and \quad \lambda_c = \frac{2\pi a}{u'_{nm}}$$

In the case of Sargassum, $\varepsilon'_r = 2.4$ at 2,45 GHz and 20°C.

The previous equation can be reorganized into the following form:

Equation 44 :

$$\frac{1}{\lambda_c^2} = \frac{\varepsilon'_r}{\lambda_0^2} - \frac{1}{\lambda_g^2}$$

The wave will propagate if:

$$\frac{1}{\lambda_c^2} < \frac{\varepsilon'_r}{\lambda_0^2} \quad that\ implies \quad \beta_c^2 < \varepsilon'_r \beta_0^2 \quad \frac{1}{\varepsilon'_r}\left(\frac{2\pi}{\boldsymbol{\lambda_c}}\right)^2 < \left(\frac{2\pi}{\boldsymbol{\lambda_0}}\right)^2$$

And:

$$\beta_c = \frac{u'_{nm}}{\boldsymbol{a}}$$

The combination of the equations 42 and 43 leads to:

$$\left(\frac{u'_{nm}}{\boldsymbol{a}}\right)^2 < \varepsilon'_r \left(\frac{2\pi}{\boldsymbol{\lambda_0}}\right)^2$$

From the precedent equation, the minimal diameter required for a wave propagation in the biomass can be deduced as:

Equation 45 :

$$a > \frac{u'_{nm}}{\beta_0} \frac{1}{\sqrt{\varepsilon'_r}} a > \frac{1.841}{51.33\sqrt{2.4}}$$

$$d > 0{,}0231\ m = 2{,}31\ cm$$

The minimal radius required to the wave propagation in a cylindrical cavity filled with Sargassum is 2.31 cm. This means, for the auger reactor, the minimal internal diameter allowed is 4.62 cm.

5.1.3 Biomass circulation

Ease of biomass circulation, product separation, and gas handling is another important point to discuss. The condensable phase of pyrolysis products induces condensation-related issues and high and heterogeneous temperatures profile due to hot spots can generate gasification reactions. This problem also includes integrating biomass input and output from the system with the minimal perturbation of the distribution of the electromagnetic field.

To ensure both biomass circulation and wave propagation, a shaftless screw is recommended. As the minimal diameter required to ensure the wave propagation is 4,62 cm when the cylindrical reactor is fully fed with biomass and 7.16 cm when empty, two types of a shaftless screw are proposed, one with an internal diameter of 6 cm and the other with 8 cm, and both with an external diameter of 9.6 cm. Both screws have a pitch of 3 cm.

Figure 5.1-2 Shaftless spiral/screw internal diameter

The shaftless screw with an internal diameter of 8 cm had a smaller thickness and a higher probability of ensuring the wave propagation. The biomass circulation for different revolutions per minute was tested. With a continuous feed rate, Figure 5.1.3. shows that 15 minutes are required at 1 rpm to reach the steady-state, for 6 minutes of the residence time for a path of 18 cm long.

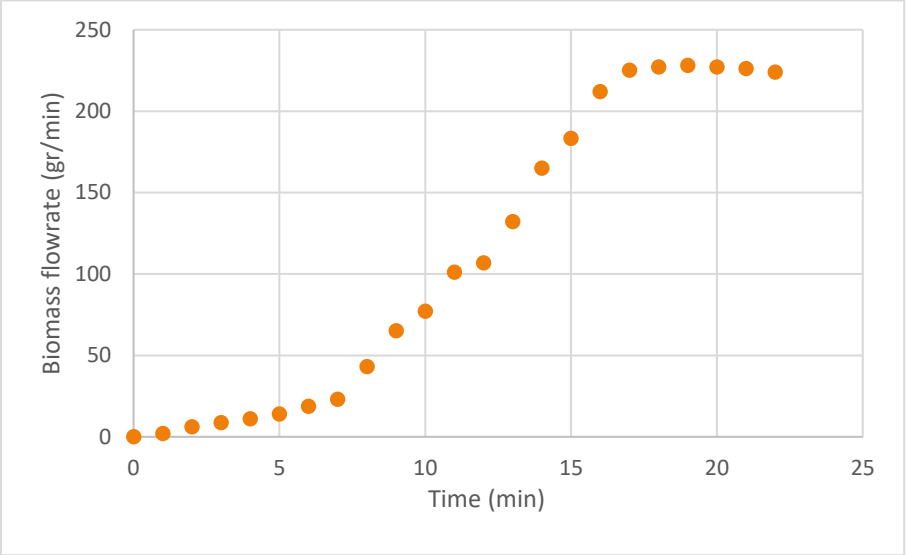

Figure 5.1-3 Biomass flowrate with time

In figure 5.1-4 it can be seen how the residence time decay with the increase of the revolutions per minutes. For a react with 60cm of length, the appropriate speed should be of 3.5 rpm for a residence time of 6 minutes

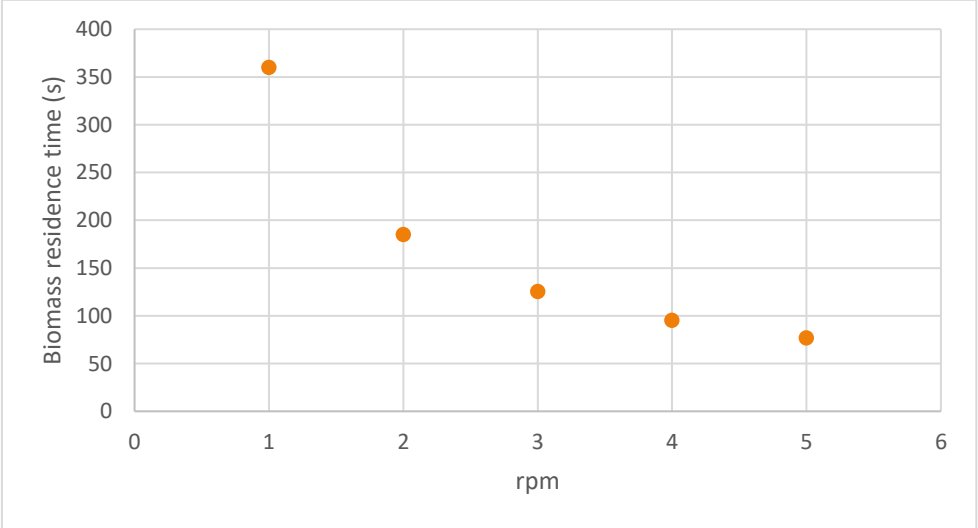

Figure 5.1-4 Biomass residence time vs shaftless screw speed

5.1.4 Biomass inlet and product's outlet

Once the biomass circulation has been validated, the second question is how to place the feed and products outlet with a minimal interference to the wave propagation patterns. In this second case, the purpose is to avoid the wave propagation inside the inlets and outlets. As is expected to have a wave propagated along all the cavity, the solution should be an exponential decay of the intensity of the standing wave when encountering the inlets and outlets of the biomass and products. In this context, the objective is to create what is called an evanescent wave by introducing a slot in which the mass can pass through without microwave leaks.

For a cylindrical waveguide and the wave propagation mode TE_{11} and reusing the equations proposed in section 5.1.2, a graphic (figure 5.1.5) which represents the wave propagation areas according to the dielectric properties of the workload and the minimal diameter required, can be obtained.

The attenuation of the wave is plotted according to the equivalent relative permittivity and the reactor diameter. In the case of the relative permittivity of 2.4, attenuation of an evanescent wave only exists if the internal diameter is greater than 2cm, meaning that, the entry and outlet's slots should have a diameter lower than 2 cm to avoid microwave leaks.

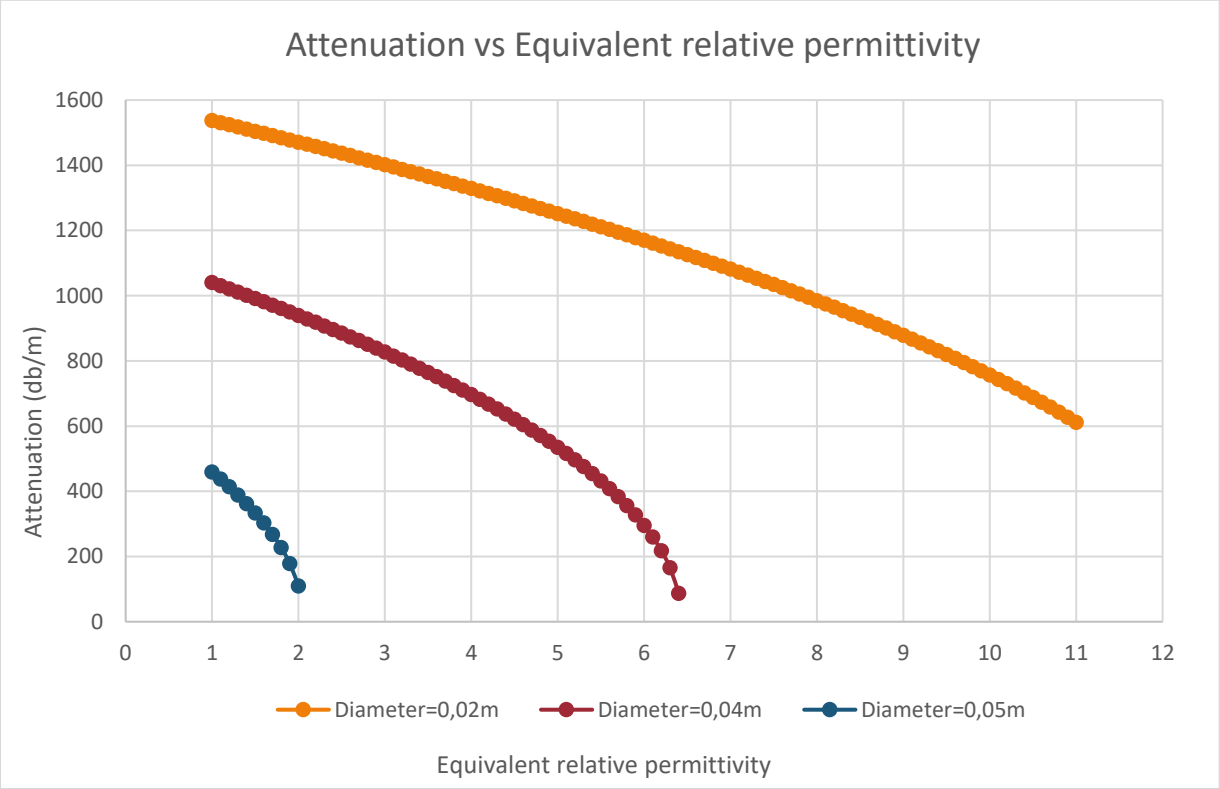

Figure 5.1-5 Attenuation vs relative permittivity of the material that fully fills the reactor

5.1.5 Power delivery

Compared to the usual pyrolysis by heat transfer from a hot wall, the challenge is to achieve high temperature increments of about 120 °C/min, as it is commonly observed that an increase in the rate of transformation of reagents results in compounds or mixtures of compounds, containing fewer secondary products. In the flax shive's pyrolysis, microwaves bring the required intense and localized heat input, in the order of 10 $MW.m^{-3}$, as commonly encountered in the domestic and industrial use of electromagnetic energy. The optimum of 13 000 $J.g^{-1}$ for obtaining a suitable mixture of extracted oils has been found and can serve as the basis for the scale up between the laboratory and the industry. Thus, pre-designs respecting the optimum energy to be provided of 13000 $J.g^{-1}$ of biomass and the required residence and rapid temperature rise times, are proposed in Table 5.1-1.

Depending on the biomass flow to be treated, the table shows the power to be absorbed and the mass in the reactor, which leads to the volume of the guiding structure. Beyond 4 $kg.h^{-1}$ the treatment is hardly possible at a frequency of 2.45GHz, considering the required powers. However, a further energy optimization by a convenient insulation and a matching of the impedances of the device should allow to further decrease these power values and therefore make this process more efficient. This way of proceeding maximizes the production of bio-oils whose composition is not very variable with the overall energy applied.

Table 5.1-1 Calculations for a continuous microwave pyrolysis process

Biomass flowrate (kg/h)	Optimal absorbed energy ($J/g_{biomass}$)	Required absorbed power (kW)	Biomass residence time (min)	Biomass loading along of the reactor (g)
1	13000	3.6	4	67
2	13000	7.2	4	133
4	13000	14.4	4	267
6	13000	21.7	4	400
10	13000	36.1	4	667

5.2 ELECTROMAGNETIC COMPATIBILITY OF THE SYSTEM

Considering all the concepts discussed before, the choice of the reactor stands by the following criteria: Cylindrical single mode cavity used as a reactor, biomass circulation using a shaftless spiral, internal diameter of the shaftless spiral > 4,62 cm, feedstock and products inlets and outlets diameter < 2 cm and cut-off element and microwave window as limiting agents of the system. The compatibility of the systems is going to be tested by two different methods, the first one by COMSOL's modelling and the second one by thermography.

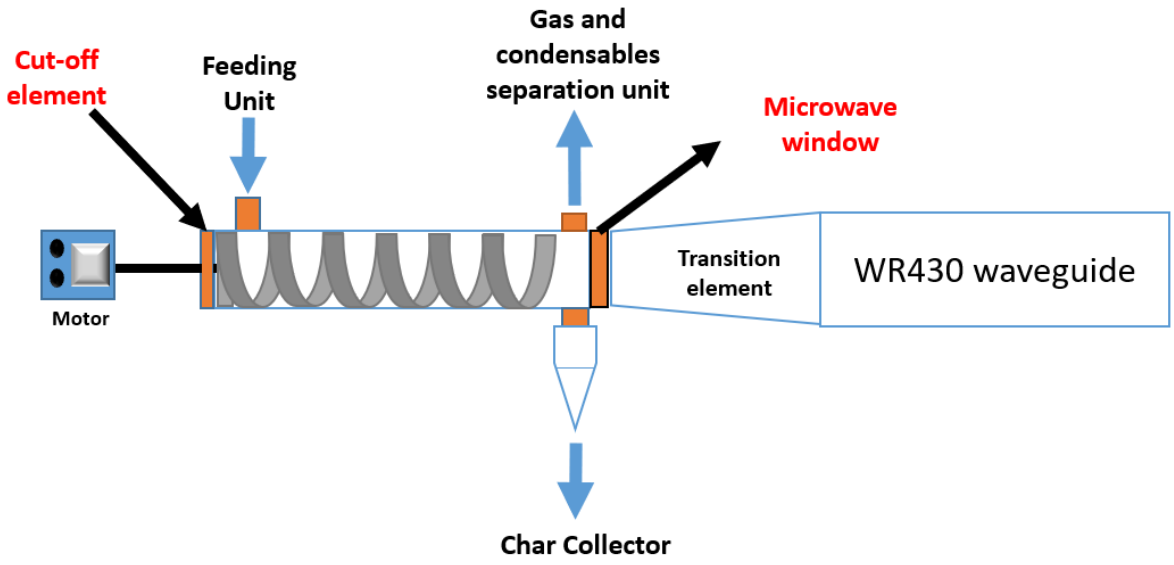

Figure 5.2-1 Microwave continous flow reactor detailed scheme

5.2.1 COMSOL's modelling: Effect of the workload dielectric properties

The effect of the electromagnetic wave propagation on the microwave heating of the biomass was also investigated using COMSOL-RF module. As explained in the section 2.5, by using thermography, it was possible to map the electric field behavior when adding different elements to a basic cylindrical reactor structure. However, to better understand the translation of the physical laws and the effect of other physical phenomena including the temperature rise and the fluid flow, a more robust system is needed. The simulation using COMSOL made possible the latter statement and allowed to better understand the obstacles when scaling up our process.

Several simulations were carried out in COMSOL, the reactors' geometry is presented in figure 5.2.1. The simulation was done using different materials combinations as well as the empty rector. The incident power in each simulation is 400 W for 360 seconds at a frequency of 2.45 GHz. This work was done by Randal de la Cruz, during his internship inside the context of this thesis.

Even though computational software is undeniably powerful to provide accurate results, the complexity involved in this real case therefore brings the need to make several assumptions to simplify the problem, thus leading to a reduced computational time. For the present simulation work, assumptions were made as follows.

- The flow of air inside the cavity is not modelled.
- The effect of biomass movement by the auger is not considered.
- Constant dielectric properties and thermal conductivity properties are applied when solving the heat transfer equations.
- The biomass is considered isotropic and homogenous.
- Simulation is performed by considering a single 2.45 GHz frequency.
- No heat transfer is considered from the reactor, surrounding cavity and environment.
- Mass transfer is assumed negligible.
- The port is excited by a transverse electric field in the x-direction.

The coupled electromagnetic and heat transfer equations involved in the microwave heating of the feedstock bed were numerically computed using COMSOL Multiphysics software. The software evaluates electromagnetic propagation from the Maxwell's equations.

To determine the electric field distribution in a medium, the guiding equation of the wave is given by:

Equation 46 :

$$\nabla.\mu_r^{-1}(\nabla.E) - k_o^2\left(\epsilon_r - \frac{j\sigma}{w\varepsilon_0}\right)E = 0$$

where:

μ_r = The relative permeability of the material

E = Electric field vector

k_0 = The wave numbers

ϵ_r = The relative permittivity of the material

σ = Electric conductivity of the material

$j = \sqrt{-1}$

ε_0= Permittivity in the free space ($8{,}854 \times 10^{-12}$ F/m).

Also, the absorbed power per unit of volume can be calculated as the temporal average of the Poynting vector on an S surface, however, if the material is neither magnetic nor conductive, the power density (W/m3) at a local point can be estimated using the following equation.

Equation 47 :

$$P_{diss} = \pi f \varepsilon'' |E|^2$$

Where:

P_{diss} = Power density dissipated (W/m³)

f : Frequency (2.45 GHz MO)

$|E|$: Electric field intensity (V/m).

ε'': Imaginary part of the permittivity

Also, for the COMSOL's modelling the following parameters must be considered:

	Properties T (293.15 K)	Value	Reference
Sargassum Powder 300µm<dp<500µm	Heat capacity (J / kg.K)	3595	[227]
	Thermal conductivity (W / m.K)	0.14	[228]
	Relative permittivity of the bed: real	2.0186	LSPC
	Relative permittivity of the bed: imaginary	0.1201	LSPC
	Relative permeability	1	LSPC
	Density of the bed (kg / m^3)	643	LSPC
	Electrical conductivity (S / m)	0	[35]
Sargassum (4,5g) + SiC (0,9g)	Heat capacity (J / kg.K)	3112	[227], Comsol
	Thermal conductivity (W / m.K)	4.41	[228]
	Relative permittivity of the bed: real	2.72	LSPC
	Relative permittivity of the bed: imaginary	0.29	LSPC
	Relative permeability	1	LSPC
	Density of the bed (kg / m^3)	675	LSPC
	Electrical conductivity (S / m)	0	Comsol
Sargassum (1.575 g) + SiC(0.9 g) + Bio-oil (2.025 g)	Heat capacity (J / kg.K)	2294	[227], Comsol
	Thermal conductivity (W / m.K)	9.96	[228]
	Relative permittivity of the bed: real	15.5	LSPC
	Relative permittivity of the bed: imaginary	1.14	LSPC
	Relative permeability	1	LSPC
	Density of the bed (kg / m^3)	1036	LSPC
	Electrical conductivity (S / m)	0	Comsol
Sargassum (1.575 g) + SiC(0.9 g) + Bio-oil (1.125 g) + Biochar (0.9 g)	Heat capacity (J / kg.K)	2217	[227], Comsol
	Thermal conductivity (W / m.K)	9.5	[228]
	Relative permittivity of the bed: real	40.9	LSPC
	Relative permittivity of the bed: imaginary	32.2	LSPC
	Relative permeability	1	LSPC
	Density of the bed (kg / m^3)	1060	LSPC
	Electrical conductivity (S / m)	0	Comsol

Table 5.2-1 Properties used for COMSOL Modelling

The effect of different dielectric properties of the load is also studied via the simulation work. As previously demonstrated, material's dielectric properties will highly affect the microwave heating. In Table 5-3, as the relative permittivity increases, the power input and the maximum temperature reached in the reactor decrease. This can be explained by a possible resistance to the electric field created by the biomass in the reactor, which causes greater reflection of the waves when the relative permittivity increases, and consequently the power absorbed by the biomass decreases.

Table 5.2-2 Absorbed power and final temperature results for different reactor's load by COMSOL simulation

Material	ε-ε*j	Absorbed power (W)	Final Temperature (°C)
Sargassum	2.0186-j*0.1201	386.86	440
Sargassum (4,5 g) + SiC (0,9 g)	2.72-j*0.29	341.06	410
Sargassum (1,575 g) + SiC (0,9) + Bio-oil (2,025)	15.5-j*1.14	200.47	358

Generally, biomass has poor interaction with microwave energy and so achieving rapid heating of the reaction medium is almost impossible. However, blending the raw biomass with SiC can alleviate the problem since SiC has the capability to absorb a high amount of microwave energy and dissipate heat to the surrounding region. Therefore, the use of SiC as a microwave-absorbent agent helps to achieve rapid heating of the low microwave-absorbing material (the biomass), thus resulting in a more uniform heating distribution throughout the sample. Dielectric properties, as indicated by ε' and ε" play an important role in microwave heating where the former relates to the ability of the sample to absorb microwave energy, known as the dielectric constant, and the latter measures the efficiency with which the microwave energy can be converted into heat, known as dielectric loss. From Figure 5.2.2, dielectric properties influence the intensity of the electric field inside the cavity. Thermal properties and dielectric properties are also normally changing with time and temperature.

It can also be seen from Figure 5.2-2 that there are always areas of high electric field intensity and others of low field intensity throughout the cavity and within the load. For the present case, achieving uniformity within the load in the radial direction was more important than in the axial direction of the bed because the shaftless spiral from the auger reactor is going to play a role in the axial temperature homogenization.

In figures 5.2-2 A, we see that in the reactor, there is a lower capacity of absorption of the electric field than in figures 5.2-2 B and 5.2-2 C; this is because the biomass in the reactor has a low relative permittivity and the wave can propagate. However, based on the calculated power input, it was determined that the reflected power was also very low. Figure 5.2-2 C shows the greatest absorption capacity of the electric field in the reactor, although it shows the greatest reflected power compared to the other cases. It can be concluded that a lower relative permittivity in the reactor allows better penetration of the electric field in the biomass, which results in better absorption of the energy by the biomass and a reduction in the reflection of the waves.

In figures 5.2-3 A and 5.2-3 B, the two black lines mark the microwave entrance of the reactor containing the biomass. Figures show that the absorption capacity of the latter is directly related to the relative permittivity of the biomass, meaning that the greater the relative permittivity is, the lower the penetration depth and the lower the wavelength is..

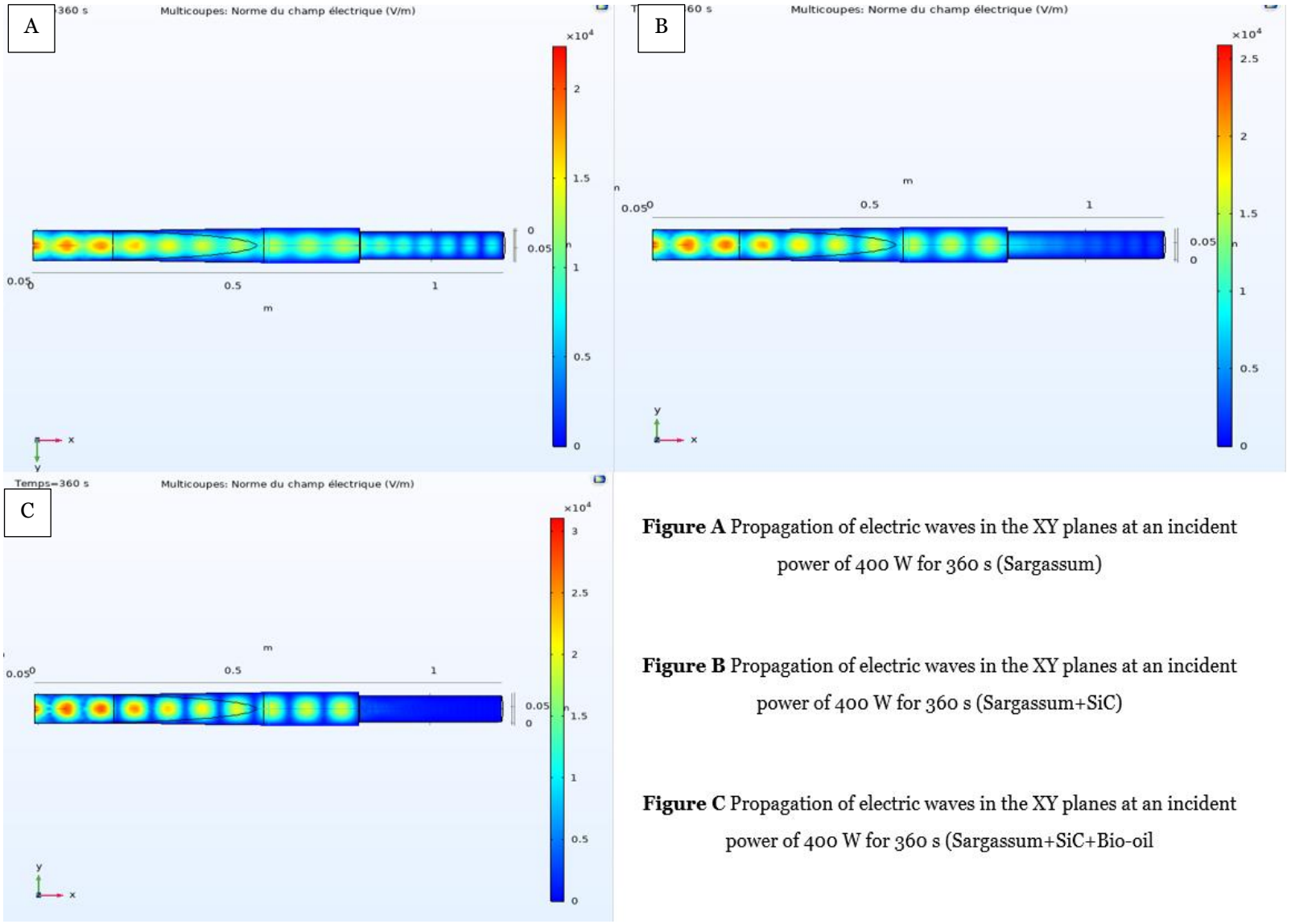

Figure A Propagation of electric waves in the XY planes at an incident power of 400 W for 360 s (Sargassum)

Figure B Propagation of electric waves in the XY planes at an incident power of 400 W for 360 s (Sargassum+SiC)

Figure C Propagation of electric waves in the XY planes at an incident power of 400 W for 360 s (Sargassum+SiC+Bio-oil

Figure 5.2-2 Propagation of the electric field: COMSOL's results

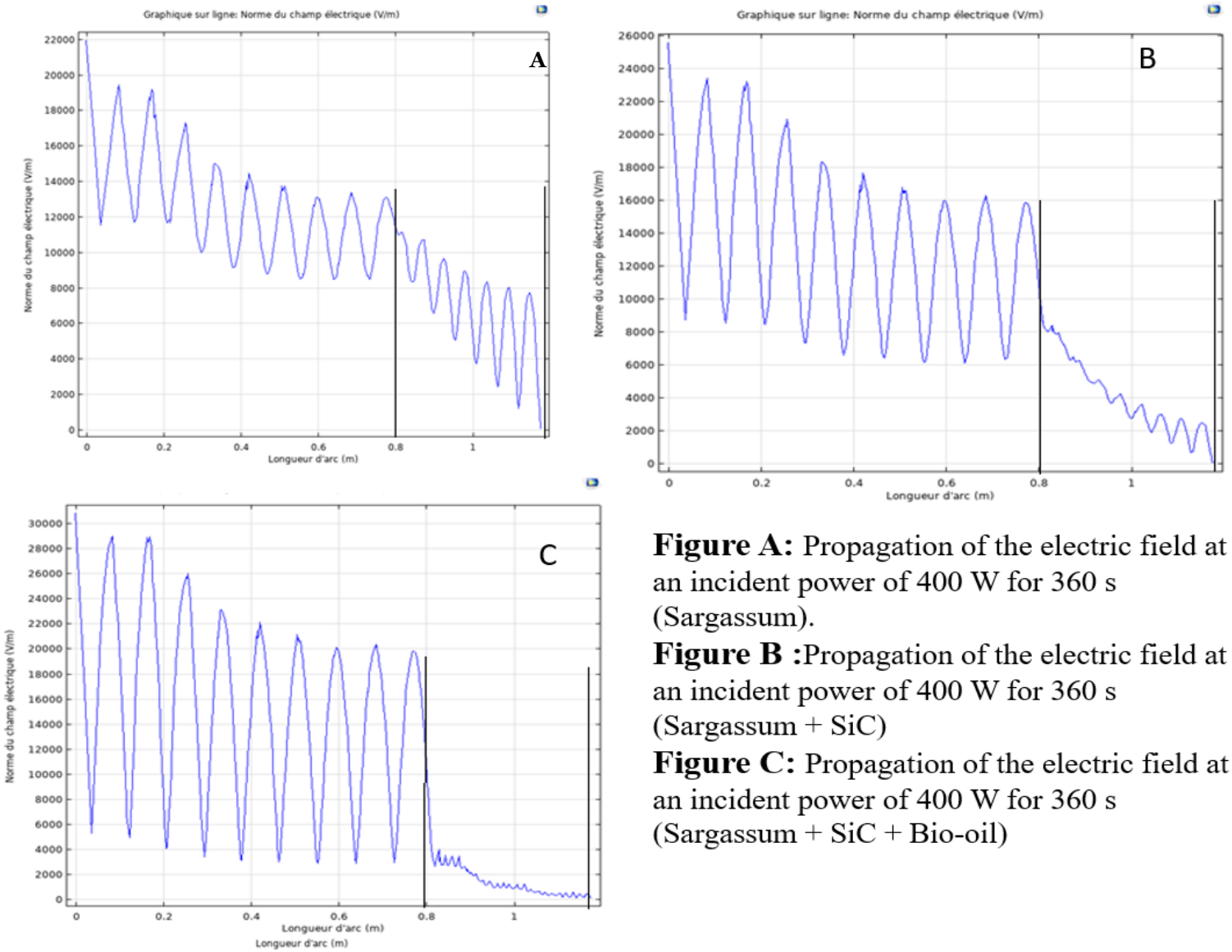

Figure A: Propagation of the electric field at an incident power of 400 W for 360 s (Sargassum).

Figure B : Propagation of the electric field at an incident power of 400 W for 360 s (Sargassum + SiC)

Figure C: Propagation of the electric field at an incident power of 400 W for 360 s (Sargassum + SiC + Bio-oil)

Figure 5.2-3 Propagation of the electric field: Arc length

5.2.2 Thermography: Mapping the electric field for the different reactor's configurations

We have measured the distribution of the electric field of the microwave energy irradiated into different reactor's configurations by using the thermal paper irradiated inside the reactor filled with air. We have calculated the wavelength of the guided electromagnetic radiation in the cylindrical cavity/reactor (λ_g) for each one of cases and results are discussed below.

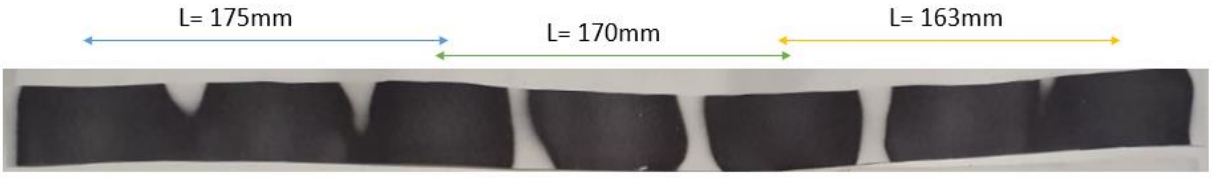

Thermal paper inside the empty reactor irradiated by 15 seconds with a incident power of 600 watt. Length 60mm

Figure 5.2-4 Thermography results for the empty reactor. Values of L= λ_g

In figure 5.2-4, we can see the maximum points of the electric field as degradation to white within the black spot. This phenomenon is part of the sensitive response of the thermal paper to the heat, which passes from white to black according to the heat produced in the point in question. The measured values of the wavelength λg inside the reactor decreased from 175 mm to 163 mm, due to experimental uncertainties in determining the length between the center of two black spots. This decrease is also due to the absorption of electromagnetic energy by the cardboard, which produces the heat needed for the thermography analysis.

A second step was to evaluate the influence of the shaftless spiral inside the reactor filled with air. Two different spirals were tested, one with 80 mm of internal diameter and a second one with 60 mm of diameter. The relevancy of this test lies in need for a right shaftless spiral that produces the minimal perturbation of the electromagnetic propagation mode, keeping the uniformity of the electrical field along the reactor. Figure 5.2-5 shows the results of the thermography analysis with the reactor with each spiral.

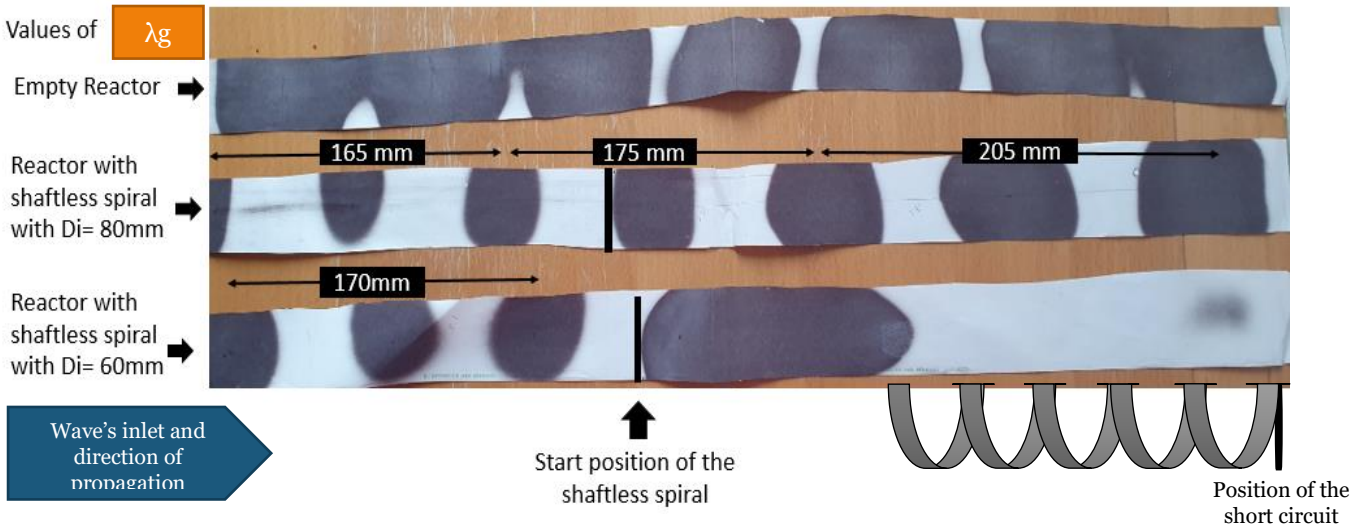

Figure 5.2-5. Thermography results of empty reactor and the reactor with two different shaftless spirals filled with air. Values of λg

The shaftless spiral with an internal diameter of 80mm, displays an increased wavelength when the wave starts traveling inside the spiral. This behavior is the response to the change of the radius of the system. The wave starts traveling in a cylindrical cavity with a diameter of 100 mm and then passes to the spiral with a diameter of 80 mm. The lower the diameter is, the higher the wavelength is. In the case of a shaftless spiral of an internal dimeter of 60 mm, the wave propagates similarly to the other cases in the cylindrical part but propagation is stopped inside the spiral. It is found a maximum point of the electric field at the very beginning of the spiral and another point at the end just before the short circuit of the system. To evaluate both behaviors, we must introduce the concept of cut-off wavelength which defines a boundary to the microwave transmission through the system.

For a cylindrical cavity with a propagation mode type TE11, the cut-off wavelength can be calculated by using the following equation:

Equation 5. 1.Cut-off wavelength equation

$$\lambda_c = \frac{2\pi a}{u'_{11}}$$

Where "a" is the internal radius if the cavity and "u'11" = 1.841 is a constant value for the propagation mode TE11.

The next table shows the results of the cut-off wavelength for the three cases presented until the moment and for the following configurations where the reactor will be filled with beech wood biomass.

Table 5.2-3 Cut-off wavelength results for empty reactor and reactor with shaftless spirals filled with air or Beech Wood

Type of system	Internal Diameter (mm)	Internal Radius (mm)	λc (mm)	$\frac{\lambda_0}{\sqrt{\varepsilon'_r}}$ (mm) Air	$\frac{\lambda_0}{\sqrt{\varepsilon'_r}}$ (mm) Beech wood
Empty Reactor	100	50	171	122	85 ,9
Reactor with shaftless spiral #1	80 *	40	137	122	85 ,9
Reactor with shaftless spiral #2	60 *	30	102	122	85 ,9

*Internal diameter of the spiral

As stated before, the wave will propagate in the reactor fully filled by the materials if:

$$\frac{1}{\lambda_c^2} < \frac{\varepsilon'_r}{\lambda_0^2}$$

and

$$\frac{1}{\lambda_g^2} = \frac{\varepsilon'_r}{\lambda_0^2} - \frac{1}{\lambda_c^2}$$

For $f = 2.45\ GHz$:

$$\lambda_0 = \frac{C}{f} = \frac{3.10^8}{2.45.10^9} = 0.1224\ m = 122.4\ mm$$

And the $\varepsilon'_r = 1$ for air and 2.03 for Beech Wood

If the reactor is full of air, only the reactors of 100 mm and 80 mm diameters can propagate the wave considering λ_c in Table 5.2-3. This result is fully in accordance with the experimental results. If the reactor is full of Beech Wood, the wave should propagate in the three cases.

After evaluating three reactor configurations without biomass, we proceeded to evaluate the system with biomass inside, in order to observe the attenuation of the wave when passing through the biomass. The biomass used for this experiment was beech wood (because Flax shives and Sargassum were not

available at that time) which have permittivity values for ε' = 2.03 and for ε'' = 0.19 at a frequency of 2.45 GHz.

The first essay was the evaluation of the biomass load on the reactor with the shaftless spiral with an internal dimeter of 80 mm. Two types of workload were evaluated, the first one was a workload all along the reactor and the second one, was a workload just inside the spiral. The results of this test are presented below in figure 5.2-6.

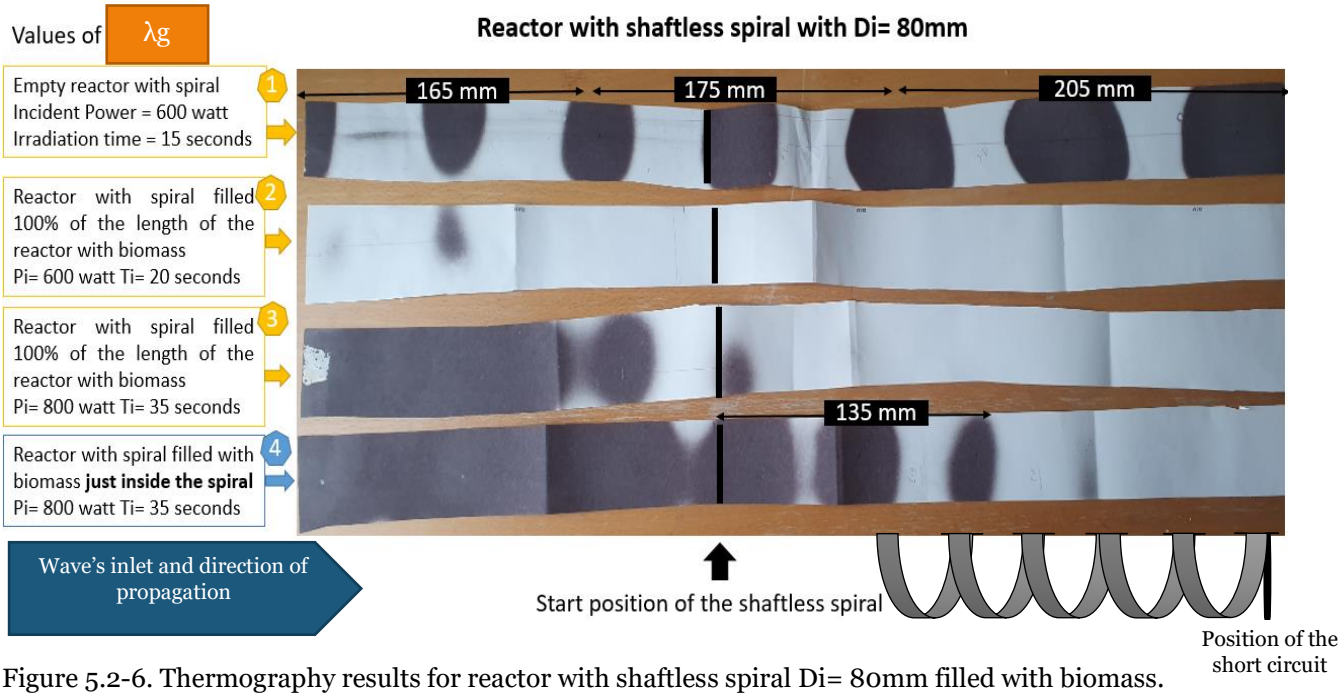

Figure 5.2-6. Thermography results for reactor with shaftless spiral Di= 80mm filled with biomass.

As mentioned in section 2.5, part of experimental arrangements is calibrating the correct incident power and irradiation time to have visible spots. In case 1, when the reactor was empty, an incident power of 600 watts for 15 seconds was enough to have a visible electric field propagation mode pattern; however, when the reactor was filled with biomass, the incident power was not enough even if the irradiation time was increased to 20 seconds (case 2).

This is due to the attenuation of the wave when it gets in contact with biomass. Still, we can obtain some conclusions. For both cases (1 and 2), the wave propagation mode pattern is similar to the λg matches for the two first spots. The third case, which has the same workload as in case two but with a higher incident power and time of contact, shows an important attenuation of the electromagnetic energy. At the same time, the wave propagates into the biomass.

In the fourth case, where the reactor was filled with biomass just inside the spiral, it is observed that before encountering the biomass, there was a large dark spot, most probably because the incident power and the irradiation time were too high for space in which the dielectric is the air, preventing for seeing the black and white zones. However, once it entered the spiral, a reduction of the wavelength was noticed with a strong energy attenuation. This behavior is reasonable, considering that the wave is

changing from air to biomass while entering inside the spiral, which has higher permittivity values, and that influences the attenuation factor.

The last test was done in the reactor with a spiral of 60 mm of internal diameter. The results are presented in Figures 5.2-7. As in the case of the spiral of 80 mm of internal diameter, an attenuation of the wave while entering the spiral was observed in this case also. However, the rapid attenuation of the wave near the start point of the spiral highlight the presence of an evanescent wave even if the dielectric medium with a higher attenuation than air is present. An evanescent wave is a standing wave with an intensity that exhibits exponential decay with distance from the boundary at which the wave was formed. This kind of configuration could be interesting for systems that require an extremely high absorption/ attenuation of energy at a precise point.

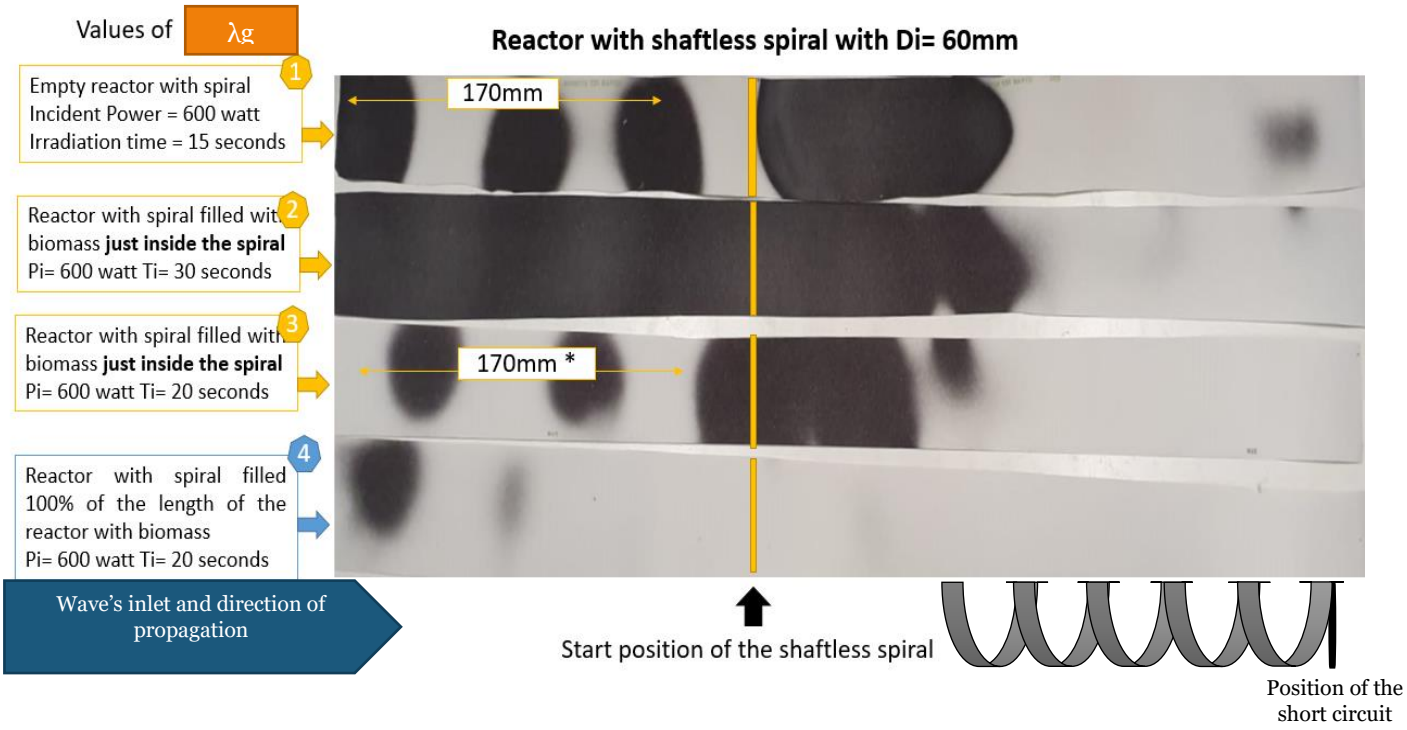

Figure 5.2-7. Thermography results for reactor with shaftless spiral Di= 60mm filled with biomass

5.3 PRELIMINARY CONCLUSIONS

A continuous pyrolysis process under microwave irradiation is possible when considering the key parameters that will allow the right pyrolysis conditions and the electromagnetic wave propagation. Choosing the type of rector according to the required operating parameters is not negligible. This decision will influence the wave propagation mode, the attenuation factor, the quantity of biomass that can be treated, and the power delivery capacity.

Two types of methods were used to verify the electromagnetic compatibility of the system. A comprehensive COMSOL-model to simulate the influence of dielectric properties of the medium and the effect on temperature was developed to understand the behavior of the electric field in a different reactor configuration. Also, a sequence of thermography experiments was carried out to validate the type of shaftless screw to be used inside the reactor.

In general, lower rotating speed will result in higher variance for particle residence time, which is unfavorable for product distribution. The temperature progress is an important parameter for reactor design. It needs careful attention for correct implementation to have the right incident power according to the thermochemical degradation phase of biomass and the evolution of the dielectric properties.

The presence of the shaftless screw inside the reactor influences the electric field propagation pattern, where for an internal diameter of 60 mm, the wave propagation is not possible.

6 GENERAL CONCLUSIONS

This thesis aimed to study the interaction between biomass and microwaves under the pyrolysis reaction to obtain the optimal operating conditions and develop a reliable and scalable microwave pyrolysis process. The biomasses were selected considering the needs of participating countries, their availability, cost, and environmental issues. These materials were studied and characterized in chemical composition, dielectric properties, devolatilization behavior, and pyrolysis product quality.

To overcome the challenges of microwave pyrolysis, a semi-batch rotatory bed reactor was used to better understand the different phenomena occurring while pyrolysis under microwave irradiation. The experiments were carried out to assess the yield and quality of the products obtained. Also, a continuous flow alternative was investigated to overcome the limitations of scaling up a microwave pyrolysis process.

First, the elemental and proximate analysis of both, Sargassum and Flax shives reflected the differences between a lignocellulosic and algae biomass composition. Flax shives presented a higher amount of carbon while Sargassum of nitrogen. Also, the percentage of hemicellulose, cellulose, and lignin were different: for Flax shives, the organic matter distribution was in accordance with the other lignocellulosic biomass, while for Sargassum, the presence of these pseudo components was not that remarkable due to the presence of other compounds as lipid in their basic structure.

To study the devolatilization behavior, the thermogravimetric analysis was carried out over different heating rates and in a temperature range from room temperature up to 100 ° Celsius. The decomposition behavior of both biomasses was very related to their chemical composition. Flax shives presented a common behavior of lignocellulosic biomass, with three stages of degradation:

1. Water evaporation
2. An abrupt mass loss related to cellulose and hemicellulose degradation
3. Finishing with the slow degradation of lignin

In the case of the Sargassum, the weight loss was more stable with temperature. The component degradation behavior was divided into four important steps, the water evaporation, then the carbohydrates, followed by the lipid, and at the end, char volatilization. It was concluded that for Flax shives, the operating conditions should be in the range of 300 - 500 °C and for Sargassum between 250 – 600°C to ensure up to 80% of weight loss.

Dielectric properties were studied for different frequencies. The first parameter evaluated was the water content. It was found that the water content increased the absorption of microwaves for both the biomasses studied. Additionally, their pyrolysis products, bio-oil, and biochar were studied. In the case of Flax shives, bio-oil did have higher dielectric properties than biochar, contrary to the Sargassum biomass in which the biochar had higher dielectric properties than bio-oil. Of the four products,

Sargassum biochar did show the more interesting dielectric properties, being considered a potential microwave absorber.

To predict the possible valorization of the microwave pyrolysis products, a chemical family's detection was performed using a GC-MS for bio-oil and the non-condensable gases. Flax shives presented a high quantity of ketones, esters, and phenols, while Sargassum in alcohol, ketones, and aromatic. However, these results concerned the number of compounds belonging to a specific chemical family. Deepening the study, the higher relevancy compounds were acetic acid, phenol, creosol, and 2-Methoxy-4-vinylphenol for Flax shives. For Sargassum, they were acetic acid, phenol, pyridine, and 2-Furancarboxaldehyde 5-Methyl. The latter was in terms of GC-MS detection. In terms of non-condensable gases, the GC-MS could not detect all the desired compounds. Still, the more relevant were carbon dioxide and ethylene for Flax shives and carbon dioxide and acetylene for Sargassum. The remaining undetected compounds were analyzed by GC-FID/TCD using standards (Hydrogen, Methane, and Carbon monoxide). It was concluded that the non-negligible presence of phenols in both biomasses could be interesting for the production of high value-added. The presence of aromatics and alcohol in Sargassum bio-oil could lead to the production of biofuels.

Microwave pyrolysis was first studied in terms of heat conversion and transfer. The response of a biomass bed to the incident power and its absorbed power capacity and induced temperature were studied. It was found a positive and linear correlation between the incident and absorbed power and the temperature. Also, a high gradient of temperature between the surface and the center of the reactor was highlighted in the rotary kiln reactor. Both types of biomasses mixed with silicon carbide presented an efficient microwave absorption and linearly positive response in terms of temperature.

The influence of incident power was measured in the pyrolysis reaction development. It is concluded that pyrolysis phases can have a variable duration depending on the power applied and that the energy is properly transmitted to the biomass, despite the thermal losses.

The influence of microwave pyrolysis operating conditions on bio-oil, biochar, and gas production was studied. It was concluded that for Flax shives, the increase of the microwave power enhanced the bio-oil production, but for the Sargassum, there was a competition between the gas and bio-oil production. The bio-oil of both biomasses was obtained in relatively high yields (up to 60%), compared to literature which can be convenient when the production of liquid biofuels or additives is targeted. Additionally, both Flax shives and Sargassum N. are also highly suitable materials for producing H2+CO-rich gas via microwave pyrolysis at high incident power.

The chemical families produced in bio-oil and non-condensable gases were also studied for the different operating conditions. For Flax shives, carboxylic acids, phenols, ketones, and aromatic compounds presented a cleared tendency with temperature compared to the other chemical families. In the case of Sargassum, the tendency was less clear due to the experimental approach. However, to compare both cases, a principal component analysis was done. The principal component analysis reflected the global trend of chemical families production for both biomasses.

As one of the steps toward optimizing the process, the optimal condition for bio-oil production was studied. It was found that even if the bio-oil production was dependent on the energy absorbed and the internal heating rate of the system, 13000 joules was the right amount of energy to be delivered per gram of biomass.

The scalable concept of microwaves pyrolysis was studied. Features such as avoiding microwave leaks for the biomass input and output and the changing patterns of the electric field when adding elements inside the reactor/ cavity were considered. This research revealed that to scale a microwave process, the electric field patterns must not be neglected, and the proper propagation of the wave inside the reactor. For a cylindrical cavity, the internal diameter of 80 mm allowed the propagation of the microwave. Moreover, the dielectric properties influenced the attenuation of the wave allowing the use of a smaller diameter. The distribution of the electric field was also evaluated by using COMSOL. The intensity of the electric field increased with an increase in the dielectric properties of the feedstock load. For example, a mixture of biomass and bio-oil allowed a higher intensity of the electric field than the biomass alone, but propagation depth and absorbed energy were less.

To conclude, microwave heating is perceived as an increasingly feasible alternative technology for producing bio-derived products with a different heating mechanism. Therefore, it can be viewed as an important pathway to improve the limitations of conventional heat transfer in the pyrolysis process. Also, even if microwave pyrolysis is relatively new, it has become an interesting option for biomass residues treatment due to its energy efficiency and high-quality products. Studying the potential of Flax shives and Sargassum N. has resulted in highly promising potential biomasses for producing fuels, additives, and chemicals.

7 PERSPECTIVES

The lack of dielectric properties information of the Flax shives and Sargassum in literature, and the influence of temperature and pressure on the dielectric constant and loss factor during microwave irradiation, is one of the next studies to be done in order to better understand the microwave pyrolysis mechanism. Also, Sargassum biochar as a microwave absorbed cannot be neglected. A deeper study of the biochar structure is recommended.

The different kinetics pathways and the influence of microwave operating conditions should be deepened and studied in terms of product quality. The fact that for two different biomasses, the chemical families were not dependent on the same ways to the incident power reflects a need to study the relationship between incident power and the pyrolysis reaction kinetics in terms of the chemical family's production and the influence of heir dielectric properties in the results.

The effect of pressure under microwave pyrolysis is another interesting parameter to be studied and the use of catalysts inside the biomass bed to improve the quality of the bio-oil obtained.

In terms of microwave thermochemical degradation. The high temperatures achieved during microwave pyrolysis lead to thin in performing gasification under microwave irradiation.

A continuous system needs to be developed and investigated for biofuel production in terms of the industrialization of microwave-assisted pyrolysis and gasification technology. This research has assisted in understanding the pyrolysis at a semi-batch scale and the path to follow to scale a process to microwave continuous flow pyrolysis. However, the pyrolysis reactions must be evaluated on the reactor proposed to understand the effect of the reactor configuration on the yield of the products. The key features of the continuous system could include a motor-driven mixer, multiple-point temperature detection, automatic temperature control, mechanisms for easy input of feedstock and discharge of solid materials and reassembling, etc.

Future work can further study the sensitivity of the COMSOL model towards operational conditions, physical properties, and other shaftless screws configurations. Finally, the model can integrate a mass- and heat transfer model to predict the electric field evolution with the pyrolysis product evolution in time. The latter would be valuable information for upscaled reactors.

8 REFERENCES

[1] M. Hoogwijk, A. Faaij, B. Eickhout, B. Devries, et W. Turkenburg, « Potential of biomass energy out to 2100, for four IPCC SRES land-use scenarios », *Biomass Bioenergy*, vol. 29, nº 4, p. 225-257, oct. 2005, doi: 10.1016/j.biombioe.2005.05.002.

[2] A. A. Arpia, W.-H. Chen, S. S. Lam, P. Rousset, et M. D. G. de Luna, « Sustainable biofuel and bioenergy production from biomass waste residues using microwave-assisted heating: A comprehensive review », *Chem. Eng. J.*, vol. 403, p. 126233, janv. 2021, doi: 10.1016/j.cej.2020.126233.

[3] T. Bridgwater, « Biomass for energy », *J. Sci. Food Agric.*, vol. 86, nº 12, p. 1755-1768, 2006, doi: https://doi.org/10.1002/jsfa.2605.

[4] E. C. Gaudino, G. Cravotto, M. Manzoli, et S. Tabasso, « From waste biomass to chemicals and energy via microwave-assisted processes », *Green Chem.*, vol. 21, nº 6, p. 1202-1235, mars 2019, doi: 10.1039/C8GC03908A.

[5] « Why European Flax®? - Le lin et le chanvre européen ». http://news.europeanflax.com/celc/4-european-flax/ (consulté le avr. 18, 2021).

[6] C. Mohabeer, L. Abdelouahed, S. Marcotte, et B. Taouk, « Comparative analysis of pyrolytic liquid products of beech wood, Flax shives and woody biomass components », *J. Anal. Appl. Pyrolysis*, vol. 127, p. 269-277, sept. 2017, doi: 10.1016/j.jaap.2017.07.025.

[7] E. M. Sulman, Y. Y. Kosivtsov, A. Sidorov, A. A. Stepacheva, et Y. Lugovoy, « Fuel gas production through low-temperature catalytic pyrolysis of Flax shives », vol. 11, p. 4439-4447, avr. 2016

[8] N. Boukaous, L. Abdelouahed, M. Chikhi, A.-H. Meniai, C. Mohabeer, et T. Bechara, « Combustion of Flax shives, Beech Wood, Pure Woody Pseudo-Components and Their Chars: A Thermal and Kinetic Study », *Energies*, vol. 11, nº 8, Art. nº 8, août 2018, doi: 10.3390/en11082146.

[9] T. M. Thompson, B. R. Young, et S. Baroutian, « Pelagic Sargassum for energy and fertiliser production in the Caribbean: A case study on Barbados », *Renew. Sustain. Energy Rev.*, vol. 118, p. 109564, févr. 2020, doi: 10.1016/j.rser.2019.109564.

[10] J. Schell, D. Goodwin, et A. Siuda, « Recent Sargassum Inundation Events in the Caribbean: Shipboard Observations Reveal Dominance of a Previously Rare Form », *Oceanography*, vol. 28, p. 8-10, sept. 2015, doi: 10.5670/oceanog.2015.70.

[11] A. C. Metaxas et R. J. Meredith, *Industrial Microwave Heating*. IET, 1983.

[12] S. S. Lam et H. A. Chase, « A Review on Waste to Energy Processes Using Microwave Pyrolysis », *Energies*, vol. 5, nº 10, Art. nº 10, oct. 2012, doi: 10.3390/en5104209.

[13] *Code of Federal Regulations: 1949-1984*. U.S. General Services Administration, National Archives and Records Service, Office of the Federal Register, 1980.

[14] A. Grebennikov, *RF and Microwave Transmitter Design*. John Wiley & Sons, 2011.

[15] J. C. Atuonwu et S. A. Tassou, « Quality assurance in microwave food processing and the enabling potentials of solid-state power generators: A review », *J. Food Eng.*, vol. 234, p. 1-15, oct. 2018, doi: 10.1016/j.jfoodeng.2018.04.009.

[16] G. D. Stefanidis, A. N. Muñoz, G. S. J. Sturm, et A. Stankiewicz, « A helicopter view of microwave application to chemical processes: reactions, separations, and equipment concepts », *Rev. Chem. Eng.*, vol. 30, nº 3, p. 233-259, juin 2014, doi: 10.1515/revce-2013-0033.

[17] D. M. Pozar, *Microwave Engineering, 4th Edition*. Wiley, 2011.

[18] A.-A. Khalid et N. I. Fawaz, « Zinc Sulfide Waveguide Analysis », *Univers. J. Electr. Electron. Eng.*, vol. 7, nº 4, p. 227-233, août 2020, doi: 10.13189/ujeee.2020.070401.

[19] F. C. Borges *et al.*, « Fast microwave assisted pyrolysis of biomass using microwave absorbent », *Bioresour. Technol.*, vol. 156, p. 267-274, mars 2014, doi: 10.1016/j.biortech.2014.01.038.

[20] S. S. Lam, W. A. Wan Mahari, A. Jusoh, C. T. Chong, C. L. Lee, et H. A. Chase, « Pyrolysis using microwave absorbents as reaction bed: An improved approach to transform used frying oil into biofuel product with desirable properties », *J. Clean. Prod.*, vol. 147, p. 263-272, mars 2017, doi: 10.1016/j.jclepro.2017.01.085.

[21] D. Beneroso, T. Monti, E. T. Kostas, et J. Robinson, « Microwave pyrolysis of biomass for bio-oil production: Scalable processing concepts », *Chem. Eng. J.*, vol. 316, p. 481-498, mai 2017, doi: 10.1016/j.cej.2017.01.130.

[22] J. Asomaning, S. Haupt, M. Chae, et D. C. Bressler, « Recent developments in microwave-assisted thermal conversion of biomass for fuels and chemicals », *Renew. Sustain. Energy Rev.*, vol. 92, p. 642-657, sept. 2018, doi: 10.1016/j.rser.2018.04.084.

[23] E. T. Kostas, D. Beneroso, et J. P. Robinson, « The application of microwave heating in bioenergy: A review on the microwave pre-treatment and upgrading technologies for biomass », *Renew. Sustain. Energy Rev.*, vol. 77, p. 12-27, sept. 2017, doi: 10.1016/j.rser.2017.03.135.

[24] C. R. Ellison, R. Hoff, C. Mărculescu, et D. Boldor, « Investigation of microwave-assisted pyrolysis of biomass with char in a rectangular waveguide applicator with built-in phase-shifting », *Appl. Energy*, vol. 259, p. 114217, févr. 2020, doi: 10.1016/j.apenergy.2019.114217.

[25] N. Benamara, « Intensification de procédés par chauffage micro-ondes pour la chimie verte », These de doctorat, Normandie, 2017. Consulté le: avr. 18, 2021. [En ligne]. Disponible sur: https://www.theses.fr/2017NORMIR13

[26] « Annual Energy Outlook 2020 ». https://www.eia.gov/outlooks/aeo/ (consulté le juill. 06, 2020).

[27] « Sustainable biofuel and bioenergy production from biomass waste residues using microwave-assisted heating: A comprehensive review », *Chem. Eng. J.*, vol. 403, p. 126233, janv. 2021, doi: 10.1016/j.cej.2020.126233.

[28] X. J. Lee, H. C. Ong, Y. Y. Gan, W.-H. Chen, et T. M. I. Mahlia, « State of art review on conventional and advanced pyrolysis of macroalgae and microalgae for biochar, bio-oil and bio-syngas production », *Energy Convers. Manag.*, vol. 210, p. 112707, avr. 2020, doi: 10.1016/j.enconman.2020.112707.

[29] B. Velimirov, J. G. Field, C. L. Griffiths, et P. Zoutendyk, « The ecology of kelp bed communities in the Benguela upwelling system: Analysis of biomass and spatial distribution », *Helgoländer Wiss. Meeresunters.*, vol. 30, nº 1-4, p. 495-518, août 1977, doi: 10.1007/BF02207857.

[30] « Green and golden seaweed tides on the rise | Nature ». https://www.nature.com/articles/nature12860 (consulté le avr. 18, 2021).

[31] « Lignocellulosic biomass: a sustainable platform for the production of bio-based chemicals and polymers - Polymer Chemistry (RSC Publishing) ». https://pubs.rsc.org/en/content/articlelanding/2015/py/c5py00263j#!divAbstract (consulté le mai 13, 2021).

[32] S. D. Stefanidis, K. G. Kalogiannis, E. F. Iliopoulou, C. M. Michailof, P. A. Pilavachi, et A. A. Lappas, « A study of lignocellulosic biomass pyrolysis via the pyrolysis of cellulose, hemicellulose and lignin », *J. Anal. Appl. Pyrolysis*, vol. 105, p. 143-150, janv. 2014, doi: 10.1016/j.jaap.2013.10.013.

[33] S. Dumitriu, *Polysaccharides: Structural Diversity and Functional Versatility, Second Edition*. CRC Press, 2004.

[34] A. Nordin, « Chemical elemental characteristics of biomass fuels », *Biomass Bioenergy*, vol. 6, nº 5, p. 339-347, janv. 1994, doi: 10.1016/0961-9534(94)E0031-M.

[35] R. Bakker et H. W. Elbersen, « Managing ash content and quality in herbaceous biomass: An analysis from plant to product », *14th Eur. Biomass Conf.*, janv. 2005.

[36] T. Li et S. Takkellapati, « The current and emerging sources of technical lignins and their applications: Sources of Technical Lignins », *Biofuels Bioprod. Biorefining*, vol. 0, juill. 2018, doi: 10.1002/bbb.1913.

[37] J. Salmon-Minotte et R. R. Franck, « Flax », in *Bast and Other Plant Fibres*, Elsevier, 2005, p. 94-175. doi: 10.1533/9781845690618.94.

[38] L. Yan, N. Chouw, et K. Jayaraman, « Flax fibre and its composites – A review », *Compos. Part B Eng.*, vol. 56, p. 296-317, janv. 2014, doi: 10.1016/j.compositesb.2013.08.014.

[39] F. Bensadoun, B. Vanderfeesten, I. Verpoest, A. W. Van Vuure, et K. Van Acker, « Environmental impact assessment of end of life options for flax-MAPP composites », *Ind. Crops Prod.*, vol. 94, p. 327-341, déc. 2016, doi: 10.1016/j.indcrop.2016.09.006.

[40] Y. Deng et Y. Tian, « Assessing the Environmental Impact of Flax Fibre Reinforced Polymer Composite from a Consequential Life Cycle Assessment Perspective », *Sustainability*, vol. 7, nº 9, Art. nº 9, sept. 2015, doi: 10.3390/su70911462.

[41] J.-W. Kim et G. Mazza, « Optimization of extraction of phenolic compounds from Flax shives by pressurized low-polarity water », *J. Agric. Food Chem.*, vol. 54, nº 20, p. 7575-7584, oct. 2006, doi: 10.1021/jf0608221.

[42] R. V. Parsons, « Selective Break-Down of Flax Shive for the Recovery of High-Value Bio-Products », p. 307.

[43] « Sustainability Assessing the Environmental Impact of Flax Fibre Reinforced Polymer Composite from a Consequential Life Cycle Assessment Perspective | HTML ». https://www.mdpi.com/2071-1050/7/9/11462/htm (consulté le mai 13, 2021).

[44] « The use of modified Flax shives in cementitious composites and the repercussion of these modifications on their behaviour in the cement matrix ». https://www.researchgate.net/publication/242421517_The_use_of_modified_flax_shives_in_cementitious_composites_and_the_repercussion_of_these_modifications_on_their_behaviour_in_the_cement_matrix (consulté le mai 13, 2021).

[45] D. Puglia, « A Review on Natural Fibre-Based Composites-Part I », *J. Nat. Fibers*, Consulté le: mai 13, 2021. [En ligne]. Disponible sur: https://www.academia.edu/22122496/A_Review_on_Natural_Fibre_Based_Composites_Part_I

[46] K. Ross et M. Giuseppe, « Characteristics of Lignin from Flax shives as Affected by Extraction Conditions », *Int. J. Mol. Sci.*, vol. 11, oct. 2010, doi: 10.3390/ijms11104035.

[47] V. B. Agbor, « Personal communication of results of analysis of a similar flax shive sample as employed in this work by the Feeds Innovation Institute at the University of Sasksatchewan for the Laboratory of Professor D. Levin, Departmet of Biosystems Engineering, University of Manitoba. » 2011.

[48] J. A. Raven et M. Giordano, « Algae », *Curr. Biol. CB*, vol. 24, nº 13, p. R590-595, juill. 2014, doi: 10.1016/j.cub.2014.05.039.

[49] F. B. Metting, « Biodiversity and application of microalgae », *J. Ind. Microbiol.*, vol. 17, nº 5, p. 477-489, nov. 1996, doi: 10.1007/BF01574779.

[50] « Refining Biomass Residues for Sustainable Energy and Bioproducts - 1st Edition ». https://www.elsevier.com/books/refining-biomass-residues-for-sustainable-energy-and-bioproducts/kumar/978-0-12-818996-2 (consulté le mai 13, 2021).

[51] P. Debiagi, M. Trinchera, A. Frassoldati, T. Faravelli, R. Vinu, et E. Ranzi, « Algae Characterization and Multistep Pyrolysis Mechanism », *J. Anal. Appl. Pyrolysis*, vol. 128, sept. 2017, doi: 10.1016/j.jaap.2017.08.007.

[52] K. Anastasakis, A. B. Ross, et J. M. Jones, « Pyrolysis behaviour of the main carbohydrates of brown macro-algae », *Fuel*, vol. 90, nº 2, p. 598-607, févr. 2011, doi: 10.1016/j.fuel.2010.09.023.

[53] « Biobased Products and Industries - 1st Edition ». https://www.elsevier.com/books/biobased-products-and-industries/galanakis/978-0-12-818493-6 (consulté le mai 13, 2021).

[54] « Microalgae Cultivation for Biofuels Production - 1st Edition ». https://www.elsevier.com/books/microalgae-cultivation-for-biofuels-production/yousuf/978-0-12-817536-1 (consulté le mai 13, 2021).

[55] « Haliseris C.Agardh, 1820 :: Algaebase ». https://www.algaebase.org/search/genus/detail/?tc=accept&genus_id=42925 (consulté le mai 13, 2021).

[56] « Sargassum natans (Linnaeus) Gaillon 1828 :: Algaebase ». https://www.algaebase.org/search/species/detail/?species_id=826&-session=abv4:AC1F22890c87922867yk358AB895 (consulté le mai 13, 2021).

[57] M. Wang et C. Hu, « Mapping and quantifying Sargassum distribution and coverage in the Central West Atlantic using MODIS observations », *Remote Sens. Environ.*, vol. 183, p. 350-367, sept. 2016, doi: 10.1016/j.rse.2016.04.019.

[58] « Identification and chemical studies of pelagic masses of Sargassum natans (Linnaeus) Gaillon and S. fluitans (Borgessen) Borgesen (brown algae), found offshore in Ondo State, Nigeria ». https://www.researchgate.net/publication/272369721_Identification_and_chemical_studies_of_pelagic_masses_of_Sargassum_natans_Linnaeus_Gaillon_and_S_fluitans_Borgessen_Borgesen_brown_algae_found_offshore_in_Ondo_State_Nigeria (consulté le avr. 18, 2021).

[59] G. N. D. Addico et K. A. A. deGraft-Johnson, « Preliminary investigation into the chemical composition of the invasive brown seaweed Sargassum along the West Coast of Ghana », *Afr. J. Biotechnol.*, vol. 15, nº 39, p. 2184-2191, sept. 2016, doi: 10.5897/AJB2015.15177.

[60] P. G. del Río, J. S. Gomes-Dias, C. M. R. Rocha, A. Romaní, G. Garrote, et L. Domingues, « Recent trends on seaweed fractionation for liquid biofuels production », *Bioresour. Technol.*, vol. 299, p. 122613, mars 2020, doi: 10.1016/j.biortech.2019.122613.

[61] G. P. B. Marquez *et al.*, « Seaweed biomass of the Philippines: Sustainable feedstock for biogas production », *Renew. Sustain. Energy Rev.*, vol. 38, p. 1056-1068, oct. 2014, doi: 10.1016/j.rser.2014.07.056.

[62] A. Maneesh, K. Chakraborty, et F. Makkar, « Pharmacological activities of brown seaweed Sargassum wightii (Family Sargassaceae) using different in vitro models », *Int. J. Food Prop.*, vol. 20, nº 4, p. 931-945, avr. 2017, doi: 10.1080/10942912.2016.1189434.

[63] T. A. Davis, B. Volesky, et R. H. S. F. Vieira, « Sargassum seaweed as biosorbent for heavy metals », *Water Res.*, vol. 34, nº 17, p. 4270-4278, déc. 2000, doi: 10.1016/S0043-1354(00)00177-9.

[64] L. Mattio, « Taxonomie du genre Sargassum (Fucales, Phaeophyceae) en Nouvelle-Calédonie et dans le Pacifique Sud. Approches morphologique et moléculaire », p. 352.

[65] H. Rabemanolontsoa et S. Saka, « Comparative study on chemical composition of various biomass species », *RSC Adv.*, vol. 3, nº 12, p. 3946-3956, févr. 2013, doi: 10.1039/C3RA22958K.

[66] Y. Peng *et al.*, « Nutritional and chemical composition and antiviral activity of cultivated seaweed Sargassum naozhouense Tseng et Lu », *Mar. Drugs*, vol. 11, nº 1, p. 20-32, déc. 2012, doi: 10.3390/md11010020.

[67] « Bioactive constituents and biochemical composition of the egyptian brown alga Sargassum Subrepandum (Forsk) ». http://www.scielo.org.mx/scielo.php?script=sci_arttext&pid=S0370-59432011000100006 (consulté le mai 13, 2021).

[68] A. V. Bridgwater, « Principles and practice of biomass fast pyrolysis processes for liquids », *J. Anal. Appl. Pyrolysis*, vol. 51, nº 1, p. 3-22, juill. 1999, doi: 10.1016/S0165-2370(99)00005-4.

[69] M. I. Jahirul, M. G. Rasul, A. A. Chowdhury, et N. Ashwath, « Biofuels Production through Biomass Pyrolysis —A Technological Review », *Energies*, vol. 5, nº 12, Art. nº 12, déc. 2012, doi: 10.3390/en5124952.

[70] C. C. D. Mohabeer, « Bio-oil production by pyrolysis of biomass coupled with a catalytic de-oxygenation treatment », p. 207.

[71] S. Keleş, K. Kaygusuz, et M. Akgün, « Pyrolysis of Woody Biomass for Sustainable Bio-oil », *Energy Sources Part Recovery Util. Environ. Eff.*, vol. 33, nº 9, p. 879-889, févr. 2011, doi: 10.1080/15567030903330652.

[72] N. Canabarro, J. Soares, C. Anchieta, C. Kelling, et M. Mazutti, « Thermochemical processes for biofuels production from biomass », *Sustain. Chem. Process.*, vol. 1, p. 22, nov. 2013, doi: 10.1186/2043-7129-1-22.

[73] A. Verma, R. Shankar, et P. Mondal, « A Review on Pyrolysis of Biomass and the Impacts of Operating Conditions on Product Yield, Quality, and Upgradation », in *Recent Advancements in Biofuels and Bioenergy Utilization*, 2018, p. 227-259. doi: 10.1007/978-981-13-1307-3_10.

[74] M. Fatih Demirbas, « Biorefineries for biofuel upgrading: A critical review », *Appl. Energy*, vol. 86, p. S151-S161, nov. 2009, doi: 10.1016/j.apenergy.2009.04.043.

[75] S. Wang *et al.*, « Effects of torrefaction on hemicellulose structural characteristics and pyrolysis behaviors », *Bioresour. Technol.*, vol. 218, p. 1106-1114, oct. 2016, doi: 10.1016/j.biortech.2016.07.075.

[76] S. Wang, B. Ru, H. Lin, et Z. Luo, « Degradation mechanism of monosaccharides and xylan under pyrolytic conditions with theoretic modeling on the energy profiles », *Bioresour. Technol.*, vol. 143, p. 378-383, sept. 2013, doi: 10.1016/j.biortech.2013.06.026.

[77] « Progress in microwave pyrolysis conversion of agricultural waste to value-added biofuels: A batch to continuous approach », *Renew. Sustain. Energy Rev.*, vol. 135, p. 110148, janv. 2021, doi: 10.1016/j.rser.2020.110148.

[78] L. Abdelouahed, S. Leveneur, L. Vernieres-Hassimi, L. Balland, et B. Taouk, « Comparative investigation for the determination of kinetic parameters for biomass pyrolysis by thermogravimetric analysis », *J. Therm. Anal. Calorim.*, vol. 129, nº 2, p. 1201-1213, août 2017, doi: 10.1007/s10973-017-6212-9.

[79] P. R. Patwardhan, R. C. Brown, et B. H. Shanks, « Understanding the Fast Pyrolysis of Lignin », *ChemSusChem*, vol. 4, nº 11, p. 1629-1636, nov. 2011, doi: 10.1002/cssc.201100133.

[80] Y.-C. Lin, J. Cho, G. A. Tompsett, P. R. Westmoreland, et G. W. Huber, « Kinetics and Mechanism of Cellulose Pyrolysis », *J. Phys. Chem. C*, vol. 113, nº 46, p. 20097-20107, nov. 2009, doi: 10.1021/jp906702p.

[81] I. Ali et A. Bahadar, « Red Sea seaweed (Sargassum spp.) pyrolysis and its devolatilization kinetics », *Algal Res.*, vol. 21, p. 89-97, janv. 2017, doi: 10.1016/j.algal.2016.11.011.

[82] « Comparative investigation for the determination of kinetic parameters for biomass pyrolysis by thermogravimetric analysis | SpringerLink ». https://link.springer.com/article/10.1007/s10973-017-6212-9 (consulté le avr. 18, 2021).

[83] S. Benzennou, J. P. Laviolette, et J. Chaouki, « Kinetic study of microwave pyrolysis of paper cups and comparison with calcium oxide catalyzed reaction », *AIChE J.*, p. aic.16471, déc. 2018, doi: 10.1002/aic.16471.

[84] C. Branca et C. Di Blasi, « Global Kinetics of Wood Char Devolatilization and Combustion », *Energy Fuels*, vol. 17, nº 6, p. 1609-1615, nov. 2003, doi: 10.1021/ef030033a.

[85] W. Jin, K. Singh, et J. Zondlo, « Pyrolysis Kinetics of Physical Components of Wood and Wood-Polymers Using Isoconversion Method », *Agriculture*, vol. 3, nº 1, p. 12-32, mars 2013, doi: 10.3390/agriculture3010012.

[86] « Kinetics of Primary Product Formation from Wood Pyrolysis | Industrial & Engineering Chemistry Research ». https://pubs.acs.org/doi/pdf/10.1021/ie000997e# (consulté le juill. 06, 2020).

[87] L. M. Romero Millán, F. E. Sierra Vargas, et A. Nzihou, « Kinetic Analysis of Tropical Lignocellulosic Agrowaste Pyrolysis », *BioEnergy Res.*, vol. 10, nº 3, p. 832-845, sept. 2017, doi: 10.1007/s12155-017-9844-5.

[88] K. Kirtania et S. Bhattacharya, « Pyrolysis kinetics and reactivity of algae–coal blends », *Biomass Bioenergy*, vol. 55, p. 291-298, août 2013, doi: 10.1016/j.biombioe.2013.02.019.

[89] S.-S. Kim, H. V. Ly, J. Kim, J. H. Choi, et H. C. Woo, « Thermogravimetric characteristics and pyrolysis kinetics of Alga Sagarssum sp. biomass », *Bioresour. Technol.*, vol. 139, p. 242-248, juill. 2013, doi: 10.1016/j.biortech.2013.03.192.

[90] X. Li, C. Yin, S. Knudsen Kær, et T. Condra, « A detailed pyrolysis model for a thermally large biomass particle », *Fuel*, vol. 278, p. 118397, oct. 2020, doi: 10.1016/j.fuel.2020.118397.

[91] W. Peng, Q. Wu, P. Tu, et N. Zhao, « Pyrolytic characteristics of microalgae as renewable energy source determined by thermogravimetric analysis », *Bioresour. Technol.*, vol. 80, nº 1, p. 1-7, oct. 2001, doi: 10.1016/S0960-8524(01)00072-4.

[92] L. A. Andrade, F. R. X. Batista, T. S. Lira, M. A. S. Barrozo, et L. G. M. Vieira, « Characterization and product formation during the catalytic and non-catalytic pyrolysis of the green microalgae Chlamydomonas reinhardtii », *Renew. Energy*, vol. 119, p. 731-740, avr. 2018, doi: 10.1016/j.renene.2017.12.056.

[93] E. Ansah, L. Wang, B. Zhang, et A. Shahbazi, « Catalytic pyrolysis of raw and hydrothermally carbonized Chlamydomonas debaryana microalgae for denitrogenation and production of aromatic hydrocarbons », *Fuel*, vol. 228, p. 234-242, sept. 2018, doi: 10.1016/j.fuel.2018.04.163.

[94] W.-H. Chen, M.-Y. Huang, J.-S. Chang, et C.-Y. Chen, « Thermal decomposition dynamics and severity of microalgae residues in torrefaction », *Bioresour. Technol.*, vol. 169, p. 258-264, oct. 2014, doi: 10.1016/j.biortech.2014.06.086.

[95] A. Marcilla, L. Catalá, J. C. García-Quesada, F. J. Valdés, et M. R. Hernández, « A review of thermochemical conversion of microalgae », *Renew. Sustain. Energy Rev.*, vol. 27, p. 11-19, nov. 2013, doi: 10.1016/j.rser.2013.06.032.

[96] X. Wang, L. Sheng, et X. Yang, « Pyrolysis characteristics and pathways of protein, lipid and carbohydrate isolated from microalgae Nannochloropsis sp. », *Bioresour. Technol.*, vol. 229, p. 119-125, avr. 2017, doi: 10.1016/j.biortech.2017.01.018.

[97] M. Saber, B. Nakhshiniev, et K. Yoshikawa, « A review of production and upgrading of algal bio-oil », *Renew. Sustain. Energy Rev.*, vol. 58, p. 918-930, mai 2016, doi: 10.1016/j.rser.2015.12.342.

[98] C. Şerbănescu, « Kinetic analysis of cellulose pyrolysis: a short review », *Chem. Pap.*, vol. 68, juill. 2014, doi: 10.2478/s11696-013-0529-z.

[99] E. Ranzi *et al.*, « Chemical Kinetics of Biomass Pyrolysis », *Energy Fuels*, vol. 22, nº 6, p. 4292-4300, nov. 2008, doi: 10.1021/ef800551t.

[100] F. R. M. Nascimento, A. M. González, E. E. Silva Lora, A. Ratner, J. C. Escobar Palacio, et R. Reinaldo, « Bench-scale bubbling fluidized bed systems around the world - Bed agglomeration and collapse: A comprehensive review », *Int. J. Hydrog. Energy*, vol. 46, nº 36, p. 18740-18766, mai 2021, doi: 10.1016/j.ijhydene.2021.03.036.

[101] A. Soria-Verdugo, M. Rubio-Rubio, E. Goos, et U. Riedel, « On the characteristic heating and pyrolysis time of thermally small biomass particles in a bubbling fluidized bed reactor », *Renew. Energy*, vol. 160, p. 312-322, nov. 2020, doi: 10.1016/j.renene.2020.07.008.

[102] Y. Liu *et al.*, « Characterization and analysis of condensates and non-condensable gases from furfural residue via fast pyrolysis in a bubbling fluidized bed reactor », *Waste Manag.*, vol. 125, p. 77-86, avr. 2021, doi: 10.1016/j.wasman.2021.02.025.

[103] Q. K. Tran, M. L. Le, H. V. Ly, H. C. Woo, J. Kim, et S.-S. Kim, « Fast pyrolysis of pitch pine biomass in a bubbling fluidized-bed reactor for bio-oil production », *J. Ind. Eng. Chem.*, vol. 98, p. 168-179, juin 2021, doi: 10.1016/j.jiec.2021.04.005.

[104] K. Papadikis, S. gu, et T. Bridgwater, « CFD modelling of the fast pyrolysis of biomass in fluidised bed reactors: Modelling the impact of biomass shrinkage », *Chem. Eng. J.*, vol. 149, p. 417-427, juill. 2009, doi: 10.1016/j.cej.2009.01.036.

[105] D. Radlein et A. Quignard, « A Short Historical Review of Fast Pyrolysis of Biomass », *Oil Gas Sci. Technol. – Rev. D'IFP Energ. Nouv.*, vol. 68, nº 4, p. 765-783, juill. 2013, doi: 10.2516/ogst/2013162.

[106] J. Zhou *et al.*, « Chapter Twelve - Pyrolysis and Gasification of Food Waste », in *Current Developments in Biotechnology and Bioengineering*, J. Wong, G. Kaur, M. Taherzadeh, A. Pandey, et K. Lasaridi, Éd. Elsevier, 2021, p. 325-344. doi: 10.1016/B978-0-12-819148-4.00012-9.

[107] D. T. Pio et L. A. C. Tarelho, « Industrial gasification systems (>3 MWth) for bioenergy in Europe: Current status and future perspectives », *Renew. Sustain. Energy Rev.*, vol. 145, p. 111108, juill. 2021, doi: 10.1016/j.rser.2021.111108.

[108] « Pyrolysis Reactors ». http://task34.ieabioenergy.com/pyrolysis-reactors/ (consulté le mai 29, 2020).

[109] J. A. Garcia-Nunez *et al.*, « Historical Developments of Pyrolysis Reactors: A Review », *Energy Fuels*, vol. 31, nº 6, p. 5751-5775, juin 2017, doi: 10.1021/acs.energyfuels.7b00641.

[110] H. Guoxin, G. Xiwu, H. Hao, F. Haojie, et W. Zheng, « Experimental studies on flow and pyrolysis of coal with solid heat carrier in a modified rotating cone reactor », *Chem. Eng. Process. Process Intensif.*, vol. 47, nº 9, p. 1777-1785, sept. 2008, doi: 10.1016/j.cep.2007.09.021.

[111] B. M. Wagenaar, W. Prins, et W. P. M. van Swaaij, « Pyrolysis of biomass in the rotating cone reactor: modelling and experimental justification », *Chem. Eng. Sci.*, vol. 49, nº 24, Part 2, p. 5109-5126, déc. 1994, doi: 10.1016/0009-2509(94)00392-0.

[112] G. Luo, D. S. Chandler, L. C. A. Anjos, R. J. Eng, P. Jia, et F. L. P. Resende, « Pyrolysis of whole wood chips and rods in a novel ablative reactor », *Fuel*, vol. 194, p. 229-238, avr. 2017, doi: 10.1016/j.fuel.2017.01.010.

[113] G. V. C. Peacocke et A. V. Bridgwater, « Ablative plate pyrolysis of biomass for liquids », *Biomass Bioenergy*, vol. 7, nº 1, p. 147-154, janv. 1994, doi: 10.1016/0961-9534(94)00054-W.

[114] F. Campuzano, R. C. Brown, et J. D. Martínez, « Auger reactors for pyrolysis of biomass and wastes », *Renew. Sustain. Energy Rev.*, vol. 102, p. 372-409, mars 2019, doi: 10.1016/j.rser.2018.12.014.

[115] C. U. Pittman *et al.*, « Characterization of Bio-oils Produced from Fast Pyrolysis of Corn Stalks in an Auger Reactor », *Energy Fuels*, vol. 26, nº 6, p. 3816-3825, juin 2012, doi: 10.1021/ef3003922.

[116] H. Zhang *et al.*, « Microwave pyrolysis of textile dyeing sludge in a continuously operated auger reactor: Char characterization and analysis », *J. Hazard. Mater.*, vol. 334, p. 112-120, juill. 2017, doi: 10.1016/j.jhazmat.2017.03.048.

[117] G. Mancini, P. Viotti, A. Luciano, M. Raboni, et D. Fino, « Full scale treatment of ASR wastes in a modified rotary kiln », *Waste Manag.*, vol. 34, nº 11, p. 2347-2354, nov. 2014, doi: 10.1016/j.wasman.2014.06.028.

[118] M. Syamsiro, M. Dwicahyo, Y. Sulistiawati, M. Ridwan, et N. Citrasari, « Development of a rotary kiln reactor for pyrolytic oil production from waste tire in Indonesia », *IOP Conf. Ser. Earth Environ. Sci.*, vol. 245, p. 012044, mars 2019, doi: 10.1088/1755-1315/245/1/012044.

[119] E. Yazdani, S. H. Hashemabadi, et A. Taghizadeh, « Study of waste tire pyrolysis in a rotary kiln reactor in a wide range of pyrolysis temperature », *Waste Manag.*, vol. 85, p. 195-201, févr. 2019, doi: 10.1016/j.wasman.2018.12.020.

[120] T. Aysu et M. M. Küçük, « Biomass pyrolysis in a fixed-bed reactor: Effects of pyrolysis parameters on product yields and characterization of products », *Energy*, vol. 64, p. 1002-1025, janv. 2014, doi: 10.1016/j.energy.2013.11.053.

[121] M. A. Aziz, R. A. Al-khulaidi, M. Rashid, M. R. Islam, et M. Rashid, « Design and fabrication of a fixed-bed batch type pyrolysis reactor for pilot scale pyrolytic oil production in Bangladesh », *IOP Conf. Ser. Mater. Sci. Eng.*, vol. 184, p. 012056, mars 2017, doi: 10.1088/1757-899X/184/1/012056.

[122] M. A. Aziz, M. A. Rahman, et H. Molla, « Design, fabrication and performance test of a fixed bed batch type pyrolysis plant with scrap tire in Bangladesh », *J. Radiat. Res. Appl. Sci.*, vol. 11, nº 4, p. 311-316, oct. 2018, doi: 10.1016/j.jrras.2018.05.001.

[123] M. U.H.Joardder (Omar), « Design and Construction of Fixed Bed Pyrolysis System and Plum Seed Pyrolysis for Bio-oil Production », *Int. J. Renew. Energy Res.*, août 2012.

[124] C. Mohabeer, L. Abdelouahed, S. Marcotte, et B. Taouk, « Comparative analysis of pyrolytic liquid products of beech wood, Flax shives and woody biomass components », *J. Anal. Appl. Pyrolysis*, vol. 127, p. 269-277, sept. 2017, doi: 10.1016/j.jaap.2017.07.025.

[125] N. Punsuwan et C. Tangsathitkulchai, « Product Characterization and Kinetics of Biomass Pyrolysis in a Three-Zone Free-Fall Reactor », *International Journal of Chemical Engineering*, févr. 04, 2014. https://www.hindawi.com/journals/ijce/2014/986719/ (consulté le mai 29, 2020).

[126] A. Campanella et M. P. Harold, « Fast pyrolysis of microalgae in a falling solids reactor: Effects of process variables and zeolite catalysts », *Biomass Bioenergy*, vol. 46, p. 218-232, nov. 2012, doi: 10.1016/j.biombioe.2012.08.023.

[127] R. K. Liew *et al.*, « Innovative production of highly porous carbon for industrial effluent remediation via microwave vacuum pyrolysis plus sodium-potassium hydroxide mixture activation », *J. Clean. Prod.*, vol. 208, p. 1436-1445, janv. 2019, doi: 10.1016/j.jclepro.2018.10.214.

[128] C. Yin, « Microwave-assisted pyrolysis of biomass for liquid biofuels production », *Bioresour. Technol.*, vol. 120, p. 273-284, sept. 2012, doi: 10.1016/j.biortech.2012.06.016.

[129] J. Robinson *et al.*, « Microwave Pyrolysis of Biomass: Control of Process Parameters for High Pyrolysis Oil Yields and Enhanced Oil Quality », *Energy Fuels*, janv. 2015, doi: 10.1021/ef502403x.

[130] M. Arafat Hossain, P. Ganesan, J. Jewaratnam, et K. Chinna, « Optimization of process parameters for microwave pyrolysis of oil palm fiber (OPF) for hydrogen and biochar production », *Energy Convers. Manag.*, vol. 133, p. 349-362, févr. 2017, doi: 10.1016/j.enconman.2016.10.046.

[131] Y.-F. Huang, P.-T. Chiueh, et S.-L. Lo, « A review on microwave pyrolysis of lignocellulosic biomass », *Sustain. Environ. Res.*, vol. 26, nº 3, p. 103-109, mai 2016, doi: 10.1016/j.serj.2016.04.012.

[132] J. Robinson *et al.*, « Microwave Pyrolysis of Biomass: Control of Process Parameters for High Pyrolysis Oil Yields and Enhanced Oil Quality », *Energy Fuels*, vol. 29, nº 3, p. 1701-1709, mars 2015, doi: 10.1021/ef502403x.

[133] L. Abdelouahed, S. Leveneur, L. Vernieres-Hassimi, L. Balland, et B. Taouk, « Comparative investigation for the determination of kinetic parameters for biomass pyrolysis by thermogravimetric analysis », *J. Therm. Anal. Calorim.*, vol. 129, nº 2, p. 1201-1213, 2017.

[134] S. S. Lam et H. A. Chase, « A Review on Waste to Energy Processes Using Microwave Pyrolysis », *Energies*, vol. 5, nº 10, Art. nº 10, oct. 2012, doi: 10.3390/en5104209.

[135] H. Al Sayegh, « Microwave pyrolysis of forestry waste », Ph.D., University of Nottingham, 2012. Consulté le: juin 20, 2021. [En ligne]. Disponible sur: https://ethos.bl.uk/OrderDetails.do?uin=uk.bl.ethos.576151

[136] M. Giorcelli, O. Das, G. Sas, M. Försth, et M. Bartoli, « A Review of Bio-Oil Production through Microwave-Assisted Pyrolysis », *Processes*, vol. 9, nº 3, Art. nº 3, mars 2021, doi: 10.3390/pr9030561.

[137] J. P. Robinson, S. W. Kingman, R. Barranco, C. E. Snape, et H. Al-Sayegh, « Microwave Pyrolysis of Wood Pellets », *Ind. Eng. Chem. Res.*, vol. 49, nº 2, p. 459-463, janv. 2010, doi: 10.1021/ie901336k.

[138] A. A. Salema, Y. K. Yeow, K. Ishaque, F. N. Ani, M. T. Afzal, et A. Hassan, « Dielectric properties and microwave heating of oil palm biomass and biochar », *Ind. Crops Prod.*, vol. 50, p. 366-374, oct. 2013, doi: 10.1016/j.indcrop.2013.08.007.

[139] A. Al Shra'ah et R. Helleur, « Microwave pyrolysis of cellulose at low temperature », *J. Anal. Appl. Pyrolysis*, vol. 105, p. 91-99, janv. 2014, doi: 10.1016/j.jaap.2013.10.007.

[140] X. Zhao, J. Zhang, Z. Song, H. Liu, L. Li, et C. Ma, « Microwave pyrolysis of straw bale and energy balance analysis », *J. Anal. Appl. Pyrolysis*, vol. 92, nº 1, p. 43-49, sept. 2011, doi: 10.1016/j.jaap.2011.04.004.

[141] A. Domínguez, J. A. Menéndez, M. Inguanzo, et J. J. Pís, « Production of bio-fuels by high temperature pyrolysis of sewage sludge using conventional and microwave heating », *Bioresour. Technol.*, vol. 97, nº 10, p. 1185-1193, juill. 2006, doi: 10.1016/j.biortech.2005.05.011.

[142] « Ex situ thermo-catalytic upgrading of biomass pyrolysis vapors using a traveling wave microwave reactor », *Appl. Energy*, vol. 183, p. 995-1004, déc. 2016, doi: 10.1016/j.apenergy.2016.09.047.

[143] O. O. D. Afolabi, M. Sohail, et C. L. P. Thomas, « Characterization of solid fuel chars recovered from microwave hydrothermal carbonization of human biowaste », *Energy*, vol. 134, p. 74-89, sept. 2017, doi: 10.1016/j.energy.2017.06.010.

[144] S. Y. Foong *et al.*, « Valorization of biomass waste to engineered activated biochar by microwave pyrolysis: Progress, challenges, and future directions », *Chem. Eng. J.*, vol. 389, p. 124401, juin 2020, doi: 10.1016/j.cej.2020.124401.

[145] M. Miura, H. Kaga, A. Sakurai, T. Kakuchi, et K. Takahashi, « Rapid pyrolysis of wood block by microwave heating », *J. Anal. Appl. Pyrolysis*, vol. 71, nº 1, p. 187-199, mars 2004, doi: 10.1016/S0165-2370(03)00087-1.

[146] J. Robinson, S. Kingman, R. Barranco, C. Snape, et H. Al-Sayegh, « Microwave Pyrolysis of Wood Pellets », *Ind. Eng. Chem. Res. - IND ENG CHEM RES*, vol. 49, déc. 2009, doi: 10.1021/ie901336k.

[147] M. Adam, « Understanding Microwave Pyrolysis of Biomass Materials », p. 230.

[148] D. Iribarren, J. Peters, et J. Dufour, « Life cycle assessment of transportation fuels from biomass pyrolysis », *Fuel*, vol. 97, p. 812-821, juill. 2012, doi: 10.1016/j.fuel.2012.02.053.

[149] L. Ubiera, I. Polaert, L. Abdelouahed, et B. Taouk, « Microwave pyrolysis of biomass in a rotatory Kiln reactor: deep characterization and comparative analysis of pyrolytic liquids products », présenté à Ampere 2019, sept. 2019. doi: 10.4995/Ampere2019.2019.9807.

[150] « (PDF) Microwave dielectric properties of agricultural biomass at high temperature in an inert environment ». https://www.researchgate.net/publication/282823064_Microwave_dielectric_properties_of_agricultural_biomass_at_high_temperature_in_an_inert_environment (consulté le mai 19, 2021).

[151] « High-temperature dielectric properties and pyrolysis reduction characteristics of different biomass-pyrolusite mixtures in microwave field », *Bioresour. Technol.*, vol. 294, p. 122217, déc. 2019, doi: 10.1016/j.biortech.2019.122217.

[152] F. Motasemi, M. T. Afzal, A. A. Salema, J. Mouris, et R. M. Hutcheon, « Microwave dielectric characterization of switchgrass for bioenergy and biofuel », *Fuel*, vol. 124, p. 151-157, mai 2014, doi: 10.1016/j.fuel.2014.01.085.

[153] Z. M. A. Bundhoo, « Microwave-assisted conversion of biomass and waste materials to biofuels », *Renew. Sustain. Energy Rev.*, vol. 82, p. 1149-1177, févr. 2018, doi: 10.1016/j.rser.2017.09.066.

[154] L. Hongqiang, Q. Yongshui, et J. Xu, « Microwave-Assisted Conversion of Lignin », 2014, p. 61-82. doi: 10.1007/978-94-017-9612-5_4.

[155] B. Krieger-Brockett, « Microwave pyrolysis of biomass », *Res. Chem. Intermed.*, vol. 20, nº 1, p. 39-49, janv. 1994, doi: 10.1163/156856794X00054.

[156] P. Payakkawan, S. Areejit, et P. Sooraksa, « Design, fabrication and operation of continuous microwave biomass carbonization system », *Renew. Energy*, vol. 66, p. 49-55, juin 2014, doi: 10.1016/j.renene.2013.10.042.

[157] B.-J. Lin *et al.*, « Modeling and prediction of devolatilization and elemental composition of wood during mild pyrolysis in a pilot-scale reactor », *Ind. Crops Prod.*, vol. 131, p. 357-370, mai 2019, doi: 10.1016/j.indcrop.2019.01.065.

[158] « Microwave rotary kiln used for calcining chemical uranium concentrate », CN201686500U, déc. 29, 2010 Consulté le: mai 19, 2021. [En ligne]. Disponible sur: https://patents.google.com/patent/CN201686500U/en

[159] J. P. Robinson *et al.*, « Scale-up and design of a continuous microwave treatment system for the processing of oil-contaminated drill cuttings », *Chem. Eng. Res. Des.*, vol. 88, nº 2, p. 146-154, févr. 2010, doi: 10.1016/j.cherd.2009.07.011.

[160] H. C. Kim, H. Y. Kim, et S.-I. Woo, « Fast pyrolysis of chlorodifluoromethane in a microwave-heated fluidized bed », *J. Chem. Eng. Jpn.*, vol. 32, nº 2, p. 171-176, 1999.

[161] Y. Li *et al.*, « Continuous pyrolysis and catalytic upgrading of corncob hydrolysis residue in the combined system of auger reactor and downstream fixed-bed reactor », *Energy Convers. Manag.*, vol. 122, p. 1-9, août 2016, doi: 10.1016/j.enconman.2016.05.055.

[162] T. Kan, V. Strezov, et T. J. Evans, « Lignocellulosic biomass pyrolysis: A review of product properties and effects of pyrolysis parameters », *Renew. Sustain. Energy Rev.*, vol. 57, p. 1126-1140, mai 2016, doi: 10.1016/j.rser.2015.12.185.

[163] « Effect of Temperature in Fluidized Bed Fast Pyrolysis of Biomass: Oil Quality Assessment in Test Units | Industrial & Engineering Chemistry Research ». https://pubs.acs.org/doi/10.1021/ie900885c (consulté le mai 18, 2021).

[164] X. Wang *et al.*, « Biomass temperature profile development and its implications under the microwave-assisted pyrolysis condition », *Appl. Energy*, vol. 99, p. 386-392, nov. 2012, doi: 10.1016/j.apenergy.2012.05.031.

[165] D. V. Suriapparao et R. Vinu, « Effects of Biomass Particle Size on Slow Pyrolysis Kinetics and Fast Pyrolysis Product Distribution », *Waste Biomass Valorization*, vol. 9, nº 3, p. 465-477, mars 2018, doi: 10.1007/s12649-016-9815-7.

[166] « Microwave pyrolysis of corn stalk bale: a promising method for direct utilization of large-sized biomass and syngas production. » https://www.cabdirect.org/cabdirect/abstract/20103270387 (consulté le mai 19, 2021).

[167] M. Bartoli, L. Rosi, A. Giovannelli, P. Frediani, et M. Frediani, « Bio-oil from residues of short rotation coppice of poplar using a microwave assisted pyrolysis », *J. Anal. Appl. Pyrolysis*, vol. 119, p. 224-232, mai 2016, doi: 10.1016/j.jaap.2016.03.001.

[168] Y.-F. Huang, P.-T. Chiueh, W.-H. Kuan, et S.-L. Lo, « Microwave pyrolysis of lignocellulosic biomass: Heating performance and reaction kinetics », *Energy*, vol. 100, p. 137-144, avr. 2016, doi: 10.1016/j.energy.2016.01.088.

[169] Z. Hu, X. Ma, et C. Chen, « A study on experimental characteristic of microwave-assisted pyrolysis of microalgae », *Bioresour. Technol.*, vol. 107, p. 487-493, mars 2012, doi: 10.1016/j.biortech.2011.12.095.

[170] « Microwave-induced selective decomposition of cellulose: Computational and experimental mechanistic study », *J. Phys. Chem. Solids*, vol. 150, p. 109858, mars 2021, doi: 10.1016/j.jpcs.2020.109858.

[171] R. S. Singh, A. Pandey, et E. Gnansounou, *Biofuels: Production and Future Perspectives*. CRC Press, 2016.

[172] A. B. Namazi, D. G. Allen, et C. Q. Jia, « Probing microwave heating of lignocellulosic biomasses », *J. Anal. Appl. Pyrolysis*, vol. 112, p. 121-128, mars 2015, doi: 10.1016/j.jaap.2015.02.009.

[173] S. Ethaib, R. Omar, S. M. M. Kamal, D. R. Awang Biak, et S. L. Zubaidi, « Microwave-Assisted Pyrolysis of Biomass Waste: A Mini Review », *Processes*, vol. 8, nº 9, Art. nº 9, sept. 2020, doi: 10.3390/pr8091190.

[174] F. Motasemi et M. T. Afzal, « A review on the microwave-assisted pyrolysis technique », *Renew. Sustain. Energy Rev.*, vol. 28, p. 317-330, déc. 2013, doi: 10.1016/j.rser.2013.08.008.

[175] A. Salema et F. Ani, « Pyrolysis of oil palm empty fruit bunch biomass pellets using multimode microwave irradiation », *Bioresour. Technol.*, vol. 125C, p. 102-107, août 2012, doi: 10.1016/j.biortech.2012.08.002.

[176] « Dielectric characterization of biodegradable wastes during pyrolysis », *Fuel*, vol. 172, p. 146-152, mai 2016, doi: 10.1016/j.fuel.2016.01.016.

[177] F. Mushtaq, T. A. Tuan Abdullah, R. Mat, et F. Ani, « Optimization and characterization of bio-oil produced by microwave assisted pyrolysis of oil palm shell waste biomass with microwave absorber », *Bioresour. Technol.*, vol. 190, mars 2015, doi: 10.1016/j.biortech.2015.02.055.

[178] V. Abdelsayed, C. R. Ellison, A. Trubetskaya, M. W. Smith, et D. Shekhawat, « Effect of Microwave and Thermal Co-pyrolysis of Low-Rank Coal and Pine Wood on Product Distributions and Char Structure », *Energy Fuels*, juill. 2019, doi: 10.1021/acs.energyfuels.9b01105.

[179] F. Huang, A. Tahmasebi, K. Maliutina, et J. Yu, « Formation of nitrogen-containing compounds during microwave pyrolysis of microalgae: Product distribution and reaction pathways », *Bioresour. Technol.*, vol. 245, p. 1067-1074, déc. 2017, doi: 10.1016/j.biortech.2017.08.093.

[180] J. D. Moseley et C. O. Kappe, « A critical assessment of the greenness and energy efficiency of microwave-assisted organic synthesis », *Green Chem.*, vol. 13, nº 4, p. 794-806, avr. 2011, doi: 10.1039/C0GC00823K.

[181] X. Zhao, M. Wang, H. Liu, L. Li, C. Ma, et Z. Song, « A microwave reactor for characterization of pyrolyzed biomass », *Bioresour. Technol.*, vol. 104, p. 673-678, janv. 2012, doi: 10.1016/j.biortech.2011.09.137.

[182] S. Zhang, Q. Dong, L. Zhang, et Y. Xiong, « High quality syngas production from microwave pyrolysis of rice husk with char-supported metallic catalysts », *Bioresour. Technol.*, vol. 191, p. 17-23, sept. 2015, doi: 10.1016/j.biortech.2015.04.114.

[183] F. Motasemi, A. A. Salema, et M. T. Afzal, « Dielectric characterization of corn stover for microwave processing technology », *Fuel Process. Technol.*, vol. 131, p. 370-375, mars 2015, doi: 10.1016/j.fuproc.2014.12.006.

[184] « Microwave Pyrolysis of Lignocellulosic Biomass », *Energy Procedia*, vol. 105, p. 41-46, mai 2017, doi: 10.1016/j.egypro.2017.03.277.

[185] M. Sekar *et al.*, « A review on the pyrolysis of algal biomass for biochar and bio-oil – Bottlenecks and scope », *Fuel*, vol. 283, p. 119190, janv. 2021, doi: 10.1016/j.fuel.2020.119190.

[186] R. Li, Z. Zhong, B. Jin, et A. Zheng, « Selection of Temperature for Bio-oil Production from Pyrolysis of Algae from Lake Blooms », *Energy Fuels*, vol. 26, nº 5, p. 2996-3002, mai 2012, doi: 10.1021/ef300180r.

[187] V. Bhola, R. Desikan, S. K. Santosh, K. Subburamu, E. Sanniyasi, et F. Bux, « Effects of parameters affecting biomass yield and thermal behaviour of Chlorella vulgaris », *J. Biosci. Bioeng.*, vol. 111, nº 3, p. 377-382, mars 2011, doi: 10.1016/j.jbiosc.2010.11.006.

[188] Y. Hong, W. Chen, X. Luo, C. Pang, E. Lester, et T. Wu, « Microwave-enhanced pyrolysis of macroalgae and microalgae for syngas production », *Bioresour. Technol.*, vol. 237, p. 47-56, août 2017, doi: 10.1016/j.biortech.2017.02.006.

[189] N. Ferrera-Lorenzo, E. Fuente, J. M. Bermúdez, I. Suárez-Ruiz, et B. Ruiz, « Conventional and microwave pyrolysis of a macroalgae waste from the Agar–Agar industry. Prospects for bio-fuel production », *Bioresour. Technol.*, vol. 151, p. 199-206, janv. 2014, doi: 10.1016/j.biortech.2013.10.047.

[190] D. Beneroso, J. M. Bermúdez, A. Arenillas, et J. A. Menéndez, « Microwave pyrolysis of microalgae for high syngas production », *Bioresour. Technol.*, vol. 144, p. 240-246, sept. 2013, doi: 10.1016/j.biortech.2013.06.102.

[191] R. Zhang, L. Li, D. Tong, et C. Hu, « Microwave-enhanced pyrolysis of natural algae from water blooms », *Bioresour. Technol.*, vol. 212, p. 311-317, juill. 2016, doi: 10.1016/j.biortech.2016.04.053.

[192] A. Domínguez *et al.*, « Conventional and microwave induced pyrolysis of coffee hulls for the production of a hydrogen rich fuel gas », *J. Anal. Appl. Pyrolysis*, vol. 79, nº 1, p. 128-135, mai 2007, doi: 10.1016/j.jaap.2006.08.003.

[193] M. Chen *et al.*, « Catalytic effects of eight inorganic additives on pyrolysis of pine wood sawdust by microwave heating », *J. Anal. Appl. Pyrolysis*, vol. 82, nº 1, p. 145-150, mai 2008, doi: 10.1016/j.jaap.2008.03.001.

[194] Y. F. Huang, W. H. Kuan, S. L. Lo, et C. F. Lin, « Hydrogen-rich fuel gas from rice straw via microwave-induced pyrolysis », *Bioresour. Technol.*, vol. 101, nº 6, p. 1968-1973, mars 2010, doi: 10.1016/j.biortech.2009.09.073.

[195] H. Lei, S. Ren, et J. Julson, « The Effects of Reaction Temperature and Time and Particle Size of Corn Stover on Microwave Pyrolysis », *Energy Fuels - ENERG FUEL*, vol. 23, juin 2009, doi: 10.1021/ef9000264.

[196] D. Beneroso, J. M. Bermúdez, A. Arenillas, et J. A. Menéndez, « Comparing the composition of the synthesis-gas obtained from the pyrolysis of different organic residues for a potential use in the synthesis of bioplastics », *J. Anal. Appl. Pyrolysis*, vol. 111, p. 55-63, janv. 2015, doi: 10.1016/j.jaap.2014.12.011.

[197] Y. Wan *et al.*, « Microwave-assisted pyrolysis of biomass: Catalysts to improve product selectivity », *J. Anal. Appl. Pyrolysis*, vol. 86, nº 1, p. 161-167, sept. 2009, doi: 10.1016/j.jaap.2009.05.006.

[198] D07 Committee, « Test Method for Ash in Wood », ASTM International. doi: 10.1520/D1102-84R13.

[199] E48 Committee, « Test Method for Moisture Analysis of Particulate Wood Fuels », ASTM International. doi: 10.1520/E0871-82R19.

[200] E48 Committee, « Test Method for Volatile Matter in the Analysis of Particulate Wood Fuels », ASTM International. doi: 10.1520/E0872-82R19.

[201] M. S. Venkatesh et G. S. V. Raghavan, « An Overview of Microwave Processing and Dielectric Properties of Agri-food Materials », *Biosyst. Eng.*, vol. 88, nº 1, p. 1-18, mai 2004, doi: 10.1016/j.biosystemseng.2004.01.007.

[202] J. T. Scanlon et D. E. Willis, « Calculation of Flame Ionization Detector Relative Response Factors Using the Effective Carbon Number Concept », *J. Chromatogr. Sci.*, vol. 23, nº 8, p. 333-340, août 1985, doi: 10.1093/chromsci/23.8.333.

[203] « Composition of gases released during olive stones pyrolysis ». https://www.infona.pl/resource/bwmeta1.element.elsevier-dab53391-b32f-3d62-a742-fb381e8c34c0 (consulté le avr. 18, 2021).

[204] V. Minkova, M. Razvigorova, E. Bjornbom, R. Zanzi, T. Budinova, et N. Petrov, « Effect of water vapour and biomass nature on the yield and quality of the pyrolysis products from biomass », *Fuel Process. Technol.*, vol. 70, nº 1, p. 53-61, 2001.

[205] A. Friedl, E. Padouvas, H. Rotter, et K. Varmuza, « Prediction of heating values of biomass fuel from elemental composition », *Anal. Chim. Acta*, vol. 544, p. 191-198, juill. 2005, doi: 10.1016/j.aca.2005.01.041.

[206] W. Zhang, T. Henschel, U. Söderlind, K.-Q. Tran, et X. Han, « Thermogravimetric and Online Gas Analysis on various Biomass Fuels », *Energy Procedia*, vol. 105, p. 162-167, mai 2017, doi: 10.1016/j.egypro.2017.03.296.

[207] Q.-V. Bach, W.-H. Chen, S.-C. Lin, H.-K. Sheen, et J.-S. Chang, « Effect of Wet Torrefaction on Thermal Decomposition Behavior of Microalga Chlorella vulgaris ESP-31 », *Energy Procedia*, vol. 105, p. 206-211, mai 2017, doi: 10.1016/j.egypro.2017.03.303.

[208] H. Kol et N. Ay, « Dielectric properties of hardwood species at microwave frequencies », *J. Wood Sci.*, vol. 50, p. 375-380, janv. 2004, doi: 10.1007/s10086-003-0575-1.

[209] « (PDF) Dielectric characterization of bentonite clay at various moisture contents and with mixtures of biomass in the microwave spectrum », *ResearchGate*, Consulté le: mai 11, 2021. [En ligne]. Disponible sur: https://www.researchgate.net/publication/322693922_Dielectric_characterization_of_bentonite_clay_at_various_moisture_contents_and_with_mixtures_of_biomass_in_the_microwave_spectrum

[210] A. Itolikar, « Microwave Dielectric Properties of Alage », déc. 2015.

[211] M. Tripathi, J. N. Sahu, P. Ganesan, P. Monash, et T. K. Dey, « Effect of microwave frequency on dielectric properties of oil palm shell (OPS) and OPS char synthesized by microwave pyrolysis of OPS », *J. Anal. Appl. Pyrolysis*, vol. 112, p. 306-312, mars 2015, doi: 10.1016/j.jaap.2015.01.007.

[212] C. Ellison, M. Mckeown, S. Trabelsi, et D. Boldor, « Dielectric Properties of Biomass/Biochar Mixtures at Microwave Frequencies », *Energies*, vol. 10, avr. 2017, doi: 10.3390/en10040502.

[213] K. Anastasakis, A. B. Ross, et J. M. Jones, « Pyrolysis behaviour of the main carbohydrates of brown macro-algae », *Fuel*, vol. 90, nº 2, p. 598-607, févr. 2011, doi: 10.1016/j.fuel.2010.09.023.

[214] A. Mathiarasu et M. Pugazhvadivu, « Studies on dielectric properties and microwave pyrolysis of karanja seed », *Biomass Convers. Biorefinery*, p. 1-11, févr. 2021, doi: 10.1007/s13399-021-01349-5.

[215] F. Motasemi, A. Salema, et M. T. Afzal, « Microwave dielectric properties of agricultural biomass at high temperature in an inert environment », *Trans. ASABE*, vol. 58, p. 869-877, janv. 2015, doi: 10.13031/trans.58.11006.

[216] C. Zhao, E. Jiang, et A. Chen, « Volatile production from pyrolysis of cellulose, hemicellulose and lignin », *J. Energy Inst.*, vol. 90, nº 6, p. 902-913, déc. 2017, doi: 10.1016/j.joei.2016.08.004.

[217] C. Di Blasi, « Modeling chemical and physical processes of wood and biomass pyrolysis », *Prog. Energy Combust. Sci.*, vol. 34, nº 1, p. 47-90, févr. 2008, doi: 10.1016/j.pecs.2006.12.001.

[218] A. K. Sadhukhan, P. Gupta, et R. K. Saha, « Modelling of pyrolysis of large wood particles », *Bioresour. Technol.*, vol. 100, nº 12, p. 3134-3139, juin 2009, doi: 10.1016/j.biortech.2009.01.007.

[219] C. C. D. Mohabeer, « Bio-oil production by pyrolysis of biomass coupled with a catalytic de-oxygenation treatment », phdthesis, Normandie Université, 2018. Consulté le: avr. 25, 2021. [En ligne]. Disponible sur: https://tel.archives-ouvertes.fr/tel-02096666

[220] S. Ge *et al.*, « Progress in microwave pyrolysis conversion of agricultural waste to value-added biofuels: A batch to continuous approach », *Renew. Sustain. Energy Rev.*, vol. 135, p. 110148, janv. 2021, doi: 10.1016/j.rser.2020.110148.

[221] J. Hunt, A. Ferrari, A. Lita, M. Crosswhite, B. Ashley, et A. E. Stiegman, « Microwave-Specific Enhancement of the Carbon–Carbon Dioxide (Boudouard) Reaction », *J. Phys. Chem. C*, vol. 117, nº 51, p. 26871-26880, déc. 2013, doi: 10.1021/jp4076965.

[222] S. Grierson, V. Strezov, G. Ellem, R. Mcgregor, et J. Herbertson, « Thermal characterisation of microalgae under slow pyrolysis conditions », *J. Anal. Appl. Pyrolysis*, vol. 85, nº 1, p. 118-123, mai 2009, doi: 10.1016/j.jaap.2008.10.003.

[223] D. D. Miller, M. W. Smith, et D. Shekhawat, « Microwave-induced selective decomposition of cellulose: Computational and experimental mechanistic study », *J. Phys. Chem. Solids*, vol. 150, p. 109858, mars 2021, doi: 10.1016/j.jpcs.2020.109858.

[224] C. Nzediegwu, M. Arshad, A. Ulah, M. A. Naeth, et S. X. Chang, « Fuel, thermal and surface properties of microwave-pyrolyzed biochars depend on feedstock type and pyrolysis temperature », *Bioresour. Technol.*, vol. 320, p. 124282, janv. 2021, doi: 10.1016/j.biortech.2020.124282.

[225] H. Luo *et al.*, « Microwave-assisted low-temperature biomass pyrolysis: from mechanistic insights to pilot scale », *Green Chem.*, vol. 23, nº 2, p. 821-827, févr. 2021, doi: 10.1039/D0GC03348K.

[226] « Micro-ondes: Tome 1, Lignes, guides et cavités - Paul François Combes - Google Livres ». https://books.google.fr/books/about/Micro_ondes.html?id=ApnOnAEACAAJ&redir_esc=y (consulté le juill. 06, 2020).

[227] A. R. Hakim, W. T. Handoyo, et A. W. Prasetyo, « A simulation study of parameters influencing microwave heating of seaweed (*Eucheuma cottonii*) », *J. Phys. Conf. Ser.*, vol. 1444, p. 012026, janv. 2020, doi: 10.1088/1742-6596/1444/1/012026.

[228] R. Try, « Étude expérimentale et modélisation dynamique d'un réacteur catalytique modulaire pour l'hydrogénation du CO2 en méthane. Energie électrique. Université de Lyon », p. 1-50, 2018.

9 PUBLICATIONS AND ORAL COMMUNICATIONS FROM THIS THESIS

1. UBIERA L, POLAERT I., DELMOTTE M., ABDELOUAHED L., TAOUK B., "Energy optimization of bio-oil production from biomass by fast pyrolysis using microwaves" Reaction Chemistry & Engineering, 2021, 6, 1884 – 1899

2. B- DE LA CRUZ R., UBIERA L., POLAERT I., "Sargasso pyrolysis under guided single-mode microwave cavity" CHISA 2021: International Congress of Chemical and Process Engineering, 15-18 March **2021** (Virtual). **ORAL**

3. C- UBIERA L, POLAERT I., DELMOTTE M., ABDELOUAHED L., TAOUK B., "Microwave intensification and energy optimization of bio-oil production from biomass by fast PyrolysisISCRE26 Delhi, 5-8 December **2021.**

4. D- UBIERA L, POLAERT I., ABDELOUAHED L., TAOUK B., "Microwave pyrolysis of biomass in a rotary kiln reactor: deep characterization and comparative analysis of pyrolytic liquids products" Congrès AMPERE2019, 17th International conference on microwave and high Frequency heating, Valencia (Spain), 9-12 September **2019**.